Masticatory muscle anatomy and functional performance of rodents and Djadochtatherioid multituberculates

Julia Rosalind Samantha May, BSc, MSc

Thesis deposited for PhD in Human Sciences

Hull York Medical School

First submitted for examination October 2024

This post-viva corrected submission December 2025

Abstract

Rodents exhibit conservative anatomy adapted for gnawing, which can be divided into four morphotype categories. This project quantifies and compares the mechanical advantage of a sample of rodents across the tree, evaluating the variation between the morphotypes during incisor and molar biting at a range of gape angles. Once the variation of rodents was established, this was compared and contrasted with that of three Cretaceous multituberculates, a fossil mammal group that has several similarities to modern rodents. Through 2D lever-arm mechanics and PCAs and MANOVAs of the data, the rodent morphotypes are compared with each other and with the multituberculate fossils. According to the results of this project, multituberculates are functionally distinct on homologous muscles but can individually be more similar to extant rodents than to each other, to a degree, and the morphotype categories within rodents are functionally distinct. The variation within each morphotype is broad, however, suggesting that assumptions should not be made about the mechanical efficiency and function of organisms based on their morphotype category without a more detailed exploration of their anatomical and functional characteristics. This project explores, supports and builds upon established interpretations of the functional difference between morphotypes and provides a stepping stone to future research on extant and fossil rodents and fossil multituberculates. Incorporation of multiple factors such as bite point and gape angle are critical to differentiating the categories, with the sample being more mechanically similar during gnawing and the extremes of high and low gape accounting for most of the variance in efficiency.

Table of Contents

Abstract 1

Table of Contents 2

Table of Figures 6

Table of Tables 8

Author's declaration 9

Acknowledgements 9

Chapter 1 – Introduction 10

Bibliography 12

Chapter 2: Comparing rodent morphotype categories through modelling of biting with the incisors at zero degrees gape. 17

2.1 – Introduction 17
2.1.1 – Quantitative comparisons of rodent gnawing 17
2.1.2 – A brief overview of Rodentia 18
2.1.3 – Morphotypes 20
2.1.4 – Mechanical advantage 26
2.1.5 – Key questions and hypotheses 28

2.2 – Materials & Methods 30
2.2.1 – Sample information 30
2.2.2 – Segmentation and alignment 33
2.2.3 – Muscle identification and mapping 34
2.2.4 – Lever-arm mechanics analyses 36
2.2.5 – Statistical analysis 41

2.3 – Results 43
2.3.1 – Archetypal taxa 43
2.3.1.1 – Protrogomorph: Aplodontia rufa (Mountain Beaver) 43
2.3.1.2 – Hystricomorph: Cavia porcellus (Domestic Guinea Pig) 51
2.3.1.3 – Myomorph: Rattus norvegicus (Brown rat) 55
2.3.1.4 – Sciuromorph: Sciurus carolinensis (Eastern Grey Squirrel) 59
2.3.2 – Remaining taxa 62
2.3.2.1 – Acomys cahirinus ('Northeast African Spiny Mouse') 62
2.3.2.2 – Bathyergus suillus ('Cape Dune Mole-rat') 63
2.3.2.3 – Cannomys badius ('Lesser Bamboo Rat') 64
2.3.2.4 – Capromys pilorides ('Desmarest's Hutia') 66

2.3.2.5 – Castor canadensis ('Northeast American Beaver') 67
2.3.2.6 – Cricetomys gambianus ('Northern Giant Pouched Rat') 69
2.3.2.7 – Ctenomys opimus ('Andean/Highland Tuco-tuco') 70
2.3.2.8 – Dasyprocta sp. ('Agouti') 72
2.3.2.9 – Dipus sagitta ('Northern Three-toed Jerboa') 74
2.3.2.10 – Erethizon dorsatum ('North American Porcupine') 75
2.3.2.11 – Georychus capensis ('Cape Mole-rat') 76
2.3.2.12 – Gerbillus watersi ('Water's Gerbil') 78
2.3.2.13 – Graphiurus nagtglasii ('Nagtglas's African Dormouse') 79
2.3.2.14 – Hydrochoerus hydrochaeris ('Capybara') 80
2.3.2.15 – Hystrix cristata ('Crested Porcupine') 82
2.3.2.16 – Lagostomus maximus ('Plains Viscacha') 84
2.3.2.17 – Laonastes aenigmamus ('Kha-nyou' or 'Laotian Rock Rat') 85
2.3.2.18 – Myocastor coypus ('Coypu') 86
2.3.2.19 – Octodon degus ('Common Degu') 87
2.3.2.20 – Pedetes capensis ('South African Springhare') 88
2.3.2.21 – Petaurista sp. ('Giant Flying Squirrel') 90
2.3.2.22 – Phyllotis gerbillus ('Peruvian Leaf-eared Mouse') 91
2.3.2.23 – Thomomys umbrinus ('Southern Pocket Gopher') 92
2.3.3 – Mechanical advantage results 94
2.4 – Discussion 99
2.4.1 – Key questions and hypotheses 99
2.4.2 – Pterygoid configurations 101
2.4.3 – Limitations of this study, and ways to expand 106
2.5 – Conclusion 108
Bibliography *109*
Chapter 3 – Gape angle, bite point, head size, and their relationship with mechanical advantage among rodent morphotypes *119*
3.1 – Introduction 119
3.1.1 – Preface 119
3.1.2 – The rodents 120
3.1.3 – Mechanical advantage and jaw-closing muscles 121
3.1.4 – Incisor biting and molar biting 123
3.1.5 – Gape angle 125

3.1.6 – Head size: a potential factor to consider _____ 130
3.1.7 – Key Questions and Hypotheses _____ 131

3.2 – Materials and Methods _____ 134
3.2.1 – Sample preparation _____ 134
3.2.2 – Simulating bite point and gape angle _____ 134
3.2.3 – Statistical analyses _____ 138
3.2.4 – Head Size Correlation Testing _____ 142

3.3 – Results _____ 145
3.3.1 – Comparing Morphotypes _____ 145
3.3.1.1 – A brief overview of observable trends in the raw data _____ 145
3.3.1.2 – Individual muscle MANOVA results _____ 149
3.3.1.3 – Principal Components Analyses results _____ 150
3.3.1.3.1 – Analysis with all muscles _____ 150
3.3.1.3.2 – Analysis without IOZM _____ 158
3.3.2 – Head Size Regression _____ 165

3.4 – Discussion _____ 166
3.4.1 – Key Questions and Hypotheses _____ 166
3.4.2 – Potential limitations _____ 172

3.5 – Conclusions _____ 177

Bibliography _____ 179

Chapter 4 – Comparing the mechanical advantage and jaw-closing musculature among rodent morphotypes and Djadochtatherioid multituberculates _____ 189

4.1. – Introduction _____ 189
4.1.1 – A brief summary _____ 189
4.1.2 – Multituberculates: a point of comparison _____ 190
4.1.3 – Key questions and hypotheses _____ 195

4.2 – Materials & Methods _____ 198
4.2.1 – Sample Preparation _____ 198
4.2.1.1 – General Sample Preparation _____ 198
4.2.1.2 – Multituberculate Fossil Reconstructions _____ 200
4.2.1.2.1 – Nemegtbaatar gobiensis _____ 200
4.2.1.2.2 – Chulsanbaatar vulgaris _____ 205
4.2.1.2.3 – Kryptobaatar dashzevegi _____ 206
4.2.2 – Lever-arm mechanics modelling _____ 207
4.2.3 – Statistical Analyses _____ 208
4.2.4 – Head size correlation testing _____ 211

4.3 – Results _____ 212
4.3.1 – Anatomy and fossil reconstructions _____ 212
4.3.1.1 – Nemegtbaatar gobiensis _____ 212
4.3.1.1.1 – Skull reconstruction _____ 216

4.3.1.1.2 – Hemimandible reconstruction 221
4.3.1.1.3 – Mandible position during incisor and molar biting 224
4.3.1.1.4 – Muscle attachments 229
4.3.1.2 – Chulsanbaatar vulgaris 237
4.3.1.3 – Kryptobaatar dashzevegi 246
4.3.2 – Lever-arm mechanics 254
4.3.2.1 – Individual muscle MANOVAs 254
4.3.2.2 – PCA results 255
4.3.2.2.1 – ADM v IOZM 255
4.3.2.2.2 – ADM v DM 264
4.3.2.3 – Head size regression 273
4.4 – Discussion 275
4.4.1 – Returning to the hypotheses 275
4.4.2 – Comparisons with older reconstructions 277
4.4.3 – Limitations and avenues for further study 282
4.5 – Conclusions 285
Bibliography 287
Chapter 5 – Discussion and conclusions 294
Bibliography 298

Table of Figures

Fig 2.1	Diagrams of the skeletal characteristics of morphotypes	21
Fig 2.2	Diagrams of the DM and ZM complexes of morphotypes	23
Fig 2.3	Tree of Rodentia with morphotype distribution shown	24
Fig 2.4	Cladogram of rodent families showing the distribution of sampled taxa.	30
Fig 2.5	Orientation of digital specimens relative to the global axes	33
Fig 2.6	Illustrative example of muscle mapping	36
Fig 2.7	Illustration of equations for calculating mechanical advantage	40
Fig 2.8	Lateral views of muscle attachments on the lateral zygomatic arch and mandible in *A. rufa*, *C. porcellus*, *R. norvegicus*, and *S. carolinensis*.	44
Fig 2.9	Lateral views of muscle attachments on the medial zygomatic arch and mandible in *A. rufa*, *C. porcellus*, *R. norvegicus*, and *S. carolinensis*.	45
Fig 2.10	Lateral views of muscle attachments on the condylar process and medial mandibular angle in *A. rufa*, *C. porcellus*, *R. norvegicus*, and *S. carolinensis*.	46
Fig 2.11	Muscle attachments panel figure for *A. cahirinus*	62
Fig 2.12	Muscle attachments panel figure for *B. suillus*	63
Fig 2.13	Muscle attachments panel figure for *C. badius*	65
Fig 2.14	Muscle attachments panel figure for *C. pilorides*	66
Fig 2.15	Muscle attachments panel figure for *C. canadensis*	67
Fig 2.16	Muscle attachments panel figure for *C. gambianus*	69
Fig 2.17	Muscle attachments panel figure for *C. opimus*	71
Fig 2.18	Muscle attachments panel figure for *D. punctata*	73
Fig 2.19	Muscle attachments panel figure for *D. sagitta*	74
Fig 2.20	Muscle attachments panel figure for *E. dorsatum*	75
Fig 2.21	Muscle attachments panel figure for *G. capensis*	77
Fig 2.22	Muscle attachments panel figure for *G. watersi*	78
Fig 2.23	Muscle attachments panel figure for *G. nagtglasii*	80
Fig 2.24	Muscle attachments panel figure for *H. hydrochaeris*	81
Fig 2.25	Muscle attachments panel figure for *H. cristata*	83
Fig 2.26	Muscle attachments panel figure for *L. maximus*	84
Fig 2.27	Muscle attachments panel figure for *L. aenigmamus*	85
Fig 2.28	Muscle attachments panel figure for *M. coypus*	86
Fig 2.29	Muscle attachments panel figure for *O. degus*	87
Fig 2.30	Muscle attachments panel figure for *P. capensis*	89
Fig 2.31	Muscle attachments panel figure for *P. petaurista*	90
Fig 2.32	Muscle attachments panel figure for *P. gerbillus*	91
Fig 2.33	Muscle attachments panel figure for *T. umbrinus*	92
Fig 2.34	Box plots of mechanical advantage by morphotype for each individual homologous muscle	96
Fig 2.35	Panel figure illustrating the three proposed configurations of pterygoid origin centroids	104

Fig 3.1 Illustration of example gape angles and bite points 135
Fig 3.2 Raw mechanical advantage (MA) data in *R. norvegicus* 148
Fig 3.3 Principal Component (PC) plots of MA in the 'ADM v IOZM' sample 151
Fig 3.4 Loading plots of the 'ADM v IOZM' PCA 154
Fig 3.5 PC plots of MA in the 'ADM v DM' sample 159
Fig 3.6 Loading plots of the 'ADM v DM' PCA 161

Fig 4.1 Rough tree of Multituberculata and the three taxa sampled 193
Fig 4.2 Photographs of the fossil *N. gobiensis* specimen 212
Fig 4.3 Volume renders of the scanned *N. gobiensis* skull 214
Fig 4.4 Volume renders of the scanned *N. gobiensis* hemimandible 215
Fig 4.5 Segmented bone and matrix of *N. gobiensis* skull 217
Fig 4.6 Reconstructed right side of *N. gobiensis* skull 219
Fig 4.7 Diagrams of proposed complete *N. gobiensis* skull 220
Fig 4.8 Diagrams of proposed complete *N. gobiensis* hemimandible 222
Fig 4.9 Illustrations of the rescaling of the scanned *N. gobiensis* hemimandible 223
Fig 4.10 Lateral view of incisor and premolar biting in *N. gobiensis* 225
Fig 4.11 Diagrams of *N. gobiensis* at incisor occlusion 227
Fig 4.12 Diagrams of *N. gobiensis* at premolar occlusion 228
Fig 4.13 Proposed muscle attachments on *N. gobiensis* skull 230
Fig 4.14 Proposed attachments on *N. gobiensis* hemimandible 231
Fig 4.15 Lateral diagram of muscle attachments in *N. gobiensis* 236
Fig 4.16 Digitised fossil skull of *C. vulgaris* 237
Fig 4.17 Segmented hemimandible of *C. vulgaris* 238
Fig 4.18 Diagrams of proposed complete *C. vulgaris* skull 239
Fig 4.19 Diagrams of right hemimandible of *C. vulgaris* 240
Fig 4.20 Diagrams of *C. vulgaris* at incisor occlusion 241
Fig 4.21 Diagrams of *C. vulgaris* at premolar occlusion 242
Fig 4.22 Proposed muscle attachments of *C. vulgaris* skull 243
Fig 4.23 Proposed muscle attachments of *C. vulgaris* hemimandible 244
Fig 4.24 Lateral diagram of muscle attachments in *C. vulgaris* 245
Fig 4.25 Diagrams of the scanned skull of *K. dashzevegi* 246
Fig 4.26 Diagrams of the scanned mandible of *K. dashzevegi* 247
Fig 4.27 Diagrams of *K. dashzevegi* at incisor occlusion 248
Fig 4.28 Diagrams of *K. dashzevegi* at premolar occlusion 249
Fig 4.29 Proposed muscle attachments on *K dashzevegi* skull 250
Fig 4.30 Proposed muscle attachments on *K dashzevegi* mandible 251
Fig 4.31 Lateral diagram of muscle attachments in *K. dashzevegi* 252
Fig 4.32 PC plots of MA in the 'ADM v IOZM' sample 256
Fig 4.33 Loading plots of the 'ADM v IOZM' sample PCA 259
Fig 4.34 PC plots of MA in the 'ADM v DM' sample 265
Fig 4.35 Loading plots of the 'ADM v DM' sample PCA 268

Table of Tables

Table 2.1	Sample information for the twenty-seven rodents	31
Table 2.2	Summary of relevant citations on the musculature of species in the sample	34
Table 2.3	Mechanical advantage of each muscle in each taxon	94
Table 2.4	Summary of phylANOVA results	97
Table 3.1	MANOVA results for individual muscle MA data	150
Table 3.2	Summary of the variance accounted for by PCs 1–4 in the 'ADM v lOZM' PCA	151
Table 3.3	MANOVA results of 'ADM v lOZM' sample PC data	158
Table 3.4	Variance accounted for by PCs 1–4 in the 'ADM v DM' PCA	159
Table 3.5	MANOVA results on the 'ADM v DM' PCA data	163
Table 3.6	MANOVA results when comparing paired morphotypes in the 'ADM v DM' PCA data	164
Table 3.7	Summary of the results of the Multiple Regression (MR) comparing MA and head size	165
Table 4.1	Sample information for the three multituberculates	199
Table 4.2	Measurements of original and scanned hemimandibles	203
Table 4.3	MANOVA results for individual muscle MA data	255
Table 4.4	Summary of the variance accounted for by PCs 1–4 in the 'ADM v lOZM' PCA	256
Table 4.5	MANOVA results of 'ADM v lOZM' sample PC data	263
Table 4.6	MANOVA results comparing multituberculates and individual rodent morphotypes in the 'ADM v lOZM' data	264
Table 4.7	Variance accounted for by PCs 1–4 in the 'ADM v DM' PCA	265
Table 4.8	MANOVA results on the 'ADM v DM' PCA data	271
Table 4.9	MANOVA results comparing multituberculates and individual rodent morphotypes in the 'ADM v DM' data	272
Table 4.10	MANOVA results comparing multituberculates and paired rodent morphotypes in the 'ADM v DM' data	272
Table 4.11	Results of MR comparing MA and head size	273

Author's declaration

I declare that this thesis is a presentation of original work and I am the sole author. This thesis was conducted with the support of my supervisors, Samuel N. Cobb and Philip G. Cox, who provided feedback and proofreading. This work has not previously been presented for a degree or other qualification at this University or elsewhere. None of the material in this thesis has yet been presented for publication at the time of submission. All sources are acknowledged as references.

Acknowledgements

Many thanks to my supervisors, Sam Cobb and Phil Cox, who have been an incredible source of knowledge, support, and feedback through the PhD. I'm very grateful to the administrative and support staff of HYMS, especially Elaine Brookes and Aziz Asghar, who were invaluable during the Covid-19 pandemic and beyond. And finally, thanks to my family, friends, and loved ones, whose kindness and support made all this possible.

All rodents studied in this project have the scans available on MorphoSource (www.morphosource.org), and *K. dashzevegi* is available on Digimorph. Specimens from National Museums Liverpool (NML) are specifically from the World Museum Liverpool, and specimens from the University Museum of Zoology, Cambridge (UMZC), were loaned by Rob Asher and Matt Lowe to the project's secondary supervisor, Phil Cox, for scanning some years ago. The novel multituberculate scans (*C. vulgaris* and *N. gobiensis*) were provided by Łucja Fostowicz-Frelik of the Institute of Paleobiology at the Polish Academy of Sciences, Warsaw (ZPAL), and Ian Corfe of the University of Helsinki. Jesse Hennekam, at the time a fellow PhD student at HYMS, took the photographs of *N. gobiensis* shown in Figure 4.2 (as well as similar photographs included in the supplementary material/data storage of the project) as I was unable to travel to Warsaw at the time. Thanks also to my friend Bridget Warren, for her help troubleshooting some R code errors.

Chapter 1 – Introduction

Rodents are a group with highly specialised autapomorphies and behaviours related to gnawing, associated with conservative anatomy (Wood, 1955, 1965; Druzinsky, 1995, 2015; Cox *et al.*, 2012; Cox and Hautier, 2015; Cox and Baverstock, 2016; McIntosh and Cox, 2016) despite their massive species diversity, dietary diversity, and habitat diversity (Vander Wall, 2001; Wilson and Reeder, 2005; Samuels, 2009; Wilson, Lacher and Mittermeier, 2016, 2017; Burgin *et al.*, 2018). However, they are not the only organisms to have evolved some of these characteristics, such as their diprotodont incisors, or diastema, or large subdivided masseter complex (Wood, 1965; Samuels, 2009; P. Cox *et al.*, 2011; Cox and Hautier, 2015); for example, multituberculates evolved in the Jurassic, before the origin of rodents, and persisted into the Eocene (Kielan-Jaworowska, Cifelli and Luo, 2004; Weaver *et al.*, 2022), eventually coexisting with and going extinct in habitats shared with rodents, resulting in disputed propositions of competitive exclusion (Matthew, 1897; Jepsen, 1949; Wilson, 1951; Simpson, 1953; McKenna, 1961; Wood, 1962, 2010; Landry, 1965; Valen and Sloan, 1966; Hopson, 1967; Clemens, Kielan-Jaworowska and Lillegraven, 1979; Ostrander, 1984; Krause, 1986; Benton, 1987; Jablonski, 2008; Adams *et al.*, 2019). Multituberculates share several distinctive characteristics with rodents despite also having their own unique autapomorphies (Kielan-Jaworowska, 1974; Kielan-Jaworowoska, Presley and Poplin, 1986; Gambaryan and Kielan-Jaworowska, 1995; Kielan-Jaworowska, Cifelli and Luo, 2004; Wilson *et al.*, 2012; Grossnickle and Polly, 2013; Adams *et al.*, 2019; Grossnickle, Smith and Wilson, 2019; Weaver and Wilson, 2021). Despite these apparent similarities and pre-existing comparisons, several questions remain not yet fully explored using modern methods and digitised samples: what is the functional significance of anatomical disparity within and across these groups, and what might this mean for our understanding of them individually and when studied together?

To compare the anatomy and functions of organisms, homologous features must be identified. This requires a systematic method that is applied consistently across the sample, which presents a number of restrictions when fossil taxa lack preservation of soft-tissues. Within these limitations, a suitable method of anatomical and functional comparison is to identify the homologous muscle attachments on the bones, and compare the efficiency of their lever arms. Rather than studying dentition or cranial features—which themselves could be a full PhD project each—this project compares the identified muscle attachments of a selection of 27 rodents and 3 multituberculate fossils, analysing the disparity between these groups and the variation within Rodentia itself. Despite their conservative anatomy, rodents are not uniform, and the shape of their anterior zygomatic root and masseter subdivisions can be categorised into four morphological groups (Brandt, 1855; Scott, Jepsen and Wood, 1937; Wood, 1955, 1965; Cox and Jeffery, 2011, 2015; Fabre *et al.*, 2012). Functional comparisons between these anatomical groups have been made before (Becht, 1953; Wood, 1965; Druzinsky, 1995, 2010; Cox and Jeffery, 2011; Cox *et al.*, 2011; Adams *et al.*, 2019; Rankin, Emry and Asher, 2020), but this project presents an opportunity to do so with a sample across the tree of rodents and compare these groups with the distantly related fossils too. This forms a framework that can be expanded with fossil rodents or more fossil multituberculates in the coming years.

This project's analyses are divided into three segments, presented here as Chapters 2, 3, and 4, which comprise the majority of the thesis. Chapter 2 identifies and quantifies homologous muscle attachments across 27 rodent taxa, and compares them using a simple bite with the incisor teeth at occlusion. Chapter 3 builds upon these data and models incisor and molar biting at a range of gape angles, evaluating how the size of an object being bitten and the type of bite used may illuminate variation and disparity within and between the anatomical categories. Chapter 4 reconstructs and identifies the musculature of three Cretaceous multituberculate taxa and compares them with the rodents using the same methods and variables as before.

Chapter 5 provides a summary Discussion synthesising the results and conclusions of each of the main chapters. As a result, this Introduction, Chapter 1, has been kept brief and light on detail. The main chapters themselves are mostly written as standalone papers; Chapters 1 and 5 are bookending sections to provide support and emphasise the throughline. Repeated text (such as in the Introductions or Material and Methods sections in certain Chapters) was removed for the print thesis, but otherwise those chapters provide all relevant introductory details on a chapter-by-chapter basis, detail that this brief summary omits. Instead, this Introduction section is merely a short prelude, establishing the broad strokes and laying out why the main chapters occur in this order, and the logic of this project's structure as a whole.

Bibliography

Adams, N.F., Rayfield, E.J., Cox, P.G., Cobb, S.N. and Corfe, I.J. (2019) 'Functional tests of the competitive exclusion hypothesis for multituberculate extinction', *Royal Society Open Science*, 6:181536. Available at: https://doi.org/10.1098/rsos.181536.

Becht, G. (1953) 'Comparative biologic-anatomical researches on mastication in some mammals', *Proc. Koninklijke Nederlandse Akademie van Wetenschappen, Ser C*, 56, pp. 508–527.

Benton, M.J. (1987) 'Progress and competition in macroevolution', *Biological Reviews*, 62(3), pp. 305–338. Available at: https://doi.org/10.1111/j.1469-185X.1987.tb00666.x.

Brandt, J.F. (1855) *Beiträge zur nähern Kenntniss der Säugethiere Russlands.*

Burgin, C.J., Colella, J.P., Kahn, P.L. and Upham, N.S. (2018) 'How many species of mammals are there?', *Journal of Mammalogy*, 99(1), pp. 1–14. Available at: https://doi.org/10.1093/jmammal/gyx147.

Clemens, W.A., Kielan-Jaworowska, Z. and Lillegraven, J.A. (eds) (1979) *Mesozoic mammals: the first two-thirds of mammalian history*. University of California Press.

Cox, P., Fagan, M.J., Rayfield, E.J. and Jeffrey, N. (2011) 'Finite element modelling of squirrel, guinea pig and rat skulls: using geometric morphometrics to assess sensitivity', *Journal of Anatomy*, 219, pp. 696–709. Available at: https://doi.org/10.1111/j.1469-7580.2011.01436.x.

Cox, P.G. and Baverstock, H. (2016) 'Masticatory muscle anatomy and feeding efficiency of the American beaver, *Castor canadensis* (Rodentia, Castoridae)', *Journal*

of Mammalian Evolution, 23, pp. 191–200. Available at: https://doi.org/10.1007/s10914-015-9306-9.

Cox, P.G., Fagan, M.J., Rayfield, E.J. and Jeffery, N. (2011) 'Finite element modelling of squirrel, guinea pig and rat skulls: Using geometric morphometrics to assess sensitivity', *Journal of Anatomy*, 219(6), pp. 696–709. Available at: https://doi.org/10.1111/j.1469-7580.2011.01436.x.

Cox, P.G. and Hautier, L. (2015) *Evolution of the Rodents: Advances in Phylogeny, Functional Morphology and Development*. Edited by P. G. Cox and L. Hautier. Cambridge University Press (Cambridge Studies in Morphology and Molecules: New Paradigms in Evolutionary Bio, 5). Available at: https://doi.org/10.1017/CBO9781107360150.

Cox, P.G. and Jeffery, N. (2011) 'Reviewing the morphology of the jaw-closing musculature in squirrels, rats, and guinea pigs with Contrast-Enhanced MicroCT', *The Anatomical Record*, 294, pp. 915–928. Available at: https://doi.org/10.1111/j.1469-7580.2011.01436.x.

Cox, P.G. and Jeffery, N. (2015) 'Chapter 13: The muscles of mastication in rodents and the function of the medial pterygoid', in P.G. Cox and L. Hautier (eds) *Evolution of the Rodents: Advances in Phylogeny, Functional Morphology and Development*. Cambridge University Press (Cambridge Studies in Morphology and Molecules: New Paradigms in Evolutionary Bio, 5), pp. 350–372. Available at: https://doi.org/10.1017/CBO9781107360150.

Cox, P.G., Rayfield, E.J., Fagan, M.J., Herrel, A., Pataky, T.C. and Jeffery, N. (2012) 'Functional evolution of the feeding system in rodents', *PLOS One*, 7(4). Available at: https://doi.org/10.1371/journal.pone.0036299.

Druzinsky, R.E. (1995) 'Incisal biting in the mountain beaver (*Aplodontia rufa*) and woodchuck (*Marmota monax*)', *Journal of Morphology*, 226(1), pp. 79–101. Available at: https://doi.org/10.1002/jmor.1052260106.

Druzinsky, R.E. (2010) 'Functional anatomy of incisal biting in *Aplodontia rufa* and sciuromorph rodents – Part 1: Masticatory muscles, skull shape and digging', *Cells Tissues Organs*, 191(6), pp. 510–522. Available at: https://doi.org/10.1159/000284931.

Druzinsky, R.E. (2015) 'Chapter 12 – The oral apparatus of rodents: variations on the theme of a gnawing machine', in P.G. Cox and L. Hautier (eds) *Evolution of the Rodents: Advances in Phylogeny, Functional Morphology and Development*. Cambridge University Press (Cambridge Studies in Morphology and Molecules: New Paradigms in Evolutionary Bio, 5), pp. 323–349. Available at: https://doi.org/10.1017/CBO9781107360150.

Fabre, P., Hautier, L., Dimitrov, D. and Douzery, E.J.P. (2012) 'A glimpse on the pattern of rodent diversification: a phylogenetic approach', *BMC Evolutionary Biology*, 12(88). Available at: https://doi.org/10.1186/1471-2148-12-88.

Gambaryan, P.P. and Kielan-Jaworowska, Z. (1995) 'Masticatory musculature of Asian taeniolabidoid multituberculate mammals', *Acta Palaeontologica Polonica*, 40(1), pp. 45–108.

Grossnickle, D.M. and Polly, P.D. (2013) 'Mammal disparity decreases during the Cretaceous angiosperm radiation', *Proceedings of the Royal Society B*, 280.

Grossnickle, D.M., Smith, S.M. and Wilson, G.P. (2019) 'Untangling the Multiple Ecological Radiations of Early Mammals', *Trends in Ecology and Evolution*, 34(10), pp. 936–949. Available at: https://doi.org/10.1016/j.tree.2019.05.008.

Hopson, J.A. (1967) 'Comments on the Competitive Inferiority of the Multituberculates', *Systematic Zoology*, 16(4), pp. 352–355. Available at: https://doi.org/10.2307/2412159.

Jablonski, D. (2008) 'Biotic interactions and macroevolution: extensions and mismatches across scales and levels', *Evolution*, 62(4), pp. 715–739. Available at: https://doi.org/10.1111/j.1558-5646.2008.00317.x.

Jepsen, G.L. (1949) 'Selection, "Orthogenesis," and the Fossil Record', *Proceedings of the American Philosophical Society*, 93(6), pp. 479–500.

Kielan-Jaworowoska, Z., Presley, R. and Poplin, C. (1986) 'The cranial vascular system in taeniolabidoid multituberculate mammals', *Philosophical Transactions of the Royal Society of London. B, Biological Sciences*, 313(1164), pp. 525–602. Available at: https://doi.org/10.1098/rstb.1986.0055.

Kielan-Jaworowska, Z. (1974) 'Multituberculate succession in the Late Cretaceous of the Gobi desert (Mongolia)', *Results of the Polish-Mongolian Palaeontological Expeditions - Part V. Palaeontologia Polonica 30*, pp. 23–44.

Kielan-Jaworowska, Z., Cifelli, L.R. and Luo, Z.-X. (2004) *Mammals from the Age of Dinosaurs: Origins, Evolution, and Structure*. Columbia University Press. Available at: https://doi.org/10.7312/kiel11918.

Krause, D.W. (1986) 'Competitive exclusion and taxonomic displacement in the fossil record; the case of rodents and multituberculates in North America', *Rocky Mountain Geology*, 24(3), pp. 95–117. Available at: http://dx.doi.org/10.2113/gsrocky.24.special_paper_3.95.

Landry, S.O. (1965) 'The Status of the Theory of the Replacement of the Multituberculata by the Rodentia', *Journal of Mammalogy*, 46(2), pp. 280–286. Available at: https://doi.org/10.2307/1377848.

Matthew, W.D. (1897) 'A revision of the Puerco Fauna.', *Bulletin of the American Museum of Natural History*, 9, pp. 259–323.

McIntosh, A.F. and Cox, P.G. (2016) 'Functional implications of craniomandibular morphology in African mole-rats (Rodentia: Bathyergidae)', *Biological Journal of the Linnean Society*, 117(3), pp. 447–462. Available at: https://doi.org/10.1111/bij.12691.

McKenna, M.C. (1961) 'A Note on the Origin of Rodents', *American Museum Novitates*, 2037, pp. 1–5.

Ostrander, G., E. (1984) 'The Early Oligocene (Chadronian) Raben Ranch Local Fauna, Northwest Nebraska: Multituberculata; with Comments on the Extinction of the Allotheria', *Transactions of the Nebraska Academy of Sciences and Affiliated Societies*, 239.

Rankin, A.H., Emry, R.J. and Asher, R.J. (2020) 'Anatomical sciuromorphy in "protrogomorph" rodents', *Palaeontologia Electronica*, 23(2). Available at: https://doi.org/10.26879/1049.

Samuels, J.X. (2009) 'Cranial morphology and dietary habits of rodents', *Zoological Journal of the Linnean Society*, 156, pp. 864–888. Available at: https://doi.org/10.1111/j.1096-3642.2009.00502.x.

Scott, W.B., Jepsen, G.L. and Wood, A.E. (1937) 'The mammalian fauna of the White River Oligocene: Part II. Rodentia', *Transactions of the American Philosophical Society*, 28(2), pp. 155–269.

Simpson, G.G. (1953) *The Major Features of Evolution*. New York Chichester, West Sussex: Columbia University Press (Columbia Biological Series, 3). Available at: https://doi.org/10.7312/simp93764.

Valen, L.V. and Sloan, R.E. (1966) 'The extinction of the multituberculates', *Systematic Zoology*, 15(4), pp. 261–278.

Vander Wall, S.B. (2001) 'The Evolutionary Ecology of Nut Dispersal', *The Botanical Review*, 67(1), pp. 74–117. Available at: https://www.jstor.org/stable/4354385.

Weaver, L.N., Fulghum, H.Z., Grossnickle, D.M., Brightly, W.H., Kulik, Z.T., Wilson Mantilla, G.P. and Whitney, M.R. (2022) 'Multituberculate Mammals Show Evidence of a Life History Strategy Similar to That of Placentals, Not Marsupials', *The American Naturalist*, 200(3), pp. 383–400. Available at: https://doi.org/10.1086/720410.

Weaver, L.N. and Wilson, G.P. (2021) 'Shape disparity in the blade-like premolars of multituberculate mammals: functional constraints and the evolution of herbivory', *Journal of Mammalogy*. Edited by R. Powell, 102(4), pp. 967–985. Available at: https://doi.org/10.1093/jmammal/gyaa029.

Wilson, D.E., Lacher, T.E. and Mittermeier, R.A. (eds) (2016) *Handbook of the Mammals of the World, Volume 6: Lagomorphs and Rodents I*. Lynx Edicions (Handbook of the Mammals of the World (HMW)).

Wilson, D.E., Lacher, T.E. and Mittermeier, R.A. (eds) (2017) *Handbook of the Mammals of the World, Volume 7: Rodents II*. Lynx Edicions (Handbook of the Mammals of the World (HMW)).

Wilson, D.E. and Reeder, D.M. (2005) *Mammal Species of the World*. Baltimore: Johns Hopkins University Press.

Wilson, G.P., Evans, A.R., Corfe, I.J., Smits, P.D., Fortelius, M. and Jernvall, J. (2012) 'Adaptive radiation of multituberculate mammals before the extinction of dinosaurs', *Nature*, 483, pp. 457–460. Available at: https://doi.org/10.1038/nature10880.

Wilson, R.W. (1951) 'Evolution of the Early Tertiary Rodents', *Evolution*, 5(3), pp. 207–215. Available at: https://doi.org/10.2307/2405460.

Wood, A.E. (1955) 'A revised classification of the rodents', *Journal of Mammalogy*, 36(2), pp. 165–187. Available at: https://doi.org/10.2307/1375874.

Wood, A.E. (1962) *The early Tertiary rodents of the family Paramyidae*. American Philosophical Society (Transactions of the American Philosophical Society).

Wood, A.E. (1965) 'Grades and clades among rodents', *Society for the Study of Evolution*, 19(1), pp. 115–130. Available at: https://doi.org/10.2307/2406300.

Wood, D.J. (2010) *The Extinction of the Multituberculates Outside North America: a Global Approach to Testing the Competition Model*. MSc Thesis. The Ohio State University. Available at: http://rave.ohiolink.edu/etdc/view?acc_num=osu1275595604.

Chapter 2: Comparing rodent morphotype categories through modelling of biting with the incisors at zero degrees gape.

2.1 – Introduction

2.1.1 – Quantitative comparisons of rodent gnawing

Rodents are adapted for gnawing, with specialised anatomy and distinctive autapomorphies suited to this function (Wood, 1965; Cox *et al.*, 2012; Druzinsky, 2015). Gnawing is a specialised biting behaviour using diprotodont incisors, and it allows rodents to access foods or perform other paramasticatory functions efficiently and effectively for their body size (such as beavers felling trees, squirrels feeding on hard acorns and walnuts, or chisel-tooth digging rodents burrowing using gnawing) (Druzinsky, 1995; Vander Wall, 2001; Cox and Baverstock, 2016; McIntosh and Cox, 2016a). Traditionally, the anatomical diversity of rodents has been categorised in a number of ways, such as by 'morphotype', a category based on a set of key hard- and soft-tissue characteristics (Wood, 1965; Cox and Jeffery, 2011; Cox and Baverstock, 2016). Comparisons of the functional differences between these morphotype categories have been made in the existing literature, but have not been tested using a large sample across the tree via quantitative methods, a gap which this thesis project aims to address. Such biomechanical analyses can tease out the relationships between form and function, in this case with respect to feeding performance during gnawing, a factor in dietary adaptation (Greaves, 1985; Sakamoto, 2010; Santana, Dumont and Davis, 2010; Santana, Grosse and Dumont, 2012; Morales-García *et al.*, 2021). In this chapter, I aim to quantitatively compare the morphotypes during a simplified bite with the incisor teeth, to see if their anatomical categories are reflected in differences of functional performance in gnawing at occlusion. This is the first assessment across the tree of Rodentia in this regard, comparing taxa of

all four morphotypes by calculating and comparing the mechanical advantage of each muscle in each taxon. This study focusses on a simplified incisor bite at zero degrees of gape, to remove the potential effects of other major variables—such as gape angle and bite point—from the analyses.

2.1.2 – A brief overview of Rodentia

Rodents are the largest order of extant mammals, consisting of 2552 species, over 40% of known mammal species (Wilson and Reeder, 2005; Burgin *et al.*, 2018). Some rodent families contain few taxa, some contain hundreds (Wilson, Lacher and Mittermeier, 2016, 2017), and representative specimens from twenty-seven families are sampled in this project. This sample, and Rodentia as group, covers a huge range of habitats, some of which require additional specialised functions such as chisel-toothed digging among some fossorial rodents (Wilson, Lacher and Mittermeier, 2016, 2017). From treetops to burrows and deserts to mangroves, and from gliding, to quadrupedal, to bipedal hopping, to scratch and chisel-toothed digging, and even to semi-aquatic swimming modes of locomotion, Rodentia has living representatives across terrestrial niches on every continent on Earth (Wilson, Lacher and Mittermeier, 2016, 2017). As a group, they thrive. Although they have great diversity in species, their morphology is quite conservative (Goswami *et al.*, 2022), and rodents possess several key autapomorphies (Wood, 1955, 1965; Cox and Hautier, 2015); despite similarities to other taxa, especially their sister clade Lagomorpha, the form of these autapomorphies are often distinctive to Rodentia. Of particular importance to this study are the autapomorphies of their masticatory system. The huge dietary diversity combined with the relative anatomical conservativeness of the morphotype categories is quite surprising; with limited dietary information available, functional testing can evaluate the impact of these anatomical differences.

Among their craniomandibular hard-tissue autapomorphies, rodents have large diprotodont upper and lower incisors (Cox and Hautier, 2015) that grow continuously with a diverse range of distinctive and complex enamel

Schmelzmusters (Wahlert, 1968; Koenigswald, 1985; Wahlert and Von Koenigswald, 1985; Martin, 1993). Despite differences in the thickness and arrangement of the bands of prisms, most rodents possess a band of hard Hunter-Schreger banded enamel on the anterior face of their incisors (Wahlert, 1968; Koenigswald and Clemens, 1992), and such an arrangement of enamel prisms—even uniserial patterns in rodents that were once incorrectly assumed to be simple and uniform (Smith *et al.*, 2019)—can contribute to fracture resistance through the dissipation of tensional stresses (Koenigswald and Clemens, 1992; Vieytes, Morgan and Verzi, 2007). Together, the two adaptations of rapid growth and hard, fracture-resistant anterior enamel allow rodents to gnaw intensively and recover rapidly from wear and minor damage to the incisors; through gnawing, they can process foods that are typically difficult to feed on, while the softer enamel on the posterior face causes the incisors to be self-sharpening as the rear surface is worn away faster than the harder anterior surface (Koenigswald, 1985; Cox *et al.*, 2012). This difference in the rate of wear is a critical anatomical characteristic of their ability to gnaw (Hunt *et al.*, 2023). Unlike lagomorphs, rodents can even engage in active self-sharpening behaviours for their lower incisors, due to their highly mobile temporomandibular joint (Druzinsky, 2015). Their glenoid fossa lacks a post-glenoid process, and is shaped like a trough that extends roughly anteroposteriorly, allowing for extensive protraction and retraction of the mandible (Cox and Hautier, 2015)—when the molars are in occlusion, the incisors are often not, and vice versa (Becht, 1953; Hiiemae and Ardran, 1968; Cox and Hautier, 2015). Behind these large incisors, rodents possess a diastema and lack other incisor teeth, as well as lacking canines and some or all of the premolars; their molars, which begin posterior to this diastema (Cox and Hautier, 2015), are diverse among taxa despite the relative similarity of incisor form and function. Disparity among incisor and molar form is interconnected with their broad diversity in diet; though rodent evolution has trended towards herbivory (Samuels, 2009), taxa can also be omnivorous, insectivorous, granivorous (Wilson, Lacher and Mittermeier, 2016, 2017), and even have more specialised diets such as vermivory (Esselstyn, Achmadi and Rowe, 2012). The morphological disparity

of molar tooth crowns and the function of cheek teeth during chewing are beyond the scope of this chapter's focus on simplified gnawing at zero gape.

Across the board, the above hard-tissue autapomorphies are adaptations for or related to gnawing; their gnawing behaviour is a constraint upon their anatomy, including their soft-tissue anatomy (Druzinsky, 2015). The anatomy of their mandibular adductor musculature is of particular note, and is the focus of this study as it is a factor in the anatomical differences between morphotypes. Through homoplasy, similar muscular characteristics and differentiations of individual muscles have developed across the order, and these are typically categorised into four groupings. These four paraphyletic groupings are referred to as 'morphotypes'.

2.1.3 – Morphotypes

The categories referred to as 'morphotypes' are not just categories of soft-tissue anatomy alone, and their history is intertwined with older systems of classification in Rodentia (Wood, 1955, 1965). They are based on observations of both hard-tissue and soft-tissue, and groups are distinguished by the following criteria: the presence and size of an infraorbital foramen; the presence or absence of a zygomatic plate; and the presence or absence of specific differentiations of the masseter muscle complex (Wood, 1965; Cox and Jeffery, 2011; Cox and Hautier, 2015; Druzinsky, 2015). Combinations of traits define the four morphotype categories: protrogomorphy, hystricomorphy, sciuromorphy, and myomorphy.

The shape and size of the infraorbital foramen varies between the morphotypes. As can be seen in Figure 2.1, in hystricomorphous taxa it is expanded greatly in size. In myomorphous taxa the foramen is relatively large compared to sciuromorphs and protrogomorphs, but smaller than in hystricomorphs (Brandt, 1855; Scott, Jepsen and Wood, 1937; Wood, 1955, 1965; Cox and Jeffery, 2011, 2015). Comparatively, in sciuromorphous taxa the foramen is small compared to the proportional size of the foramen in myomorphs and hystricomorphs, and in protrogomorphous taxa it is also

typically small (Brandt, 1855; Scott, Jepsen and Wood, 1937; Wood, 1955, 1965).

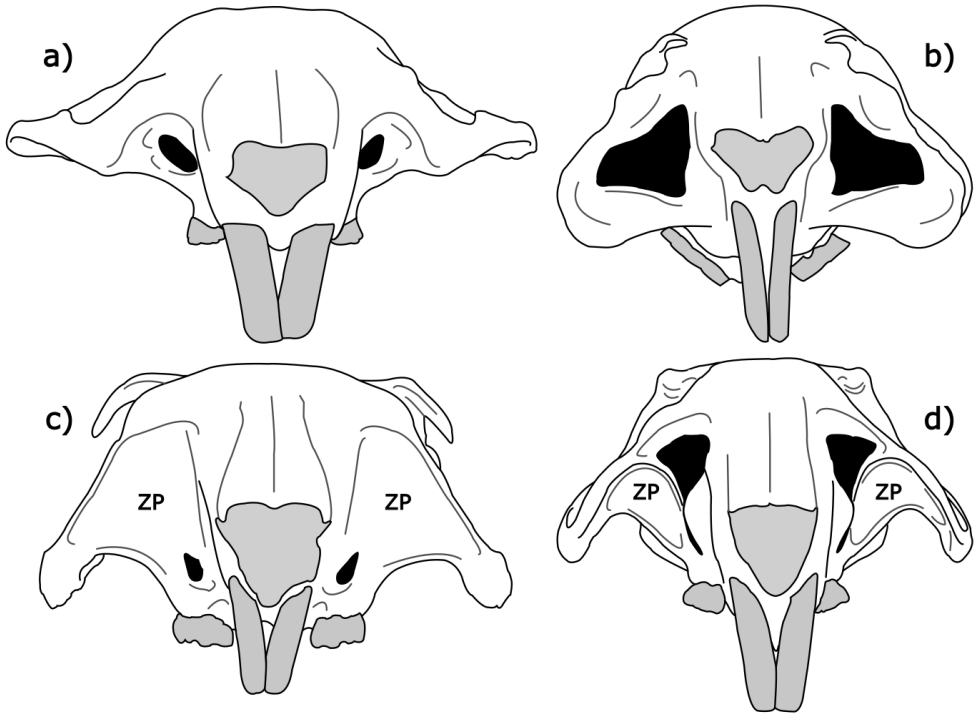

Figure 2.1: Diagrams of frontal views of a) protrogomorphy, b) hystricomorphy, c) sciuromorphy, d) myomorphy, using the four 'archetypal' taxa discussed in detail in the Results section: *Aplodontia rufa*, *Cavia porcellus*, *Sciurus carolinensis*, and *Rattus norvegicus*. The infraorbital foramena are filled in black, the teeth and nares are light grey, and the zygomatic plates (where present) are labelled ZP roughly in their centres. This figure is based on the concept and structure of an existing figure (Hautier, Cox and Lebrun, 2015), but redrawn here using the scanned specimens in this study. The panels are not to scale relative to each other.

Sciuromorphous and myomorphous taxa also possess a zygomatic plate, a feature absent in both other morphotypes (Fabre *et al.*, 2012; Cox and Hautier, 2015). The zygomatic plate is a steeply sloping large surface on the anteroventral zygomatic root, which forms the ventrolateral wall of the infraorbital foramen in myomorphs and serves as a site for muscle attachment of a portion of the masseter (Brandt, 1855; Scott, Jepsen and Wood, 1937; Wood, 1955, 1965; Cox *et al.*, 2011, 2011; Fabre *et al.*, 2012; Cox and Jeffery, 2015). In protrogomorphy, typically no portion of the masseter attaches to the rostrum (Wood, 1965). Figure 2.1 displays these four configurations; note the varying shapes of the anterior zygomatic root associated with these differences, and the larger size of the zygomatic plate in the sciuromorph than the myomorph.

Adductor muscles in mammals are roughly arranged into three groups: the temporalis, the masseter, and the pterygoids. In herbivores, the masseter tends to be enlarged, and this is particularly extreme in Rodentia with the masseter often accounting for around 70% of the masticatory muscle mass (Cox and Jeffery, 2015). One particular paper (Cox and Jeffery, 2011) provides detailed analyses of these muscle subdivisions through contrast-enhanced computed tomography, and will be referenced here as it addresses shared taxa with Figures 2.1 and 2.2. The muscle information of that paper will be presented in the following sentences.

The temporalis is typically differentiated into two portions, a medial portion originating from the lateral surface of the cranium, and a lateral portion that partially originates from the fascia overlying the medial temporalis; they respectively insert medial to and on the coronoid process. The masseter is divided into a superficial portion, a deep portion, and a zygomaticomandibularis portion. The superficial portion originates below the infraorbital foramen and inserts on the aponeuroses of the deep portion, the posterolateral surface of the angle of the mandible, and the medial surface of the angle. The deep portion can be further differentiated into two parts in many taxa, with the anterior portion originating from the zygomatic plate in myomorphs and sciuromorphs, and the posterior portion originating from the lateral and ventral surfaces of the zygomatic arch; when undivided, the deep portion originates from the ventrolateral surfaces of the zygomatic arch. Both subdivisions—or the undivided deep masseter—insert all along the masseteric ridge. In all rodents, the zygomaticomandibularis portion is formed from either two (sciuromorphs and *A. rufa*) or three (myomorphs, bathyergids, and hystricomorphs) subdivisions: the two consistent subdivisions originate from the medial surface of the zygomatic arch and insert on the lateral surfaces of the mandible; the additional third subdivision originates from the rostrum, passes posteroventrally through the expanded infraorbital foramen, and inserts ventrolateral to the first lower molar. In some taxa, the rodent masseteric complex can also include a small 'posterior masseter' near the TMJ, originating from the dorsal face of the posterior

zygomatic root and inserting on the postcondyloid process (Druzinsky, 2010; Cox and Jeffery, 2011). The two pterygoid muscles consist of one 'medial' or 'internal', and one 'lateral' or 'external' muscle (Cox and Jeffery, 2011, 2015). The internal pterygoid originates from the pterygoid fossa and inserts on the medial surface of the mandibular angle, dorsal to the insertion of the superficial masseter. The external pterygoid originates on the alisphenoid and lateral pterygoid process, and inserts on the medial condyloid process. In this study, the muscular nomenclature of Cox and Jeffery, 2011 is used, as it is consistent across taxa and these names of the muscle subdivisions are easily understood when compared with some older nomenclatures.

Figure 2.2 displays some of the morphotypes' soft-tissue differences, which will be expanded on in this Chapter's Results subsection. All morphotypes are para/polyphyletic groups that exist due to widespread homoplasy and convergent evolution, though protrogomorphy is thought to be the ancestral condition (Wood, 1965; Fabre *et al.*, 2012; Cox and Hautier, 2015; Cox, Faulkes and Bennett, 2020; Rankin, Emry and Asher, 2020). Figure 2.3 shows the distribution of morphotypes across Rodentia. Note that myomorphy and hystricomorphy both occur in Gliridae, within the squirrel-related assemblage (Fabre *et al.*, 2012; Cox and Hautier, 2015).

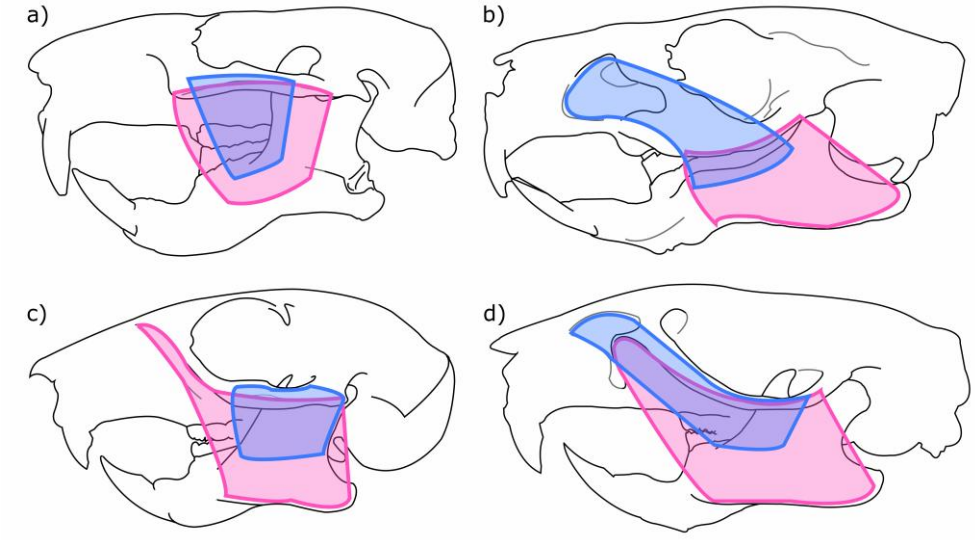

Figure 2.2: Lateral diagrams of the masseter configurations of: a) protrogomorphy, b) hystricomorphy, c) sciuromorphy, d) myomorphy. Panels c) and d) show the anterior expansion of the deep masseter (pink) onto the zygomatic plate in those morphotypes. Panels b) and d) display the anterior expansion on the zygomaticomandibularis complex (blue) through the infraorbital foramen in those morphotypes. These panels are not to scale.

Hystricomorphy and protrogomorphy both occur in Ctenohystrica, the guinea pig-related assemblage (Fabre *et al.*, 2012; Cox and Hautier, 2015). In Ctenohystrica, protrogomorphy occurs within Bathyergidae (Cox, Faulkes and Bennett, 2020), as the bathyergids have a proposed classification as protrogomorphs due to their lack of an expanded infraorbital foramen or anterior expansion of the masseter onto the rostrum, both of which partially define hystricomorphy, in opposition to their traditional classification as hystricomorphs due to their undifferentiated deep masseters (Cox, Faulkes and Bennett, 2020).

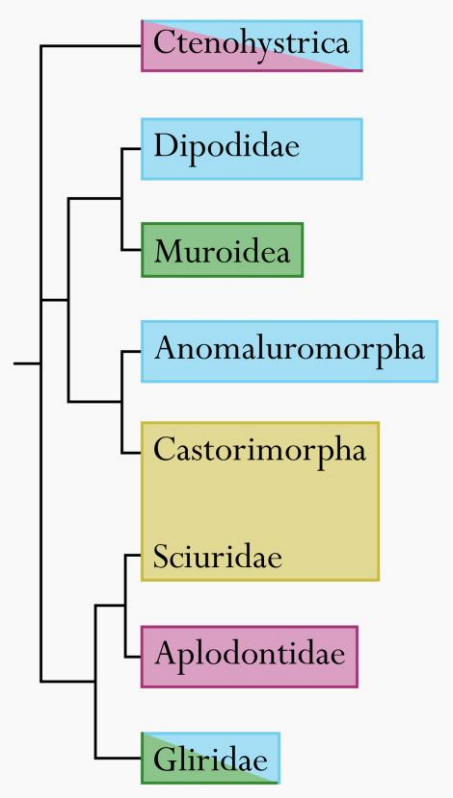

Figure 2.3: A phylogenetic tree of Rodentia which displays the morphotypes of selected clades, recoloured and updated from Hautier, Cox & Lebrun 2015, itself adapted from Fabre *et al* 2012. Hystricomorphs are highlighted in blue, myomorphs in green, protrogomorphs in pink, and sciuromorphs in yellow.

Existing comparisons of morphotypes have been primarily anatomical, although functional assertions have been made, including through estimations of bite force, and stress analysis via Finite Element Analysis (FEA) (Druzinsky, 1995; Cox and Jeffery, 2011; Cox *et al.*, 2011; Adams *et al.*, 2019). For example, it has been proposed that the anterior expansion of the deep masseter in sciuromorphs is an adaptation to favour bite force production at the incisors (Wood, 1965) to improve efficiency by around 5% (Druzinsky, 2010), while the enlarged infraorbital portion of the zygomaticomandibularis complex in hystricomorphs is an adaptation to favour bite force production at the molars (Becht, 1953) to improve efficiency by around 10–20% (Cox, Kirkham and Herrel, 2013). It has also been suggested that the infraorbital portion of the zygomaticomandibularis plays an especially notable role in making the masticatory system a second-class

lever in molar biting (Becht, 1953; Cox, 2017), adding force without significantly contributing to strain or deformation within the skull (Cox, 2017). In FEA comparisons, higher skull stresses have been calculated in sciuromorphs and myomorphs, interpreted as a trade-off with the expansion of the jaw-closing muscles to increase bite force (Adams *et al.*, 2019).

Generally, there are relatively few studies comparing the masticatory biomechanics of the different morphotype categories; most related studies have focussed on specific taxa individually or in small groups of selected taxa, as broad morphotype functional differences were not the focus of those papers. For example feeding of specific taxa *in vivo* has been studied via electromyography but these papers did not aim to make functional comparisons between the designated morphotypes; instead they evaluated masticatory mechanics and jaw movements, muscle forces throughout the chewing cycle, or the mechanical roles of specific individual muscles in particular (Hiiemae and Ardran, 1968; Weijs and Dantuma, 1975; Byrd, 1981). Individual taxa and small groups have also been studied through both physical dissection and anatomical observation of muscle scars on skulls and mandibles (Hiiemae, 1971; Satoh, 1998, 1999; Olivares, Verzi and Vassallo, 2004; Druzinsky, 2010; McIntosh and Cox, 2016a; Cox, Faulkes and Bennett, 2020) and through digital dissection and muscle identification (Cox and Jeffery, 2011; Adams *et al.*, 2019) though the majority of these analyses did not compare the morphotypes through these methods. In addition, quantitative assessment of rodent feeding has sometimes focussed on measuring or estimating bite force specifically (Nies and Ro, 2004; Freeman and Lemen, 2008). GMM has been used to compare cranial or mandibular shape between taxa of the same morphotype, and taxa of different morphotypes (Hautier *et al.*, 2008; Samuels and Valkenburgh, 2009; Gómez Cano, Hernández Fernández and Álvarez-Sierra, 2013; Hautier, Cox and Lebrun, 2015; Samuel *et al.*, 2015; Samuel, Parés-Casanova and Olopade, 2016) or for the purpose of comparing one taxon with a selection of taxa to assess its similarity to different morphotypes (Rankin, Emry and Asher, 2020).

Though functional assertions have been made about the morphotypes, comparisons have often been restricted due to sample limitations and technological limitations in earlier years; this paper is an expansion in sample scope using modern digital methods, while remaining focussed on morphotype comparisons specifically. For functional comparisons between taxa, I must select a characteristic to compare. I selected mechanical advantage.

2.1.4 – Mechanical advantage

Mechanical advantage is the ratio between the in-lever and the out-lever of a mechanical system (Hildebrand *et al.*, 1985). The in-lever is the tangent distance between the pivot and the vector of the force applied, and the out-lever is the distance between the pivot and the point where the output force is being measured. As a result, mechanical advantage is a ratio, providing an estimation of what proportion of input force is converted into output force. It can be greater than 1 if the in-lever is longer than the out-lever, but in the case of incisor biting in rodents that is not possible; the incisors meet anterior to all muscle attachments. Within the context of masticatory biomechanics, the pivot is the jaw joint, the input force vector is the muscle's line of action, and the output force occurs at the bite point. Thus, the mechanical advantage of an individual muscle provides a numerical measurement of the muscle's mechanical efficiency. It is important to note that despite the colloquial meaning of the word "advantage", I do not intend to make a value judgement; increasing mechanical advantage is a trade-off in anatomy as it is one characteristic of a broader anatomical and functional system.

Mechanical advantage can be used to compare the functional performance of specific muscles in organisms, as well as the whole masticatory system if all relevant muscles are used to calculate a resultant vector. Mechanical advantage has been applied to anatomy and functions far beyond biting, including studies of limbs and gaits (Biewener *et al.*, 2004;

Olberding *et al.*, 2019; Basu and Hutchinson, 2022) and breathing (Troyer *et al.*, 1998). Across vertebrate life it has also been used in studies of biting mechanics specifically, to compare organisms by feeding ecology or assess the interaction between form and function for known diets (Ledevin and Koyabu, 2019; Navalón *et al.*, 2019; Morales-García *et al.*, 2021), to compare biting efficiency at a particular stage of development or throughout the growth of a specific taxon (Dechow and Carlson, 1990; García-Morales *et al.*, 2003; Young, 2006; Tanner *et al.*, 2010), to assess evolutionary trends of functional morphology within a group (Santana, Grosse and Dumont, 2012; Nabavizadeh, 2016; Ma *et al.*, 2022), and to compare efficiency and function on particular teeth (Greaves, 1983, 1985; Devlin and Wastell, 1986; Sakamoto, 2010; Nabavizadeh, 2016; Echeverría *et al.*, 2017; Huby *et al.*, 2019; Kunz and Sakamoto, 2024). In rodents themselves, it has been applied to entire masticatory systems (Cox, 2017) and to individual muscles (Ball and Roth, 1995; Velhagen and Roth, 1997; Satoh, 1999; Druzinsky, 2010; Swiderski and Zelditch, 2010; Casanovas-Vilar and Van Dam, 2013; Renaud *et al.*, 2015; Cox and Baverstock, 2016; Gomes Rodrigues, Šumbera and Hautier, 2016; McIntosh and Cox, 2016a, 2016b; Cox, 2017; Echeverría *et al.*, 2017; Jones and Law, 2018; West and King, 2018; Cox *et al.*, 2020).

As yet unanswered questions can be addressed by assessing mechanical advantage, such as whether the anatomical differences between the morphotypes are reflected in the functional characteristics of individual homologous muscles. Comparing mechanical advantage among this sample is a mathematical comparison of the locations of muscle attachments relative to the jaw joint and bite point. Whereas GMM, for example, would be focussed on the shape space of the morphotypes, mechanical advantage is a measure of the mechanical efficiency of the muscles' spatial configuration; this fits this study's focus on functional comparisons of the different morphotypes during gnawing. Furthermore, rather than comparing data which are affected by factors not quantifiable in the available scans of bones (such as muscle mass, pennation, muscle fibre lengths, the organism's body size, or the skull and mandible's material properties and partitioning of stress

and strain), mechanical advantage provides a point of comparison that is relatively decoupled from these absent variables. Morphotypes mostly vary in the arrangement of their muscle attachments, and mechanical advantage directly compares the input-to-output force ratio of these arrangements.

2.1.5 – Key questions and hypotheses

As established, this chapter aims to evaluate potential functional differences between the four morphotypes during gnawing. In order to compare the functional performance of the morphotypes, I must establish and quantify the anatomy of a large sample, including those taxa which lack existing study or digitisation of their musculature. The sample in question consists of 27 extant rodents, and the muscles and morphotypes of each taxon will be identified systematically and categorised in this chapter. Once these muscles are identified, I can compare them using lever-arm mechanics, determining the mechanical advantage of each individual muscle. These calculated mechanical advantages can then be compared statistically, and I can test for differences between the morphotype categories on homologous muscles.

I will analyse two particular key questions using these data. Firstly, is there an observable difference in mechanical advantage between the four morphotypes during gnawing at zero degrees of gape? The morphotype categories are distinct in anatomy, but the quantitative data can identify whether or not the morphotypes are distinct from one another in function as well. For example, if sciuromorphs group distinctly from hystricomorphs in these data, this could fit with the existing interpretation that sciuromorphy is an optimisation for incisor bite force (Wood, 1965; Druzinsky, 2010). However, if the categories do not clearly differ, then the analysis would not support such assertions of functional difference. Rather than combining the in-levers of muscles (when certain muscle differentiations are absent in three of the four morphotypes), I will keep them separate to compare homologous muscles individually in this analysis. I hypothesise (**H1.1**) that the morphotype categories will not be distinctly different in these results, and

that the broad disparity within morphotype categories will result in their mechanical advantage ranges overlapping with those of other morphotypes. By comparing the mechanical advantages of each morphotype on each muscle using a box plot, this can be visually identified, and the group means can be compared statistically. Between anatomical disparity and the uneven sampling of morphotypes due to availability and their distribution across the tree, I expect each morphotype to show broad ranges in mechanical advantage. Since this is an examination of incisor biting, and rodents are adapted for gnawing, it would not be unsurprising if the morphotypes were similar in these analyses, being adapted for their shared function. More detailed questions can be answered with more complex analyses, and this simplified zero-gape test at a single bite point provides a foundation for expansion in Chapter 3 to assess other factors.

Secondly, is there a statistically significant phylogenetic signal in the mechanical advantage data? Morphotypes are para/polyphyletic categories (Fabre *et al.*, 2012; Cox and Hautier, 2015), but this does not necessarily preclude phylogenetic constraints from affecting the anatomy and muscular arrangement of these taxa, especially since most masticatory muscle divisions in rodents have homologous counterparts regardless of morphotype. A phylogenetic signal, if present, could affect the signal (or lack thereof) from the morphotypes. I must test it as a potential factor in the variation in mechanical advantage across the sample. I hypothesise (**H1.2**) this test will not identify a significant correlation, due to the para/polyphyletic nature of the groups and the variation and diversity within each morphotype category. If my hypothesis is correct, this may imply that morphotype categories are primarily categories of homologous anatomy and may lack functional distinction, or perhaps imply that functional morphology is being significantly affected by variables beyond morphotype category alone.

2.2 – Materials & Methods

2.2.1 – Sample information

I selected 27 rodent taxa from 20 families (Table 2.1) for this study to provide a broad sample across the tree that covers representatives of all four morphotypes, without oversampling from the most speciose families of the tree. All micro computed tomography (µCT) scans are available on MorphoSource (www.morphosource.org), and each consists of a skull and mandible (sometimes scanned together, sometimes separately) from a single individual. These µCT scans were obtained primarily from museum collections, and a complete table of specimen numbers, institutions, MorphoSource Media IDs and scanning locations is included here in Table 2.1. Where skulls and mandibles were scanned separately, their Media IDs are ordered respectively. Each taxon has a sample size of n=1 (i.e. a single scan per taxon).

These taxa are all representatives of different families or subfamilies within Rodentia. A simple cladogram of rodent clades is shown in Figure 2.4. Clade names are removed from this cladogram for clarity. Due to the difference in how many families there are that contain taxa of a selected morphotype, the sampling skews towards hystricomorphous taxa (with 14

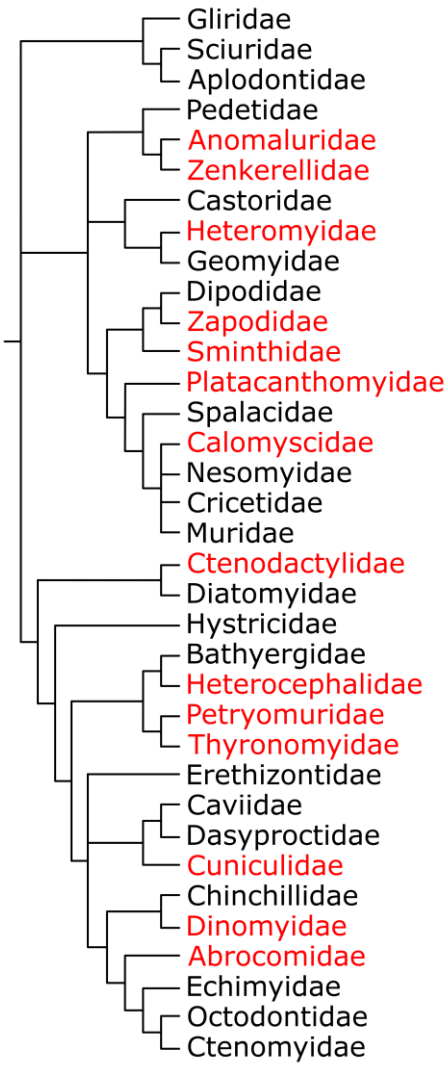

Figure 2.4: A cladogram of rodent families redrawn and simplified from a recent tree in the literature (D'Elía, Fabre and Lessa, 2019) with unrepresented families in this study marked as red text.

hystricomorphs, 6 myomorphs, 4 sciuromorphs, and 3 protrogomorphs according to the categorisations used in this project), but avoids a potential skew from oversampling individual clades.

Species	Common name	Family	From	Catalogue Number	Media ID
Graphiurus nagtglasii	Nagtglas's African dormouse	Gliridae	UMZC	E.1909	000048253 000048254
Petaurista petaurista	Giant flying squirrel	Sciuridae	UMZC	E.1475	000048251 000048252
Sciurus carolinensis	Grey squirrel	Sciuridae	Liverpool	SC11	000047051
Aplodontia rufa	Mountain beaver	Aplodontidae	MNHN	1354	000049500 000049502
Pedetes capensis	South African springhare	Pedetidae	UMZC	E.1446	000048261 000048262
Castor canadensis	Northeast American beaver	Castoridae	UMZC	E.1831	000048257 000048258
Thomomys umbrinus	Southern pocket gopher	Geomyidae	NML	19.8.98.8	000047047
Dipus sagitta	Northern three-toed jerboa	Dipodidae	UMZC	E.3165	000048259 000048260
Cannomys badius	Lesser bamboo rat	Spalacidae	UMZC	E.2850	000048804 000048469
Cricetomys gambianus	Northern giant pouched rat	Nesomyidae	UMZC	E.2262	000050458 000048467
Phyllotis gerbillus	Peruvian leaf-eared mouse	Cricetidae	UMZC	E.2597	000050454 000048468
Acomys cahirinus	Northeast African spiny mouse	Muridae	UMZC	E.2278	000048255 000048256
Gerbillus watersi	Water's gerbil	Muridae	UMZC	E.1971	000050400 000048466
Rattus norvegicus	Brown rat	Muridae	Liverpool	RN4	000047050
Laonastes aenigmamus	Laotian rock rat	Diatomyidae	Anthony Herrel	KY213	000047067
Hystrix cristata	Crested porcupine	Hystricidae	UMZC	E.3406	000048271 000048272
Bathyergus suillus	Cape dune mole-rat	Bathyergidae	NML	19.8.75.14	000046728 000046758
Georychus capensis	Cape mole-rat	Bathyergidae	NML	D.300	000046565 000046641
Erethizon dorsatum	North American porcupine	Erethizontidae	UMZC	E.3506	000048267 000048268
Cavia porcellus	Domestic guinea pig	Caviidae	Liverpool	CP3	000047035
Hydrochoerus hydrochaeris	Capybara	Caviidae	UMZC	E.3768	000048269 000048270
Dasyprocta punctata	Agouti	Dasyproctidae	UMZC	E.3621	000048265 000048266
Lagostomus maximus	Plains viscacha	Chinchillidae	UMZC	E.3555	000048273 000048274
Capromys pilorides	Desmarest's hutia	Echimyidae	UMZC	E.3371	000048263 000048264

Myocastor coypus	Coypu	Echimyidae	UMZC	E.3370	000048275 000048276
Octodon degus	Common Degu	Octodontidae	UMZC	E.3288	000047319
Ctenomys opimus	Highland tuco-tuco	Ctenomyidae	UMZC	E.3261	000050401 000048470

Table 2.1: Sample information, including their catalogue numbers and MorphoSource Media IDs. NML: World Museum at National Museums Liverpool. UZMC: University Museum of Zoology, Cambridge. MNHN: Museum National d'Histoire Naturelle, Paris.

Some families are sampled here with representatives from different subfamilies, such as Echimyidae being represented by *Myocastor coypus* from the subfamily Echimyinae, and *Capromys pilorides* from the subfamily Capromyinae. The families and subfamilies that are not represented tend to be small, typically represented by very few genera. The only families within Muroidea that are unrepresented here are Calomyscidae and Platacanthomyidae (D'Elía, Fabre and Lessa, 2019), which have only one and two extant genera respectively. In suborder Castorimorpha, only Heteromyidae is unrepresented and is the largest unrepresented family in this sample (D'Elía, Fabre and Lessa, 2019). Within Anomaluromorpha, two subfamilies are not represented: Anomaluridae, which contains two extant genera, and Zenkerellidae, which contains one extant species (D'Elía, Fabre and Lessa, 2019). Of the major families of Hystricognathi, six are not represented in this sample: Cuniculidae and Thyronomyidae, which are represented by one extant genus each, Abrocomidae, which contains two extant genera, and the monotypic extant groups Dinomyidae, Petromuridae and Heterocephalidae (D'Elía, Fabre and Lessa, 2019). One of Caviidae's three subfamilies is not represented, Dolichotinae, which contains two extant genera (D'Elía, Fabre and Lessa, 2019). In Gliridae, the subfamilies Glirinae (2 genera) and Leithinae (6 extant genera) are not represented here (Petrova et al, 2024). There are no large branches of the tree that are left completely unrepresented by this sample, and it provides multiple representatives of all morphotypes. All the specimens are well-preserved and mostly or entirely complete skulls paired with their original mandibles, with no uncertainty introduced by having to use a mandible/hemimandible from a different individual. All specimens are of adults.

2.2.2 – Segmentation and alignment

Most of the scans were of isolated bony specimens, though some were intact heads. None of the µCT scans of these specimens were contrast-enhanced; the resulting absence of identifiable muscle tissue prevents certain kinds of functional analyses that require full muscles, but lever-arm mechanics can be conducted using the areas of the attachments on the bones.

I segmented these µCT scans using Avizo version 9.2 (Thermo Fisher Scientific, Waltham, MA, USA), through a combination of thresholding and manual segmentation to isolate the bone. Because this analysis focusses on specific muscles, particularly thin bones irrelevant to these results such as nasal turbinates or sections of the orbital wall were not rigorously included in the segmentations. Once the specimens were segmented, I virtually replaced or reconstructed damaged, broken, or missing parts relevant to the study using mirroring and translation/rotation in accordance with established practice (Lautenschlager, 2016). Most commonly this was required for a snapped zygomatic arch or mandibular angle on one side of a specimen, and

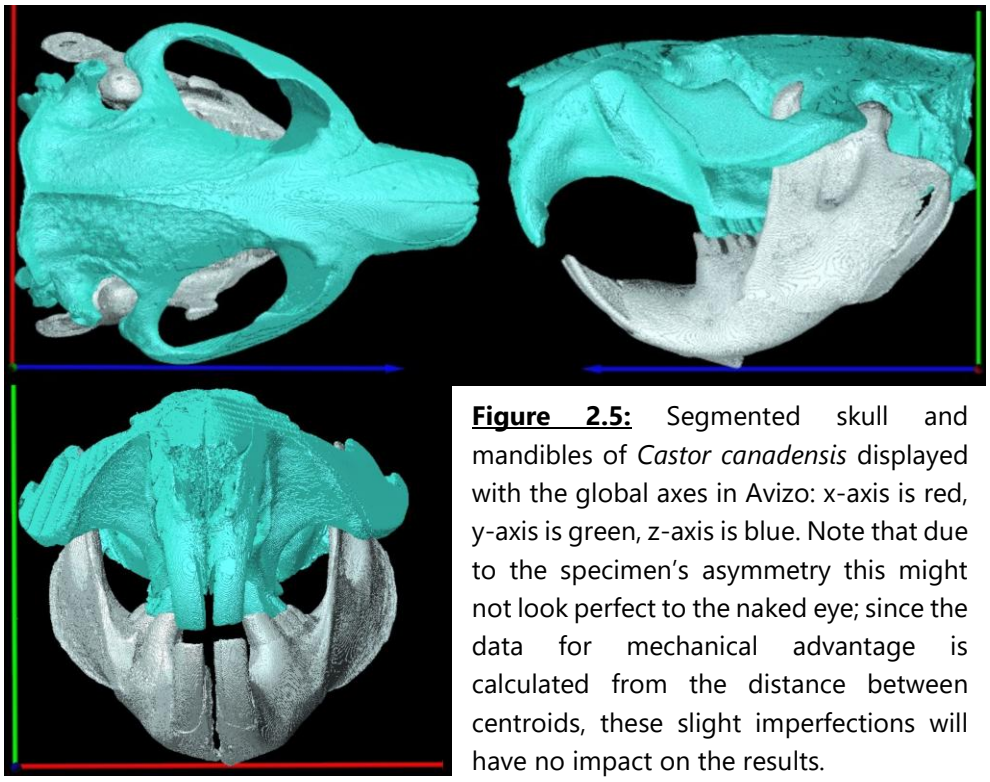

Figure 2.5: Segmented skull and mandibles of *Castor canadensis* displayed with the global axes in Avizo: x-axis is red, y-axis is green, z-axis is blue. Note that due to the specimen's asymmetry this might not look perfect to the naked eye; since the data for mechanical advantage is calculated from the distance between centroids, these slight imperfections will have no impact on the results.

in all cases the intact side was in good condition. I aligned the specimens identically for consistency: in these segmented surface files, the most lateral point on the right zygomatic arch is aligned with the yz-plane, the posterior extent of the cranium is aligned with the xy-plane, and the mandible is positioned with the condyle articulated and the molar cheek teeth at occlusion, with the specimen being positioned in the y-dimension so that the lowest point of the body of the mandible was aligned with the xz-plane. This is displayed in Figure 2.5.

In some specimens, mandibles were still in articulation when scanned, in others they were separate, but even in cases with articulated mandibles I still adjusted the articulation where necessary to ensure alignment of the mandible and skull at molar occlusion.

2.2.3 – Muscle identification and mapping

Across the sample, some taxa have far more existing papers on their musculature and feeding than others. A selection of existing citations is contained in Table 2.2. Some taxa lacked detailed papers on musculature during the time of this study.

Species	**Citations**
A. cahirinus	
A. rufa	Druzinsky, 1995, 2010; Samuels, 2009
B. suilllus	Samuels, 2009; McIntosh and Cox, 2016a, 2016b; Cox, Faulkes and Bennett, 2020
C. badius	
C. pilorides	Woods and Howland, 1979
C. canadensis	Samuels, 2009; Cox and Baverstock, 2016
C. porcellus	Woods, 1972; Byrd, 1981; Cox and Jeffery, 2011
C. gambianus	
C. opimus	Woods, 1972; Olivares, Verzi and Vassallo, 2004; Becerra, Casinos and Vassallo, 2013; Álvarez, Perez and Verzi, 2013; Echeverría *et al.*, 2017
D. punctata	Windle, 1897; Woods, 1972; Álvarez, Perez and Verzi, 2013; Álvarez and Pérez, 2019
D. sagitta	
E. dorsatum	Woods, 1972; Samuels, 2009
G. capensis	McIntosh and Cox, 2016a, 2016b; Cox, Faulkes and Bennett, 2020

G. watersi	
G. nagtglasii	Maier, Klingler and Ruf, 2002
H. hydrochaeris	Woods, 1972; Samuels, 2009; Álvarez, Perez and Verzi, 2013
H. cristata	Toldt, 1905; Turnbull, 1970; Morris, Cox and Cobb, 2022
L. maximus	
L. aenigmamus	Cox, Kirkham and Herrel, 2013
M. coypus	Woods, 1972; Woods and Howland, 1979
O. degus	Woods, 1972; Olivares, Verzi and Vassallo, 2004
P. capensis	Woods, 1972; Cox, 2017
P. petaurista	
P. gerbillus	
R. norvegicus	Moore, 1967; Turnbull, 1970; Hiiemae, 1971; Weijs, 1973; Maier, Klingler and Ruf, 2002; Samuels, 2009; Cox and Jeffery, 2011
S. carolinensis	Ball and Roth, 1995; Cox and Jeffery, 2011
T. umbrinus	Wahlert, 1985

Table 2.2: Citations regarding muscle attachment information in the sample, where present. These papers either focussed on or tangentially involved the identified muscle attachments of these taxa in their analyses.

Due to the inconsistency of available information during data gathering, I initially mapped the muscles of these specimens without reading existing identifications of muscles in these taxa. If existing material had been referenced during the initial mapping, it would have biased the method. I visually identified the muscle attachments based on the surface topography of the bones. I selected four taxa (one of each morphotype category, *A. rufa*, *C. porcellus*, *R. norvegicus*, *S. carolinensis*) with relatively extensive existing literature to be the first to be mapped, and then identified and mapped the muscles; I compared these to the literature to note differences before moving on to the rest of the sample, which included taxa that lacked such physical or digital dissections. I used these four 'archetypal' taxa as my baseline for comparison when mapping other taxa and identifying homologous muscles. The visual identification of muscles was conducted with as few preconceptions as possible; for example, I did expect *Hystrix cristata* to be identified as a hystricomorph, but I conducted comparisons with existing literature post-hoc, to identify areas where the muscles in this paper may differ from established literature where soft-tissue was available. This may result in some uncertainties or conflicts with existing research, such as interpreting *Graphiurus nagtglasii* with a potential posterior masseter based

on the topography of the bones when the limited existing literature does not discuss such a muscle in this taxon.

I identified the muscle attachments on the skulls and mandibles for the masseter subdivisions, the temporalis, and the pterygoids and mapped them in Avizo. I marked the edges of each attachment using a B-spline, to produce a clear visual outline of the shape on the surface. Then, I used the Surface Editor to manually select the surface triangles of the muscle attachment, and exported each attachment as a .stl file. An example of these mapped surfaces is shown in Figure 2.6. I imported the stl files into Blender (www.blender.org), and identified and recorded the coordinates of the centre of each surface; these coordinates are the muscle centroids used for the lever-arm mechanics.

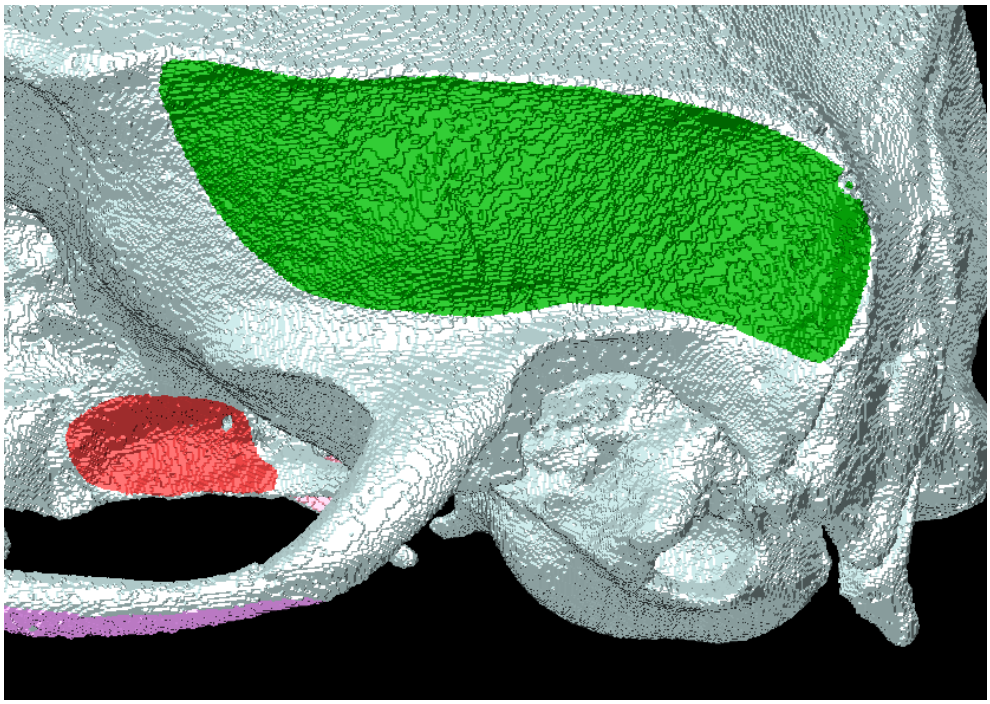

Figure 2.6: Mapped muscle attachments in the skull of *R. norvegicus*, with the view centring on the Temporalis origin (green). From this angle, the Posterior Deep Masseter origin (pink) can be observed on the lateral face of the zygomatic arch, and the External Pterygoid (red) origin is visible on the alisphenoid.

2.2.4 – Lever-arm mechanics analyses

Qualitative visual comparison alone cannot differentiate the functional significance of minor anatomical differences between individuals

or groups, especially given the number of taxa and muscles being compared. Quantitative analyses can compare them more clearly and 2D lever-arm mechanics, specifically, can evaluate the functional performance of each muscle. 2D lever-arm mechanical methods can lead to inaccuracies when estimating bite force (Davis *et al.*, 2010; Greaves, 2012), which is a limitation of this study. The calculation of mechanical advantage is here being used to compare the functional variation of these muscle attachments in two dimensions, and the simplification of removing the mediolateral component of the muscle vectors causes the study to focus on the anteroposterior and dorsoventral components of the muscle configuration.

In addition to the extraction of centroid coordinates of the mapped muscle attachments (as outlined earlier in subheading 2.2.3) I landmarked the TMJ using two landmarks on each side (one on the mandible, one on the skull). I also landmarked the tips of the upper and lower incisors, so their coordinates could be averaged to represent the bite point. Wear or damage to the tooth tips could be a potential source of error.

Since the lever-arm mechanics conducted in this chapter are of an incisor bite, but mandibles were aligned at molar occlusion, the muscle insertions and condyle had to be translated accordingly to simulate an incisor bite. I used the landmarks to do this with a simple translation and rotation of their coordinates, rather than manual translation of the bones in Avizo; potentially, this could lead to an inaccurate configuration with overlapping tooth volumes of the molars. Due to the alignment of the specimens, the two axes of these analyses are the z-axis (anteroposterior) and the y-axis (dorsoventral). To conduct the analysis in 2D, the mediolateral axis (x-axis) was ignored; due to the consistent alignment of specimens during segmentation, this could be achieved by simply not using x-coordinates in the calculations.

I translated the landmark coordinates of the TMJ and all muscle insertion centroid coordinates anteriorly by the z-distance between the upper and lower incisor landmarks, shown in Equation (1), where z_1 is the z-axis coordinate of the upper incisor tip once the left and right landmarks are

averaged, and z_0 is the averaged lower incisor tip at molar occlusion. However, protraction of the mandible in rodents is a process with a vertical/rotation component individual to each taxon, due to the shape of their incisors, jaw joint, rostrum and mandibles; this can be clearly observed by examining any of the rodents studied in this sample and shown in lateral view figures in the results. To account for this, I applied a rotation to the muscle insertion centroid coordinates, rotating them by an angle that caused y-displacement equal to the distance between the y-coordinates of the upper and lower incisor landmarks—this effectively translates and rotates the mandible into incisor occlusion at a gape of zero degrees at the incisors, though it does not account for the small vertical displacement of the TMJ during protraction. I calculated the rotation required for each taxon using Pythagoras' theorem in Equations (2.1–2.3) and the law of cosines in Equation (2.4). In Equations (2.1–2.3) z_1 is the z-coordinate of the upper incisor landmark, z_0 is the lower incisor landmark, z_c is the TMJ, and y_1, y_0, and y_c are the y-coordinates of the upper incisor, lower incisor and TMJ landmarks respectively. In Equation (2.4), θ is the angle of rotation applied to simulate incisor occlusion.

$$Mandible\ Protraction\ Distance = z_1 - z_0 \quad (1)$$

$$a = \sqrt{(z_1 - z_0)^2 + (y_1 - y_0)^2} \quad (2.1)$$

$$b = \sqrt{(z_c - z_1)^2 + (y_c - y_1)^2} \quad (2.2)$$

$$c = \sqrt{(z_c - z_0)^2 + (y_c - y_0)^2} \quad (2.3)$$

$$\theta = \cos^{-1}\left(\frac{b^2 + c^2 - a^2}{2bc}\right) \quad (2.4)$$

$$z_x = (z_\alpha - z_c)\cos\theta - (y_\alpha - y_c)\sin\theta + z_c \quad (3.1)$$

$$y_x = (z_\alpha - z_c)\sin\theta - (y_\alpha - y_c)\cos\theta + y_c \quad (3.2)$$

Once this angle and protraction distance had been calculated, I applied them to the muscle insertion z- and y-coordinates to translate the muscle insertions into a simulation of incisor occlusion. This was conducted using Equations (3.1) and (3.2), where z_χ and y_χ represent the calculated coordinates of a muscle insertion centroid at incisor biting, z_α and y_α are the

coordinates of the centroid prior to its translation, z_c and y_c are the coordinates of the TMJ which functions as the centre of rotation, and θ remains the rotation applied to simulate the occlusion of the incisor tips.

With the specimens mapped, landmarked, aligned, and at simulated incisor occlusion, a 2D lever-arm mechanics calculation could be conducted. I averaged the left- and right-side muscle centroid coordinates, as selecting only one side of centroids could result in the data being affected slightly by asymmetry. The in-lever (the perpendicular distance between the muscle vector and the TMJ) of each muscle was calculated using Equation (4), where z_i and y_i are the z- and y-coordinates of a muscle insertion and z_o and y_o are the coordinates of that muscle's origin. The out-lever is the vector between the TMJ and the bite point, in this case the landmarks of the tip of the lower incisor, and was calculated using Equation (5), where z_b and y_b represent the averaged z- and y-coordinates of the landmarks for the upper and lower incisor tips. Mechanical advantage was calculated for each muscle using Equation (6), dividing the in-lever by the out-lever. All of these calculations were performed systematically in Microsoft Excel (Microsoft Corporation) and the spreadsheets are included in the supplementary material. For incisor biting, the masticatory system will function as a third-class lever, as the force is applied between the pivot (the TMJ) and the load (the bite at the incisor tips). Figure 2.7 illustrates these equations in *R. norvegicus*.

$$In\ lever = \frac{|(z_i - z_o)(y_o - y_c) - (z_o - z_c)(y_i - y_o)|}{\sqrt{(z_i - z_o)^2 + (y_i - y_o)^2}} \quad (4)$$

$$Out\ lever = (((y_b - y_c)^2) + ((z_b - z_c)^2))^{0.5} \quad (5)$$

$$Mechanical\ Advantage = \frac{In\ lever}{Out\ lever} \quad (6)$$

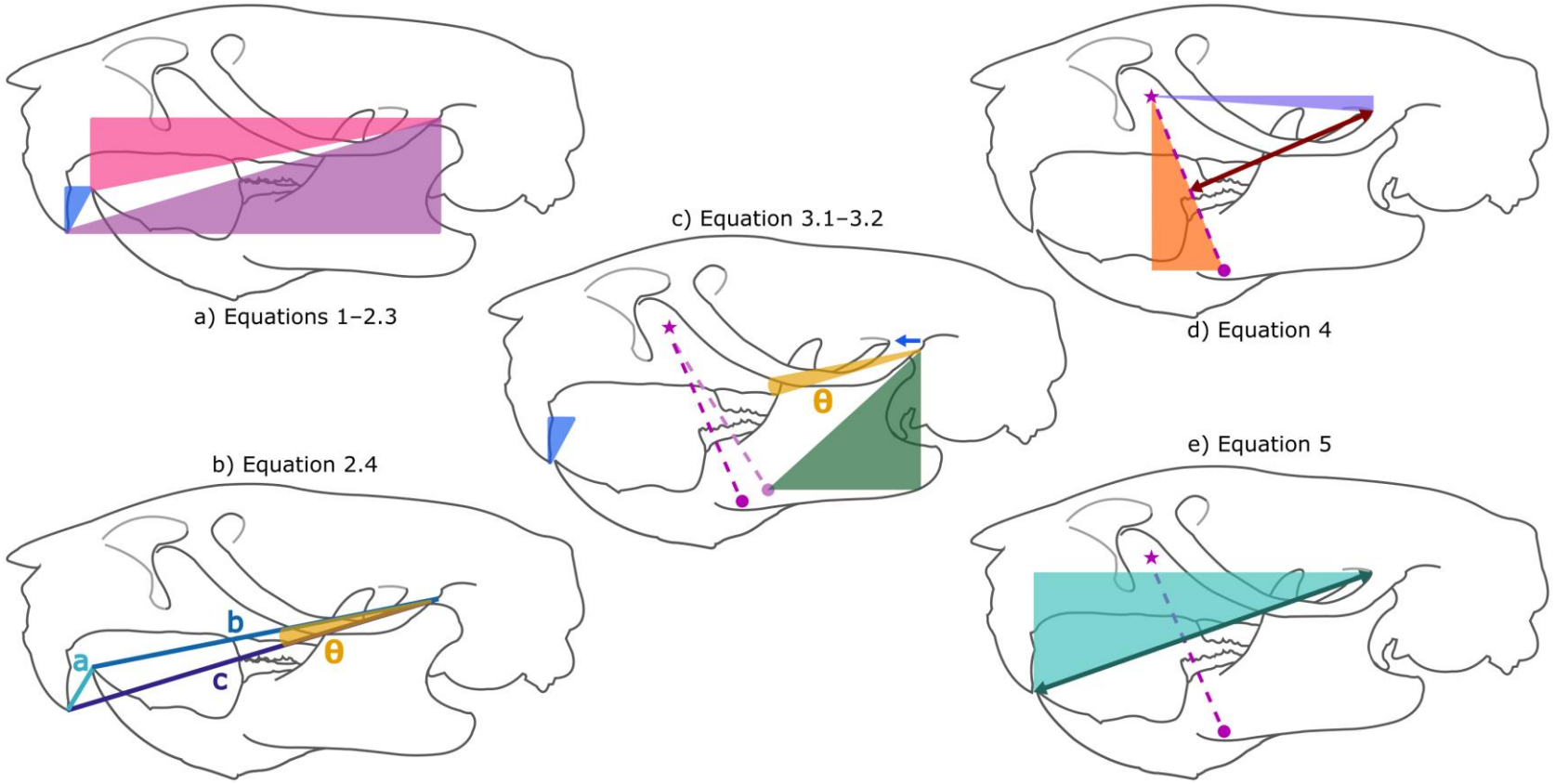

Figure 2.7: *R. norvegicus* in lateral view, approximately illustrating the equations: **a)** shows the calculation of lengths *a, b,* and *c*; **b)** shows how angle theta is calculated for the scalene triangle defined by *a, b, c*; **c)** shows the protraction and rotation of the lower jaw to define the new Anterior Deep Masseter (purple) insertion centroid position; **d)** shows the calculation of the in-lever; **e)** shows the calculation of the incisor out-lever. This figure is not strictly to scale.

2.2.5 – Statistical analysis

The results of these lever-arm mechanics analyses were then statistically analysed using a phylANOVA (Garland *et al.*, 1993) and test for Blomberg's K (Blomberg, Garland and Ives, 2003) in RStudio (RStudio Team (2022) 'RStudio: Integrated Development for R'. Boston, MA: RStudio. Available at: http://www.rstudio.com/). The phylANOVA is a multivariate analysis of variance that assesses the differences between groups within a phylogenetic framework, by testing the significance of the difference between the means of pre-defined groups (in this case, the rodent morphotypes). The simultaneous test for Blomberg's K identifies the strength of the phylogenetic signal within the data. These tests do not assume a normal distribution, and can be conducted on a dataset with one input variable—in this case, the input variable is the calculated mechanical advantages of an individual homologous muscle. Conducting this analysis requires the following packages when using RStudio: 'ape' (Paradis and Schliep, 2019), 'geiger' (Pennell *et al.*, 2014), 'nlme' (Pinheiro, Bates, and R Core Team, 2022) and 'phytools' (Revell, 2012).

An individual phylANOVA had to be performed for each muscle, and the code was written accordingly. I used an existing phylogenetic tree of Euarchontoglires (Morris, Cobb and Cox, 2018) with the taxa absent in my analyses removed. Taxa were dropped from the tree using the 'drop.tips' function if they lacked the muscle subdivision being analysed. I assigned all taxa in each analysis to their morphotype. I ran the phylANOVA using the muscle as the trait and the morphotypes as the groups to be compared, with the number of simulations (nsim) set at 1000. The test of Blomberg's K was conducted simultaneously. The code used, input files, and tree file are included in the thesis's supplementary material.

If the group means are significantly different according to the phylANOVA, then these data would imply that morphotypes are functionally distinct in terms of mechanical advantage during gnawing, and identify which homologous muscle or muscles in question are or are not significantly different. Altogether, from the muscle mapping and other landmarking to

this statistical test, these methods can address the hypotheses and key questions of this chapter. Performing this analysis for an incisor bite and only a gape of zero provides the simplest analysis; the effect of gape or different bite points is not considered, and an incisor bite was selected due to rodents' adaptation for gnawing with their incisors. The only variable analysed in these tests are the lever-arms, which are affected by shape.

2.3 – Results

2.3.1 – Archetypal taxa

2.3.1.1 – Protrogomorph: *Aplodontia rufa* (Mountain Beaver)

A. rufa (Aplodontidae) was the first protrogomorphous taxon to be muscle mapped in this study, and the other protrogomorphous taxa in the sample will be compared to it. *A. rufa* was selected because the other taxa assigned as protrogomorphous in this sample (*B. suillus* and *G. capensis*) have disputed classifications and complications in their proposed derived protrogomorphy (such as possessing an undifferentiated **Deep Masseter (DM)**) (Cox, Faulkes and Bennett, 2020). As such, protrogomorphy is the least strictly defined category in this sample, with the fewest extant representatives.

According to existing research, *A. rufa* possesses a masseter divided into four portions, two of which are further subdivided into two portions each (Druzinsky, 2010). I used visual examination of the skull and mandible to identify and map muscle attachment sites on this specimen, then this was compared with the existing literature; there are no differences between the muscle subdivisions identified in my analysis and the literature (Druzinsky, 1995, 2010). Figures 2.8, 2.9, and 2.10 show the attachment sites and rough illustrative muscle shapes of all four archetypal taxa in lateral view. The figure captions are shown together after the full-page panel figures, to allow the figures themselves to be displayed at the largest possible size. The names of muscles in the main text will use bold coloured text to aid in interpreting the diagrams and to avoid potential confusion of muscles with similar names or acronyms in the text. Due to the lack of a Suprazygomatic Temporalis (**ZT**) in other studied taxa, and a lack of a Posterior Masseter (**PM**) identified during this study in all but *G. nagtglasii*, these muscles were not included in the lever-arm mechanics analyses and are not displayed on the Figures. Like all rodents, *A. rufa* possesses a **Superficial Masseter (SM)**, a deep masseter complex, a zygomaticomandibularis masseter (ZM) complex, a differentiated

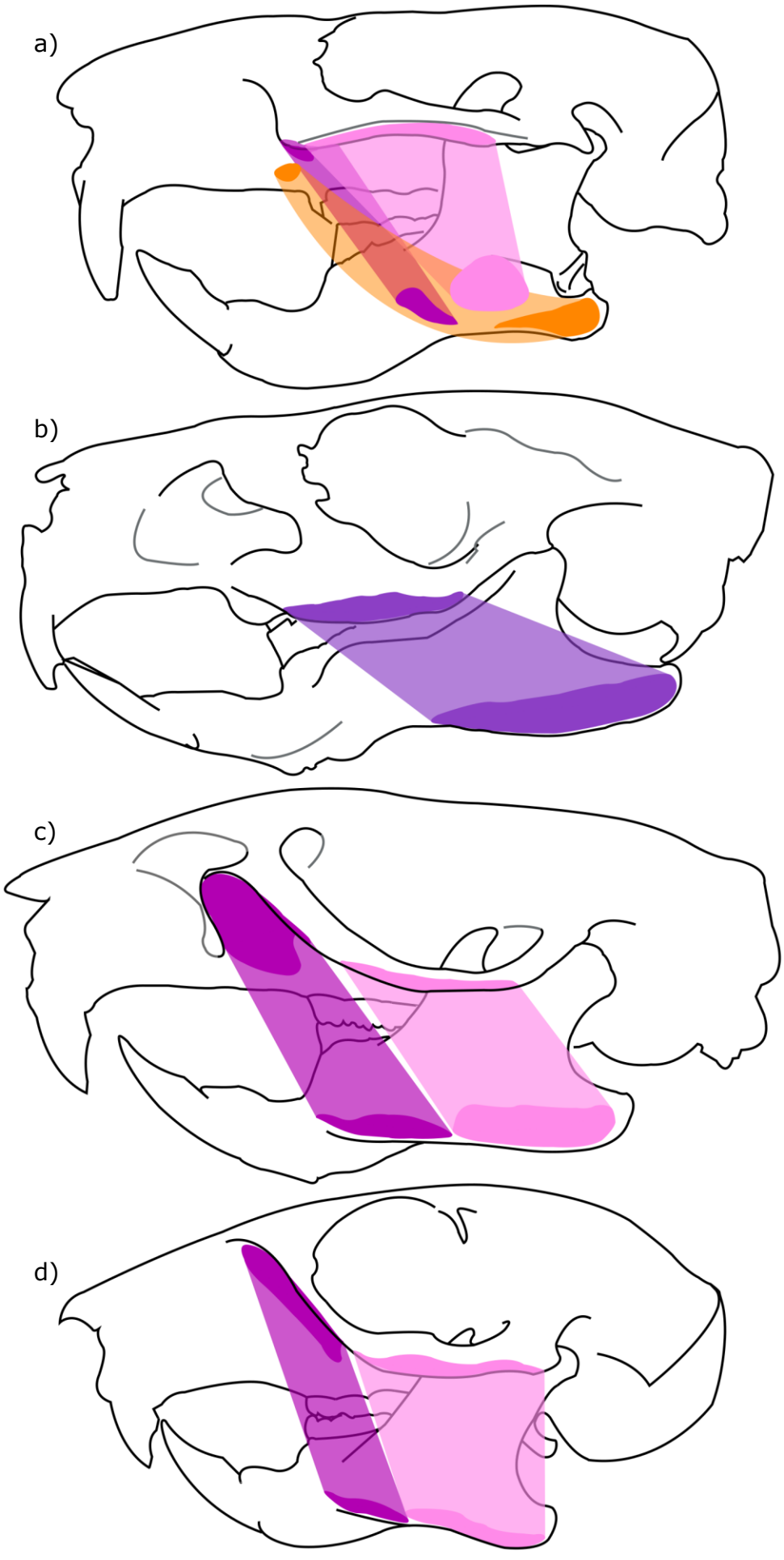
a)
b)
c)
d)

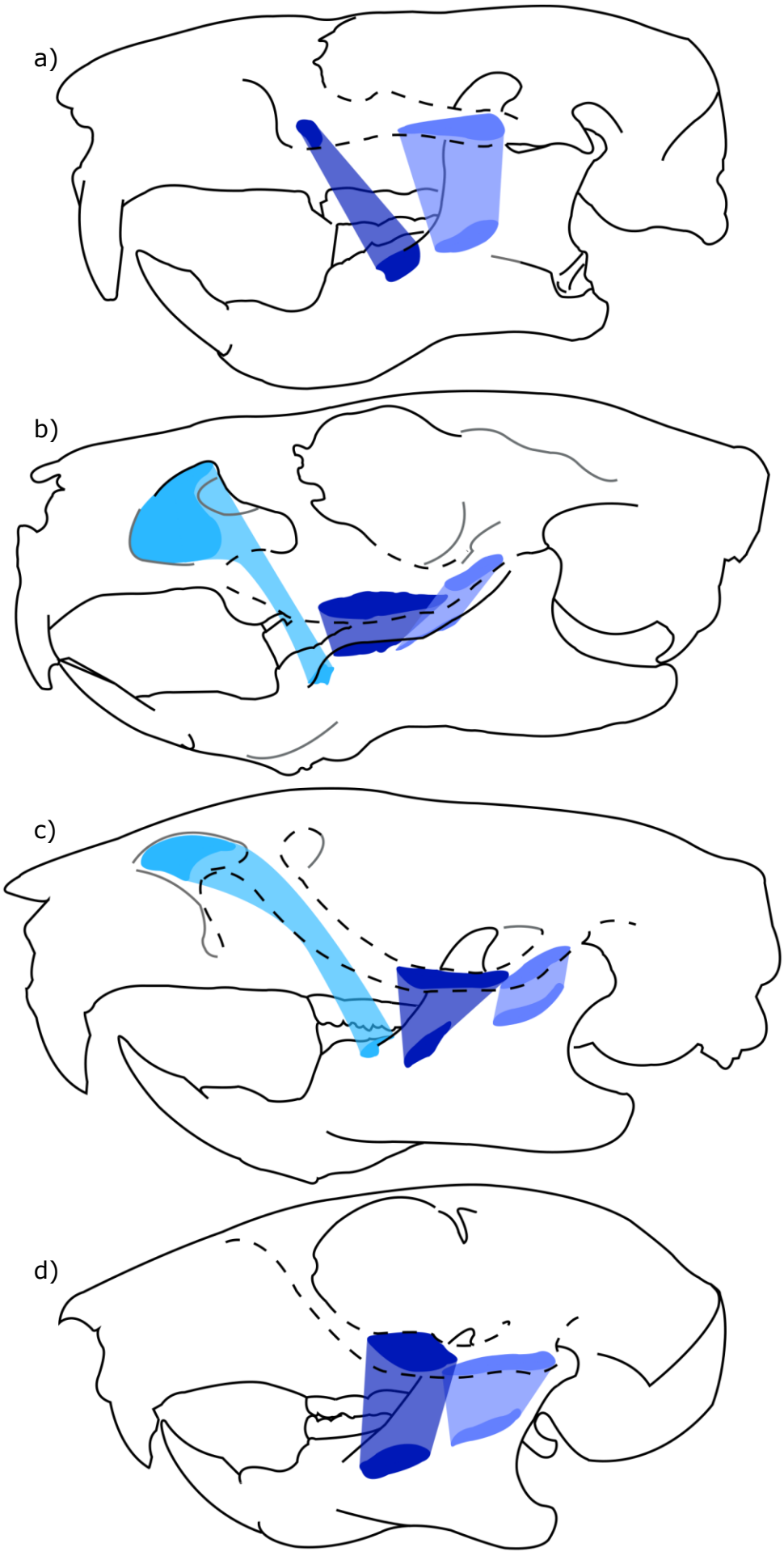
a)
b)
c)
d)

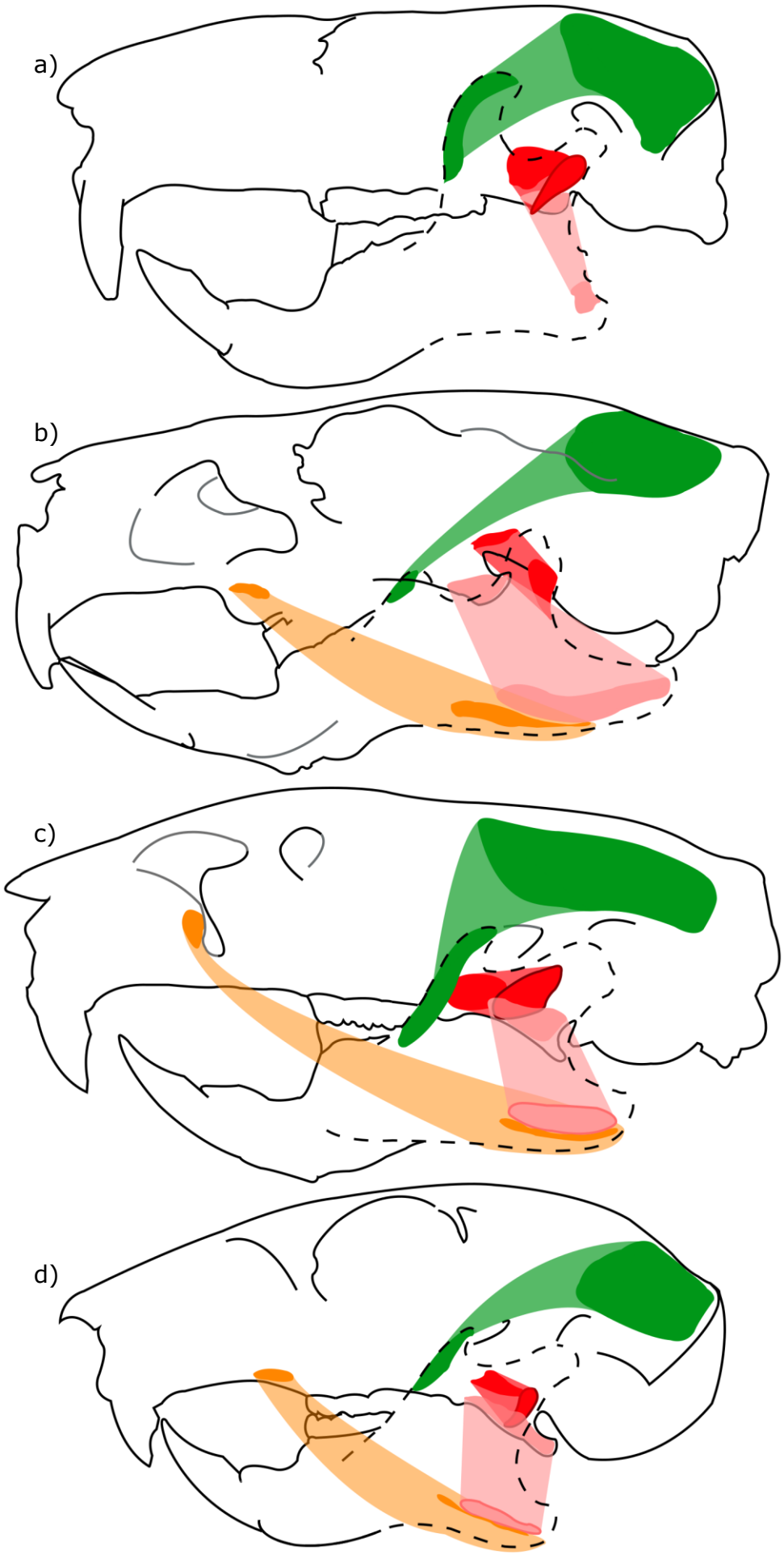
a)
b)
c)
d)

Figure 2.8: Mapped muscle attachment sites for the **ADM**, **PDM**, and **DM** in a) *A. rufa*., b) *C. porcellus*, c) *R. norvegicus*, d) *S. carolinensis*. The panels are not to scale relative to each other. All such figures in this study use the same colour key for representing muscles, and match those of the text. Approximate illustrative muscle shapes are shown as translucent layers, showing the rough path muscles take from origin to insertion. In *A. rufa*, the **SM** is also in this figure, as it inserts on the ventrolateral surface of the mandible with no *pars reflexa*. All of these images are traced over lateral screenshots of the 3D models in Avizo, simplified for clarity of presentation.

Figure 2.9: Mapped muscle attachment sites for the **IOZM**, **AZM**, and **PZM** in a) *A. rufa*., b) *C. porcellus*, c) *R. norvegicus*, d) *S. carolinensis*. The panels are not to scale relative to each other. Dashed outlines are used to indicate that an attachment is on the medial surface of a bone, in this case, primarily the zygomatic arch.

Figure 2.10: Mapped muscle attachment sites for the **SM**, **T**, **EP**, and **IP** in a) *A. rufa*., b) *C. porcellus*, c) *R. norvegicus*, d) *S. carolinensis*. The panels are not to scale relative to each other. Dashed outlines are used to indicate that an attachment is on the medial surface of a bone, in this case, the mandible. The zygomatic arch is removed from this figure, to fully expose the mandible. The **SM** is shown in panels b), c), and d) as the *pars reflexa* was the most identifiable attachment surface of the muscle, and was mapped.

Temporalis (T), and two pterygoid muscles: an **Internal Pterygoid (IP)** and an **External Pterygoid (EP)** (Druzinsky, 2010; Cox and Jeffery, 2011).

In *A. rufa*, I interpret the deep masseter as being differentiated into two portions: an **Anterior Deep Masseter (ADM)**, and a **Posterior Deep Masseter (PDM)**, an interpretation in agreement with existing study despite the difference in nomenclature (Druzinsky, 2010). I identified the ZM complex as being differentiated into two portions as well: the **Anterior Zygomaticomandibularis (AZM)** and **Posterior Zygomaticomandibularis (PZM)**. This also agrees with the literature (Druzinsky, 2010). The **SM** is here interpreted as originating from the maxilla, on the ventral surface of the anterior zygomatic root. This origin is anterior and dorsal to the upper cheek teeth, and medial and ventral to the inferred attachment of the **ADM**. There is no notable tubercle or other structure associated with this origin in *A. rufa* that I can identify, as is sometimes present in other rodents. The **SM** has no *pars reflexa* in this taxon that I am able to identify (which most rodents are

here identified to possess) and instead is mapped as inserting in a prominent fossa on the lateral surface of the angle of the mandible; the angle of *A. rufa*'s mandible possesses a prominent lateral protrusion, and the **SM** is interpreted here as inserting on the ventral surface of this protrusion. These interpretations of the **SM** mostly align with established reconstructions (Druzinsky, 2010), one notable difference will be discussed once the **IP** origin has been discussed.

The **ADM** and **PDM** originate from the ventrolateral surface of the zygomatic arch and insert on the lateral face of the body of the mandible. The **ADM** originates anteriorly on the zygomatic arch, from a distinct fossa on the most anterior region of the zygomatic root's ventral surface. The **ADM** was interpreted as inserting in a fossa dorsal to the anterior end of the masseteric line, a distinct ridge and topographic change on the body of the mandible. The **PDM** originates on the ventrolateral surface of the zygomatic arch itself, posterolateral to the origin of the **ADM**. Whereas the **ADM**'s origin is roughly rounded, the **PDM**'s origin is elongate and bordered on its medial margin by the prominent ridge that forms the ventral edge of the zygomatic arch. The **PDM**'s origin extends anteriorly to the attachment of the **ADM**, and posteriorly to a distinct change in the shape of the ventral zygomatic arch, approximately level anteroposteriorly with the coronoid process. The **PDM** inserts posteriorly to the **ADM**, but the margins of its insertion are less clearly defined, as is often the case in this sample. These interpretations are in agreement with the literature, and are not novel (Druzinsky, 2010).

The ZM complex is divided into two portions in *A. rufa*, both in the literature (Druzinsky, 2010) and in this study's identification. In all taxa in the sample, this muscle is differentiated into either two (anterior or posterior) or three portions (anterior, posterior and infraorbital). In *A. rufa*, I identify the **AZM** and **PZM** as originating from the medial surface of the zygomatic arch, posterior to the anterior root, and anterior to the TMJ; this is in agreement with the literature (Druzinsky, 2010). The **AZM**'s origin is interpreted as being on the medial surface of the zygomatic root (Druzinsky, 2010), and is here identified as occurring lateral to the bulk of the root itself; this region of bone

is curved and slopes slightly, and is visually distinct from the surrounding bone when the zygomatic arch is viewed medially. The inflection in the surface of the bone from the root to the arch is quite clear, and here suggested to mark the posterolateral extent of this origin. I identified the **PZM** as originating posteriorly to this, on an elongate fossa on the medial surface of the zygomatic arch, in agreement with existing study (Druzinsky, 2010). The relative smoothness of the lateral face of the body of the mandible and coronoid process makes clear identification of the insertions of both the **AZM** and **PZM** difficult based on bones alone; however, there is a visual change in topography identifying faint attachment sites at the base of the coronoid process, anteromedial to the lateral protrusion on the mandible's angle. As in the case of the deep masseter's portions, the **AZM**'s insertion was easier to identify than the **PZM**'s. I interpreted the **AZM** as inserting dorsal to the **ADM**, on a rough patch anterior to the attachment of the coronoid process. The **PZM**'s insertion was mapped posteriorly to this, on a shallow fossa on the lateral face of the base of the coronoid process. Both of these insertions fit with established study (Druzinsky, 2010).

The **PM** originates posterior to the **PDM** and **PZM** (Druzinsky, 2010). Here, this was identified as a narrow fossa on the ventrolateral surface of the posterior zygomatic arch, lateral to the TMJ; on most taxa, such a clear attachment was absent, hence it not being identified in most taxa in this sample. I interpreted it as inserting on the lateral face of the mandible, anteroventral to the condylar process, and dorsal to the lateral protrusion on the angle. Both its origin and insertion as interpreted here match with the existing study (Druzinsky, 2010), though I chose not to illustrate such an infrequently occurring muscle on the figures.

The **T** in all taxa is differentiated into at least two portions, the medial and lateral temporalis; the lateral temporalis originates largely from the fascia of the medial temporalis, making accurate separation of their origins impossible (Cox and Jeffery, 2011, 2015). As a result, both portions are here represented using a singular **T** attachment, one origin and one insertion. I identify this origin in *A. rufa* as on the dorsal cranium, primarily from the

parietal bone, with its posterior margin delineated by a prominent nuchal crest. On each side, there is a ridge lateral to the sagittal midline, the superior temporal line, which marks the medial extent of the origin. The origin's anterolateral margin is unclear due to the shape of the skull, but its anterior extent is here interpreted as reaching no further than the end of each medial edge of the origin. This muscle passes through the posterior region of the orbit, curving to insert on the coronoid process itself, and was mapped on the superior and anterior surfaces of the coronoid process, based on the surface topography of this region. Although the existing study uses dissection and can discuss the separated subdivisions of the temporalis, my interpretations here align with the existing identification of the medial temporalis (Druzinsky, 2010). *A. rufa* also possesses a **ZT** (Druzinsky, 2010), here identified as originating from the dorsal surface of squamosal at the posterior zygomatic root, and curving around the medial surface of the zygomatic arch to an interpreted insertion on a fossa anterior to the insertion of the **PM**; this fossa is on the lateral surface of the coronoid process, near its base. Once again, the **ZT** interpretations agree with the literature, but with no **ZT** being observed in the other taxa, this subdivision is not part of the figures, nor the analyses to come.

All rodent taxa possess two pterygoid muscles: **IP** and **EP**. The **IP** originates from the medial pterygoid plate (Druzinsky, 2010), as in all taxa in this sample and inserts on the medial face of the angle of the mandible (Druzinsky, 2010). I identified the **EP** as inserting on the medial surface of the condylar process, ventral to the condyle, in agreement with the literature (Druzinsky, 2010).

In *A. rufa*, I identified the **EP** as originating from the alisphenoid/squamosal, on the anteroventral surface of the posterior zygomatic root, medial to the TMJ; this is aligned with the existing study (Druzinsky, 2010) but the attachment of this particular muscle is interpreted in this study to vary among Rodentia based on the topography of the bones. Rather than discussing multiple taxa as examples before introducing them and their anatomy or comparing with the literature, this interpretation is later

displayed in Figure 2.35 in the Discussion section, where this subject is discussed in detail under subheading '2.4.2 – Pterygoid configurations'. In some taxa, such as *A. rufa*, there is relatively little anteroposterior or mediolateral distance between the two origins of the pterygoids, but a relatively large dorsoventral distance between them—this pterygoid origin configuration is hereafter referred to as 'dorsal offset', though most dorsal offset taxa have the origin of the **EP** occurring more medially than *A. rufa* does due to the shape of the posterior zygomatic root and its attachment to the cranium. 'Dorsal', 'anterior', and 'lateral' offset (with clear examples shown in Figure 2.35) are three loose categories interpreted in this sample, with some taxa showing particularly exaggerated or extreme examples of these arrangements; a comparison of these different configurations and their characteristics is made in the Discussion section, since this is an interpretation across the whole sample rather than being specific to *A. rufa* alone and is beyond the scope of a species-specific subheading.

Existing physical dissection (Druzinsky, 2010) describes in *A. rufa* a portion of the **SM** curving to insert on the ventromedial surface of the mandible, anterior and medial to the attachment of the muscle referred to herein as **IP** (Druzinsky, 2010). This could not be identified from the isolated skull and mandibles in this study, and is not mapped.

2.3.1.2 – Hystricomorph: *Cavia porcellus* (Domestic Guinea Pig)

C. porcellus (Caviidae) was the archetypal specimen for mapping hystricomorphs, and the first hystricomorphous taxon to be mapped. The literature establishes it as possessing a masseter divided into three portions, of which the ZM is further differentiated into three subdivisions (Cox and Jeffery, 2011), an assessment my own reconstruction here agrees with. As in *A. rufa*, visual examination of the skull's surface was used to identify the muscle attachment sites in this study, and the identified muscles and their origins and insertions are displayed in Figures 2.8, 2.9, and 2.10.

Unlike *A. rufa*, *C. porcellus* has an undifferentiated **DM** and an infraorbital portion of the ZM complex, the **Infraorbital Zygomaticomandibularis** (**IOZM**), but both taxa possess several homologous muscles: **SM**, **AZM** and **PZM**, a differentiated **T**, and an **IP** and **EP** are all identifiable on this specimen. This interpretation of subdivisions concurs with the literature, though Byrd was unable to differentiate the ZM complex, nor the **T**, into separate subdivisions (Woods, 1972; Byrd, 1981; Cox and Jeffery, 2011).

In *C. porcellus*, I identify the **SM** as originating on a fossa on the ventral surface of the anterior zygomatic root; this agrees with the existing research (Byrd, 1981; Cox and Jeffery, 2011). In hystricomorphs, the infraorbital foramen is large, and the ventral surface of the zygomatic root is oriented more horizontally than that of the myomorphs and sciuromorphs (which possess a zygomatic plate) (Brandt, 1855; Scott, Jepsen and Wood, 1937; Wood, 1955, 1965; Cox and Jeffery, 2011, 2015). I identified the origin of the **SM** in *C. porcellus* as more laterally positioned compared to that of other morphotypes, lateral to the anterior cheek teeth and occurring on the zygomatic root itself; this interpretation is also in agreement with the literature (Cox *et al.*, 2011). This **SM** origin configuration (with the origin on the zygomatic root) is typical of hystricomorphs. Since there is no identifiable muscle attachment on the ventral surface of the mandibular angle that I can see, nor an identifiable attachment ventral to that of the **DM** on the lateral face, I interpreted that the muscle then curves into a *pars reflexa* to insert on the medial surface of the angle in a prominent fossa. This interpretation of a *pars reflexa* is also consistent with the existing study of the masseter in this taxon, and in other rodents, though some papers interpret the insertion as being divided into multiple regions. For example, Byrd and Woods interpret the attachment of the *pars reflexa* on the lateral face as reaching up almost to the condylar process, and they also identify an additional insertion surface on the ventral surface of the angle not identified in this study (Woods, 1972; Byrd, 1981). Without those insertions being observed in this study or in the other taxa studied, these previously proposed elements of the **SM** are not

represented in the mechanical advantage analysis of this specimen. This **SM** insertion I identify is ventral and anterior to a second fossa, here interpreted as the insertion of **IP** as in *A. rufa*.

I identified the undifferentiated **DM** as originating on the ventrolateral surface of the zygomatic arch, which aligns with existing study (though Woods subdivides the fibres into 'superficial', 'posterior' and 'deep' portions) (Woods, 1972; Byrd, 1981; Cox and Jeffery, 2011), and is here observed to be more similar in position to the origin of the **PDM** in taxa with a differentiated deep masseter complex, rather than their **ADM**. In this scan, the origin is a clear elongate attachment surface on the ventral margin of the zygomatic arch, extending anteriorly along the surface but not far enough anteriorly to reach the anterior zygomatic root, and extending posteriorly onto the squamosal portion of the posterior zygomatic root, lateral to the TMJ. The **DM** is here identified as inserting on the lateral face of the mandible's angle, dorsal to the masseteric line, an interpretation in agreement with the literature (Woods, 1972; Byrd, 1981; Cox and Jeffery, 2011).

The ZM complex is differentiated into three portions in this specimen: the **IOZM**, the **AZM**, and the **PZM**. This is an interpretation that concurs with existing study (Cox and Jeffery, 2011), but Byrd misidentifies the fibres of the **IOZM** as being a portion of the **DM** (Byrd, 1981) and Woods does not separate the **IOZM** and **AZM**, instead treating them as a single muscle subdivision (Woods, 1972). The **IOZM** is possessed by taxa of all morphotypes except sciuromorphs. In hystricomorphs, it originates on the rostrum; this origin takes the form of a large, distinct fossa on the lateral face of the maxilla, anterior to the large infraorbital foramen (Brandt, 1855; Scott, Jepsen and Wood, 1937; Wood, 1955, 1965; Cox and Jeffery, 2011, 2015). The **IOZM** passes through the foramen and curves down over the ventral root of the zygomatic arch (the ventral margin of the foramen), to insert at the anterior end of a prominent elongate fossa lateral to the cheek teeth; this interpretation agrees with the existing study of this taxon despite Byrd's reference to this as part of the **DM** and Woods's description of it as combined

with the **AZM** (Woods, 1972; Byrd, 1981; Cox and Jeffery, 2011). The fossa observed in this study is lateral to the coronoid process, and the lateral margin of the fossa is a prominent ridge that extends posteriorly to the condylar process. As was identified in later mapping, few hystricomorphs in the studied sample share this configuration; most lack this prominent elongate fossa lateral to the coronoid process, and instead the **IOZM** attaches on the lateral face of the mandible's body anterior to the root of the coronoid process and medioventral to the first lower molar. In agreement with the literature (Woods, 1972; Byrd, 1981; Cox and Jeffery, 2011), the **AZM** and **PZM** are here identified as originating from the medial surface of the zygomatic arch on a pair of shallow fossae, and inserting in the elongate fossa posteriorly to the **IOZM** insertion. As can be observed in Figure 2.9, the **AZM** and **PZM** have quite short muscle lengths in *C. porcellus* when compared with those of *A. rufa*, again due to the zygomatic arch being level with the upper molars; the length of a muscle is not necessarily relevant to the in-lever of that muscle, but this is mentioned here as to draw attention to how the muscle configurations can differ in ways that the mechanical advantage data might not capture.

As in *A. rufa*, the **T** is differentiated into medial and lateral portions (Cox and Jeffery, 2011), but only the medial portion is mapped, as previously discussed. Some older papers divide the temporalis into three portions, using modern nomenclature these would be the medial and lateral portions and an additional "orbital" portion (Woods, 1972). The **T** originates from the dorsal surface of the parietal bones, reaching posteriorly almost to the small nuchal crest, and medially extending at least to the suture between the parietals and squamosal. This is in agreement with the literature (Cox and Jeffery, 2011), including Byrd's paper which treats the subdivisions of the **T** as unified and describes only the attachments of the medial portion (Byrd, 1981) and the identification of the "posterior" (medial) part of the temporalis in Woods's paper (Woods, 1972). When in dorsal view, the attachments are particularly clear in this specimen, since the anteromedial margin of the insertion is more distinct than in most taxa, giving a clearly visible impression of the extent of

the shallow fossa of the attachment. The **T** passes through the posterior part of the orbit and is here identified as inserting on the tip and anterior surface of the coronoid process, an interpretation that again agrees with the literature (Woods, 1972; Byrd, 1981; Cox and Jeffery, 2011).

Similarly to *A. rufa*, the **IP** is identified here and in the literature as originating from the medial pterygoid plate (Byrd, 1981; Cox and Jeffery, 2011), but the origin of the **EP** is quite different to that of *A. rufa*. Here, the **EP** is interpreted as originating from a fossa on the alisphenoid medial to the TMJ, and this is displaced mediolaterally relative to the **IP** rather than the displacement being primarily dorsal as in *A. rufa*; as such, this configuration is referred to hereafter as 'lateral offset' (see Discussion and Figure 2.35 for further details). Existing papers describe this muscle differently, as originating from the alisphenoid and lateral pterygoid process (Woods, 1972; Byrd, 1981), and from "the adjacent edge of the maxillary bone" (Woods, 1972); I did not identify these other origin sites described in the older papers. Both muscles insert on the medial surface of the mandible, with **IP** inserting on the angle, posterodorsal to the insertion of **SM**, and **EP** inserting on the medial surface of the condylar process, ventral to the condyle; these interpretations regarding the origins and insertions of the pterygoids are broadly consistent with the existing literature (Woods, 1972; Byrd, 1981; Cox and Jeffery, 2011).

2.3.1.3 – Myomorph: *Rattus norvegicus* (Brown rat)

R. norvegicus (Murinae) was the archetypal myomorph selected and the first myomorph analysed; the other myomorphs were compared with it. Its masseter is identified in the literature as being divided into three main portions, and the Deep and ZM complexes are differentiated into two and three portions respectively (Weijs, 1973; Cox and Jeffery, 2011). That being said, one major paper does not divide the Deep and ZM complexes similarly when describing their form, and instead refers to the **IOZM** as a portion of the DM complex while combining the **PDM** with the **AZM** and **PZM** into a single 'Deep Masseter' (Hiiemae, 1971); given this decision, comparisons between that study and this thesis are limited but will be made where

possible. In a similar vein, another paper does not differentiate the **ADM** and **PDM** (Turnbull, 1970). The subdivisions described in recent study (Cox and Jeffery, 2011) were identified in my analysis here. Whereas the primary characteristics of the hystricomorphous configuration are associated with a large infraorbital foramen and relatively horizontal anterior zygomatic root, myomorphs are distinctive for their steeply inclined zygomatic plate and narrower infraorbital foramen (Fabre *et al.*, 2012; Cox and Hautier, 2015). Figures 2.8, 2.9, and 2.10 display the identified muscle attachments in lateral view.

Unlike in hystricomorphs, I do not identify *R. norvegicus*'s **SM** as originating on the zygomatic root itself. As is identified in the literature (Turnbull, 1970; Hiiemae, 1971; Weijs, 1973; Cox and Jeffery, 2011) and here in my own analysis, it originates on the ventrolateral surface of the maxilla, ventral to the infraorbital foramen and anterior to the maxillary zygomatic root and upper tooth row, similarly to that of *A. rufa*. The muscle possesses a *pars reflexa*, inserting on the medial surface of the angle of the mandible, ventral to the insertion of the **IP**; this interpretation is consistent with the literature (Hiiemae, 1971; Weijs, 1973; Cox and Jeffery, 2011), though one paper subdivides the **SM** with a *pars reflexa* and a portion inserting on the ventral surface of the mandible (Turnbull, 1970).

The Deep Masseter is differentiated into an **ADM** and **PDM** in all myomorphous taxa in this study, and this agrees with the majority of the literature on myomorphs including this taxon (Hiiemae, 1971; Weijs, 1973; Cox and Jeffery, 2011) though one paper does not separate the two subdivisions (Turnbull, 1970). I identify the **ADM** as originating from the ventral surface of the zygomatic plate, a skeletal characteristic specific to myomorphs and sciuromorphs. The maxillary zygomatic root curves upwards towards the infraorbital foramen, before curving steeply down to form the lateral wall of the foramen and attaches to the rostrum low on the maxilla; this forms a wide, inclined surface that curves steeply. The **ADM**'s attachment on this plate is a large, clearly defined fossa, and the muscle passes steeply downwards to insert on the anterior end of the masseteric line, on the lateral

face of the mandible. These origin and insertion attachment surfaces are very clear, and are identified both here and in the literature (Hiiemae, 1971; Weijs, 1973; Cox and Jeffery, 2011).

The **PDM** originates on the ventrolateral surface of the zygomatic arch (Weijs, 1973; Cox and Jeffery, 2011), though Hiiemae expands this to incorporate the **AZM** and **PZM** (Hiiemae, 1971). Here, I identify the origin as extending ventrally to the ventral margin of the arch and it appears to extend anteriorly to the beginning of the zygomatic plate, and posteriorly almost to the squamosal root of the arch. The **PDM** inserts on the posterolateral face of the mandibular angle, towards the posterior end of the masseteric line (Weijs, 1973; Cox and Jeffery, 2011), though Hiiemae seemingly identifies this insertion as extending anteriorly to around the level of the second molar (Hiiemae, 1971).

Homologous to *C. porcellus*, the ZM complex in this analysis and a recent reconstruction is differentiated into three portions: the **IOZM**, the **AZM**, and the **PZM** (Cox and Jeffery, 2011). As in *C. porcellus*, the **IOZM** originates on the rostrum, on a fossa anterior to the infraorbital foramen (Turnbull, 1970; Hiiemae, 1971; Weijs, 1973; Maier, Klingler and Ruf, 2002; Cox and Jeffery, 2011)) and though Hiiemae refers to this as a portion of the DM complex and Turnbull gives it its own name distinct from the ZM complex ("M. maxillomandibularis") both papers clearly identified the same origin surface that I do here (Turnbull, 1970; Hiiemae, 1971). The muscle then passes through the foramen and curves downwards to insert on the mandible, on a fossa lateral to the tooth row (Turnbull, 1970; Hiiemae, 1971; Weijs, 1973; Cox and Jeffery, 2011). In agreement with the literature that differentiates the two portions (Weijs, 1973; Cox and Jeffery, 2011), I identify that the **AZM** and **PZM** originate on the medial surface of the zygomatic arch, the former from a fossa on the jugal, the latter from a fossa that extends posteriorly onto the squamosal root of the zygomatic arch. In *R. norvegicus*, the root of the incisor can be observed to form a distinct protrusion on the lateral face of the mandible, which makes precise identification of the insertions of the **AZM** and **PZM** difficult here because it is hard to tell if topographical changes in

the bone's surface in the region are associated with this protrusion itself or with muscle attachments. The **AZM** is interpreted here as inserting laterally on the root of the coronoid process, anterior to the protrusion formed by the root, while the **PZM** is interpreted as inserting posterior to it, in what appears to be a prominent elongate fossa that terminates anterior to the condylar process; these interpretations agree with the literature even if the two subdivisions are not separated in Turnbull's paper (Turnbull, 1970; Weijs, 1973; Cox and Jeffery, 2011).

The **T** is once again mapped with a single origin and insertion regardless of potential differentiation—existing papers identify two subdivisions, one medial and one lateral (Hiiemae, 1971; Weijs, 1973; Cox and Jeffery, 2011)—and this origin is clear on the parietal bones in *R. norvegicus*. The superior temporal line connects to the nuchal crest to form the medial and posterior margins of the origin as interpreted here, which extends ventrolaterally to the squamosal root of the zygomatic arch. This region appears proportionally larger than the origins of the other taxa, though the anterior margin of the origin cannot be so clearly identified. This specific origin was earlier shown in Figure 2.6. The **T** inserts on the coronoid process and was mapped on the anterior surface. These interpretations of the origin and insertion of this portion of the temporalis fit with the literature (Hiiemae, 1971; Weijs, 1973; Cox and Jeffery, 2011).

R. norvegicus possesses an **IP** and **EP**. Similarly to the other taxa, the **IP** is identified here and in the literature as originating on the lateral surface of the medial pterygoid plate (Turnbull, 1970; Hiiemae, 1971; Cox and Jeffery, 2011). The **EP** originates differently to some rodents, however, here identified as being displaced anteriorly relative to **IP** (associated with the different shapes of the pterygoids, squamosal and alisphenoid) and positioned anteroventral to the posterior zygomatic root, on the cranium itself; it originates on a fossa on the lateral face of the alisphenoid, posterior to the cheek teeth, an interpretation in agreement with some of the literature (Turnbull, 1970; Cox and Jeffery, 2011). In contrast, Hiiemae identifies the **EP** origin as occurring further posterior and dorsal to this interpretation, still on

the alisphenoid but more similar to the origin in a 'dorsal offset' taxon, and apparently expanding the **IP**'s origin into the area I mapped the **EP** (Hiiemae, 1971). Since the anteroposterior distance between the two origins is notably greater than the mediolateral and dorsoventral distance, this is here classified as 'anterior offset', a category mostly identified among the myomorphous taxa in this sample (the only non-myomorphous anterior offset taxon being *G. nagtglasii*). These categories are shown in Figure 2.35 and compared in the Discussion section. The **IP** inserts on the medial surface of the angle of the mandible, dorsal to the insertion of the **SM**, and **EP** inserts on the medial surface of the condylar process, ventral to the TMJ. This interpretation of the **IP** origin differs from one paper which identifies the insertion as extending to cover much of the angular process (Turnbull, 1970), but otherwise both interpretations of the **IP** and **EP** insertions made here are in keeping with the literature (Hiiemae, 1971; Weijs, 1973; Cox and Jeffery, 2011).

2.3.1.4 – Sciuromorph: *Sciurus carolinensis* (Eastern Grey Squirrel)

S. carolinensis (Sciurinae) was the first sciuromorphous taxon analysed. In agreement with the existing literature (Ball and Roth, 1995; Cox and Jeffery, 2011), its masseter is here divided into three portions, and the deep and ZM complexes are each differentiated into a further two portions (anterior and posterior each). Similarly to myomorphs, the anterior zygomatic root curves dorsally to form a zygomatic plate; however, in sciuromorphs there is no enlarged infraorbital foramen, nor its associated subdivision of the ZM complex seen in the myomorphs and hystricomorphs (Brandt, 1855; Scott, Jepsen and Wood, 1937; Wood, 1955, 1965; Turnbull, 1970; Fabre *et al.*, 2012; Cox and Hautier, 2015). Figures 2.8, 2.9, and 2.10 display the configuration of the attachments in lateral view, as for the other taxa.

The **SM** in *S. carolinensis* is here identified as originating on the ventrolateral surface of the maxilla; this is in agreement with the literature, which sometimes describes the origin as associated with the "masseteric tubercule" (Ball and Roth, 1995; Cox and Jeffery, 2011). Despite the lack of an

enlarged infraorbital foramen, I identify its placement as similar to that of *R. norvegicus*; anterior to the tooth row and zygomatic root, though the margins of the origin are difficult to identify on the CT specimen due to its lower resolution (when compared with the other 'archetype' scans) obscuring small topographical variations. I interpret the muscle as inserting in a prominent fossa on the medial surface of the angle, implying the presence of a *pars reflexa*—the presence of a *pars reflexa* and the **SM** attaching here is also established in existing study (Cox and Jeffery, 2011), though some identify fibres of the **SM** as partially inserting on the lateral surface of the ramus in addition to this *pars reflexa* (Ball and Roth, 1995).

In *S. carolinensis*, the deep masseter is differentiated into an **ADM** and **PDM** (Ball and Roth, 1995; Cox and Jeffery, 2011). In agreement with the literature (Cox and Jeffery, 2011), I identify the former as originating from the prominent fossa on the anteroventral surface of the zygomatic plate, though its attachment surface does appear to extend anteriorly onto the rostrum where it fuses with the zygomatic plate.

I interpret the **ADM** as passing down to insert on the lateral face of the mandible, towards the anterior end of the masseteric line—an interpretation in agreement with existing study (Ball and Roth, 1995; Cox and Jeffery, 2011). Meanwhile, I identify the **PDM** as originating from the ventrolateral surface of the zygomatic arch, in a distinct elongate fossa. The muscle inserts on the lateral face of the mandible, posterior on the masseteric line and towards the angle. Neither of these interpretations regarding the attachments of the **PDM** conflict with one of the existing papers (Cox and Jeffery, 2011), but the insertion I identify differs slightly from the other paper, which positions the insertion posterior and dorsal to where I do (Ball and Roth, 1995), seemingly close to insertion of the **IP** when viewed in lateral view. That paper instead seemingly treats what I identify as being the **PDM** insertion as an extension of the **ADM** insertion (Ball and Roth, 1995).

The ZM complex is differentiated into an **AZM** and **PZM** (Ball and Roth, 1995; Cox and Jeffery, 2011). I and the literature (Ball and Roth, 1995; Cox and Jeffery, 2011) both identify the **AZM** as originating from the medial

surface of the zygomatic arch, and inserting on the lateral face of the root of the coronoid process. Likewise, I agree that the **PZM** originates posteriorly on the medial surface of the zygomatic arch, close to the glenoid fossa, and inserts on the lateral face of the mandible, ventral to the condylar process (Ball and Roth, 1995; Cox and Jeffery, 2011). Both of these insertions are in shallow fossae.

The **T** in *S. carolinensis* has a similar form to the three previous taxa with its subdivision into medial and lateral portions in the literature (Ball and Roth, 1995; Cox and Jeffery, 2011) and is again mapped in this study as only the medial temporalis origin. I identify the muscle as originating from the dorsal cranium, with its dorsal margin marked by the superior temporal line, and its posterior margin marked by the shallow nuchal crest. It extends laterally to the posterior zygomatic root, and curves to insert on the coronoid process. These interpretations align with those of the medial temporalis in existing study though they can provide greater detail on the margins of its insertion (Ball and Roth, 1995; Cox and Jeffery, 2011). As in the other archetypal taxa, the **T** insertion is mapped primarily on the anterior face of the coronoid process.

The **IP** originates from the medial pterygoid plate, and inserts on the medial surface of the angle of the mandible, dorsal to the insertion of the **SM**; this interpretation is in agreement with the previously established interpretation of this muscle (Ball and Roth, 1995; Cox and Jeffery, 2011) though Ball and Roth partition the muscle into three distinct layers and go into greater detail identifying where these layers insert. I identify the **EP** as originating on the alisphenoid/squamosal, medial to the posterior zygomatic root and similarly to *A. rufa*, an interpretation that aligns with the literature (Ball and Roth, 1995; Cox and Jeffery, 2011). As a result, *S. carolinensis* is classified as dorsal offset in this study. The **EP** inserts on the medial surface of the condylar process, again in agreement with existing interpretations (Ball and Roth, 1995; Cox and Jeffery, 2011).

2.3.2 – Remaining taxa

2.3.2.1 – *Acomys cahirinus* ('Northeast African Spiny Mouse')

A. cahirinus (Deomyinae) lacks existing literature on its muscle subdivisions and their configuration, leaving this section with no direct comparisons to make to the literature. I identify it here as possessing all the same differentiation of muscles as the selected archetypal myomorph, *R. norvegicus*: an **SM**, **ADM** and **PDM**, **IOZM**, **AZM**, and **PZM**, a differentiated **T** represented by a single attachment for the Medial portion, **IP**, and **EP**. The attachments are shown in Figure 2.11, as the prior taxa were displayed in Figures 2.8, 2.9, and 2.10. All muscles also originate from and attach to the same bones as in *R. norvegicus*, though the **EP** is notably distinct in its origin. Here, I interpret the **EP** as originating more dorsally and posteriorly than its origin in *R. norvegicus*. It is therefore classified as a 'dorsal offset'. Despite this small difference, *A. cahirinus* was classified here as a myomorph due to its present but narrow infraorbital foramen, zygomatic plate, and the differentiation of its muscles.

When compared with *R. norvegicus*, some of the muscles in *A. cahirinus* (such as the **AZM** and **PZM**) appear to have their insertions further posterior than their origins on the medial surface of the zygomatic arch, resulting in shallower slopes for their lines of action in Figure 2.11. That being said, precise mapping of

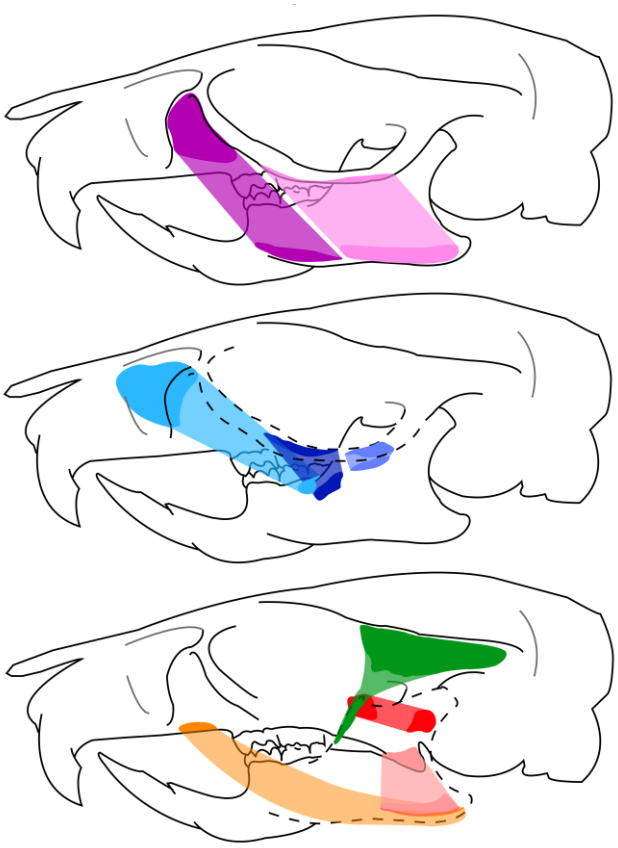

Figure 2.11: Muscle attachments in *Acomys cahirinus*.

the insertions of these two muscles is difficult in this taxon due to the subtlety of topographic change in this region. Other muscles are generally similar to those of *R. norvegicus*. Future studies of their soft-tissue may confirm or dispute these interpretations.

2.3.2.2 – *Bathyergus suillus* ('Cape Dune Mole-rat')

B. suillus (Bathyergidae) possesses some differentiation of muscles in common with *A. rufa*, but with some key differences that it shares with *G. capensis* (the other member of Bathyergidae): an **SM**, an undifferentiated **DM** (in contrast to *A. rufa*'s differentiated deep masseter), **IOZM** (which *A. rufa* lacks) **AZM** and **PZM**, **T**, **IP**, and **EP**. Existing papers identify these same muscles (McIntosh and Cox, 2016b; Cox, Faulkes and Bennett, 2020). The attachments of these muscles are shown in Figure 2.12. All the muscles it shares with *A. rufa* originate from and attach to the same bones as in *A. rufa*. The '**IOZM**' identified here does not actually pass through the infraorbital foramen and instead attaches on a fossa posterodorsal to the anterior zygomatic root; despite the lack of an enlarged foramen, this is referred to as an **IOZM** in this thesis due the similarity of its origin on the rostrum, unlike the other portions of the ZM complex. This interpretation of the **IOZM** origin was also made independently in existing research (McIntosh and Cox, 2016b; Cox, Faulkes and Bennett, 2020). The **EP**

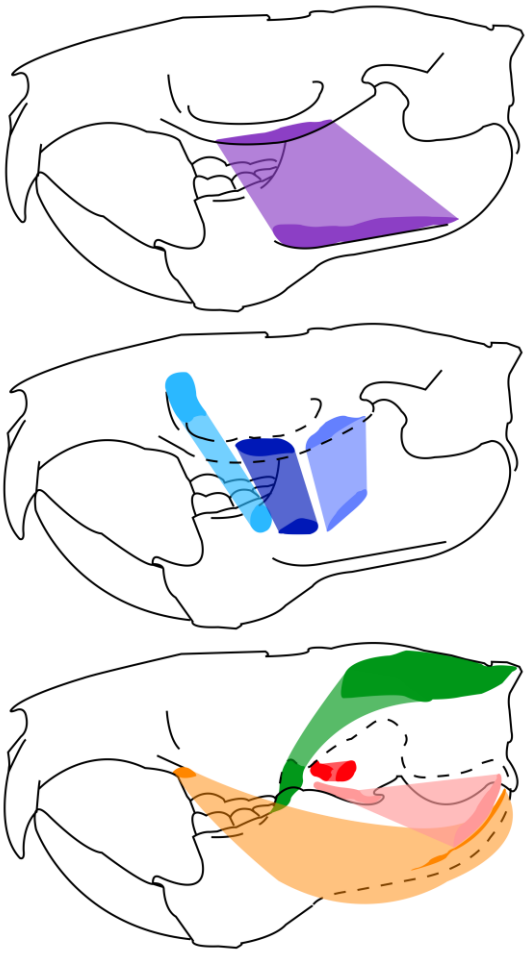

Figure 2.12: Muscle attachments in *Bathyergus suillus*.

is categorised as 'dorsal offset', as in *A. rufa*, but appears to originate more medially and on the anterior face of the alisphenoid/squamosal rather than the ventral face.

Existing study identified the **T** origin as extending much further forward on the skull, almost to the anterior zygomatic root (McIntosh and Cox, 2016b; Cox, Faulkes and Bennett, 2020); this is perhaps the most notable difference between the literature and this study's reconstruction and would result in a more anterior centroid for the **T** origin. Despite the presence of an **IOZM** and the undifferentiated **DM**—proposed in the literature to be due to *B. suillus* having derived protrogomorphy from a hystricomorphous ancestor (Cox, Faulkes and Bennett, 2020)—*B. suillus* was classified in this analysis as a protrogomorph due to the configuration of the **SM** and **DM** on the anterior zygomatic, and due to the lack of an enlarged infraorbital foramen (a distinct feature of hystricomorphs). When compared with the other assigned protrogomorphs, notable differences are visible. For example, in this analysis I identify that the infraorbital foramen is larger (though still greatly reduced) in *G. capensis*, and the muscle identified as **IOZM** does not pass through the infraorbital foramen and instead originates behind the zygomatic root similarly to that of *B. suillus*; this is an interpretation the literature also aligns with across Bathyergidae (Cox, Faulkes and Bennett, 2020). *A. rufa* was identified here as possessing a differentiated deep masseter that both these taxa lack, but itself lacks an **IOZM** or equivalent. Both *B. suillus* and *G. capensis* are proposed to have evolved from hystricomorphs (Cox, Faulkes and Bennett, 2020) and this may be responsible for their distinctive differences when compared with *A. rufa*.

2.3.2.3 – *Cannomys badius* ('Lesser Bamboo Rat')

C. badius (Spalacidae), displayed in Figure 2.13 is here identified as possessing the characteristic muscle differentiation of a myomorph: **SM**, differentiated **ADM** and **PDM**, differentiated **IOZM**, **AZM** and **PZM**, **T**, **IP**, and **EP**. Existing papers on the musculature of Spalacidae either omit detail regarding this species (Endo *et al.*, 2001) or do not discuss muscle

differentiation of their sample in detail (Fournier, Hautier and Gomes Rodrigues, 2021); this means there are no direct points of comparison for the interpretations made here.

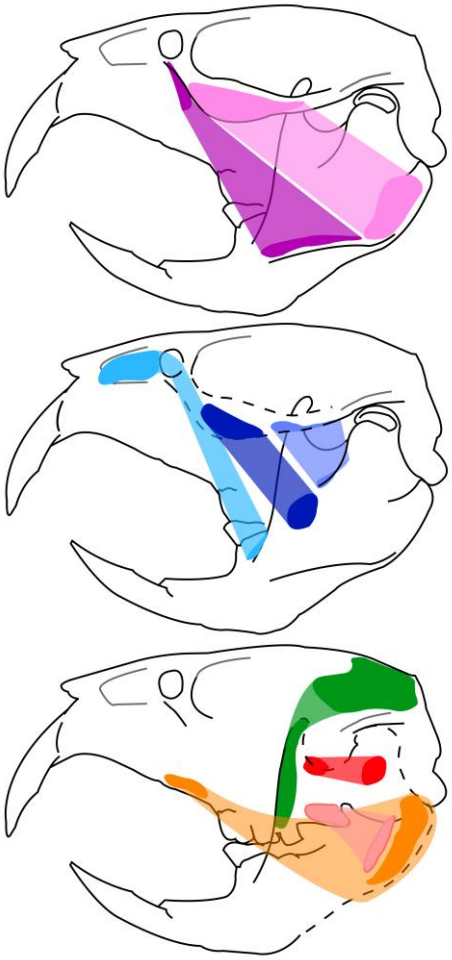

Figure 2.13: Muscle attachments in *Cannomys badius*.

All muscles seem to originate from and attach to the same bones as in *R. norvegicus*, though some variations in configuration are notable. The **IOZM** appears to be oriented more steeply than in most other rodents with the muscle, correlating with *C. badius*'s relatively tall, short head and that the anterior zygomatic root attaches so far dorsally relative to the tooth row; in incisor occlusion, the muscle is here proposed to curve almost into a crescent-shape around the small zygomatic plate in order to reach its insertion. Unlike *R. norvegicus*, and similarly to *A. cahirinus* and *C. gambianus*, the **EP** origin is categorised as dorsal offset, though it should be noted that with the shortness of *C. badius*'s head and the lack of anteroposterior space between the rearmost molar and the pterygoid plate, there would be no physical space for an anterior offset **EP** origin. *A cahirinus*, *C. badius*, and *C. gambianus* are the only three of the six myomorphs in this sample that are interpreted to have a dorsal offset **EP**, rather than the anterior offset of the other three. Due to its muscle differentiations, zygomatic plate, and small infraorbital foramen, *C. badius* was classified in this analysis as a myomorph. Unfortunately, none of these detailed observations on this particular species can be compared with existing studies at present.

2.3.2.4 – *Capromys pilorides* ('Desmarest's Hutia')

C. pilorides (Capromyinae) displays in Figure 2.14 the muscle differentiation of a hystricomorph: **SM**, **DM**, differentiated **IOZM**, **AZM** and **PZM**, **T**, **IP**, and **EP**. Existing research (Woods and Howland, 1979) also identifies three portions to the ZM complex, but: identifies a **PM**; differentiates the **SM** into two separate portions (the anterior of which inserts on the ventrolateral surface of the alveolar sheath); differentiates the **DM** into anterior and posterior portions; divides the **T** into medial and lateral portions; and differentiates the **IP** into multiple layers. None of these are traits I identify or map here.

The muscles I identified originate from and insert on the same bones as in *C. porcellus*, though the **AZM** and **PZM** were here interpreted as attaching lateral to the coronoid process (as can be observed in Figure 2.14)—rather than medial to it in an elongate fossa—along the lateral face of the mandible, and there is no elongated fossa lateral to the coronoid process as in *C. porcellus*, *H. hydrochaeris* or *L. maximus*.

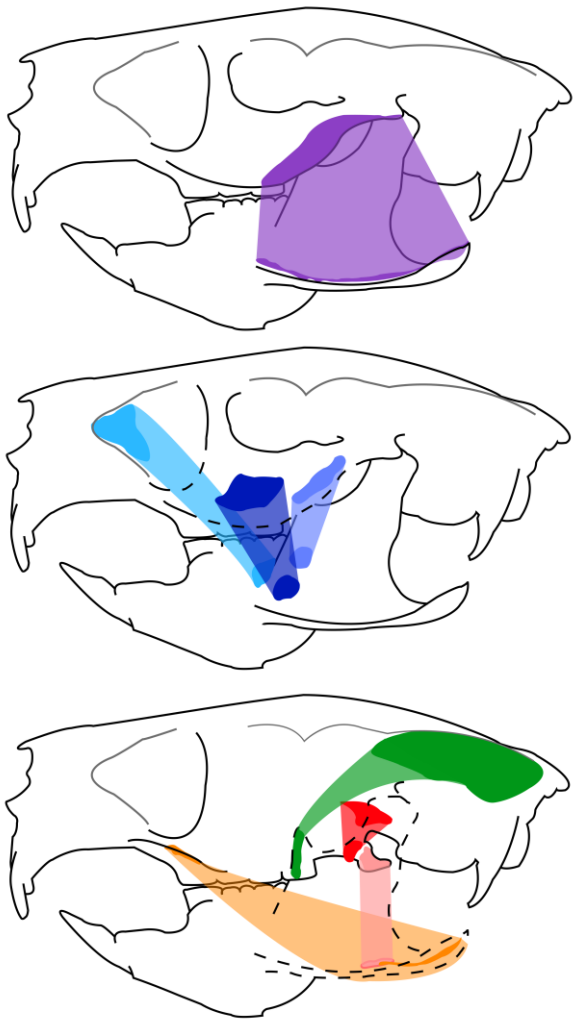

Figure 2.14: Muscle attachments in *Capromys pilorides*.

The **EP**'s origin is dorsal offset, originating on the ventral surface of the alisphenoid/squamosal, and almost directly dorsal to the **IP** origin, similarly to *A rufa*. *C. pilorides* possesses a lateral 'shelf' on the angle of the mandible that flares outwards towards a posterior protrusion at the tip of the angle;

this is a characteristic that *C. porcellus* lacks, but is shared with other hystricomorphs to varying degrees of prominence (*C. opimus, M. coypus,* and *O. degus*). Due to its undifferentiated **DM** and large infraorbital foramen, *C. pilorides* was categorised as a hystricomorph. The muscles identified in this analysis are missing some subdivisions from an existing paper on capromyids; for the muscles I and they both identified, the origins and insertions I describe are broadly in agreement (Woods and Howland, 1979).

2.3.2.5 – *Castor canadensis* ('Northeast American Beaver')

C. canadensis (Castoridae) is here identified to possess all the same differentiation of muscles as *S. carolinensis*, the selected sciuromorph: **SM**, differentiated **ADM** and **PDM**, differentiated **AZM** and **PZM**, **T**, **IP**, and **EP**. This interpretation disagrees with an existing dissection paper (Cox and Baverstock, 2016) in four regards due to the limitations of only using the bone surfaces. I interpreted a *pars reflexa* for the **SM** based on the topography of the medial surface of the mandible, and what appear to be a fossa for the **SM** and a fossa for the **IP** insertion dorsal to it, but the dissection identifies that the **SM** only inserts on the ventral margin of the angular process and does not a *pars reflexa* at all (Cox and Baverstock, 2016). It seems that what I here identify as the **SM** insertion may be part of the **IP** insertion, according to that dissection (Cox and Baverstock, 2016). That dissection does not differentiate the **AZM** and **PZM** into two portions (Cox and Baverstock, 2016), but I do here

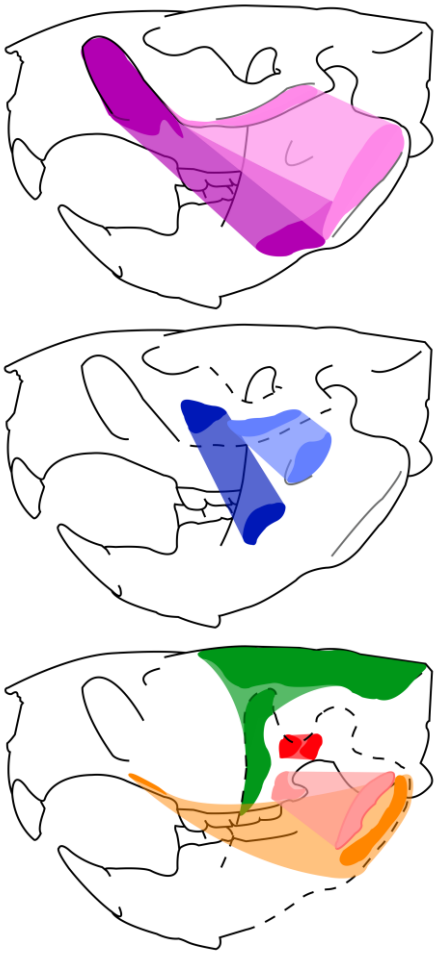

Figure 2.15: Muscle attachments in *Castor canadensis*.

based on an apparent inflections between two fossae on the medial zygomatic arch and lateral face of the mandible. I did not identify a **PM** as they described (Cox and Baverstock, 2016), but it appears that the fossa I identify here as the **PZM** insertion is described as the **PM** insertion in that dissection. The identification of the **EP** origin based on bone surfaces here also does not match the dissection, which places it on the lateral surface of alisphenoid (Cox and Baverstock, 2016); here, I mapped a fossa on the alisphenoid dorsal to the pterygoid plates and classified it as dorsal offset, but according to the dissection this taxon would be lateral offset according to the classifications here. In this reconstruction, these muscles originate from and attach to the same bones as in *S. carolinensis*, including the categorisation of the **EP** origin as dorsal offset, originating on the alisphenoid/squamosal almost directly dorsal to the pterygoid plate as can be seen in the figure for this taxon, Figure 2.15.

C. canadensis has a tall head relative to its length, with a stout zygomatic arch that is elevated relative to the tooth row; as a result, the **ADM** and **PDM** both have long muscle lengths with slightly shallower slopes than in *S. carolinensis* and many other taxa, with the **PDM** apparently inserting on and dorsal to a prominent ridge on the angle of the mandible; this interpretation aligns with the dissection paper (Cox and Baverstock, 2016). The **AZM** and **PZM** both exhibit a distinct orientation from their counterparts in *S. carolinensis* due to their positions and the curvature of the mandible, and here interpreted to insert on two prominent fossae (these fossae are likely clear due to the physical size of the taxon and these muscles, the insertions of these muscles are not usually so sharply defined in this sample) on the lateral face of the mandible, resulting in a shallowly sloping line of action that is oriented differently to the dorsal/retracting pull of these muscles in *S. carolinensis*. The **AZM** insertion here does seem to align with that described in the dissection paper for the there-undifferentiated ZM. Due to its muscle differentiation, zygomatic plate, and lack of an infraorbital foramen, *C. canadensis* was classified in both this analysis and others as a sciuromorph (Cox and Baverstock, 2016).

With the study using 2D lever-arm mechanics, the misidentification of a *pars reflexa* may have little effect on calculation of the **SM**'s mechanical advantage, and the lack of a **PM** is not explored in the quantitative data as so few taxa were here identified as having one to compare at all. The only muscle likely to see a substantial difference in estimation of its mechanical advantage between this study and if these quantitative methods were applied to the existing dissection reconstructions, is the **EP**. As a result, though the differences between this reconstruction and the dissection are significant, they may have little actual impact on the quantitative data here.

2.3.2.6 – *Cricetomys gambianus* ('Northern Giant Pouched Rat')

C. gambianus (Nesomyidae) lacks existing descriptions of its musculature in detail to compare against. Here, it is determined to possess the same muscles as *R. norvegicus:* **SM**, **ADM** and **PDM**, **IOZM**, **AZM** and **PZM**, **T**, **IP**, and **EP**. The configuration is shown in Figure 2.16. All these muscles also originate from and insert on the same bones as in *R. norvegicus*; as briefly alluded to in previous sections, *C. gambianus* possesses a dorsal offset **EP** origin similar to that of *A. cahirinus* and *C. badius*, on the more anterior face

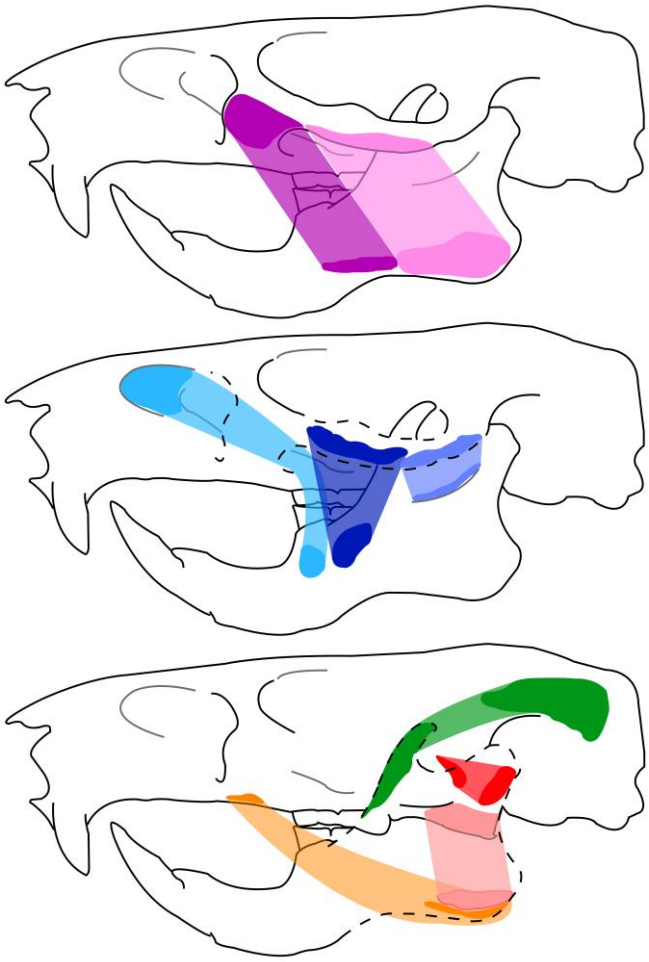

Figure 2.16: Muscle attachments in *Cricetomys gambianus*.

of the alisphenoid/squamosal compared to the more ventral position in *A. rufa*.

Visually, there are no especially notable differences in the configuration of the other muscles when compared to *R. norvegicus* or to other myomorphs within this sample. However, it shares some anatomical similarities with some hystricomorphs that resulted in some initial indecision in assigning it the category of a myomorph (such as its especially large infraorbital foramen, and its less obvious zygomatic plate than other myomorphs).

There is a notable fossa on the lateral surface of the condylar process, anteroventral to the condyle and extending anteriorly to the coronoid process; this is interpreted to be where **PZM** inserts, and visually appears similar to the elongate fossae in *C. porcellus* and *L. maximus*, both of which are hystricomorphs and have homologous portions of the ZM complex inserting there. Despite the visual similarity of *C. gambianus* to those hystricomorphs, it is distinct from them due to its differentiated **ADM** and **PDM**, and its zygomatic plate. *C. gambianus* was classified as a myomorph here based on these characteristics. Its zygomatic plate is proportionally quite small and the infraorbital foramen proportionally quite wide for a myomorph, resulting in the distinctive slightly hystricomorph-like shape of its anterior zygomatic root.

2.3.2.7 – *Ctenomys opimus* ('Andean/Highland Tuco-tuco')

Ctenomys opimus (Ctenomyidae) is of a well-studied genus (Woods, 1972; Olivares, Verzi and Vassallo, 2004; Becerra, Casinos and Vassallo, 2013; Álvarez, Perez and Verzi, 2013; Becerra *et al.*, 2014; Echeverría *et al.*, 2017); though most of these studies focus on different species, one assessing 24 species across the genus does identify the same muscle subdivision across *Ctenomys*, including in *C. opimus* (Echeverría *et al.*, 2017). Here, *C. opimus* is

identified as having the muscle differentiation of hystricomorphs: **SM**, undifferentiated **DM**, differentiated **IOZM**, **AZM** and **PZM**, **T**, **IP**, and **EP**. The left angle of the mandible was broken in this specimen, but the right hemimandible had an intact angle, which was used to replace the missing section. The muscles present all attach to the same bones as in *C. porcellus* (see Figure 2.17).

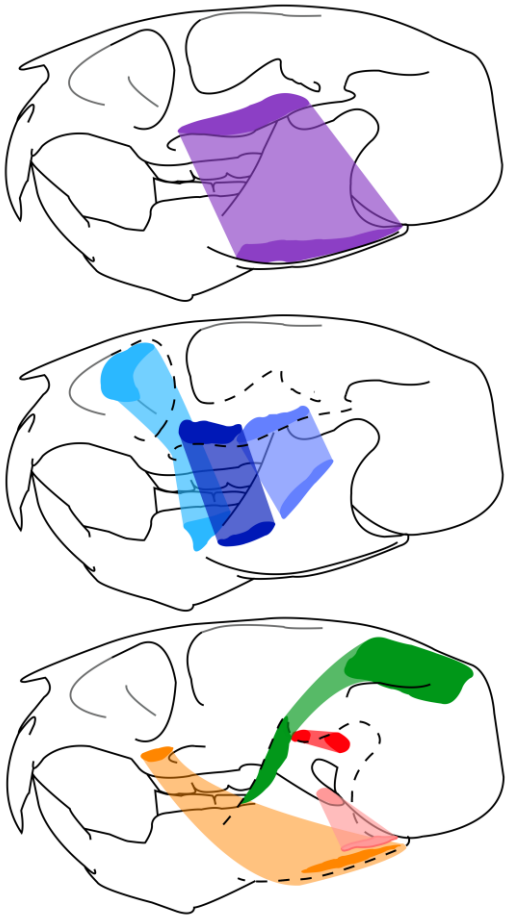

Figure 2.17: Muscle attachments in *Ctenomys opimus*.

The **SM** is here interpreted to have a *pars reflexa* that inserts on the ventromedial surface of the mandible's angle; like *C. pilorides*, *M. coypus*, and *O. degus*, *C. opimus* possesses a lateral 'shelf' on the angle of the mandible that flares outwards into a posterior protrusion at the tip of the angle, and it is on the ventral and medial surfaces of this structure that the **SM** inserts. As is common in this sample, existing study on this genus identifies this *pars reflexa* as well as fibres inserting on the ventral surface of the mandible (which would be further lateral to the identified insertion here) though such papers are not of this species (Woods, 1972). Though the paper that does include *C. opimus* does not describe or illustrate its musculature—and omits the **EP** entirely—the figures and descriptions provided there do fit with the interpreted attachments identified here (Echeverría *et al.*, 2017). Some papers do not differentiate the **AZM** and **PZM** in the analysis of the *Ctenomys* species they studied, and omit the **EP**, but include the other subdivisions, origins, and insertions discussed here (Becerra, Casinos and Vassallo, 2013; Becerra *et al.*, 2014). Typically, the origins and insertions described in other

Ctenomys species are similar to those I identify here (Woods, 1972; Becerra, Casinos and Vassallo, 2013; Becerra *et al.*, 2014; Echeverría *et al.*, 2017), though Woods does not subdivide the ZM complex and some papers describe a **PM** in the genus that I was unable to identify, originating dorsally to the **DM** and inserting on the lateral face of the condylar process (Woods, 1972; Olivares, Verzi and Vassallo, 2004). Despite the lack of detail on this individual species, I believe that the broader study of the genus implies that none of my interpretations here are likely to be novel or surprising except, perhaps, that of the **EP** origin.

Unlike *C. porcellus*, the origin of the **EP** in *C. opimus* is classified here as dorsal offset rather than lateral, seemingly originating on the anteroventral surface of the alisphenoid/squamosal almost directly dorsal to the origin of the **IP**. Existing study describes the **EP** of other *Ctenomys* species originating on the lateral pterygoid plate and alisphenoid (Woods, 1972; Olivares, Verzi and Vassallo, 2004). This taxon lacks the elongate fossa for ZM insertion lateral to the coronoid process that is seen in *C. porcellus*. This seems to agree with some papers on various species (Woods, 1972; Becerra *et al.*, 2014; Echeverría *et al.*, 2017), but differs from that of *C. tuconax* (Becerra, Casinos and Vassallo, 2013). Due to its large infraorbital foramen with an **IOZM**, and its undifferentiated **DM**, *C. opimus* was classified here as a hystricomorph.

2.3.2.8 – *Dasyprocta* sp. ('Agouti')

This individual of the genus *Dasyprocta* (Dasyproctidae), displays the muscle differentiation of a hystricomorph: **SM**, an undifferentiated **DM**, differentiated **IOZM**, **AZM** and **PZM**, **T**, **IP**, and **EP**. One paper discusses the musculature of *D. punctata* specifically (Woods, 1972), while another discusses a different species within the genus (Álvarez and Pérez, 2019); since the species of this particular individual is not known, it shall be compared with both of these papers. The configuration of the muscle attachments is shown in Figure 2.18.

These muscles are here identified to mostly originate from and attach to the same bones as in *C. porcellus*, though it lacks the elongate lateral fossa of ZM-complex insertion in *C. porcellus* and *L. maximus*. The existing paper on *D. punctata* describes the **IOZM**, **AZM**, and **PZM** insertions similarly, but groups the ZM complex into a single muscle rather than subdividing it (Woods, 1972). In two other species of *Dasyprocta* the ZM complex is also stated to insert lateral to the coronoid process (Álvarez and Pérez, 2019). Though that paper does not describe the muscle attachments in detail, their figures seem to imply they identify the **SM** insertion inserts on the ventral surface of the mandibular angle, with no mention of a *pars reflexa* (Álvarez and Pérez, 2019); here, I do interpret a *pars reflexa* and mapped the insertion on the medial face of the angle, which aligns with the description given in the paper that specifically examined *D. punctata* (Woods, 1972). In addition, the **DM** is here proposed to insert all along the masseteric line, which disagrees with the insertion described for *D. punctata* (Woods, 1972), where the muscle inserts anteriorly on the masseteric line and does extend so far posteriorly. That paper also describes a **PM** which I did not identify in this study (Woods, 1972). Other papers do interpret the **DM** as inserting all the way along the masseteric ridge to the posterior tip of the angle in other species of *Dasyprocta* (Álvarez and Pérez, 2019), which agrees with my interpretation here. The **T** and **IP** and origins and insertions I identify match those describe in the literature (Woods, 1972), though the paper by Álvarez

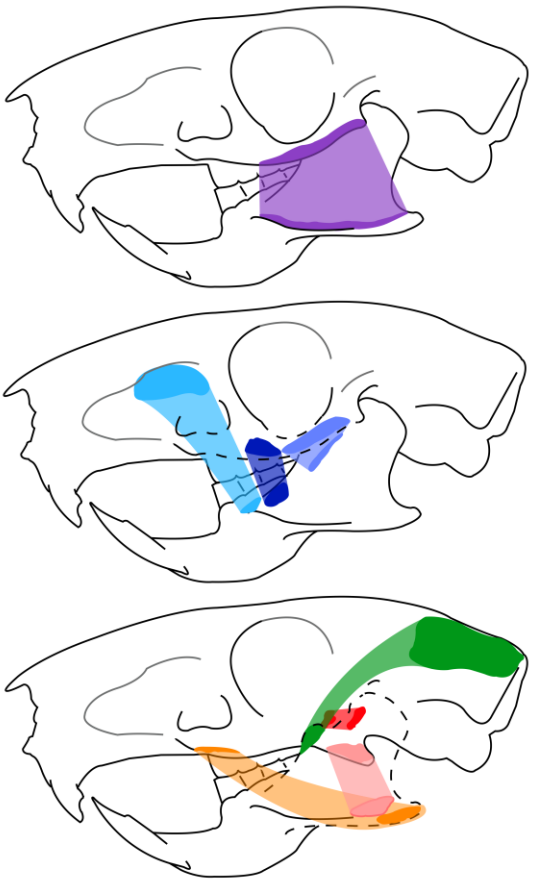

Figure 2.18: Muscle attachments in *Dasyprocta punctata*.

and Perez does not discuss either the temporalis or the pterygoids. The origin of the **EP** is here classified as dorsal offset, originating on the ventral surface of the alisphenoid/squamosal similarly to *A. rufa*. The paper on *D. punctata* described the **EP** as originating on the alisphenoid and lateral pterygoid plate (Woods, 1972).

Due to the similarity to the characteristics described for *D. punctata* as discussed above (the **SM** insertion and **DM** insertion in particular) this specimen is assigned to that species, despite the substantial difference regarding the insertions of the **AZM** and **PZM** (Woods, 1972). Due to its large infraorbital foramen and muscle differentiations, *D. punctata* was classified in this analysis as a hystricomorph.

2.3.2.9 – *Dipus sagitta* ('Northern Three-toed Jerboa')

D. sagitta (Dipodidae) has the muscle differentiation of a hystricomorph: **SM**, undifferentiated **DM**, differentiated **IOZM**, **AZM** and **PZM**, **T**, **IP**, and **EP**. It has no existing detailed papers regarding its musculature, so comparisons cannot be drawn between this interpretation and the literature. The left zygomatic arch was broken in this specimen, but the missing region was replaced using a mirror of the intact right zygomatic.

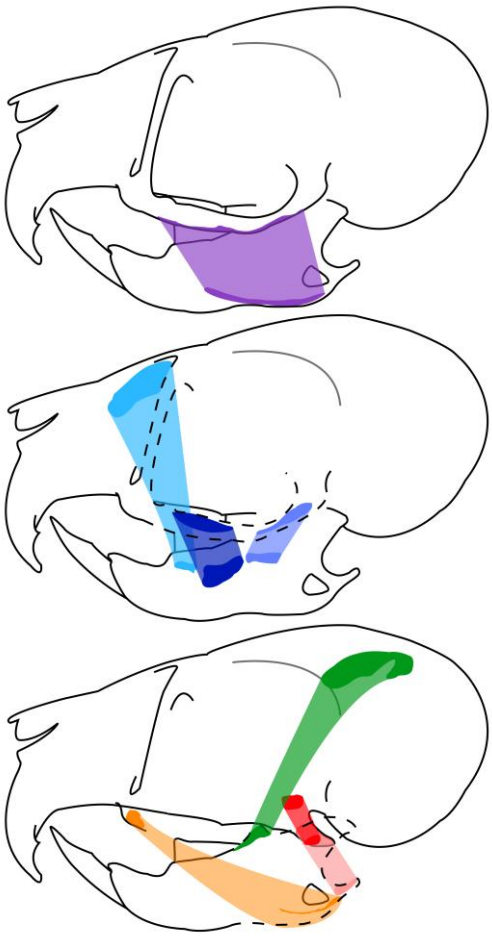

Figure 2.19: Muscle attachments in *Dipus sagitta*.

Its muscles apparently originate from and insert on the same bones as in *C. porcellus*,

though the **IOZM**, **AZM**, and **PZM** in *D. sagitta* were interpreted as inserting lateral to the coronoid with no elongate fossa. As can be observed in Figure 2.19, *D. sagitta* has a relatively small mandible with a relatively large dorsal and posterior cranium (*G. watersi*, a myomorph, also exhibits a small mandible and expanded dorsal/posterior skull and thin zygomatic, but its muscle differentiation is not the same as in *D. sagitta*).

Due to the relatively short mandible and 'low', thin zygomatic arch, *D. sagitta*'s **AZM** and **PZM** appear to be oriented in opposing directions anteroposteriorly (with the insertion posterior to the origin for **AZM**, but vice versa for **PZM**). The **T** and **IOZM** both appear to possess very steep lines of action in Figure 2.19 due to the relatively tall skull. The origin of **EP** in this taxon is identified on the ventral surface of the alisphenoid/squamosal and classed as dorsal offset, almost directly dorsal to the origin of **IP**. Due to its proportionally large infraorbital foramen and muscle differentiations, *D. sagitta* was classified as a hystricomorph.

2.3.2.10 – *Erethizon dorsatum* ('North American Porcupine')

E. dorsatum (Erethizontidae) is here identified as possessing the muscle differentiation of a hystricomorph: **SM**, **DM**, **IOZM**, **AZM** and **PZM**, **T**, **IP**, and **EP**. All these same muscle subdivisions are identified in the literature though the existing paper groups the ZM complex into a single muscle, along with a **PM** that was not identified

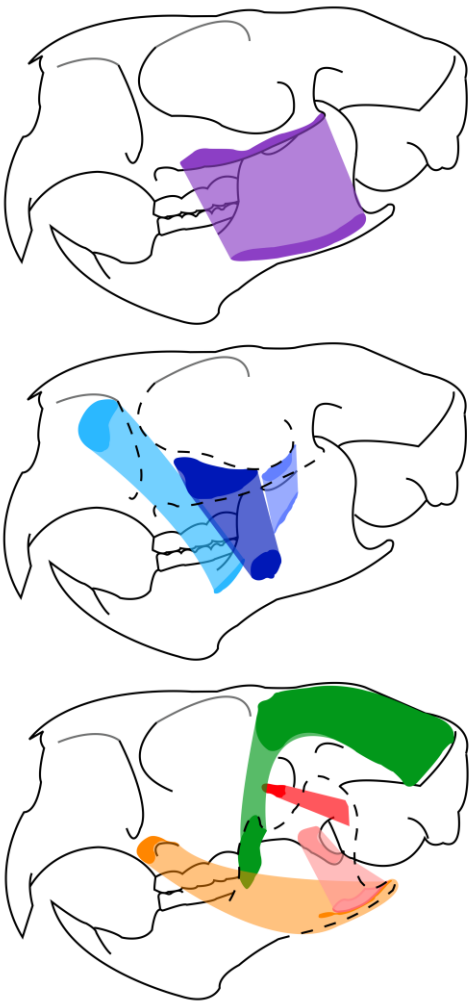

Figure 2.20: Muscle attachments in *Erethizon dorsatum*.

here (Woods, 1972). The muscular configuration is shown in Figure 2.20.

These muscles have the same bone origins and insertions as *C. porcellus*, though the **IOZM**, **AZM**, and **PZM** were here interpreted as attaching lateral to the coronoid process with no elongate fossa; this interpretation aligns with the literature (Woods, 1972). *E. dorsatum*'s **EP** is classified here as dorsal offset, originating on the anteroventral surface of the alisphenoid/squamosal; in the literature, it is described as mostly originating from the lateral pterygoid plate (Woods, 1972), substantially ventral to my interpretation. Compared to most hystricomorphs, *E. dorsatum* appears to have an almost vertical line of action on its **AZM** and **PZM**, with little anteroposterior distance between the origins and insertions during molar biting (and therefore a slight retractive pull in incisor biting). The **SM** (including its *pars reflexa* insertion), **DM**, **T** and **IP** origins and insertions, and **EP** insertion, identified here align with those described in the literature, although Woods subdivides the **IP** into three layers (Woods, 1972). Due to its enlarged infraorbital foramen, and the differentiation of its muscles, *E. dorsatum* was classified in this analysis as a hystricomorph.

2.3.2.11 – *Georychus capensis* ('Cape Mole-rat')

G. capensis (Bathyergidae) is here identified as displaying the muscle differentiation of a hystricomorph, but with an unusually reduced infraorbital foramen and the superficial/deep masseter configuration of a protrogomorph, as was noted in *B. suillus*. Though there is controversy in the literature, this is an interpretation that aligns with a recent analysis of musculature in Bathyergidae (Cox, Faulkes and Bennett, 2020). *G. capensis* possesses a **SM**, undifferentiated **DM**, differentiated **IOZM**, **AZM** and **PZM**, **T**, **IP**, and **EP**. All these muscles also originate from and attach to the same bones as in *A. rufa* and *C. porcellus*, and the attachments are shown in Figure 2.21.

Though *G. capensis* does possess an **IOZM**, like that of *B. suillus* it does not actually pass through the infraorbital foramen, instead originating within the foramen; this interpretation aligns with the literature (Cox, Faulkes and Bennett, 2020) but is in slight contrast to *B. suillus*, which does not possess an enlarged infraorbital foramen at all, instead being more similar to the foramen of sciuromorph rodents. *A. rufa* also lacks an enlarged infraorbital foramen. Despite this difference from *A. rufa*, the presence of an **IOZM**-equivalent muscle anterior to the orbit, and the undifferentiated **DM**—proposed in the literature to be due to its derived protrogomorphy from an ancestor that was hystricomorphous, like in *B. suillus* (Cox, Faulkes and Bennett, 2020)—*G. capensis* was classified in this analysis as a protrogomorph based on the configuration of the **SM** and **DM**.

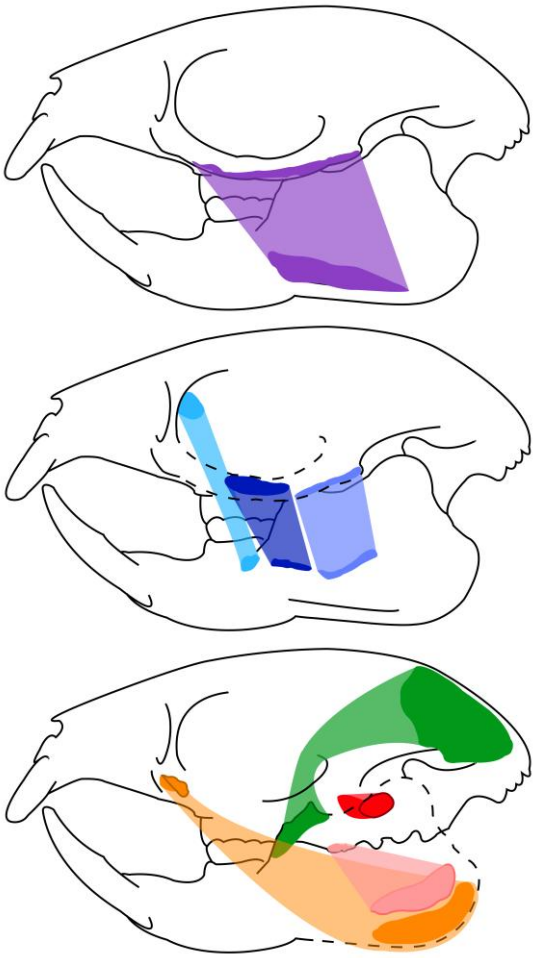

Figure 2.21: Muscle attachments in *Georychus capensis*.

As can be observed in Figure 2.21, the insertions of the **IOZM**, **AZM**, and **PZM** occur lateral to the coronoid process, on the lateral face of the mandible. This agrees with the literature, as digital dissection identifies the ZM complex as inserting on the lateral face of the mandible, ventral to the coronoid process (Cox, Faulkes and Bennett, 2020). Both *B. suillus* and *G. capensis* have disputed classifications in the literature (Cox, Faulkes and Bennett, 2020) and share characteristics with two morphotypes, but as the expanded infraorbital foramen is such a distinctive characteristic of

hystricomorphs, they are here excluded from the category. The **EP** origin is classified as dorsal offset in *G. capensis*, positioned ventrally on the alisphenoid/squamosal, similarly to *A. rufa*.

2.3.2.12 – *Gerbillus watersi* ('Water's Gerbil')

G. watersi (Gerbillini) displays the muscle differentiation of a myomorph: **SM**, differentiated **ADM** and **PDM**, differentiated **IOZM**, **AZM** and **PZM**, **T**, **IP**, and **EP**. This is a taxon with little published study, and no existing muscular reconstructions on this particular species. The right zygomatic arch of this specimen was broken posterior to the zygomatic plate and anterior to the squamosal; the missing segment was replaced virtually with the intact left zygomatic arch. All muscles are here identified to originate from and attach to the same bones as in *R. norvegicus*, and the **EP** origin is also classified as anterior offset, as it is positioned on a flattened patch of the alisphenoid close to its suture with the squamosal; as in *P. gerbillus*, the anterior distance is less increased relative to the dorsal distance, when compared with the larger difference in *R. norvegicus* and *G. nagtglasii*. Its muscle attachments are shown in Figure 2.22.

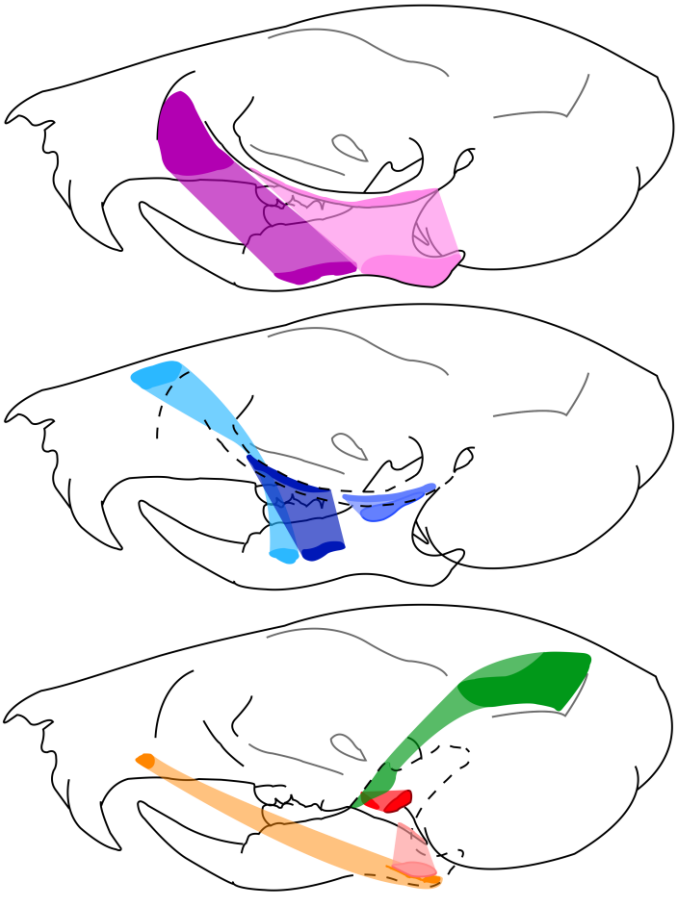

Figure 2.22: Muscle attachments in *Gerbillus watersi*.

Like *D. sagitta*, it possesses a relatively large posterior cranium with large auditory bullae, and a relatively small

mandible, compared to the majority of rodents studied here. However, the orientations of its muscles, are not as atypical as those of *D. sagitta* with the exception of **T**, which is visibly longer compared to the mandible size, than the **T** of other myomorphs. Though the thin zygomatic arch and its proximity to the teeth make some of the attachments on Figure 2.22 more difficult to read at this scale, the origins and insertions are placed on the bones similarly to other myomorphs, as previously discussed. The condylar process extends quite far dorsally, when visually compared with the lower edge of the zygomatic arch, relative to other taxa; based on the inferred insertion of **EP**, this and the shape of the pterygoid plate makes *G. watersi* quite unusual in that its **EP** is a longer muscle in 3D than its **IP**. Due to its zygomatic plate, narrow infraorbital foramen, and muscle differentiations, *G. watersi* was classified here as a myomorph.

2.3.2.13 – *Graphiurus nagtglasii* ('Nagtglas's African Dormouse')

G. nagtglasii (Gliridae) has muscle differentiation consistent with hystricomorphs: **SM**, undifferentiated **DM**, differentiated **IOZM**, **AZM** and **PZM**, **T**, **IP**, and **EP**. One of the few papers on the musculature of this species focusses only on the ZM/'medial' masseter, and also identifies these three subdivisions of that complex (Maier, Klingler and Ruf, 2002), while another only discusses the **SM** and **DM** (Hennekam, 2022). This species is the representative of Gliridae in this sample, a family in the squirrel-related clade that contains both hystricomorphs and myomorphs (Hautier, Cox and Lebrun, 2015).

Based on the appearance of an attachment site and possible insertion, *G. nagtglasii* is here interpreted to contain a **PM**, similar to *A. rufa*. All muscles except for the **PM** seem to originate from and attach to the same bones as in *C. porcellus* and their attachments are shown in Figure 2.23, but the **EP** origin is identified here in a fossa on the lateral face of the alisphenoid and categorised as anterior offset; this makes it the only hystricomorph in the

anterior offset category, which may perhaps be a result of phylogenetic constraints.

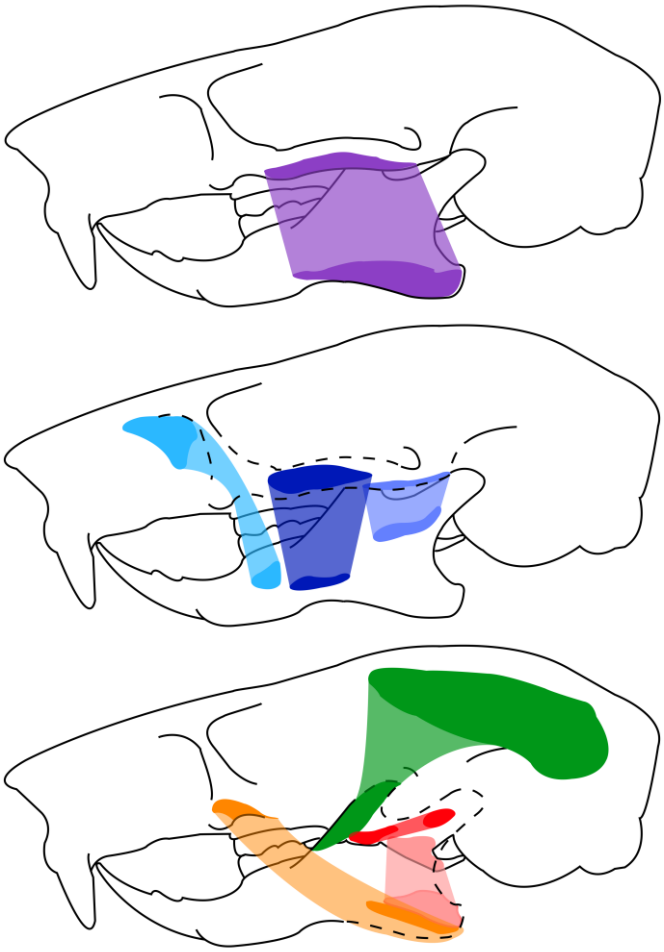

Figure 2.23: Muscle attachments in *Graphiurus nagtglasii*.

The existing paper that mentions the **SM** does not mention a *pars reflexa*, which I do identify based on the presence of a fossa here; that paper marks the muscle on the lateral face of the angle only, but makes no detailed description of its insertion (Hennekam, 2022). Similarly to most other hystricomorphs in this analysis, the ZM complex inserts lateral to the coronoid process, with no elongate fossa like that of *C. porcellus*. Due to its large infraorbital foramen and muscle differentiations, *G. nagtglasii* was classified in this analysis as a hystricomorph. Despite the proposed presence of a **PM** and its (unique among the hystricomorphs) anterior offset **EP** origin configuration, the shape of the zygomatic arch and arrangement of muscles do not match those of the assigned protrogomorphs.

2.3.2.14 – *Hydrochoerus hydrochaeris* ('Capybara')

H. hydrochaeris (Hydrochoerinae), despite a few unique characteristics in their orientations, possesses the muscle differentiation typical of a hystricomorph: **SM**, undifferentiated **DM**, differentiated **IOZM**, **AZM** and **PZM**, **T**, **IP**, and **EP**. The attachments are shown in Figure 2.24. Most

of these muscles are here suggested to originate from and attach to the same bones as in *C. porcellus*, with one notable exception that has a distinct origin position. The **IOZM** is here inferred to originate within the infraorbital foramen high up close to the dorsal margin of the foramen, the zygomatic arch here is broad and exhibits a clear fossa that aligns clearly with the insertion. The main paper that discusses the muscles of this taxon does not to mention this origin as being like this (Woods, 1972); perhaps I am only identifying the posterior extent of the origin, or of a different muscle? But if the origin mapped here is correct, this arrangement (not dissimilar to that of *G. capensis*, although the foramen is much larger proportionally) results in a relatively upright and straight **IOZM** line of action when in molar occlusion as shown in the figure, pulling the lower jaw upwards. If incorrect and the **IOZM** actually originates anteriorly to the foramen, the resulting muscle shape would have to be an exaggerated crescent-shape quite unlike any other rodent taxon, even more extreme than the shape of the muscle during incisor biting in *C. badius*.

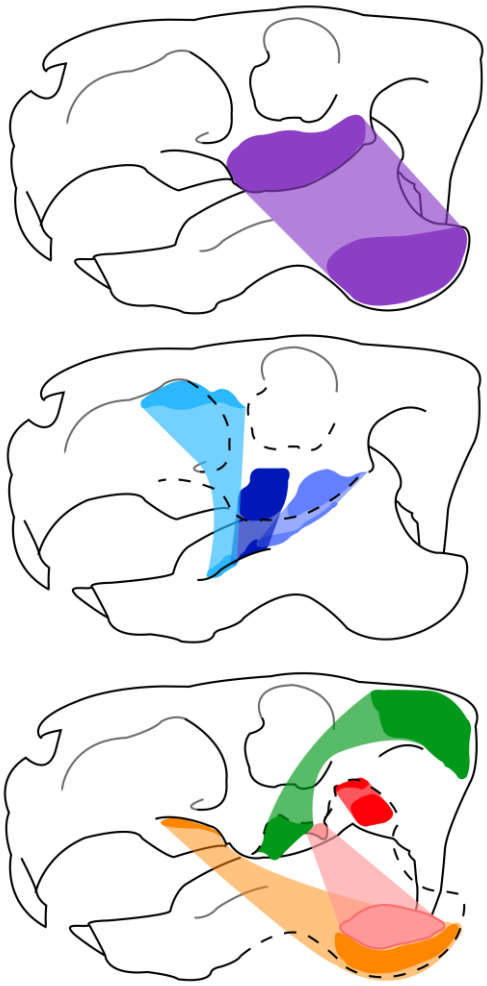

Figure 2.24: Muscle attachments in *Hydrochoerus hydrochaeris*.

The ZM complex as a whole was interpreted as inserting lateral to the coronoid process in an elongate fossa (as in *C. porcellus* and *L. maximus*)—which the literature concurs with (Woods, 1972)—but the relatively long rostrum and short zygomatic arch results in an unusual orientation of these muscles as a group, pulling posteriorly in all three muscles in incisor biting;

rodents typically exhibit an overall anterior line of action in most of these muscles, likely as part of their adaptation for gnawing, but given the relatively massive physical size of this species, the potential mechanical disadvantage when gnawing could perhaps be mitigated due to the mass of the muscles and the magnitude of the bite force produced.

The **SM** is here identified to have a *pars reflexa*, though the Woods does not explicitly discuss this muscle for this taxon, nor the **DM**, **AZM**, **PZM**, or **T**, **IP**, and **EP**, all of which he omits discussing in the case of *Hydrochoerus* (Woods, 1972). In the absence of specific discussion, I assume the attachments he noted in *Hydrochoerus* matched those of *Proechimys*; if so, *H. hydrochoeris* may have a portion of the **SM** that inserts on the ventral surface of the angle (Woods, 1972), and an **EP** that originates from the alisphenoid and lateral pterygoid plate(Woods, 1972), but the other muscle origins and insertions he identified were likely similar to those identified here. The other paper that includes analysis using the muscles of *H. hydrochoeris* does not subdivide the masseter or discuss its attachments (Álvarez, Perez and Verzi, 2013). Though Woods does not discuss the muscle in this taxon, *H. hydrochaeris* displays perhaps the clearest example of lateral offset of the **EP** origin identified in this sample, as can be observed in Figure 2.35; the upper molar tooth row extends back posterior to the relatively small pterygoid plates, and the **EP** is here suggested to originate in a well-defined fossa medial to the trench-like TMJ. The posterior extent of the tooth row would render a dorsal or anterior offset anatomically implausible by obstructing the muscle. Due to its large infraorbital foramen and muscle differentiations, *H. hydrochaeris* was classified here as a hystricomorph despite the unusual placement of the **IOZM** origin proposed here.

2.3.2.15 – *Hystrix cristata* ('Crested Porcupine')

H. cristata (Hystricidae) displays the muscle differentiation characteristic of hystricomorphs: **SM**, undifferentiated **DM**, differentiated **IOZM**, **AZM** and **PZM**, **T**, **IP**, and **EP**. This interpretation of its subdivisions aligns with the literature though some do not subdivide the **AZM** and **PZM**

and treat them as a single 'ZM' (Toldt, 1905; Turnbull, 1970; Morris, Cox and Cobb, 2022). The angle of the left hemimandible was broken off in this specimen, but was replaced using the intact right hemimandible. All muscles are here identified to originate from and attach to the same bones as in *C. porcellus*, and the **EP** origin on the alisphenoid is categorised as lateral offset due to the shape of the bones in the area displacing it laterally. The attachments are show in Figure 2.25.

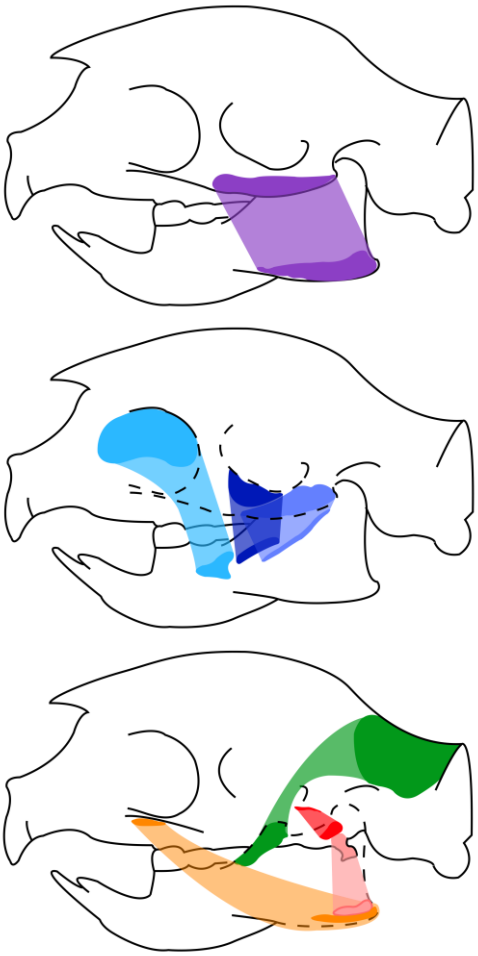

Figure 2.25: Muscle attachments in *Hystrix cristata*.

In *H. cristata* the ZM complex appears to insert on three distinct fossae lateral to the coronoid process, along the lateral face of the mandible; there is no deep elongate fossa lateral to the coronoid process for their attachment as in *C. porcellus*. Existing studies agree with this (Toldt, 1905; Turnbull, 1970).

Existing reconstructions can struggle to separate the fibres of the **SM** and **DM** (Toldt, 1905; Turnbull, 1970), making it difficult to tell if the **SM** in isolation has fibres which insert on the ventral mandible, though they also describe a *pars reflexa* (Toldt, 1905; Turnbull, 1970), as I identify here. Most of the muscle attachments I identify align with those described in the literature, and Turnbull describes the **EP** origin as occurring on the alisphenoid dorsal to **IP** the origin, similarly to the configuration observable in Figure 2.25. Due to its enlarged infraorbital foramen and undifferentiated **DM** *H. cristata* was classified in this analysis as a hystricomorph.

2.3.2.16 – *Lagostomus maximus* ('Plains Viscacha')

L. maximus (Chinchillidae) is here identified to possess the same differentiation of muscles as the selected hystricomorph, *C. porcellus*: **SM**, undifferentiated **DM**, differentiated **IOZM**, **AZM** and **PZM**, **T**, **IP**, and **EP**. There is little published information that explicitly mentions the muscle subdivisions of this species, with one only mentioning the **DM**, **IOZM**, **T**, and a **PM** that I do not identify here (Morgan *et al.*, 2007), but this does not discuss the nature of the attachments of these muscles; there is nothing I can confidently compare my interpretations to. The mapped attachments are shown in Figure 2.26. These originate from and insert on the same bones as in *C. porcellus*. In *L. maximus* the **PZM** is here interpreted as inserting in an elongate fossa lateral to the coronoid process, like that observed in *C. porcellus* though this fossa is less deep than its equivalent in *C. porcellus*; the **IOZM** and **AZM** both insert in their own fossae anterior to this. The **EP** originates from a prominent fossa medial to the TMJ, similarly to *C. porcellus*, and was therefore classified as lateral offset. *L. maximus*'s visibly long mandible compared to its skull (relative to other rodent taxa in the sample) results in visually similar slopes for the **SM** and **DM** when compared with *C. porcellus*, which has a proportionally similar skull and mandible. *L. maximus* was classified in this analysis as a hystricomorph based on its large infraorbital foramen and its

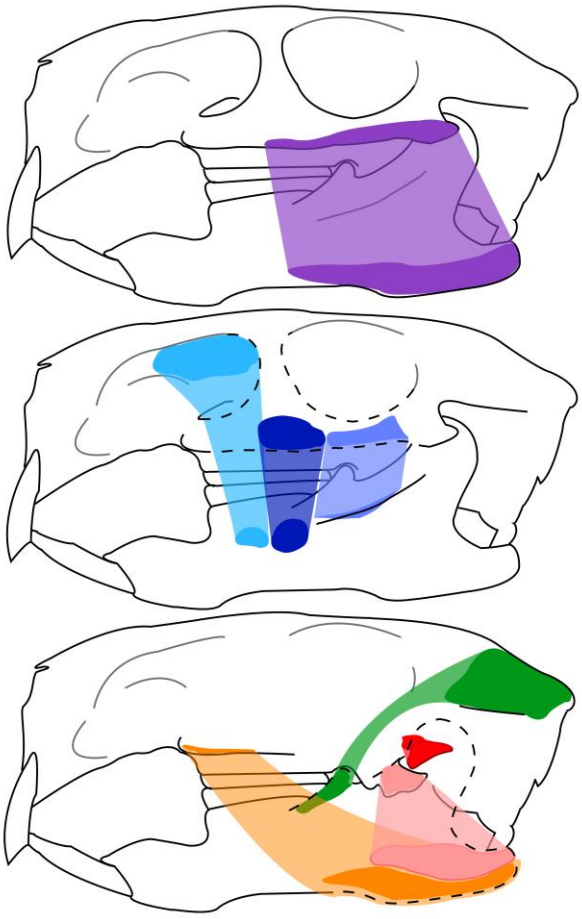

Figure 2.26: Muscle attachments in *Lagostomus maximus*.

muscle differentiation, and of all the hystricomorphs in the sample this taxon appears to be the most visually similar to *C. porcellus*'s configuration.

2.3.2.17 – *Laonastes aenigmamus* ('Kha-nyou' or 'Laotian Rock Rat')

L. aenigmamus (Diatomyidae) has the muscle differentiation of a hystricomorph, but with a number of distinct characteristics in the orientation of these muscles. Existing papers identify the same muscle divisions on the skull that I reidentify here (Hautier and Saksiri, 2009), though one paper identifies additional subdivisions of the **IOZM** that I do not (Cox, Kirkham and Herrel, 2013). It is here identified to possess an **SM**, undifferentiated **DM**, differentiated **IOZM**, **AZM** and **PZM**, **T**, **IP**, and **EP**. The attachments are shown in Figure 2.27. These originate from and insert on the same bones as in *C. porcellus*. This agrees with existing dissections, for example where the **AZM** and **PZM** are described as inserting on the lateral face of the mandible (Hautier and Saksiri, 2009) with no elongate fossa like that of *C. porcellus*. I identify a *pars reflexa* in the **SM**, which existing study does identify in addition to fibres inserting on the ventral surface of the angle (Hautier and Saksiri, 2009).

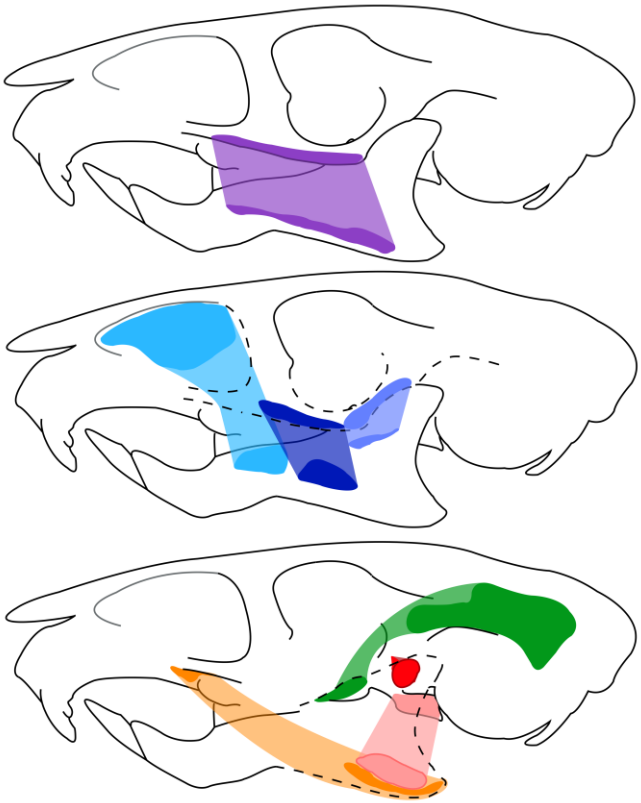

Figure 2.27: Muscle attachments in *Laonastes aenigmamus*.

L. aenigmamus has the longest skull in proportion to its dorsoventral height among the sample. This correlates with relatively short muscle length

for some muscles such as the **DM**. The **EP** was mapped on a rough patch of the alisphenoid almost directly dorsal to the origin of the **IP**, and was classified as dorsal offset; existing study identifies the origin as on the alisphenoid, maxillary, and lateral pterygoid plate (Hautier and Saksiri, 2009). For the most part, the muscle origins and insertions I mapped here (with the exception of the insertions of AZM and PZM) are in agreement with the existing dissection (Hautier and Saksiri, 2009). With its enlarged infraorbital foramen and muscle differentiation, *L. aenigmamus* was classified as a hystricomorph.

2.3.2.18 – *Myocastor coypus* ('Coypu')

M. coypus (Echimyinae) displays the typical muscle differentiation of a hystricomorph: **SM**, undifferentiated **DM**, differentiated **IOZM**, **AZM** and **PZM**, **T**, **IP**, and **EP**. These identified subdivisions are known in existing literature, though the fibres of the **AZM** and **PZM** are often inseparable, and a **PM** is described (Woods, 1972; Woods and Howland, 1979). The identified attachments are shown in Figure 2.28.

These muscles originate from and attach to the same bones as in *C. porcellus*, and the **EP** similarly originates from a fossa medial to the TMJ as was classified here as lateral offset, though existing papers describe it as originating from the lateral pterygoid plate, alisphenoid, and maxillary (Woods, 1972; Woods and Howland, 1979). The ZM

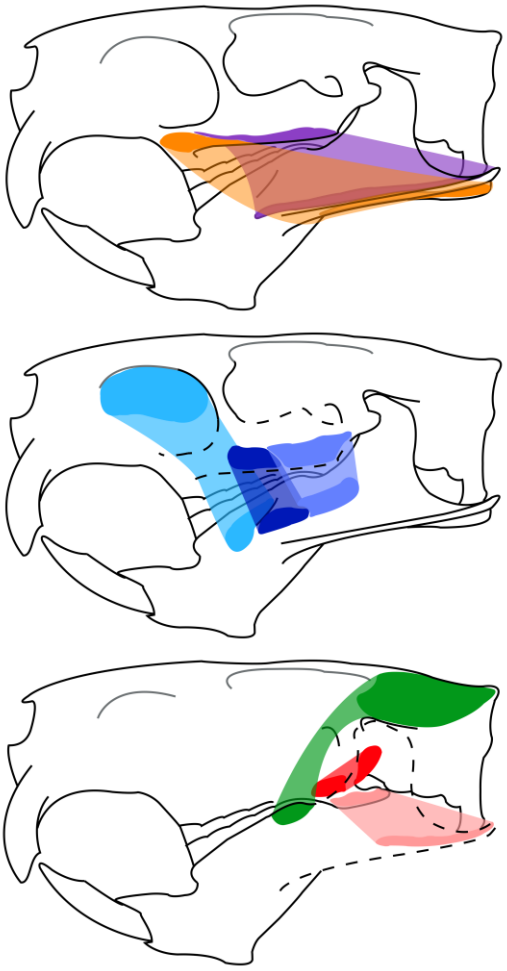

Figure 2.28: Muscle attachments in *Myocastor coypus*.

complex insertions identified here agree with the literature, which identifies them as inserting lateral to the coronoid process (Woods, 1972; Woods and Howland, 1979). Mapping the insertion of the **T** was difficult due to the reduced coronoid process; in the literature it is said to insert on the process (Woods and Howland, 1979) or "a flattened area of the dorsal surface of the mandible" (Woods, 1972), which may differ from where it was mapped here. Similarly to *C. opimus*, *C. pilorides*, and *O. degus*, *M. coypus* has a prominent 'shelf' on the lateral face of the angle, upon which the **DM** inserts, and in this case it results in a very short muscle length relative to the head length. I identify a *pars reflexa* for the insertion of the **SM**, though studies also identify fibres inserting on the ventral surface of the mandible (Woods, 1972; Woods and Howland, 1979). Aside from these stated differences, the attachments I identify match those described in the literature (Woods, 1972; Woods and Howland, 1979). With its enlarged infraorbital foramen and muscle differentiation, *M. coypus* was classified in this as a hystricomorph.

2.3.2.19 – *Octodon degus* ('Common Degu')

O. degus (Octodontidae) exhibits the same muscle differentiation as *C. porcellus*: **SM**, undifferentiated **DM**, differentiated **IOZM**, **AZM** and **PZM**, **T**, **IP**, and **EP**. Existing papers identify a **PM** in addition to these (Woods, 1972; Olivares, Verzi and Vassallo, 2004). The angle of the left hemimandible was absent in this specimen, but was reconstructed using the

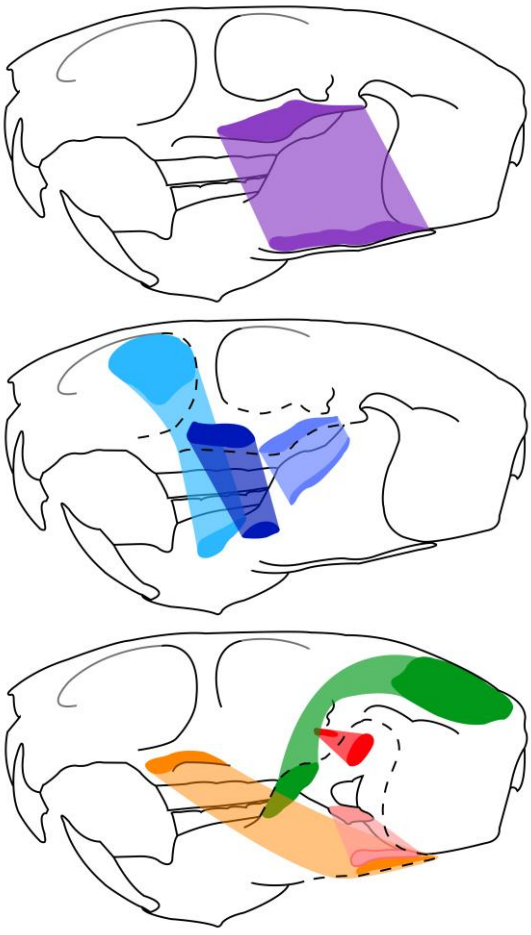

Figure 2.29: Muscle attachments in *Octodon degus*.

intact right hemimandible via mirroring and translation in Avizo. All muscles are here identified to originate from and attach to the same bones as in *C. porcellus*, and the **EP** is classified as lateral offset, originating from a fossa medial to the TMJ, though the literature describes its origin as from the alisphenoid and lateral pterygoid plate (Woods, 1972).

Due to relatively low position of the pterygoid plate and the high position of the posterior zygomatic root, relative to the tooth row, this results in a visually large dorsal distance between the two, as can be observed in Figure 2.29. Given the apparent attachment in this fossa, the pterygoid origin configuration was classified as lateral rather than dorsal offset despite this large dorsoventral distance between the two origins; existing papers describe its origin on the alisphenoid and lateral pterygoid. The portions of the ZM complex are here identified to insert lateral to the coronoid process with no elongate fossa like that of *C. porcellus*, in agreement with the existing study (Woods, 1972). Compared to some taxa, the zygomatic arch is elevated relative to the tooth row, to the point that the tip of the coronoid process is visible from a lateral view at molar occlusion; this correlates with tall, steep orientations for the **DM** and **PZM**. Aside from the **EP** origin, the attachments identified here align with those in the literature (Woods, 1972). Due to its muscle differentiation and its large infraorbital foramen, *O. degus* was classified in this analysis as a hystricomorph.

2.3.2.20 – *Pedetes capensis* ('South African Springhare')

P. capensis (Pedetidae) is identified here to possess the differentiation of a hystricomorph: **SM**, undifferentiated **DM**, differentiated **IOZM**, **AZM** and **PZM**, **T**, **IP**, and **EP**. Existing papers identify a **PM** in addition (Offermans and De Vree, 1989; Cox, 2017), but I do not. These muscles originate from and insert on the same bones as in *C. porcellus*, and their attachments are shown in Figure 2.30.

The **EP** was here classified as dorsal offset, originating from a fossa dorsal to the pterygoid plate; existing reconstructions seem to place this muscle slightly anterior to this, on the maxillary, with the origin extending anteriorly above the cheek teeth (Offermans and De Vree, 1989; Cox, 2017). The insertions of the ZM complex here agree with the existing study (Offermans and De Vree, 1989), and the **IOZM** insertion in particular is unusually large among this sample, associated with its especially large origin. The tall rostrum and huge infraorbital foramen, combined with the shortness of the head, result in an orientation for the large **IOZM** that does not curve substantially around the anterior zygomatic root to insert.

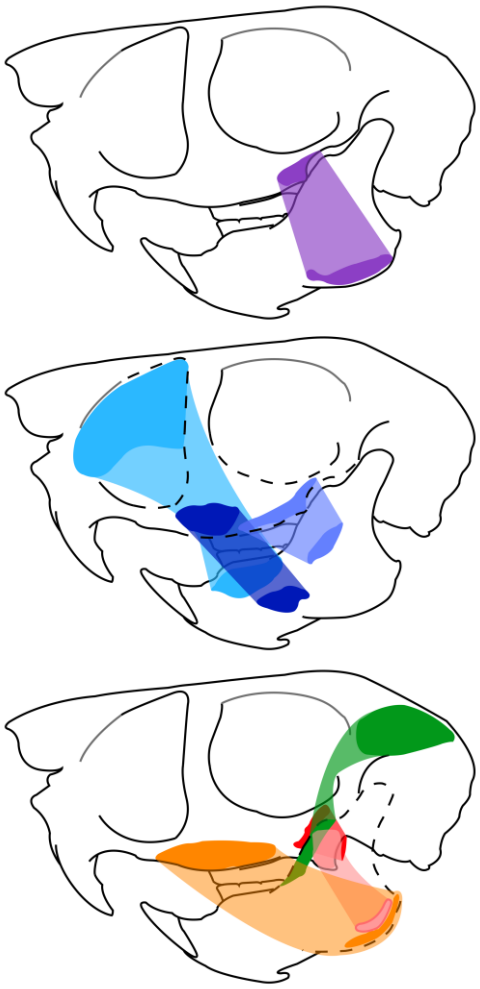

Figure 2.30: Muscle attachments in *Pedetes capensis*.

The **SM** appears to originate on a prominent fossa that is more lateral and posterior on the zygomatic arch than in other hystricomorphous taxa, and is here identified to insert low on the medial surface of the angle in a *pars reflexa*; existing papers align with this interpretation of the **SM**'s attachments (Woods, 1972; Offermans and De Vree, 1989). The **DM** inserts on a prominent shelf on the lateral face of the angle (similar to *M. coypus*, but curved due to the shape of the angle); the existing dissection paper agrees (Offermans and De Vree, 1989), but places the origins of the **DM** and **SM** visibly further forward. The coronoid process is shallow and not very strongly defined, but the insertion of the **T** was easily mapped; the older dissection's **T** matches this (Offermans and De Vree, 1989). Aside from specific differences

(e.g. the **EP** origin) discussed here, my interpretations align with the existing dissection (Offermans and De Vree, 1989). *P. capensis* was classified in this analysis as a hystricomorph, due to its large infraorbital foramen and its muscle differentiation.

2.3.2.21 – *Petaurista* sp. ('Giant Flying Squirrel')

This species of the genus *Petaurista* (Pteromyini), here assigned to *P. petaurista*, displays the typical muscle differentiation of a sciuromorph: **SM**, differentiated **ADM** and **PDM**, differentiated **AZM** and **PZM**, **T**, **IP**, and **EP**. Existing papers do identify this species as a sciuromorph (Cox, 2008), implying this differentiation, but unfortunately there is no detailed description or dissection to compare with the specific attachment sites I identify here. The first upper molars are missing on this specimen, but the mandible could be aligned using the remaining cheek teeth. Similarly to other sciuromorphs, it does not have an enlarged infraorbital foramen, and the zygomatic plate is oriented steeply. Like some other squirrels (such as *S. carolinensis*, and *Miopetaurista* (Casanovas-Vilar *et al.*, 2018)), *P. petaurista* has a postorbital processes on the frontal bone that does not connect to the zygomatic arch to form a postorbital bar. All muscles originate from and insert on the same bones as in *S.*

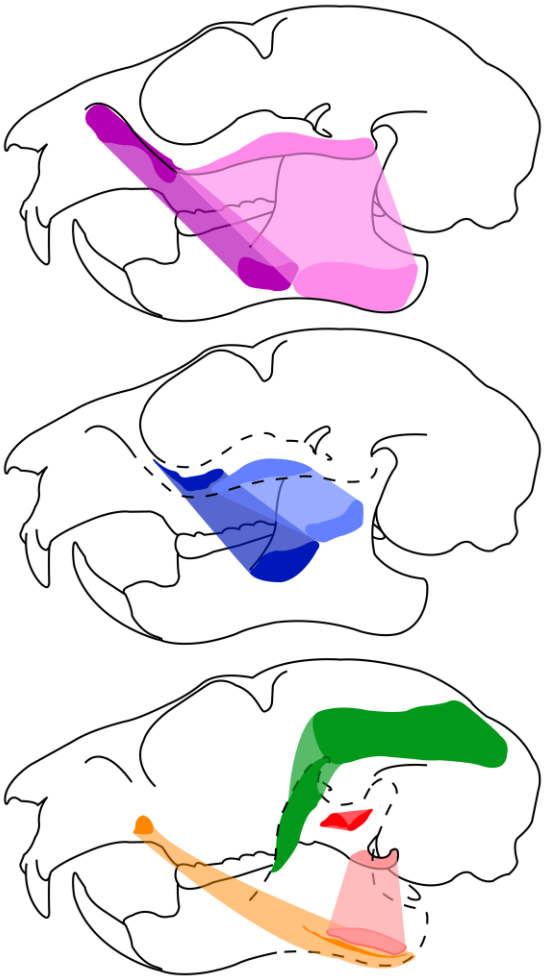

Figure 2.31: Muscle attachments in *Petaurista petaurista*.

carolinensis, with a *pars reflexa* for the **SM**. The attachments are shown in Figure 2.31.

The **EP** was classified here as dorsal offset (the same classification as *S. carolinensis*) originating from the ventral surface of the alisphenoid/squamosal. The **AZM** and **PZM** slope to have an anterior pull, in contrast to the apparent posterior-pulling orientation in *S. carolinensis*. *P. petaurista* was classified in this analysis as a sciuromorph, due to its muscle differentiation, zygomatic plate, and lack of an enlarged infraorbital foramen.

2.3.2.22 – *Phyllotis gerbillus* ('Peruvian Leaf-eared Mouse')

P. gerbillus (Cricetidae) has the same differentiation of muscles as *R. norvegicus*: **SM**, differentiated **ADM** and **PDM**, differentiated **IOZM**, **AZM** and **PZM**, **T**, **IP**, and **EP**. No detailed study could be found discussing the musculature of this species to compare against. All muscles are here proposed to originate from and attach to the same bones as in *R. norvegicus*. The attachments are shown in Figure 2.32.

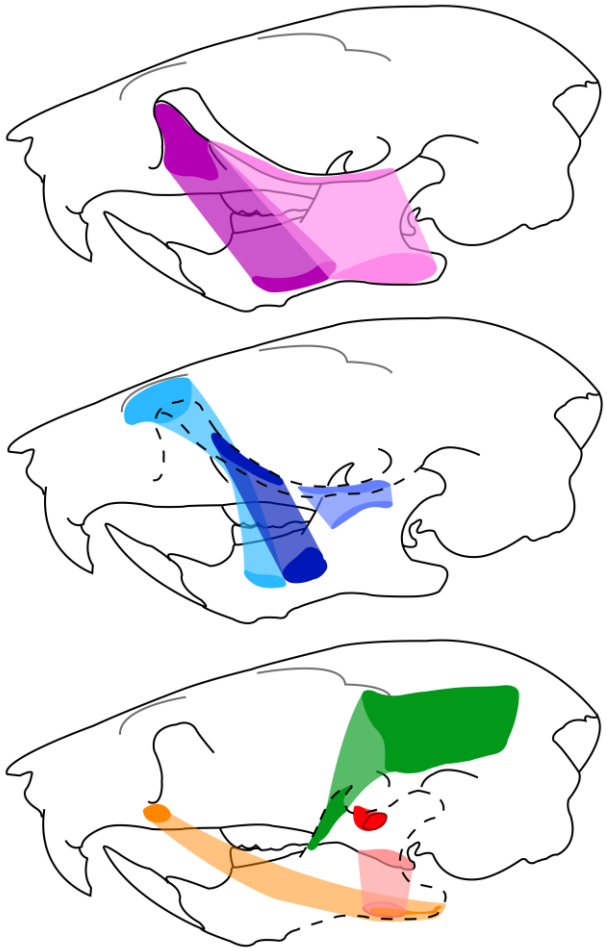

Figure 2.32: Muscle attachments in *Phyllotis gerbillus*.

The insertions of the **ADM** and **PDM** are here interpreted to be quite posterior relative to their origins when in molar occlusion. The 'domed' shape of the dorsal skull in lateral view and position of the **IOZM**

origin results in a line of action for the muscle that appears to curve relatively little in order to reach its insertion, when in molar occlusion. All three differentiated portions of the ZM complex are interpreted as inserting lateral to the coronoid process in a trio of associated fossae, with the **PZM** further from the **AZM** as is common, separated by the incisor root.

As in *R. norvegicus*, the **EP** origin is classified as anterior offset, identified as a rough patch on the posterior alisphenoid; similarly to *G. watersi*, this is closer to the suture with the squamosal than in *R. norvegicus* or *G. nagtglasii*, making the proportional difference in anteroposterior and dorsoventral distances between the **EP** and **IP** origins smaller than that observed in other anterior offset taxa. Despite these apparent irregularities, *P. gerbillus* was classified in this analysis as a myomorph, based on the differentiation of its muscles, zygomatic plate, and narrow enlarged infraorbital foramen.

2.3.2.23 – *Thomomys umbrinus* ('Southern Pocket Gopher')

T. umbrinus (Geomyidae) possesses the muscle differentiation of a sciuromorph: **SM**, differentiated **ADM** and **PDM**, differentiated **IOZM**, **AZM** and **PZM**, **T**, **IP**, and **EP**. An existing study of several species within Geomyidae provides a point of comparison, although the dissection conducted was on *T. bottae*, not *T. umbrinus* (Wahlert, 1985). Despite the distinctive shape of the lateral face of the mandible (with

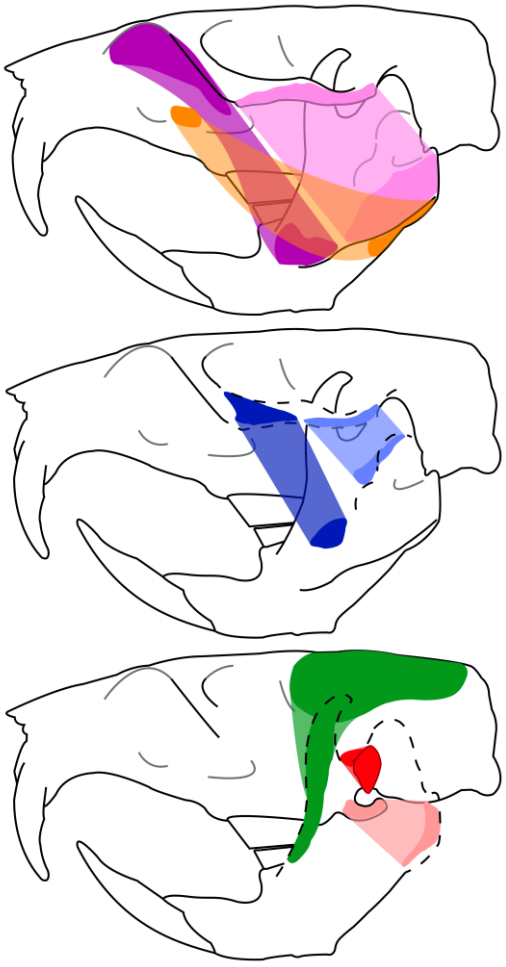

Figure 2.33: Muscle attachments in *Thomomys umbrinus*.

prominent crests and protrusions on the angle), all muscles are here thought to originate from and insert on the same bones as in *S. carolinensis*, and the **EP** origin was classified as dorsal offset, originating on the ventral surface of the alisphenoid/squamosal. The attachments are shown in Figure 2.33.

The **SM** is quite unusual, however, inserting on a prominent fossa on the ventral surface of the mandibular angle, with no identifiable *pars reflexa*; this agrees with the existing study, which identifies the **SM** as attaching on the ventromedial face of the angle (Wahlert, 1985). Both portions of the ZM complex insert lateral to the coronoid process, with the **PZM** inserting medially to the bulge of the incisor root. The **IP** insertion occurs alone on the medial face of the angle, similarly to that of *A. rufa* though the shape of the mandibular angle is very different when comparing these two taxa. The tall head, high zygomatic arch relative to the teeth, and curved mandible correlate with very long muscles for the **ADM**, **PDM**, **AZM**, and **PZM** (similarly to those observable in *C. badius*, which has a similarly curved mandible). The existing dissection describes the **IP** originating from the sphenopterygoid canal (no figure is shown there), but the identification of the **T** origin seems to be in agreement with mine, exempting additional subdivisions I did not identify or map (Wahlert, 1985). Wahlert describes part of the **T** as inserting medial to the coronoid process (Wahlert, 1985). Wahlert describes the insertions of the DM and ZM complexes collectively, inserting together in a large triangular fossa on the lateral face of the mandible (Wahlert, 1985). Unfortunately, most of the discussion on muscle attachments in that paper lacks detail that could be useful to compare with specific subdivisions here, and there are no figures providing a point of visual comparison.

With its zygomatic plate, lack of an enlarged infraorbital foramen, and differentiated deep masseter, *T. umbrinus* was classified in this analysis as a sciuromorph.

2.3.3 – Mechanical advantage results

Table 2.3 contains the raw data results of the mechanical advantage calculations for an incisor bite at zero degrees of gape. The taxa are arranged by their assigned morphotypes: fourteen hystricomorphs, six myomorphs, three protrogomorphs and four sciuromorphs.

Taxon	M	Mechanical Advantage (Zero Gape Incisor Bite)								
		SM	ADM	P/DM	IOZM	AZM	PZM	T	EP	IP
C. pilorides	H	0.663		0.349	0.756	0.529	0.230	0.263	0.004	0.074
C. porcellus	H	0.535		0.454	0.679	0.268	0.045	0.252	0.121	0.305
C. opimus	H	0.637		0.476	0.701	0.531	0.310	0.197	0.107	0.353
D. punctata	H	0.547		0.211	0.709	0.402	0.205	0.327	0.089	0.152
D. sagitta	H	0.626		0.414	0.645	0.448	0.001	0.202	0.134	0.208
E. dorsatum	H	0.589		0.417	0.812	0.464	0.050	0.365	0.148	0.210
G. nagtglasii	H	0.568		0.442	0.668	0.387	0.104	0.118	0.034	0.231
H. hydrochaeris	H	0.725		0.459	0.549	0.272	0.054	0.263	0.037	0.373
H. cristata	H	0.635		0.360	0.628	0.287	0.069	0.325	0.066	0.073
L. maximus	H	0.596		0.241	0.558	0.349	0.121	0.237	0.088	0.219
L. aenigmamus	H	0.624		0.456	0.636	0.445	0.155	0.177	0.073	0.118
M. coypus	H	0.527		0.406	0.631	0.307	0.128	0.342	0.082	0.267
O. degus	H	0.661		0.393	0.718	0.445	0.210	0.338	0.136	0.303
P. capensis	H	0.735		0.401	0.958	0.798	0.442	0.363	0.270	0.402
A. cahirinus	M	0.533	0.636	0.441	0.461	0.308	0.173	0.056	0.144	0.208
C. badius	M	0.568	0.613	0.500	0.705	0.412	0.092	0.084	0.169	0.201
C. gambianus	M	0.640	0.665	0.459	0.782	0.320	0.106	0.102	0.136	0.129
G. watersi	M	0.665	0.756	0.475	0.844	0.552	0.239	0.268	0.124	0.222
P. gerbillus	M	0.648	0.754	0.518	0.814	0.610	0.228	0.127	0.076	0.143
R. norvegicus	M	0.727	0.723	0.461	0.688	0.178	0.014	0.097	0.092	0.226
A. rufa	P	0.595	0.684	0.494		0.607	0.307	0.039	0.157	0.253
B. suillus	P	0.509		0.550	0.588	0.430	0.180	0.257	0.157	0.318
G. capensis	P	0.679		0.451	0.589	0.449	0.180	0.314	0.108	0.359
C. canadensis	S	0.555	0.814	0.466		0.554	0.286	0.164	0.118	0.369
P. petaurista	S	0.787	0.788	0.474		0.608	0.333	0.173	0.164	0.004
S. carolinensis	S	0.667	0.748	0.489		0.393	0.132	0.152	0.206	0.152
T. umbrinus	S	0.669	0.730	0.354		0.477	0.124	0.136	0.109	0.335

Table 2.3: Mechanical advantage results for the rodent sample during an incisor bite at zero gape. The empty, grey cells indicate that the taxon lacks the corresponding muscle. Values for the **DM** are highlighted in matching purple. The morphotypes (column '**M**'), are represented with a capitalised letter as shorthand: 'H' for hystricomorphy, 'M' for myomorphy, 'P' for protrogomorphy, and 'S' for sciuromorphy.

Some simple observations can be made within this table. The mechanical advantage of the **ADM**, where present, is notably higher than the mechanical advantage of the **PDM** or undifferentiated **DM**; this is a result of the **ADM**'s origins and insertions being anterior to those of the **PDM** and **DM**, which results in a longer in-lever. Taxa with an **ADM** therefore possess an additional muscle subdivision which has a higher mechanical advantage. Similarly, other muscles with origins anterior on the skull, such as the **SM** and **IOZM**, clearly tend towards higher mechanical advantages than muscles with shorter in-levers (e.g. **IP** or **EP**), as would be expected. However, there are outliers to this pattern due to the configuration of muscles in individual species. For example, *P. capensis*'s exhibits higher mechanical advantage than most other taxa on many muscles in the sample; this may be associated with the proportional shortness of its skull and mandible.

P. capensis's **AZM**, for example, possesses the highest mechanical advantage of the **AZM** at 0.798, greater than the mechanical advantage of any **SM**; even though the **SM** has one of the most anterior origins of any homologous muscle in the sample, the insertion being so far posterior on the angle can cause it to have a lower mechanical advantage than other muscles with a relatively posterior origin and anterior insertion. The individual variation of each taxon is not the focus of this study and will not be explored further in this thesis unless it relates clearly to broader comparisons. Comparing the morphotypes to one another is more easily accomplished visually and statistically than using Table 2.3.

These data are represented visually in Figure 2.34, a combined box plot showing the mechanical advantage of each muscle for each morphotype. Each morphotype is colour coded as in Figure 2.3. Due to the difference in sample size between hystricomorphs and other taxa, the ranges of these data should not be compared between morphotypes based on this box plot, but comparison of the means and boxes shows that the morphotypes display visually similar mechanical advantage on each muscle.

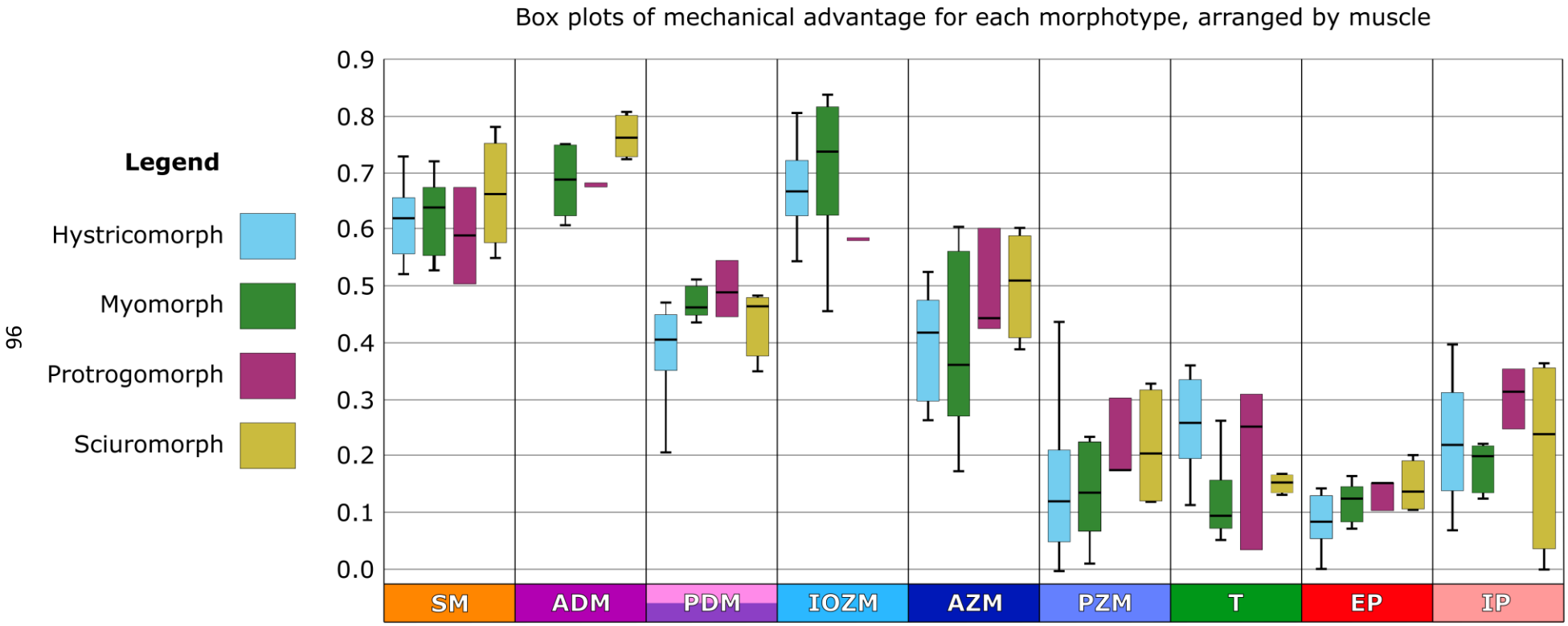

Figure 2.34: Box plot of mechanical advantage results. Hystricomorphs are in blue, myomorphs are in green, protrogomorphs are in pink, and sciuromorphs are in yellow. The muscles are arranged along the x-axis. The mean of a morphotype's mechanical advantage is marked by the black line within its box.

On Figure 2.34, a couple of details can be observed. For the **ADM**, the sciuromorphs exhibit slightly higher mechanical advantage, exceeding *A. rufa* and the majority of the myomorphs. For the **PDM**, protrogomorphs, myomorphs, and most sciuromorphs exhibit higher mechanical advantage than most hystricomorphs. Despite having the largest sample size, hystricomorphs only sometimes show the largest range of mechanical advantages on a given muscle, namely for the **DM** and **PZM**. Myomorphs show the largest range for the **IOZM** and **AZM**, sciuromorphs have the largest range for the **IP**, and protrogomorphs show the largest range on the **T** despite only having three taxa. For the **SM** and **EP**, the range of mechanical advantage in each morphotype is at its most consistent.

		SM	ADM	P/DM	IOZM	AZM	PZM	T	EP	IP
Phylogenetic signal	Blomberg's K	0.360	0.601	0.527	0.566	0.633	0.636	**1.007**	**0.706**	0.603
	p	0.951	0.436	0.355	0.256	0.091	0.072	**0.02**	**0.032**	0.102
Difference between Morphotypes	F	0.258	2.197	2.166	0.520	0.284	0.149	5.635	1.039	0.903
	p	0.957	0.477	0.439	0.827	0.945	0.981	0.144	0.755	0.774

Table 2.4: Table compiling the results of the phylANOVA, a statistical test that identifies the strength of the phylogenetic signal within the data and compares the difference between pre-defined groups (in this case, the morphotypes).

A phylogenetic ANOVA was performed for each individual muscle, comparing the mechanical advantage and using the morphotypes as the pre-defined groupings to compare, as outlined in the Materials & Methods section. The results of all these analyses are compiled in Table 2.4. The F-statistic determines whether the means of the morphotypes' mechanical advantages are significantly different. For all muscles, the p-value is greater than 0.05, and the null hypothesis cannot be rejected; the ANOVAs find no significant difference between the morphotypes' group means on any of the tested muscles. Blomberg's K measures the strength of the phylogenetic signal within the data. Only two muscles display a significant p-value for the K-test, the **T** ($p = 0.002$) and **EP** (0.032). In the case of the **T**, the K of ~1 implies that the variation is within the range of what would be expected under Brownian motion. In the case of the **EP**, its mechanical advantages are less similar than would be expected under Brownian motion. This implies

there is a phylogenetic signal affecting the mechanical advantage of the **EP**; this may be associated with the variation described in the three configurations of its origin in the earlier anatomical Results subheadings.

2.4 – Discussion

2.4.1 – Key questions and hypotheses

Throughout the Results subheading for each species, I established situations where muscles were not identified by me, but were identified in pre-existing analyses. For brevity, this will not be reiterated here after the extensive taxon-by-taxon information presented above, but the **EP** origins, presence of a **PM**, and insertion of the **SM** were often points where these reconstructions differed from published work, even if the 2D lever-arm mechanics data is less affected by this than 3D analysis would have been.

Recapping from the Introduction, these methods aimed to identify if there is an observable difference in mechanical advantage between the four morphotypes during gnawing at zero degrees of gape. I hypothesised (**H1.1**) that the morphotypes would not be significantly different in these results, and that the broad disparity within morphotype categories would result in their mechanical advantage ranges overlapping with each other. Secondly, I hypothesised (**H1.2**) that there would be no significant phylogenetic signal in the mechanical advantage data, likely due to the para/polyphyletic nature of the groups and the variation and diversity within each morphotype category.

The phylANOVA results clearly support **H1.1**. No muscle possesses a statistically significant difference between morphotypes in these results. This implies that the variance in mechanical advantage among these rodents is determined by different factors beyond morphotype alone, factors not tested in this simple analysis. All the morphotypes clearly show broad ranges in mechanical advantage for each muscle; this might be correlated with the wide variation in diet or function/behaviour within each group, factors which can be partially assessed using the variables explored in Chapter 3. As for **H1.2**, it is partially refuted as there are statistically p-values in the K tests of the **T** and **EP**. In the case of the **T**, the variation is within the range of Brownian motion. In the case of the **EP**, the variation is less than would be expected

under Brownian motion. No subdivision of the masseter exhibits a statistically significant phylogenetic signal.

There are observable differences and patterns that, despite not being statistically significant, are worth discussing here. For example, in the raw mechanical advantage results, it can be clearly observed that anterior muscles tend to have a higher mechanical advantage than posterior muscles, because their anterior position gives a longer in-lever, as expected. Anterior expansion of muscles—whether a muscle is differentiating or simply extending its attachments anteriorly—could contribute to this across a masticatory system, making the system as a whole more efficient. Previous studies have inferred that hystricomorphs are more specialised for chewing than for gnawing, compared to sciuromorphs (Becht, 1953; Wood, 1965; Druzinsky, 2010; Cox, Kirkham and Herrel, 2013). If comparing the **ADM** and **DM**, the differentiation of the deep masseter in myomorphs, sciuromorphs, and *A. rufa* could provide an increased bite force due to the addition of the higher mechanical advantage anterior portion. It can be observed here that in sciuromorphs, the **ADM** shows consistently high mechanical advantage, in keeping with the established theory that they are specialised for incisor gnawing. In contrast, hystricomorphs lack an **ADM**, but their **IOZM** is not significantly different from that of other morphotypes, which could imply that they are not adapted for higher bite forces with the incisors. The fact that sciuromorphs (which possess an **ADM** and lack an **IOZM**) cannot be clearly distinguished in mechanical advantage either may suggest that the **ADM** in sciuromorphs may serve a similar role to the **IOZM**, as an anteriorly-extended muscle for increased mechanical advantage of their masticatory system at large as an adaptation towards gnawing as has been previously suggested (Wood, 1965; Druzinsky, 2010). Perhaps, similarly, the presence of the atypical **IOZM** noted in *B. suillus* and *G. capensis* might fulfil a role like the **ADM** in *A. rufa* as a large anterior muscle with high mechanical advantage? If this is correct, then during their evolution from hystricomorphous ancestors (Cox, Faulkes and Bennett, 2020), rather than differentiating their deep masseter as in *A. rufa*, the bathyergids may have retained the **IOZM** for a similar

mechanical function despite the reduction of the infraorbital foramen relative to hystricomorphs. Evaluating this hypothesis in depth would require further exploration of the mechanical similarities and differences between the **ADM** and **IOZM**. The two muscle subdivisions will be compared in the analyses of Chapter 3.

For the most part, the granular detail of the muscle attachments in these taxa were discussed on a taxon-by-taxon basis in the Results section. Some anatomical observations in the existing literature could not be identified in this study, due to the difference in method and sample, and these were also discussed under their taxon subheadings where relevant.

In summary the Key Questions that were laid out have been answered, **H1.1** is supported, and **H1.2** is partially refuted as two muscles do have a phylogenetic signal.

2.4.2 – Pterygoid configurations

After muscle mapping I assigned the pterygoid muscles to three categories based on the arrangement of their origins: dorsal, lateral, and anterior offset. From what I can find, this does not seem to have been discussed in existing research (likely due to the relative lack of comparison in these specific muscle origins between taxa, let alone across the tree) and the interpretation here is novel. These assigned categories have no observable impact on the comparison of morphotype groups as a whole, and appear to be a minor variation associated with the morphology of the bones in the area.

Since the Lever-Arm mechanics analysis is in 2D, the differences between the dorsal and lateral categories are not quite accounted for by the mechanical advantage data. As such the muscle vectors and lengths for the **EP** were effectively analysed as two groups in the quantitative analyses: the four anterior-offset myomorphs, and all other taxa with dorsal or lateral offsets. This might be why the **EP** exhibits a significant phylogenetic signal. Perhaps a future analysis with the muscle's data categorised by the assigned

configuration category, for 3D mechanical advantage, could explore the effects of the potential variation in this muscle's origin.

The differences between and identification of these categories will be discussed in more detail here. Due to the lack of soft-tissue in these scans, these are inferred characteristics based on the bone surfaces and should be treated with due scepticism. These category labels appear to be three 'end members' of a continuous spectrum, as the possible origin of the **EP** is restricted by the posterior extent of the tooth row, the shape of the zygomatic arch, squamosal and alisphenoid, and other developmental restrictions that may be imposed by soft-tissues in the area that do not show on these scans. These three categories should not be treated as hard and defined classifications, instead they are an observation of three suggested patterns in the placement of the origin. The most extreme and easily visible example of each category is displayed diagrammatically in Figure 2.35.

Unfortunately, existing research to compare this categorisation with is very limited. At the time of this study, there was no comprehensive published analysis of the **EP** origins across Rodentia. It is possible that the attachment surfaces are being misinterpreted in this analysis, and that the **EP** does not in fact originate in these ways. Existing study that inclined the **EP** typically kept observations of variation in the position of the muscle brief, or the **EP** was only mentioned in passing, or without diagrams or visual aids that have visual detail to compare with these models (Turnbull, 1970; Satoh, 1999). Existing research characterises the **EP** as originating from the squamosal, alisphenoid or pterygoid wing in mammals (Turnbull, 1970). According to some of the descriptions and figures in Turnbull's book, in some mammals the external pterygoid's origin can be divided into an area that extends onto the pterygoid wing (which might be similar to the anterior offset discussed here), and a region that originates from the alisphenoid or the alisphenoid and squamosal (perhaps the dorsal and lateral offsets discussed here) (Turnbull, 1970). If this comparison is correct—and the limitations of verbal description make that unclear—it may be that the **EP** origin is quite large in rodents and I am only identifying the most pronounced part of its origin in

each specimen; I may only be mapping one of the two 'heads' Turnbull describes, but without soft-tissue data I cannot know for certain. An analysis of the soft-tissue via physical or digital dissection could identify whether some of these taxa have one 'head' being more prominent than the other (which could explain the differences in identified attachments here), and connect this to the potential variation in the direction of pull and the function of the muscle in different taxa.

For comparison, Turnbull identified the **EP** of *Sciurus niger* as originating from above the **IP**, with its origin extending to posterior to rearmost upper molar (Turnbull, 1970). In my analysis I categorised the muscle in *S. carolinensis* as 'dorsal offset', and identified it as originating from the alisphenoid/squamosal. They are different species of the genus *Sciurus*, and based on Turnbull's description and figure, I might have classified the muscle as 'anterior offset' if *S. niger* had been in this sample. Turnbull does study *R. norvegicus*, and identifies the **EP** as originating from the lateral face of the pterygoid, behind the teeth (Turnbull, 1970); my own identification of it in this study agrees with this interpretation, and assigns it to the 'anterior offset' category, though other papers disagree and identify the origin as occurring posterodorsal to this, which that I would classify as 'dorsal offset' (Hiiemae, 1971). Turnbull also identifies the **EP** of *Hystrix* (no species given) as originating dorsal and lateral to the **IP** (Turnbull, 1970). In my analysis, I classified it as 'lateral offset', an interpretation that independently came to a similar conclusion as this previous description. Unfortunately, Turnbull only studied a small number of rodents in that particular book, and describes none that fit with the observations I here assign to the 'dorsal offset' category; nonetheless, I feel that this existing description of the variation in the origin of this muscle suggests that my identification of these patterns here is not without precedent within Mammalia.

Taxa with an anterior offset configuration tend to have a relatively large anteroposterior distance between the pterygoid plate where the **IP** attaches and the rearmost upper molar, and have a notable fossa anterodorsal to the medial pterygoid plate itself. *R. norvegicus* is the

representative shown in Figure 2.35. Based on the position of the mandible at occlusion, the identified insertion, the interpreted positions of the other jaw closing muscles and the lack of a clearly defined attachment elsewhere, this fossa was interpreted as being the **EP** origin. At the extreme, the anteroposterior–distance between the muscle centroids is much longer than the dorsoventral distance between the two origins, but in taxa with pterygoid plates that extend further ventrally these two distances can be more similar. Due to the position of hard-tissue or inferred soft-tissue, dorsal or lateral attachment appears to be less plausible in this taxon, requiring deflection around the condylar process and jaw joint that would obstruct or impair the functioning of the muscle. The zygomatic arch seemingly tends not to attach high up relative to the tooth row in anterior offset taxa (as it does in some taxa in the sample) though this may be part of the sampling rather than associated with this category itself.

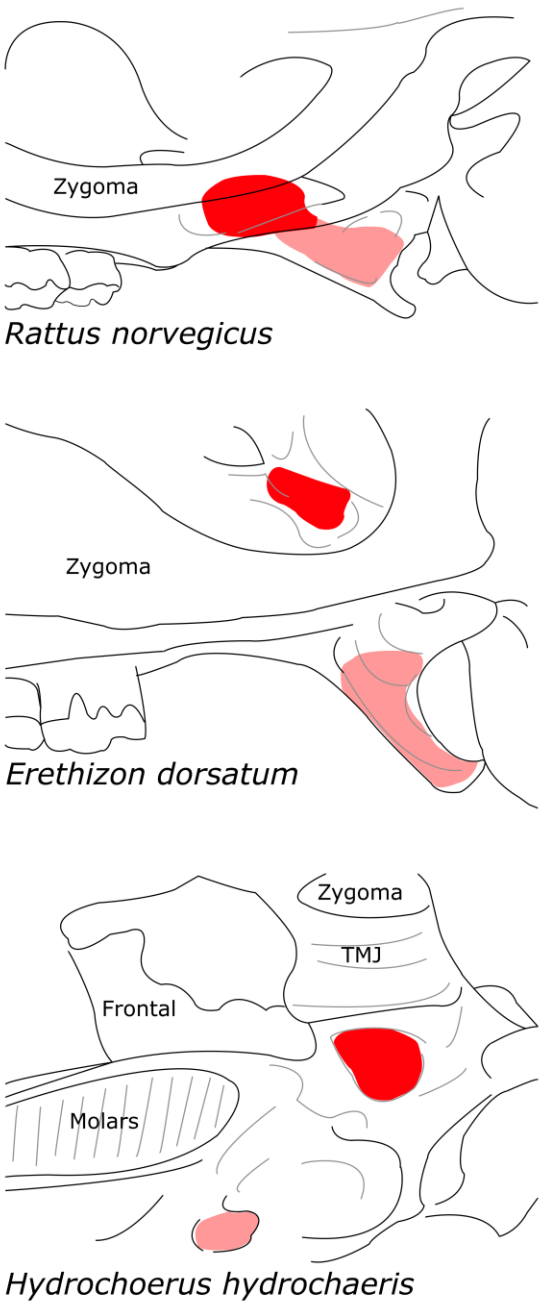

Figure 2.35: Panel figure displaying the category of three selected taxa. The muscle attachments are shown in colour (**EP**, and **IP**). *R. norvegicus* in left lateral view is the representative of the anterior offset category; *E. dorsatum* in left lateral view represents the dorsal offset; and *H. hydrochaeris* in ventral view represents the lateral offset.

Taxa with a 'dorsal offset' origin form the largest group among the sample, spread across morphotypes. *E. dorsatum* is shown in Figure 2.35. These taxa lack the apparent fossae of those classified as anterior offset and lateral offset, and typically have a flattened, rough, or faintly defined region on the anterior or ventral alisphenoid or squamosal. From this apparent attachment to the insertion on the mandible, there do not appear to be any hard-tissue obstructions the muscle would have to curve around, and the proposed path of the muscle would not interfere with the inferred paths of the other jaw muscles, or with the movement of the mandible, or with the closure of the cheek teeth. Typically, this results in an origin for the **EP** that is almost directly above the origin of the **IP** when viewed from the side; the mediolateral distance between the two attachments is smaller than that of those described as 'lateral offset', which have a different origin on the zygomatic root.

'Lateral offset' is defined by the presence of a prominent fossa medial to the TMJ. Functionally, the dorsal distance between the two origins can be similar to dorsal offset (making them appear similar in lateral view diagrams like those in the Results section) but the origin is displaced laterally away from the alisphenoid suture and towards the TMJ and zygomatic root. Unfortunately, this cannot be accounted for in 2D Lever-arm mechanics data such as this—this is why these categories were not analysed quantitatively in this study despite being a point of interest identified after data collection, they would require entirely different 3D analyses supported by anatomical data and dissection information that was not available for this study. Expanding into such an analysis was deemed beyond the scope and focus of this project on the morphotype categories. In lateral offset taxa, the shape of the posterior tooth row clearly obstructs any possible anterior or dorsal origin; the muscle would have to curve around the tooth row or else obstruct the occlusion of the posterior molars. With little or no observable origin medially, the prominent fossa was interpreted as the muscle's origin, and is at its most clear and extreme in *H. hydrochaeris*, shown in Figure 2.35. In *H.*

hydrochaeris, the displacement of the **EP** origin even results in its origin occurring notably posterior to the **IP**.

2.4.3 – Limitations of this study, and ways to expand

Ultimately, the variation among muscle configuration is greater in scope than the results of this study alone. Twenty-seven taxa out of over two thousand species forms a limited sample despite its broad distribution across families, and the lack of soft-tissue information for many taxa compounds this limitation in terms of restricting the kind of hypotheses that can be tested. Future anatomical or dissection data, projects studying of the external pterygoid across Rodentia, or other analyses could evaluate the accuracy of the interpretations herein, and their potential significance. As should be clear from the Results section and differing muscle identifications to existing papers, soft-tissue information could substantially increase the accuracy of muscle mapping: the **EP** origins, the differentiations of the **T**, and the presence and configuration of the **PM** are all notable points that could be improved. Furthermore, this analysis can only compare muscles that taxa possess; I chose not to produce a resultant vector and compare the entire muscular system of these taxa against all other taxa, as there are 'blank datapoints' where subdivisions of certain muscles are absent. There may be differences in their mechanical systems beyond the scope of this specific focus on the mechanical advantage of homologous muscles. It must also be noted that the muscles compared in this study are homologous in anatomy and arrangement, but this does not necessarily indicate homology of function. These results alone are not conclusive in implying homology of function among the groups due to the observable variation within each muscle.

Earlier in this Discussion, I made a comparison between the **IOZM** and **ADM**, suggesting that the **IOZM**'s enlarged size and high mechanical advantage in hystricomorphs may be performing a similar function as the

ADM in myomorphs and sciuromorphs. The two muscles will be compared in Chapter 3, but the potential intricacies of comparing them are not possible to explore fully through these methods, as it is limited by the lack of contrast-enhanced CT or dissection-based evaluation of the muscle tissues beyond their attachment surfaces in this study. The infraorbital foramen is notably enlarged in hystricomorphs compared to myomorphs, and therefore provides much more space for the **IOZM**, and enlargement of this muscle (which originates anterior to the **ADM**) could offset a potential difference in performance from **DM** differentiation alone; variations in muscle mass, pennation, or other anatomical characteristics that are not preserved on the bones could add significant complexity to these data, or illuminate differences between the morphotypes that are absent in this study.

Such soft-tissue analyses are beyond the scope of this project and the material available, but should be kept in mind when considering the limitations of these conclusions. Mechanical advantage does not differentiate between morphotypes in these results, and one of the shortcomings of these simple at-occlusion analyses is the basis of Chapter 3—the effect of gape and bite point on mechanical advantage, and whether these additional factors can illuminate differences between morphotypes.

2.5 – Conclusion

According to the analyses conducted, morphotypes do not have significantly different functional performance in terms of mechanical advantage at a simulated 0° gape incisor bite. As such, they do not appear to be categories of distinct functions, and therefore their patterns of muscle efficiency may be primarily impacted by other factors, such as potential evolutionary and developmental constraints (like the undifferentiated **DM** and differentiated **IOZM** of *B. suillus* and *G. capensis*) or by other factors such as diet or gape that have applied selective pressure for small specialisations.

However, they do possess anatomical differences and homologies in terms of muscle differentiation within and between their categories, and variation between taxa in the placement of muscles' origins and insertions. Whatever potential functional implications these differences may have could not be determined by these specific analyses.

Evaluation of a range of gapes, comparisons of incisor biting and molar biting, and incorporation of gape as a proxy of diet could all compare morphotypes with greater complexity and address several of these other factors. Chapter 3 will evaluate these in detail, to further compare these established groupings.

Bibliography

Adams, N.F., Rayfield, E.J., Cox, P.G., Cobb, S.N. and Corfe, I.J. (2019) 'Functional tests of the competitive exclusion hypothesis for multituberculate extinction', *Royal Society Open Science*, 6:181536. Available at: https://doi.org/10.1098/rsos.181536.

Álvarez, A. and Pérez, M.E. (2019) 'Deep changes in masticatory patterns and masseteric musculature configurations accompanied the eco-morphological evolution of cavioid rodents (Hystricognathi, Caviomorpha)', *Mammalian Biology*, 96, pp. 53–60. Available at: https://doi.org/10.1016/j.mambio.2019.03.009.

Álvarez, A., Perez, S.I. and Verzi, D.H. (2013) 'Ecological and phylogenetic dimensions of cranial shape diversification in South American caviomorph rodents (Rodentia: Hystricomorpha)', *Biological Journal of the Linnean Society*, 110(4), pp. 898–913. Available at: https://doi.org/10.1111/bij.12164.

Ball, S.S. and Roth, V.L. (1995) 'Jaw muscles of new world squirrels', *Journal of Morphology*, 224(3), pp. 265–291. Available at: https://doi.org/10.1002/jmor.1052240303.

Basu, C. and Hutchinson, J.R. (2022) 'Low effective mechanical advantage of giraffes' limbs during walking reveals trade-off between limb length and locomotor performance', *Proceedings of the National Academy of Sciences of the United States of America*, 119(28: e2108471119). Available at: https://doi.org/10.1073/pnas.2108471119.

Becerra, F., Casinos, A. and Vassallo, A.I. (2013) 'Biting performance and skull biomechanics of a chisel tooth digging rodent (*Ctenomys tuconax*; Caviomorpha; Octodontoidea)', *Journal of Experimental Zoology Part A: Ecological Genetics and Physiology*, 319(2), pp. 74–85. Available at: https://doi.org/10.1002/jez.1770.

Becerra, F., Echeverría, A.I., Casinos, A. and Vassallo, A.I. (2014) 'Another one bites the dust: Bite force and ecology in three caviomorph rodents (Rodentia, Hystricognathi)', *Journal of Experimental Zoology Part A: Ecological Genetics and Physiology*, 321(4), pp. 220–232. Available at: https://doi.org/10.1002/jez.1853.

Becht, G. (1953) 'Comparative biologic-anatomical researches on mastication in some mammals', *Proc. Koninklijke Nederlandse Akademie van Wetenschappen, Ser C*, 56, pp. 508–527.

Biewener, A.A., Farley, C.T., Roberts, T.J. and Temaner, M. (2004) 'Muscle mechanical advantage of human walking and running: implications for energy cost', *Journal of Applied Physiology*, 97, pp. 2266–2274. Available at: https://doi.org/10.1152/japplphysiol.00003.2004.

Blomberg, S.P., Garland, T. and Ives, A.R. (2003) 'Testing for phylogenetic signal in comparative data: behavioural traits are more labile', *Evolution*, 57(4), pp. 717–745. Available at: https://doi.org/10.1111/j.0014-3820.2003.tb00285.x.

Brandt, J.F. (1855) *Beiträge zur nähern Kenntniss der Säugethiere Russlands*.

Burgin, C.J., Colella, J.P., Kahn, P.L. and Upham, N.S. (2018) 'How many species of mammals are there?', *Journal of Mammalogy*, 99(1), pp. 1–14. Available at: https://doi.org/10.1093/jmammal/gyx147.

Byrd, K.E. (1981) 'Mandibular movement and muscle activity during mastication in the guinea pig (*Cavia porcellus*)', *Journal of Morphology*, 170(2), pp. 147–169. Available at: https://doi.org/10.1002/jmor.1051700203.

Casanovas-Vilar, I., Garcia-Porta, J., Fortuny, J., Sanisidro, Ó., Prieto, J., Querejeta, M., Llácer, S., Robles, J., Bernardini, F. and Alba, D.M. (2018) 'Oldest skeleton of a fossil flying squirrel casts new light on the phylogeny of the group', *eLIFE*, 7:e39270. Available at: https://doi.org/10.7554/eLife.39270.

Casanovas-Vilar, I. and Van Dam, J. (2013) 'Conservatism and adaptability during squirrel radiation: what is mandible shape telling us?', *PLOS One*, 8(4:e61298). Available at: https://doi.org/10.1371/journal.pone.0061298.

Cox, P.G. (2008) 'A quantitative analysis of the Eutherian orbit: Correlations with masticatory apparatus', *Biological Reviews*, 83(1), pp. 35–69. Available at: https://doi.org/10.1111/j.1469-185X.2007.00031.x.

Cox, P.G. (2017) 'The jaw is a second-class lever in *Pedetes capensis* (Rodentia: Pedetidae)', *PeerJ*, 5:e3741. Available at: https://doi.org/10.7717/peerj.3741.

Cox, P.G. and Baverstock, H. (2016) 'Masticatory muscle anatomy and feeding efficiency of the American beaver, *Castor canadensis* (Rodentia, Castoridae)', *Journal of Mammalian Evolution*, 23, pp. 191–200. Available at: https://doi.org/10.1007/s10914-015-9306-9.

Cox, P.G., Fagan, M.J., Rayfield, E.J. and Jeffery, N. (2011) 'Finite element modelling of squirrel, guinea pig and rat skulls: Using geometric morphometrics to assess sensitivity', *Journal of Anatomy*, 219(6), pp. 696–709. Available at: https://doi.org/10.1111/j.1469-7580.2011.01436.x.

Cox, P.G., Faulkes, C.G. and Bennett, N.C. (2020) 'Masticatory musculature of the African mole-rats (Rodentia: Bathyergidae)', *PeerJ*, 8:e8847. Available at: https://doi.org/10.7717/peerj.8847.

Cox, P.G. and Jeffery, N. (2011) 'Reviewing the morphology of the jaw-closing musculature in squirrels, rats, and guinea pigs with Contrast-Enhanced MicroCT', *The Anatomical Record*, 294, pp. 915–928. Available at: https://doi.org/10.1111/j.1469-7580.2011.01436.x.

Cox, P.G. and Jeffery, N. (2015) 'Chapter 13: The muscles of mastication in rodents and the function of the medial pterygoid', in P.G. Cox and L. Hautier (eds) *Evolution of the Rodents: Advances in Phylogeny, Functional Morphology and Development*. Cambridge University Press (Cambridge Studies in Morphology and Molecules: New Paradigms in Evolutionary Bio, 5), pp. 350–372. Available at: https://doi.org/10.1017/CBO9781107360150.

Cox, P.G., Kirkham, J. and Herrel, A. (2013) 'Masticatory biomechanics of the Laotian rock rat, *Laonastes aenigmamus*, and the function of the zygomaticomandibularis muscle', *PeerJ*, 1:e160. Available at: https://doi.org/10.7717/peerj.160.

Cox, P.G., Morris, P.J.R., Hennekam, J.J. and Kitchener, A.C. (2020) 'Morphological and functional variation between isolated populations of British red squirrels (*Sciurus vulgaris*)', *Journal of Zoology*. Edited by N. Bennett, 312(4), pp. 271–283. Available at: https://doi.org/10.1111/jzo.12829.

Cox, P.G., Rayfield, E.J., Fagan, M.J., Herrel, A., Pataky, T.C. and Jeffery, N. (2012) 'Functional evolution of the feeding system in rodents', *PLOS One*, 7(4). Available at: https://doi.org/10.1371/journal.pone.0036299.

Cox, Philip G and Hautier, Lionel (2015) *Evolution of the Rodents: Advances in Phylogeny, Functional Morphology and Development*. Edited by P. G. Cox and L. Hautier. Cambridge University Press (Cambridge Studies in Morphology and Molecules: New Paradigms in Evolutionary Bio, 5). Available at: https://doi.org/10.1017/CBO9781107360150.

Davis, J.L., Santana, S.E., Dumont, E.R. and Grosse, I.R. (2010) 'Predicting bite force in mammals: Two-dimensional versus three-dimensional lever models', *Journal of Experimental Biology*, 213(11), pp. 1844–1851. Available at: https://doi.org/10.1242/jeb.041129.

Dechow, P.C. and Carlson, D.S. (1990) 'Occlusal force and craniofacial biomechanics during growth in Rhesus monkeys', *American Journal of Physical Anthropology*, 83(2), pp. 219–237.

D'Elía, G., Fabre, P.H. and Lessa, E.P. (2019) 'Rodent systematics in an age of discovery: Recent advances and prospects', *Journal of Mammalogy*, 100(3), pp. 852–871. Available at: https://doi.org/10.1093/jmammal/gyy179.

Devlin, H. and Wastell, D.G. (1986) 'The mechanical advantage of biting with the posterior teeth', *Journal of Oral Rehabilitation*, 13(6), pp. 607–610. Available at: https://doi.org/10.1111/j.1365-2842.1986.tb00684.x.

Druzinsky, R.E. (1995) 'Incisal biting in the mountain beaver (*Aplodontia rufa*) and woodchuck (*Marmota monax*)', *Journal of Morphology*, 226(1), pp. 79–101. Available at: https://doi.org/10.1002/jmor.1052260106.

Druzinsky, R.E. (2010) 'Functional anatomy of incisal biting in *Aplodontia rufa* and sciuromorph rodents – Part 1: Masticatory muscles, skull shape and digging', *Cells Tissues Organs*, 191(6), pp. 510–522. Available at: https://doi.org/10.1159/000284931.

Druzinsky, R.E. (2015) 'Chapter 12 – The oral apparatus of rodents: variations on the theme of a gnawing machine', in P.G. Cox and L. Hautier (eds) *Evolution of the Rodents: Advances in Phylogeny, Functional Morphology and Development*. Cambridge University Press (Cambridge Studies in Morphology and Molecules: New Paradigms in Evolutionary Bio, 5), pp. 323–349. Available at: https://doi.org/10.1017/CBO9781107360150.

Echeverría, A.I., Becerra, F., Buezas, G.N. and Vassallo, A.I. (2017) 'Bite it forward … bite it better? Incisor procumbency and mechanical advantage in the chisel-tooth and scratch-digger genus *Ctenomys* (Caviomorpha, Rodentia)', *Zoology*, 125, pp. 53–68. Available at: https://doi.org/10.1016/j.zool.2017.08.003.

Endo, H., Satoh, K., Cuisin, J., Stafford, B. and Kimura, J. (2001) 'Morphological adaptation of the masticatory muscles and related apparatus in Asian and African Rhizomyinae species', *Mammal Study*, 26(2), pp. 101–108. Available at: https://doi.org/10.3106/mammalstudy.26.101.

Esselstyn, J.A., Achmadi, A.S. and Rowe, K.C. (2012) 'Evolutionary novelty in a rat with no molars', *Biology Letters*, 8(6), pp. 990–993. Available at: https://doi.org/10.1098/rsbl.2012.0574.

Fabre, P., Hautier, L., Dimitrov, D. and Douzery, E.J.P. (2012) 'A glimpse on the pattern of rodent diversification: a phylogenetic approach', *BMC Evolutionary Biology*, 12(88). Available at: https://doi.org/10.1186/1471-2148-12-88.

Fournier, M., Hautier, L. and Gomes Rodrigues, H. (2021) 'Evolution towards fossoriality and morphological convergence in the skull of Spalacidae and Bathyergidae (Rodentia)', *Journal of Mammalian Evolution*, 28(3), pp. 979–993. Available at: https://doi.org/10.1007/s10914-021-09550-z.

Freeman, P.W. and Lemen, C.A. (2008) 'Measuring bite force in small mammals with a piezo-resistive sensor', *Journal of Mammalogy*, 89(2), pp. 513–517. Available at: https://doi.org/10.1644/07-MAMM-A-101R.1.

García-Morales, P., Buschang, P.H., Throckmorton, G.S. and English, J.D. (2003) 'Maximum bite force, muscle efficiency and mechanical advantage in children with vertical growth patterns', *European Journal of Orthodontics*, 25, pp. 265–272. Available at: https://doi.org/10.1093/ejo/25.3.265.

Garland, T., Dickerman, A.W., Janis, C.M., Jason, A., Garland, T., Dickerman, A.W., Janis, C.M. and Jones, J.A. (1993) 'Phylogenetic analysis of covariance by computer simulation', *Systematic Biology*, 42(3), pp. 265–292. Available at: https://www.jstor.org/stable/2992464.

Gomes Rodrigues, H., Šumbera, R. and Hautier, L. (2016) 'Life in burrows channelled the morphological evolution of the skull in rodents: the case of African mole-rats (Bathyergidae, Rodentia)', *Journal of Mammalian Evolution*, 23, pp. 175–189. Available at: https://doi.org/10.1007/s10914-015-9305-x.

Gómez Cano, A.R., Hernández Fernández, M. and Álvarez-Sierra, M.Á. (2013) 'Dietary ecology of Murinae (Muridae, Rodentia): a geometric morphometric approach', *PLOS One*, 8(11 e79080). Available at: https://doi.org/10.1371/journal.pone.0079080.

Goswami, A., Noirault, E., Coombs, E.J., Clavel, J., Fabre, A.-C., Halliday, T.J.D., Churchill, M., Curtis, A., Watanabe, A., Simmons, N.B., Beatty, B.L., Geisler, J.H., Fox, D.L. and Felice, R.N. (2022) 'Attenuated evolution of mammals through the Cenozoic', *Science*, 378(6618), pp. 377–383. Available at: https://doi.org/10.1126/science.abm7525.

Greaves, W.S. (1983) 'A functional analysis of carnassial biting', *Biological Journal of the Linnean Society*, 20(4), pp. 353–363. Available at: https://doi.org/10.1111/j.1095-8312.1983.tb01596.x.

Greaves, W.S. (1985) 'The generalised carnivore jaw', *Zoological Journal of the Linnean Society*, 85(3), pp. 267–274. Available at: https://doi.org/10.1111/j.1096-3642.1985.tb01506.x.

Greaves, W.S. (2012) *The Mammalian Jaw*. Cambridge: Cambridge University Press. Available at: https://doi.org/10.1017/CBO9781139060851.

Hautier, L., Cox, P.G. and Lebrun, R. (2015) 'Chapter 10 – Grades and clades among rodents: the promise of geometric morphometrics', in *Evolution of the Rodents: Advances in Phylogeny, Functional Morphology and Development*. (Cambridge Studies in Morphology and Molecules: New Paradigms in Evolutionary Bio, 5), pp. 277–299. Available at: https://doi.org/10.1017/CBO9781107360150.

Hautier, L., Michaux, J., Marivaux, L. and Vianey-Liaud, M. (2008) 'Evolution of the zygomasseteric construction in Rodentia, as revealed by a geometric morphometric analysis of the mandible of *Graphiurus* (Rodentia, Gliridae)', *Zoological Journal of the Linnean Society*, 154(4), pp. 807–821. Available at: https://doi.org/10.1111/j.1096-3642.2008.00453.x.

Hautier, L. and Saksiri, S. (2009) 'Masticatory muscle architecture in the Laotian rock rat *Laonastes aenigmamus* (Mammalia, Rodentia): new insights into the evolution of hystricognathy', *Journal of Anatomy*, 215(4), pp. 401–410. Available at: https://doi.org/10.1111/j.1469-7580.2009.01130.x.

Hennekam, J.J. (2022) 'Comparative morphology of the dormouse skull and the influence of size and ecology', *Journal of Anatomy*, 240(5), pp. 914–935. Available at: https://doi.org/10.1111/joa.13596.

Hiiemae, K. (1971) 'The structure and function of jaw muscles in rat (*Rattus norvegicus* L.). III. The mechanics of the muscles', *Zoological Journal of the Linnean Society*, 50(1), pp. 111–132. Available at: https://doi.org/10.1111/j.1096-3642.1971.tb00754.x.

Hiiemae, K. and Ardran, G.M. (1968) 'A cinefluorographic study of mandibular movement during feeding in the rat (*Rattus norvegicus*)', *Journal of Zoology*, 154, pp. 139–154. Available at: https://doi.org/10.1111/j.1469-7998.1968.tb01654.x.

Hildebrand, M., Bramble, D.M., Liem, K.F. and Wake, D.B. (eds) (1985) *Funcitonal Vertebrate Morphology*. Cambridge, MA and London, UK: Harvard University Press. Available at: https://doi.org/10.4159/harvard.9780674184404.

Huby, A., Lowie, A., Herrel, A., Vigouroux, R., Frédérich, B., Raick, X., Kurchevski, G., Godinho, A.L. and Parmentier, E. (2019) 'Functional diversity in biters: the evolutionary morphology of the oral jaw system in pacus, piranhas and relatives (Teleostei: Serrasalmidae)', *Biological Journal of the Linnean Society*, 127, pp. 722–741. Available at: https://doi.org/10.1093/BIOLINNEAN%2FBLZ048.

Hunt, T.C., Grejtak, T., Kodangal, D., Varma, S., Rinaldi, C.E., Pathak, S., Krick, B.A. and Erickson, G.M. (2023) 'Microstructurally driven self-sharpening mechanism in beaver incisor enamel facilitates their capacity to fell trees', *Acta Biomaterialia*, 158, pp. 412–422. Available at: https://doi.org/10.1016/j.actbio.2022.12.051.

Jones, K. and Law, C.J. (2018) 'Differentiation of craniomandibular morphology in two sympatric *Peromyscus* mice (Cricetidae: Rodentia)', *Mammal Research*, 63, pp. 277–283. Available at: https://doi.org/10.1007/s13364-018-0364-2.

Koenigswald, W. von (1985) 'Evolutionary trends in the enamel of rodent incisors', in W.P. Luckett and J.L. Hartenberger (eds) *Evolutionary Relationships among Rodents*. Boston, MA: Springer (NATO Advanced Science Institutes (ASI) Series, 92), pp. 403–422. Available at: https://doi.org/10.1007/978-1-4899-0539-0_15.

Koenigswald, W. von and Clemens, W.A. (1992) 'Levels of complexity in the microstructure of mammalian enamel and their application in studies of systematics', *Scanning Microscopy*, 6(1), pp. 195–218. Available at: https://digitalcommons.usu.edu/microscopy/vol6/iss1/16.

Kunz, C. and Sakamoto, M. (2024) 'Elevated evolutionary rates of biting biomechanics reveal patterns of extraordinary craniodental adaptations in some herbivorous dinosaurs', *Palaeontology*, 67(e12689). Available at: https://doi.org/10.1111/pala.12689.

Lautenschlager, S. (2016) 'Reconstructing the past: Methods and techniques for the digital restoration of fossils', *Royal Society Open Science*, 3(10:160342). Available at: https://doi.org/10.1098/rsos.160342.

Ledevin, R. and Koyabu, D. (2019) 'Patterns and constraints of craniofacial variation in Colobine monkeys: disentangling the effects of phylogeny, allometry and diet', *Evolutionary Biology*, 46, pp. 14–34. Available at: https://doi.org/10.1007/s11692-019-09469-7.

Ma, W., Pittman, M., Butler, R.J., Lautenschlager, S., Ma, W., Pittman, M., Butler, R.J. and Lautenschlager, S. (2022) 'Macroevolutionary trends in theropod dinosaur feeding mechanics', *Current Biology*, 32(3), pp. 677–686. Available at: https://doi.org/10.1016/j.cub.2021.11.060.

Maier, W., Klingler, P. and Ruf, I. (2002) 'Ontogeny of the medial masseter muscle, pseudo-myomorphy, and the systematic position of the Gliridae (Rodentia, Mammalia)', *Journal of Mammalian Evolution*, 9(4), pp. 253–269. Available at: https://doi.org/10.1023/A:1023979212759.

Martin, T. (1993) 'Early rodent incisor enamel evolution: Phylogenetic implications', *Journal of Mammalian Evolution*, 1(4), pp. 227–254. Available at: https://doi.org/10.1007/BF01041665.

McIntosh, A.F. and Cox, P.G. (2016a) 'Functional implications of craniomandibular morphology in African mole-rats (Rodentia: Bathyergidae)', *Biological Journal of the Linnean Society*, 117(3), pp. 447–462. Available at: https://doi.org/10.1111/bij.12691.

McIntosh, A.F. and Cox, P.G. (2016b) 'The impact of gape on the performance of the skull in chisel-tooth digging and scratch digging mole-rats (Rodentia: Bathyergidae)', *Royal Society Open Science*, 3(10). Available at: https://doi.org/10.1098/rsos.160568.

Moore, W.J. (1967) 'Muscular function and skull growth in the laboratory rat (*Rattus norvegicus*)', *Journal of Zoology*, 152(3), pp. 287–296. Available at: https://doi.org/10.1111/j.1469-7998.1967.tb01645.x.

Morales-García, N.M., Gill, P.G., Janis, C.M. and Ray, E.J. (2021) 'Jaw shape and mechanical advantage are indicative of diet in Mesozoic mammals', *Communications Biology*, 4(333). Available at: https://doi.org/10.1038/s42003-021-01757-3.

Morgan, C.C., Olivares, A.I., Álvarez, A. and Verzi, D.H. (2007) 'Myoskeletal specialisations for digging in the rodent *Lagostomus maximus* (Caviomorpha, Chinchillidae)', in *Resúmenes del IX Congreso y 6 Jornadas de Educación*. *IX Congreso y 6 Jornadas de Educación*, La plata, Argentina: Sociedad de Ciencias Morfológicas

de La Plata, p. 55. Available at: https://sedici.unlp.edu.ar/bitstream/handle/10915/37447/Documento_completo.pdf?sequence=1.

Morris, P.J.R., Cobb, S.N.F. and Cox, P.G. (2018) 'Convergent evolution in the Euarchontoglires', *Biology Letters*, 14(8:20180366). Available at: https://doi.org/10.1098/rsbl.2018.0366.

Morris, P.J.R., Cox, P.G. and Cobb, S.N.F. (2022) 'The biomechanical significance of the elongated rodent incisor root in the mandible during incision', *Scientific Reports*, 12(3819). Available at: https://doi.org/10.1038/s41598-022-07779-z.

Nabavizadeh, A. (2016) 'Evolutionary trends in the jaw adductor mechanics of ornithischian dinosaurs', *Anatomical Record*, 299, pp. 271–294. Available at: https://doi.org/10.1002/ar.23306.

Navalón, G., Bright, J.A., Marugán-Lobón, J. and Rayfield, E.J. (2019) 'The evolutionary relationship among beak shape, mechanical advantage, and feeding ecology in modern birds', *Evolution*, 73(3), pp. 422–435. Available at: https://doi.org/10.1111/evo.13655.

Nies, M. and Ro, J.Y. (2004) 'Bite force measurement in awake rats', *Brain Research Protocols*, 12(3), pp. 180–185. Available at: https://doi.org/10.1016/j.brainresprot.2003.11.003.

Offermans, M. and De Vree, F. (1989) 'Morphology of the masticatory apparatus in the springhare, *Pedetes capensis*', *Journal of Mammalogy*, 70(4), pp. 701–711. Available at: https://doi.org/10.2307/1381705.

Olberding, J.P., Deban, S.M., Rosario, M.V. and Azizi, E. (2019) 'Modelling the determinants of mechanical advantage during jumping: Consequences for spring- and muscle-driven movement', in *Integrative and Comparative Biology*. Oxford University Press, pp. 1515–1524. Available at: https://doi.org/10.1093/icb/icz139.

Olivares, A.I., Verzi, D.H. and Vassallo, A.I. (2004) 'Masticatory morphological diversity and chewing modes in South American caviomorph rodents (family Octodontidae)', *Journal of Zoology*, 263(2), pp. 167–177. Available at: https://doi.org/10.1017/S095283690400500X.

Paradis, E. and Schliep, K. (2019) 'ape 5.0: an environment for modern phylogenetics and evolutionary analyses in R.', *Bioinformatics*, 35, pp. 526–528.

Pennell, M.W., Eastman, J.M., Slater, G.J., Brown, J.W., Uyeda, J.C., Fitzjohn, R.G., Alfaro, M.E. and Harmon, L.J. (2014) 'Geiger v2.0: An expanded suite of methods for fitting macroevolutionary models to phylogenetic trees', *Bioinformatics*, 30(15), pp. 2216–2218. Available at: https://doi.org/10.1093/bioinformatics/btu181.

Petrov, T.V., Panitsina, V.A., Bodrov, S.Y, Abramson, N.I. (2024) 'The mitochondrial genome of the critically endangered enigmatic Kazakhstani endemic *Selvinia betpakdalaensis* (Rodentia: Gliridae) and its phylogenetic relationships with other dormouse species', *Scientific Reports*, 14(1):22259. Available at: https://doi.org/10.1038/s41598-024-73703-2.

Pinheiro, J., Bates, D., and R Core Team (2022) 'nlme: Linear and Nonlinear Mixed Effects Models'.

Rankin, A.H., Emry, R.J. and Asher, R.J. (2020) 'Anatomical sciuromorphy in "protrogomorph" rodents', *Palaeontologia Electronica*, 23(2). Available at: https://doi.org/10.26879/1049.

Renaud, S., Gomes Rodrigues, H., Ledevin, R., Pisanu, B., Chapuis, J.-L. and Hardouin, E.A. (2015) 'Fast evolutionary response of house mice to anthropogenic disturbance on a Sub-Antarctic island', *Biological Journal of the Linnean Society*, 114, pp. 513–526. Available at: https://doi.org/10.1111/bij.12454.

Revell, L.J. (2012) 'phytools: An R package for phylogenetic comparative biology (and other things)', *Methods in Ecology and Evolution*, 3(2), pp. 217–223. Available at: https://doi.org/10.1111/j.2041-210X.2011.00169.x.

Sakamoto, M. (2010) 'Jaw biomechanics and the evolution of biting performance in theropod dinosaurs', *Proceedings of the Royal Society B: Biological Sciences*, 277(1698), pp. 3327–3333. Available at: https://doi.org/10.1098/rspb.2010.0794.

Samuel, O.M., Parés-Casanova, P.M., Nwaogu, I.C. and Olopade, J.O. (2015) 'Geometric morphometrics of the skull of two African rodents, *Thryonomys swinderianus* and *Cricetomys gambianus*', *Annals of Experimental Biology*, 3(2), pp. 21–30. Available at: https://repositori.udl.cat/bitstream/10459.1/49015/1/023177.pdf.

Samuel, O.M., Parés-Casanova, P.M. and Olopade, J.O. (2016) 'Comparative mandible geometric morphometrics of two African rodents, *Thryonomys swinderianus* and *Cricetomys gambianus* (Rodentia: Thryonomyidae and Nesomyidae)', *Research Journal of the Costa Rican Education University*, 8(2), pp. 249–254. Available at: https://www.scielo.sa.cr/pdf/cinn/v8n2/1659-4266-cinn-8-02-00249.pdf.

Samuels, J.X. (2009) 'Cranial morphology and dietary habits of rodents', *Zoological Journal of the Linnean Society*, 156, pp. 864–888. Available at: https://doi.org/10.1111/j.1096-3642.2009.00502.x.

Samuels, J.X. and Valkenburgh, B.V. (2009) 'Craniodental adaptations for digging in extinct burrowing beavers', *Journal of Vertebrate Paleontology*, 29(1), pp. 254–268. Available at: https://doi.org/10.1080/02724634.2009.10010376.

Santana, S.E., Dumont, E.R. and Davis, J.L. (2010) 'Mechanics of bite force production and its relationship to diet in bats', *Functional Ecology*, 24(4), pp. 776–784. Available at: https://doi.org/10.1111/j.1365-2435.2010.01703.x.

Santana, S.E., Grosse, I.R. and Dumont, E.R. (2012) 'Dietary hardness, loading behaviour, and the evolution of skull form in bats', *Evolution*, 66(8), pp. 2587–2598. Available at: https://doi.org/10.5061/dryad.d548646j.

Satoh, K. (1998) 'Balancing function of the masticatory muscles during incisal biting in two murid rodents, *Apodemus speciosus* and *Clethrionomys rufocanus*', *Journal of Morphology*, 236(1), pp. 49–56. Available at: https://doi.org/10.1002/(SICI)1097-4687(199804)236:1<49::AID-JMOR3>3.0.CO;2-J.

Satoh, K. (1999) 'Mechanical advantage of area of origin for the external pterygoid muscle in two murid rodents, *Apodemus speciosus* and *Clethrionomys rufocanus*', *Journal of Morphology*, 240, pp. 1–14. Available at:

https://doi.org/10.1002/(sici)1097-4687(199904)240:1%3C1::aid-jmor1%3E3.0.co;2-d.

Scott, W.B., Jepsen, G.L. and Wood, A.E. (1937) 'The mammalian fauna of the White River Oligocene: Part II. Rodentia', *Transactions of the American Philosophical Society*, 28(2), pp. 155–269.

Smith, C.E., Hu, Y., Hu, J.C.C. and Simmer, J.P. (2019) 'Characteristics of the transverse 2D uniserial arrangement of rows of decussating enamel rods in the inner enamel layer of mouse mandibular incisors', *Journal of Anatomy*, 235(5), pp. 912–930. Available at: https://doi.org/10.1111/joa.13053.

Swiderski, D.L. and Zelditch, M.L. (2010) 'Morphological diversity despite isometric scaling of lever arms', *Evolutionary Biology*, 37, pp. 1–18. Available at: https://doi.org/10.1007/s11692-010-9081-8.

Tanner, J.B., Zelditch, M.L., Lundrigan, B.L. and Holekamp, K.E. (2010) 'Ontogenetic change in skull morphology and mechanical advantage in the Spotted Hyena (*Crocuta crocuta*)', *Journal of Morphology*, 271, pp. 353–365. Available at: https://doi.org/10.1002/jmor.10802.

Toldt, C. von (1905) 'Der winkelforsatz des unterkiefers beim Menschen und bei den Saugetieren und die Beziehunger der kaumuskeln zu demselben', *Sitz Kaiserlund Akademie Wiss Wein mathem-naturw Klasse, II Teil*, 114, pp. 315–476.

Troyer, A., Legrand, A., Gevenois, P.-A. and Wilson, T.A. (1998) 'Mechanical advantage of the human parasternal intercostal and triangularis sterni muscles', *The Journal of Physiology*, 513(3), pp. 915–925. Available at: https://doi.org/10.1111/j.1469-7793.1998.915ba.x.

Turnbull, W.D. (1970) *Mammalian Masticatory Apparatus*. Chicago: Field Museum Press (Fieldiana (Geology)). Available at: https://doi.org/10.5962/bhl.title.5442.

Vander Wall, S.B. (2001) 'The Evolutionary Ecology of Nut Dispersal', *The Botanical Review*, 67(1), pp. 74–117. Available at: https://www.jstor.org/stable/4354385.

Velhagen, W.A. and Roth, V.L. (1997) 'Scaling of the mandible in squirrels', *Journal of Morphology*, 232, pp. 107–132. Available at: https://doi.org/10.1002/(SICI)1097-4687(199705)232:2<107::AID-JMOR1>3.0.CO;2-7.

Vieytes, E.C., Morgan, C.C. and Verzi, D.H. (2007) 'Adaptive diversity of incisor enamel microstructure in South American burrowing rodents (family Ctenomyidae, Caviomorpha)', *Journal of Anatomy*, 211(3), pp. 296–302. Available at: https://doi.org/10.1111/j.1469-7580.2007.00767.x.

Wahlert, J.H. (1968) 'Variability of rodent incisor enamel as viewed in thin section, and the microstructure of the enamel in fossil and recent rodent groups', *Breviora*, 309, pp. 1–18.

Wahlert, J.H. (1985) 'Skull morphology and relationships of geomyoid rodents', *American Museum Novitates*, 2812. Available at: https://core.ac.uk/download/pdf/18227657.pdf.

Wahlert, J.H. and Von Koenigswald, W. (1985) 'Specialized enamel in incisors of eomyid rodents', *American Museum Novitates*, 2832, pp. 1–12.

Weijs, W.A. (1973) 'Morphology of muscles of mastication in albino-rat, *Rattus norvegicus* (Berkenhout, 1769)', *Acta morphologica neerlando-Scandinavica*, 11(4), pp. 321–340.

Weijs, W.A. and Dantuma, R. (1975) 'Electromyography and mechanics of mastication in the albino rat', *Journal of Morphology*, 146(1), pp. 1–33. Available at: https://doi.org/10.1002/jmor.1051460102.

West, A.G. and King, C.M. (2018) 'Variation in mandible shape and body size of house mice *Mus musculus* in five separate New Zealand forest habitats', *New Zealand Journal of Zoology*, 45(2), pp. 136–153. Available at: https://doi.org/10.1080/03014223.2017.1411955.

Wilson, D.E., Lacher, T.E. and Mittermeier, R.A. (eds) (2016) *Handbook of the Mammals of the World, Volume 6: Lagomorphs and Rodents I*. Lynx Edicions (Handbook of the Mammals of the World (HMW)).

Wilson, D.E., Lacher, T.E. and Mittermeier, R.A. (eds) (2017) *Handbook of the Mammals of the World, Volume 7: Rodents II*. Lynx Edicions (Handbook of the Mammals of the World (HMW)).

Wilson, D.E. and Reeder, D.M. (2005) *Mammal Species of the World*. Baltimore: Johns Hopkins University Press.

Windle, B.C.A. (1897) 'On the myology of *Dolichotis patagonica* and *Dasyprocta isthmica*', *Journal of Anatomy and Physiology*, 31(3), pp. 343–353.

Wood, A.E. (1955) 'A revised classification of the rodents', *Journal of Mammalogy*, 36(2), pp. 165–187. Available at: https://doi.org/10.2307/1375874.

Wood, A.E. (1965) 'Grades and clades among rodents', *Society for the Study of Evolution*, 19(1), pp. 115–130. Available at: https://doi.org/10.2307/2406300.

Woods, C.A. (1972) 'Comparative myology of jaw, hyoid, and pectoral appendicular regions of New and Old World hystricomorph rodents', *Bulletin of the American Museum of Natural History*, 147(3), pp. 115–198. Available at: https://core.ac.uk/download/pdf/18223600.pdf.

Woods, C.A. and Howland, E.B. (1979) 'Adaptive radiation of Capromyid rodents: anatomy of the masticatory apparatus', *Journal of Mammalogy*, 60(1), pp. 95–116. Available at: https://doi.org/10.2307/1379762.

Young, J.W. (2006) 'Ontogeny of muscle mechanical advantage in capuchin monkeys (*Cebus albifrons* and *Cebus apella*)', *Journal of Zoology*, 267(4), pp. 351–362. Available at: https://doi.org/10.1017/S0952836905007521.

Chapter 3 – Gape angle, bite point, head size, and their relationship with mechanical advantage among rodent morphotypes

3.1 – Introduction

3.1.1 – Preface

Rodents exhibit a huge range of dietary diversity, including in the material properties of their food and the size of food objects. Despite this they are functionally and anatomically conservative, exhibiting convergence of their masticatory systems and an anatomy specialised for gnawing (Wood, 1965; Cox *et al.*, 2012; Druzinsky, 2015). Biomechanical analyses can evaluate the functional performance of organisms during feeding, and compare anatomical and functional characteristics; these can tease out the evolutionary trends, anatomical specialisations, functional specialisations, or dietary specialisations of those organisms (Greaves, 1985; Sakamoto, 2010; Santana, Dumont and Davis, 2010; Morales-García *et al.*, 2021). By quantifying the anatomical configurations known in rodents, their functional efficiency during gnawing and chewing can be assessed in the form of mechanical advantage at a range of gape angles as a proxy for the size of the food object being bitten. Quantitative analysis and comparison of the patterns in mechanical efficiency amongst the different muscular configurations seen in rodents, at a range of gapes and bite points, has not yet been conducted with a sample across the tree. This study seeks to address this knowledge gap in order to provide a new evaluation of the mechanical variation among rodents, and the functional differences between categories.

3.1.2 – The rodents

The sample of rodents used here and their distinctive characteristics as an Order, and of the morphotype categories, were discussed extensively in Chapter 2, subheadings 2.1.2 and 2.1.3. This information will not be repeated here, and only their key characteristics are reiterated below.

All rodents have a large masseter complex that can be divided into superficial, deep, and zygomaticomandibularis subdivisions (in the nomenclature used in this study), some of which possess further distinct subdivisions (Druzinsky, 2010; Cox and Jeffery, 2011). In hystricomorphs, the deep masseter is not subdivided further. In myomorphs, sciuromorphs, and a protrogomorph (*Aplodontia rufa)*, the deep masseter is divided into anterior and posterior portions, with the anterior portion originating from the zygomatic plate in myomorphs and sciuromorphs; the zygomatic plate, a broad sloping surface on the anteroventral zygomatic root, is itself a characteristic feature of myomorphs and sciuromorphs, absent in the other morphotypes (Fabre *et al.*, 2012; Cox, Faulkes and Bennett, 2020). In both myomorphs and hystricomorphs the infraorbital foramen is expanded relative to its size in sciuromorphs, though the presence of the zygomatic plate in myomorphs limits this relative difference in size when compared with the much larger infraorbital foramen in hystricomorphs (Brandt, 1855; Scott, Jepsen and Wood, 1937; Wood, 1955, 1965). Through their expanded infraorbital foramina, myomorphs and hystricomorphs possess an additional portion of their zygomaticomandibularis masseter, an infraorbital section that passes through the foramen to originate on the rostrum (here, the '**IOZM**'). These groups are all para/polyphyletic, with hystricomorphy observed in Anomaluromorpha, Ctenohystrica, Dipodidae and Gliridae; myomorphy present in both Muridae and Gliridae; protrogomorphy in Aplodontidae and Bathyergidae; and sciuromorphy occurring in Castorimorpha and Sciuridae (Fabre *et al.*, 2012; Cox and Hautier, 2015; Cox, Faulkes and Bennett, 2020). These categories exist due to widespread homoplasy and convergent evolution across the order, with protrogomorphy

thought to be the ancestral condition based on observations of extant and fossil rodents (Wood, 1965).

Though anatomical comparisons are relatively straightforward, we can also conduct quantitative comparisons of function. Rodents may be differentiated into these four anatomical categories, but to what extent do these anatomical morphotype categories reflect variation in function? To answer such a question, one must decide how to define and compare their function, and what factors should be assessed as part of these analyses. In Chapter 2, this consisted of mechanical advantage at zero degrees gape.

3.1.3 – Mechanical advantage and jaw-closing muscles

Mechanical advantage was discussed in detail in Chapter 2, subheading 2.1.4, and will be briefly reestablished here, with some further detail. It is a measure of the efficiency of a mechanical system; it is the ratio of the system's in-lever to its out-lever, which determines the proportion of input force mechanically converted into output force (Hildebrand *et al.*, 1985). It is important to note that a higher mechanical advantage is not necessarily an adaptational 'advantage', as it is one characteristic of a broader anatomical and functional system—the term is not a value judgement. Mechanical advantage is here calculated using lever-arm mechanics. Broadly, lever systems can be divided into three types: first-, second-, and third-class. In a first-class lever, the joint is between the load and the muscle force; in a second-class lever, the load is between the joint and the muscle force; and in a third-class lever, the muscle force is between the joint and the load.

Typically, jaws function as third-class levers in biting with anterior teeth (as the muscle attachments occur posterior to the incisors and anterior to the jaw joint), but in some rodents have been proposed to behave as second-class levers during biting with the molars, where the muscle vector and attachments of anteriorly-positioned muscles can more often be anterior to the active bite point (Turnbull, 1970; Cox, 2017). Since the hard-tissues of

the jaws are rigid, the mechanical advantage of each muscle can be calculated using lever-arm mechanics, and then compared between muscles or taxa. However, biological organisms are not entirely hard and even bones themselves respond to stress and strain; being a mixture of compliant and rigid body mechanisms, such methods will not account for lost work due to the natural deformation of the system. Factors such as the curvature of soft-tissue and elastic components of the system can be incorporated into some models, and doing so illuminates these shortcomings of rigid models in isolation (Harkness-Armstrong *et al.*, 2020). Though mechanical advantage is not affected by such properties, rigid-models are not perfect replicas of life due to simplifications made in their methods. The method used in this study focusses on the mechanical efficiency of the configuration of the jaw muscles in 2D space. *In vivo* observations and comparisons may be more complex.

Despite its limitations, mechanical advantage has been applied in the field of biomechanics far beyond feeding alone. As alluded to briefly in Chapter 2, it has been applied broadly to identify the function of muscles by comparing them, such as identifying the roles of muscles during breathing (Troyer *et al.*, 1998), or by comparing limbs and their functions such as gait and jumping (Biewener *et al.*, 2004; Olberding *et al.*, 2019; Basu and Hutchinson, 2022) or comparing morphology and other functions of limbs besides movement (Elner and Campbell, 1981). Comparisons of mechanical advantage can also be applied to study ontogeny and growth patterns (García-Morales *et al.*, 2003; Young, 2006; Tanner *et al.*, 2010).

Within the context of masticatory mechanics and diet, mechanical advantage has been applied across a huge range of organisms. It has been applied to rodents specifically in the past, to individual muscles (Ball and Roth, 1995; Velhagen and Roth, 1997; Satoh, 1999; Druzinsky, 2010; Swiderski and Zelditch, 2010; Casanovas-Vilar and Van Dam, 2013; Renaud *et al.*, 2015; Cox and Baverstock, 2016; Gomes Rodrigues, Šumbera and Hautier, 2016; McIntosh and Cox, 2016a, 2016b; Cox, 2017; Echeverría *et al.*, 2017; Jones and Law, 2018; West and King, 2018; Cox *et al.*, 2020, 2020), to entire masticatory systems (Cox, 2017), or to compare the effects of incisor procumbency

(Echeverría *et al.*, 2017). It has also been applied to assess the function of individual muscles, efficiency, and jaw mechanics in vertebrates besides rodents (e.g. van Eijden *et al.*, 1988; Westneat, 2003). Mechanical advantage can be used across groups of organisms to identify evolutionary trends or patterns in the functional performance of jaw shapes and their generalisation or specialisation of anatomy or function (Greaves, 1985; Sakamoto, 2010; Nabavizadeh, 2016; Huby *et al.*, 2019; Kunz and Sakamoto, 2024). Mechanical advantage can also be applied to assess changes in function and specialisation with growth (Weijs, Brugman and Klok, 1987; Dechow and Carlson, 1990; Tanner *et al.*, 2010), or when combined with diet (Morales-García *et al.*, 2021). It can be applied to estimating bite forces specifically (Osborn, 1996; Wroe *et al.*, 2008; Godinho *et al.*, 2018), but its effectiveness for these estimations—in comparison to using size and mandible shape to estimate bite-force—is currently disputed regarding rodents (Ginot *et al.*, 2019).

In specific taxa where supporting data (such as high-speed video) permits, assessments can be used to evaluate more complex feeding mechanics in greater detail (Grubich, Rice and Westneat, 2008). Similarly, muscle size can be a factor in differences in performance between groups (Throckmorton and Dean, 1994), but the lack of physical dissections or digital contrast-enhanced dissections or other measures of muscle size in many taxa at the time of this study means it cannot be assessed as a factor at present; with the available specimens and sample, mechanical advantage is a valuable parameter to measure and assess. Other factors can also be incorporated to identify potential trends in the variation of mechanical advantage in this sample: the bite point, and the gape angle of the jaws. These are the two key factors this chapter expands to assess.

3.1.4 – Incisor biting and molar biting

Bite point—the point along the dental arcade at which the food item contacts the teeth—is known to impact mechanical advantage (Devlin and

Wastell, 1986). If the bite point is changed, then in broad and generalised terms the in-levers of muscles typically stay the same but the out-lever shortens or lengthens, thus affecting the ratio between the two measurements. In the context of rodents, this allows us to compare their functional performance for both incisor biting (i.e. gnawing) and molar biting (i.e. chewing), to identify the variance within the sample and between morphotypes at both bite points, and evaluate existing comparisons of morphotypes for these different biting behaviours (Becht, 1953; Wood, 1965; Druzinsky, 2010; Cox *et al.*, 2012; Cox, Kirkham and Herrel, 2013; Cox, 2017). For the analyses conducted in this project, characteristics of tooth morphology such as incisor procumbency or molar cusp morphology are not tested as variables. The project's focus is on the configuration of muscles and comparisons between morphotype categories, not the individual variations in the morphology and specialisation of teeth.

For simplicity, the difference between these two bite points in this study is isolated to the propalinal movement of the mandible in two dimensions. The shift to incisor biting increases the out-lever, because the distance between the TMJ and incisor tips is greater than the distance between the TMJ and the first molar. Although a longer out-lever—the denominator in the calculation of mechanical advantage—will result in lower mechanical advantage for an incisor bite than from a molar bite, the effect on the in-lever may not necessarily be so uniform. The transition from molar to incisor biting is not simply an increase in the out-lever in a rodent. Rodents cannot occlude at their incisors and molars simultaneously (Hiiemae and Ardran, 1968), and to transition from molar to incisor occlusion the lower jaw must move forwards and partially open; as a result, incisor biting even at zero degrees gape has the mandible protracted and rotated downwards when compared with zero degrees of gape at molar biting. This movement of the mandible affects the muscles' insertions relative to their origins in space, and therefore affects the mechanics of the individual jaw-closing muscles by changing their in-levers. Since each muscle has its own in-lever, the proportional difference in mechanical advantage between incisor and molar

biting varies slightly from muscle to muscle. That is to say, the pattern of which muscles are contributing to the variance in mechanical advantage might differ between bite points. The mobility of the temporomandibular joint (TMJ) also means that the jaw is positioned differently within its joint when comparing the two bite points, affecting the coordinates of the TMJ used for the calculation—this must be incorporated to accurately identify the change in the out-lever and in-levers.

Studies comparing individual rodents or a sample of multiple rodents, sometimes across morphotypes, that test or model incisor gnawing and molar biting tend to interpret taxa or groups as optimising for one bite point or another through comparisons of bite force, skull stress, or efficiency. For example, sciuromorphs are thought to be more efficient at incisor biting than protrogomorphs (Druzinsky, 2010), and hystricomorphs are stated to be specialised towards molar chewing while sciuromorphs specialise towards gnawing and myomorphs are generalists (Cox *et al.*, 2012). This study can further explore these established interpretations by comparing the variance between the groups. Furthermore, rodents are proposed to converge in form for the function of gnawing (Druzinsky, 2015). By comparing them with both incisor and molar biting, I can see if these data show reduced variation in mechanical advantage when gnawing. However, these analyses by themselves would be missing a crucial piece of the puzzle; a proxy for diet, such as different food object sizes.

3.1.5 – Gape angle

Gape angle is a measurable component of the mechanics of biting in living organisms. It is the angle to which the jaw has opened at a specific point in a masticatory cycle. On a life-size scale, it directly interacts with the size of the food objects in the organism's diet, and the mechanical behaviours of that bite (Wheelwright, 1985). Larger food objects require a larger gape angle to fit the object between the teeth. This is inextricable from both the mechanical efficiency of the spatial arrangement of muscles (Herring and

Herring, 1974; Santana, Dumont and Davis, 2010) and the physical characteristics of the muscle soft-tissues themselves, such as muscle mass, pennation, fibre length, or other properties (Taylor and Vinyard, 2009; Hartstone-Rose, Perry and Morrow, 2012). Without data regarding muscle stretch or material properties, and the lack of soft-tissue data for most of this sample, evaluating the relationship between gape and soft-tissue adaptations/anatomy is beyond the scope of this study. Instead, this study focusses on the configuration of these muscles and lever-arm mechanics calculations based on their moment arms, as the muscle configuration is a characteristic that defines each morphotype. Gape angle provides a proxy for food object size, assessing how the efficiency of organisms and groups can vary when comparing low gapes to high gapes.

Gape has been applied across many groups of taxa to assess several factors. Diet itself has been studied extensively, both with performance at specific gapes and assessments of maximum gape (Hampton and Moon, 2013; Terhune *et al.*, 2015; Fricano and Perry, 2019). Some studies have centred on mechanical factors such as muscle stretch and the orientation of muscles to assess how gape effects efficiency (Herring and Herring, 1974; Eng *et al.*, 2009). When paired with electromyography or kinematic data, functional interpretations regarding gape and gape cycles can be tested *in vivo* (Herring, Grimm and Grimm, 1979; Wang *et al.*, 2007; Pröschel, Jamal and Morneburg, 2008; Ross *et al.*, 2010). Functional and anatomical interpretations in observed extant taxa, including around gape, can be applied to similar taxa (Herring, 1980; Ross and Iriarte-Diaz, 2014); this established principle will be applied in Chapter 4 when studying fossil multituberculates in comparison with extant rodents. Similarly, gape can be assessed across groups to identify evolutionary and functional trends (Weijs, 1994; Grossnickle, 2020). Gape can also be a part of analysing other anatomical or mechanical characteristics, such as TMJs and their adaptations (Sun, Liu and Herring, 2002), how skulls distribute stress and strain (Christiansen and Adolfssen, 2005; Bourke *et al.*, 2008; Santana, Grosse and Dumont, 2012), or trends in bite force production in taxa (Dumont and Herrel,

2003; Christiansen and Adolfssen, 2005; Christiansen, 2008; Dumont *et al.*, 2009; Santana, Dumont and Davis, 2010; Santana, Grosse and Dumont, 2012), any of which can be combined or connected back to feeding ecology specifically (Anapol and Lee, 1994; Rodríguez-Robles, Bell and Greene, 1999; Taylor and Vinyard, 2005; Ross and Iriarte-Diaz, 2014; Ledogar *et al.*, 2018; Laird *et al.*, 2023). Masticatory behaviours to circumvent the need for higher gape during biting can also be studied and assessed (Helfman and Clark, 1986; Vinyard *et al.*, 2003; Van Wassenbergh, Heindryckx and Adriaens, 2017).

Of particular interest due to their noted specialisation for extreme gape, and disputed morphotype classification, are taxa in the family Bathyergidae (McIntosh and Cox, 2016b, 2016a; Van Wassenbergh, Heindryckx and Adriaens, 2017). In this sample the representatives of this family are *Bathyergus suillus* and *Georychus capensis*, two taxa assigned as protrogomorphs in the analyses of the previous chapter. Of these burrowing taxa, *G. capensis* digs using its incisors to dig whereas *B. suillus* digs using its forelimbs (McIntosh and Cox, 2016b; Van Wassenbergh, Heindryckx and Adriaens, 2017). Incisor digging is performed at high initial gape, with smaller initial gapes used when digging in harder soil (Van Wassenbergh, Heindryckx and Adriaens, 2017). Together these taxa illuminate how gape can interact with the function of the jaws outside of feeding alone, and this is reflected in their mechanical efficiency at different gapes; for example, the mechanical advantage of the temporalis muscle is notably higher in chisel-toothed diggers than in scratch diggers (McIntosh and Cox, 2016b, 2016a). That study also compared mechanical advantage at a range of gapes, similarly to the method employed to assess gape in this chapter, and thus can provide some context for my approach. They noted a particular pattern of decreasing mechanical advantage as gape increased, up to a turning point after which mechanical advantage begin to rise—in particular, this threshold occurred at 40° gape in *B. suillus*, the scratch digger, and around 90° gape in the chisel-toothed diggers, clear evidence that the chisel-toothed diggers are optimised to reduce the inefficiency of increasing gape angle, making them more efficient at biting for extreme gape angles (McIntosh and Cox, 2016a).

When conducting my own mechanical advantage analyses, I would expect to see variation in mechanical advantage at a range of gape angles, where some muscles will change their trend of mechanical advantage with gape.

Although these mechanical functions are connected to the craniomandibular and muscular anatomy of organisms, such extreme gapes as 80–90° are not relevant to the subject of feeding itself where most organisms are concerned. This is particularly the case since gnawing allows rodents to access hard or proportionally large food items using shallow 'scraping' bites at narrower gape angles; heteromyid rodents and squirrels are highly specialised seed predators, and utilise gnawing in this manner (Hulme and Benkman, 2002). For example, among small rodents, only squirrels have sufficiently strong jaw musculature and bite forces to bite through the hard outer surface of nuts like *Juglans nigra* (the Eastern American Black Walnut), using gnawing (Emry and Thorington, 1984; Vander Wall, 2001). Grey squirrels (*Sciurus carolinensis*, included in this sample) also feed on acorns throughout the winter by using shallow bites to breach the hull as well as other specialised behaviours, such as caching to soften the hull and excising the embryo from White Oak acorns prior to burial to prevent germination (after which the acorns become less nutritious) while the nuts are cached (Vander Wall, 2001). Rather than a simple incisor bite at high gape to crack a freshly foraged hard food object, squirrels instead use specialised behaviours to optimise their efficiency and performance. Similarly, beavers gnaw down trees using shallow gnawing bites where their mechanical advantage decreases at a lower rate than other sciuromorphs as gape increases (similarly to the pattern previously alluded to in chisel-toothed diggers), with the existing biomechanical analysis testing a gape of 30° (Cox and Baverstock, 2016), significantly below the preservation of efficiency at extreme gape previously discussed in chisel-toothed digging Bathyergids. This behavioural adaptation in beavers is also paired with physical adaptations, such as the shape and angle of the incisors, to specialise beavers for biting through thick hard materials (i.e. bark and wood) at a high gape (Stefen, Habersetzer and Witzel, 2016). High gape is sometimes required for

a mechanical behaviour but is not necessarily the only solution to accessing a large food object, especially not when gnawing is possible for the organism.

As a result, although the gape angles exhibited by rodents may have the capacity for extreme gape for a particular function as in certain Bathyergidae, the majority of feeding behaviours exhibited by the group will be unlikely to include such extreme gapes. An existing study on two murid rodents identified the optimal gape during gnawing (based on the peak in bite force) as 20°, at around 40% of an individual's maximum gape angle (Williams, Peiffer and Ford, 2009). For this study, I selected a gape range based on these established patterns of gape and efficiency in rodents. Ultimately gape is not neatly separable from the other mechanical characteristics of biting and the adaptations associated with these characteristics, and will be explored as a variable of potential significance in this study.

Currently, the primary gap in existing knowledge is a comparison of efficiency at different gapes across the tree and multiple specimens of each morphotype. Many analyses mentioned earlier in this subsection focus on estimations of bite force rather than efficiency, or gape cycles rather than simple bites, or study a smaller sample of taxa or individual species or contrast two distinctly different groups. It is less common to assess mechanical advantage's variation with gape, to differentiate possible functional specialisations among paraphyletic groupings. The perception that rodents have converged functionally while maintaining a degree of anatomical diversity within the group, developing different anatomical 'solutions' for gnawing, can be assessed with the methods of this study. These methods and the conclusions drawn could provide a point of comparison or contrast for future studies on rodents or other groups that may be constrained by a specific masticatory function.

3.1.6 – Head size: a potential factor to consider

In some animals, trends in head size can be correlated with trends in bite force (Verwaijen, Van Damme and Herrel, 2002; Herrel *et al.*, 2005; Nogueira, Peracchi and Monteiro, 2009). A larger head size within a species will correlate strongly with having larger muscle masses, which will contribute to the measured or estimated bite forces. Trends in head size have not been compared as frequently with mechanical advantage itself; such comparisons have been primarily made in the context of either ontogeny, or size variation between taxa. In hyenas, mechanical advantage reaches maturity at 22 months even though maturity of skull size is not achieved until 29 months and skull shape at 35 months of age (Tanner *et al.*, 2010). In some taxa, size is suggested to be more important to diet and feeding than morphology itself; for example, in birds, body size and mechanical advantage covary with feeding ecology more significantly than beak shape does (Navalón *et al.*, 2019). Even when gape angle is maintained, a taxon with a larger physical size—or longer jaws alone—has a larger distance between teeth and can thus bite larger objects. However, rodents can use gnawing to mitigate the limitations of their small size and process foods that are typically accessible by larger mammals: for example, some rodents use gnawing and coprophagy (rather than rumination) to break down tough vegetation such as grasses (Hirakawa, 2001), and squirrels can eat hard seeds such as white oak acorns that no other mammal of their size has a strong enough bite to access, using small bites despite the large size of the acorns (Vander Wall, 2001). With the broader context in mind and the size range of different species of rodents in this sample, size needs to be ruled out as a significant factor in the variance.

Mechanical advantage is a ratio and therefore the measurement itself is size independent, but this does not mean that it cannot correlate with or interact with size; a mechanical advantage of 0.4 is a mechanical advantage of 0.4 whether the organism in question is the size of an elephant or the size of an elephant shrew, but the diets and behaviours of those organisms are different. In purely mechanical terms, larger muscles can mitigate a low mechanical advantage by simply applying more input force during the bite

to generate a comparable bite force, or allow for faster movement of the jaws where speed is important. Mechanical advantage does not necessarily illuminate what an organism can eat when viewed in isolation, and the limited availability of dietary information for so many of the studied taxa means that this study's interpretations based on mechanical advantage are inherently limited, especially if size could hypothetically be responsible for a significant portion of the variance. Although dietary information and cranial dissection data are absent for most taxa and other masticatory factors such as tooth crown morphology are beyond the scope of this study, head size can be tested for a correlation with mechanical advantage.

If head size is significantly correlated with mechanical advantage, that could overlap with or affect interpretation of the differences between morphotype categories; *Hydrochoerus hydrochaeris* and other especially large taxa could potentially skew the data when comparing groups. Size must either be ruled out as a contributing factor if it does not correlate, or accounted for when drawing conclusions if it does correlate. Rather than being a full Key Question of this study, it is a factor that needs to be checked and ruled out if its effect on the variance is not significant.

3.1.7 – Key Questions and Hypotheses

This chapter aims to expand on the topics discussed throughout this introduction, and build on the methods and conclusions of Chapter 2, which analysed a simple bite at zero gape using the incisors. The following key questions and hypotheses will be tested.

Firstly, do these data allow the morphotypes to be differentiated? And if so, which muscles are contributing to this potential variance associated with gape? The morphotypes exhibit anatomical differences, and functional assertions have been made based on these, as previously discussed in this introduction; the answers to these questions can explore existing predictions, as well as testing whether the functional differences between the morphotypes' mechanical advantages are significantly different. I

hypothesise (**H2.1**) that the morphotypes will be significantly different now that gape has been introduced as a variable, and that gape will have an observable association with the variance in mechanical advantage. The previous chapter examined biting at zero gape, i.e. at occlusion; in life, this is not how biting is performed. By incorporating gape, we can attain a more complete view of the bite cycle. The existing research on gape and mechanical advantage both within Rodentia and beyond, outlined previously, would suggest that gape will be a significant factor in functional variation—since gape in this study is a proxy for the size of the object being bitten, and mechanical advantage can be a proxy for the material properties of the food (with higher advantage providing access to tougher foods for the same muscle input force), analysing these two variables does connect with the functional context of diet. In the results of Chapter 2, the morphotypes were not significantly different. The dimensionality of the data will need to be reduced to easily identify variation and trends of mechanical advantage with gape, and lever-arm mechanics analysis and subsequent Principal Components Analyses and MANOVAs will together test this hypothesis. The effects of different gape angles and muscles on the variation in mechanical advantage can be observed visually using the loading plots produced by the PCAs.

Secondly, can the comparisons of these different bite points allow the morphotypes to be differentiated? For example, in the past it has been inferred that sciuromorphs are anatomically adapted towards gnawing, and hystricomorphs are adapted to perform better during molar chewing (Druzinsky, 2010; Cox *et al.*, 2012); will a similar division be visible in this study? With gnawing allowing food items to be broken down in small bites for further processing, and rodents moving their jaw between both positions, these data may be able to differentiate the groups even if gnawing alone cannot, despite the removal of related factors such as tooth cusp morphology in these methods. I hypothesise (**H2.2**) that the variance of the incisor PCA will be smaller than that of the molar counterpart, with rodent taxa being closer towards the mean for gnawing when compared to chewing.

Though it is too loose to make a formal hypothesis, I also expect that there will be visible overlap between morphotype categories on multiple PCs, and that some taxa will be more similar to those of a different morphotype than to those of their own morphotype. I anticipate this due to the para/polyphletic nature of the categories and the degree of homoplasy and anatomical convergence across the tree (Samuels, 2009; Hautier, Cox and Lebrun, 2015). Comparing the PC plots and the means of each morphotype category at each bite point will allow both of these hypotheses to be tested.

More granular muscle-specific and taxon-specific variation in mechanical advantage is beyond the scope of these hypotheses and this project. Major outliers to a group and observable patterns regarding the morphotype categories will be discussed, but not a detailed muscle-by-muscle or taxon-by-taxon breakdown of all the raw data of mechanical advantage calculated.

3.2 – Materials and Methods

3.2.1 – Sample preparation

The sample used in this analysis is the same as the sample used in Chapter 2, established detail will not be reiterated here. It consists of 27 rodent species from 20 families across the tree of Rodentia, each with a single individual specimen—this provides a representative sample across the phylogenetic tree, and multiple representatives of each morphotype category. I isolated and segmented the bones in Avizo version 9.2 (Thermo Fisher Scientific, Waltham, MA, USA) and positioned the mandible/hemimandibles at molar occlusion. I aligned the specimens consistently relative to the global axes. I landmarked the surface file(s) of each specimen at the anterior tip of the upper and lower first cheek teeth, the upper and lower incisor tips, and the centres of the upper and lower articulation surfaces of the TMJ. The muscle attachments on the skulls and mandibles for the masseter, the temporalis, and the pterygoids were all identified and mapped in Avizo, and the coordinates of the centre of each surface were identified in Blender to provide the muscle centroids, as outlined in Chapter 2 subheadings 2.2.1, 2.2.2, and 2.2.3. No new muscle attachment segmentation or bony landmarking was required for the analyses in this chapter.

3.2.2 – Simulating bite point and gape angle

The equations used to calculate mechanical advantage in Chapter 2 could be reused for a simulated incisor bite without alteration. However, the mandibles had been landmarked at molar occlusion; as discussed in the introduction, since rodents cannot occlude both their molar teeth and their incisors simultaneously, simulating an incisor bite requires a translation and rotation of the mandible to bring the incisor tips together. Figure 3.1 displays a diagram of *R. norvegicus* in lateral view, illustrating how the skull and jaws are positioned at low and high gape, and during incisor and molar biting.

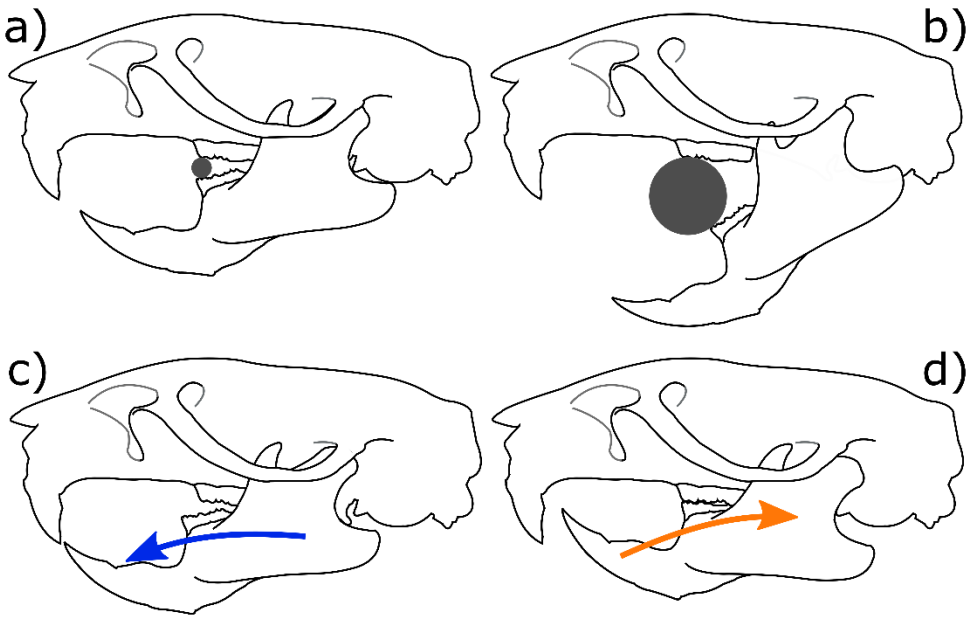

Figure 3.1: *Rattus norvegicus* in lateral view, displaying a) biting at 10° gape, b) biting at 30° gape, c) mandible protraction for incisor biting, d) mandible retraction for molar biting. The coloured arrows show the movement of the mandible required for each bite point.

Rather than manually translating and rotating the mandible into incisor occlusion in Avizo and then applying this transformation to all the muscle surface files, I used trigonometry in 2D (with the left- and right-side landmark coordinates averaged) to simulate incisor occlusion. I used the distances between the upper and lower incisor tip landmarks at molar occlusion to calculate the required protraction of the mandible and vertical opening of the mouth needed to bring the incisor tips together for an incisor bite.

These are shown as Equations (1) and (2) for the translation and rotation, respectively. The anteroposterior component of this translation was applied to the TMJ landmarks to simulate the protraction of the mandible at the jaw joint. This anterior translation and mandible rotation was then applied to the muscle centroids on the mandible so that at gape 'zero' with the incisor tips at occlusion, the muscle centroids on the mandible were positioned as they would be if the mandible had been translated into this occlusion. As stated regarding the sample preparation, the specimens were aligned consistently to the global axes. As a result, the z-axis is the anteroposterior

axis of the specimen and the y-axis is the dorsoventral axis of the specimen. The x-axis is omitted as these are 2D analyses.

$$Mandible\ Protraction\ Distance = z_1 - z_0 \quad (1)$$

$$a = \sqrt{(z_1 - z_0)^2 + (y_1 - y_0)^2} \quad (2.1)$$

$$b = \sqrt{(z_c - z_1)^2 + (y_c - y_1)^2} \quad (2.2)$$

$$c = \sqrt{(z_c - z_0)^2 + (y_c - y_0)^2} \quad (2.3)$$

$$\theta = \cos^{-1}\left(\frac{b^2 + c^2 - a^2}{2bc}\right) \quad (2.4)$$

$$z_x = (z_\alpha - z_c)\cos\theta_x - (y_\alpha - y_c)\sin\theta_x + z_c \quad (3.1)$$

$$y_x = (z_\alpha - z_c)\sin\theta_x - (y_\alpha - y_c)\cos\theta_x + y_c \quad (3.2)$$

Equation (1) calculates the anterior translation applied to the mandible landmarks to simulate protraction for incisor biting, where z_1 is the z-axis coordinate of the upper incisor tip once the left and right landmarks are averaged, and z_0 is the averaged lower incisor tip. I used the four equations grouped under Equation (2) to calculate the required rotation of the mandible landmarks to bring the incisor tips into occlusion once protracted. The distance between the incisor tips (a), distance from the upper incisor tips to the TMJ (b), and distance from the lower incisor tips to the TMJ (c) were calculated using Pythagoras' theorem as shown in Equations (2.1), (2.2), and (2.3). In these equations, z_1 is the z-coordinate of the upper incisor landmark, z_0 is the lower incisor landmark, z_c is the TMJ, and y_1, y_0, and y_c are the y-coordinates of the upper incisor, lower incisor and TMJ landmarks respectively. I used the law of cosines to calculate the required rotation to be applied to simulate incisor occlusion (angle θ) using Equation (2.4). I used Equations (3.1) and (3.2) to calculate the new z- and y-coordinates for a selected muscle insertion centroid and to subsequently simulate intervals of gape angles at 5° increments from 5° to 40° for both bite points. In the two equations included under Equation (3), z_χ and y_χ represent the calculated coordinates of a muscle centroid at incisor biting, z_α and y_α are the coordinates of the centroid prior to its translation, z_c and y_c are the

coordinates of the TMJ which functions as the centre of rotation, and the rotation applied for the specified gape angle is represented as θ_X.

Mechanical advantage was then calculated using Equations (4), (5), and (6). In Equation (4), z_i and y_i are the z- and y-coordinates of a muscle's insertion centroid and z_o and y_o are the coordinates of the muscle's origin centroid. In Equation (5), the labels of z_b and y_b represent the z- and y-coordinates of the tooth landmarks for the selected bite point, i.e. the averaged z- and y-coordinates of the incisor tip landmarks, or first molar landmarks. Figure 2.7, in subheading 2.2.4 of the thesis, illustrated these equations visually in *R. norvegicus*.

$$In\ lever = \frac{|(z_i - z_o)(y_o - y_c) - (z_o - z_c)(y_i - y_o)|}{\sqrt{(z_i - z_o)^2 + (y_i - y_o)^2}} \quad (4)$$

$$Out\ lever = (((y_b - y_c)^2) + ((z_b - z_c)^2))^{0.5} \quad (5)$$

$$Mechanical\ Advantage = \frac{In\ lever}{Out\ lever} \quad (6)$$

For many of the taxa in this study (*Acomys cahirinus, Cannomys badius, Capromys pilorides, Dasyprocta punctata, Dipus sagitta, Erethizon dorsatum, Gerbillus watersi, Hydrochoerus hydrochaeris, Hystrix cristata, Lagostomus maximus, Laonastes aenigmamus, Phyllotis gerbillus, Pedetes capensis* and *Petaurista petaurista*), detailed quantitative information on their known or tested gapes during feeding is simply not available yet. *G. watersi*, for example, has almost no available anatomical or functional information at all beyond its limited taxonomical and ecological study (Rothschild, Hartert and Jordan, 1901; Lay, 1983). Other taxa do have existing study or quantitative data of gape for members of their genera if not the studied species, including (in order of the cited papers) *Aplodontia*, *Thomomys*, *Cricetomys*, *Graphiurus*, *Cavia*, *Rattus*, *Sciurus*, *Ctenomys*, *Octodon*, *Myocastor*, and *Castor* (Druzinsky, 1995, 2010; Hanson, Newmark and Stanley, 2007; Cox and Jeffery, 2011; Cox *et al.*, 2012; Becerra *et al.*, 2014; Schultz *et al.*, 2014; Stefen, Habersetzer and Witzel, 2016), as well as measurements and studies

of gape of rodent taxa that are not in this sample (Williams, Peiffer and Ford, 2009; Van Wassenbergh, Heindryckx and Adriaens, 2017).

I selected 40° as the upper limit, which would be high for most taxa but not pushing into extreme gape angles that most taxa might not be able to physically achieve. I tested increments of 5° to reduce the total number of datapoints in the overall analysis by a factor of eight without losing too much sensitivity, as opposed to calculating in increments of 1° and having a much larger, more unwieldy dataset. A zero-gape calculation was not conducted in these analyses, as teeth are not at true tip-to-tip occlusion during biting, and zero degrees of gape would imply the rodent was not biting a physical food item. As is, 27 taxa with either 8 or 9 muscles each, studied at eight increments of gape for two bite points is still a total dataset of over 3000 calculated estimates of mechanical advantage. The following statistical analyses were used to compare the morphotype categories concisely and identify potential patterns within or between categories.

3.2.3 – Statistical analyses

A MANOVA is a statistical analysis that compares three or more dependent variables against one independent variable (Wilks, 1932). It tests for the significance of the difference between the means of the group categories that are the independent variable, and how strongly the independent variable accounts for that difference between the groups. In this study, it provides a convenient quantitative test of the difference between the means of mechanical advantage for the morphotype categories, by treating morphotype as the independent variable. The dependent variables are selected differently for the three sets of MANOVA analyses that will be conducted in this study. For these analyses, Pillai's Trace (Pillai, 1955) and its associated F statistic and p-value are included in the Results section. Only the results of statistical significance will be considered impactful, but the limitations of inputs for a MANOVA dictate how it must be run; this study includes three sets of MANOVA analyses to cover different needs.

A MANOVA cannot be conducted if the number of dependent variables exceeds the number of cases. In this study, the number of cases is the number of taxa, at 27, and the number of dependent variables is the number of data points of mechanical advantage for a given taxon. For the full sample analysis, there are far more dependent variables than 27, with each taxon having eight calculations of mechanical advantage for each muscle present. As a result, a MANOVA of the full set cannot be conducted using the raw data. Instead, a MANOVA was conducted for each muscle separately, analysing the mechanical advantage data at the studied gape angles for all taxa that possess that muscle; this comprises the first set of MANOVAs. The **Infraorbital ZygomaticoMandibularis (IOZM)** is absent in five taxa (the sciuromorphs, and *A. rufa*), all of which possess an **Anterior Deep Masseter (ADM)**, so the **ADM** data of those taxa was compared with the **IOZM** to maintain the inclusion of the full sample. However, the **Deep Masseter (DM)** of hystricomorphs was compared with both the **Anterior Deep Masseter (ADM)** and the **Posterior Deep Masseter (PDM)** in the 'individual muscle' MANOVAs; this compares the **DM** with both its subdivisions in the taxa where those subdivisions are present, allowing these data to test existing interpretations about the **ADM** being an adaptation for increased mechanical advantage compared to the undifferentiated **DM** alone (Druzinsky, 2010). Since the **ADM** and **PDM** are so closely connected and difficult to separate, I believe this is a sound comparison, though it will need to be kept in mind when examining the results. The MANOVA test for most muscles will be primarily focussed on evaluating the significance of the difference between morphotypes with respect to the mechanical advantage of individual homologous muscles, but the MANOVAs described specifically above will illuminate the potential significance of the differentiations that define morphotypes. This is something that a broader analysis cannot do as clearly, or without using subsamples of taxa. This forms a set of 20 MANOVA analyses that are compiled into a table in the Results subheading. However, this muscle-by-muscle approach fails to evaluate the broader picture of the masticatory system as a whole; this is the gap addressed by the other two sets of MANOVAs.

The raw data has far too many datapoints to identify trends visually or evaluate the broader patterns; to produce visual comparisons and identify the relative contribution of different variables, a statistical analysis is required to reduce the dimensionality of the data and tease out the significant results from the noise. To answer these broader questions, a set of Principal Components Analyses (PCAs) were conducted. In this thesis, the names of muscles will follow the colour coordination system established in Chapter 2; in the Results section, the Loading Plots of the PCAs will share this colouring system to help cross-reference discussion in the text with the correct data in the results.

The mechanical advantage results were compiled into a table. Each row was an individual taxon, with the data arranged in columns of increasing gape, muscle by muscle. Since only sciuromorphs and *A. rufa* lack an **IOZM**, two separate PCAs were conducted. In both analyses, all taxa are included. In the first analysis, the **IOZM** is compared with the **ADM**, and the **DM** is compared with the **PDM**; since myomorphs possess both the **IOZM** and the **ADM** the muscles have to be compared in two tests, as follows. The **IOZM** of all taxa that possess it are compared to the **ADM** of sciuromorphs and *A. rufa*, and the **ADM** of all taxa that possess it are compared to the **IOZM** of hystricomorphs and bathyergid protrogomorphs. In the second PCA, the data for the **IOZM** is removed from the dataset, and the **ADM** and **PDM** are both compared with the **DM**; this allows comparison of the effect of the differentiation of the **DM** without having to remove taxa due to the absence of the **IOZM** in some taxa.

I conducted the PCAs using PAST version 4 (Hammer, Harper and Ryan, 2001), and I exported and compiled the results into spreadsheets in Microsoft Excel. I produced PC plots of PC 1 vs PC 2 and PC 3 vs PC 4 and exported them as .stl files, and I exported the loading plots directly from PAST as .stl files. These PC plots and the loading plots for molar and incisor biting for the full sample of taxa—and the subsample of taxa possessing an **IOZM**—are compiled into panel figures in the Results section. I colour-coded the datapoints on the PC plots by their morphotype category for clear visual

comparison. I drew translucent convex hulls and filled them with the corresponding morphotype colour for easier visibility of the distribution of each morphotype and comparisons of the PC space occupied by each group. These convex hulls should not be misinterpreted as implying that the PC scores of that morphotype can or cannot extend beyond the existing isolated datapoints and further out into the PC space if new taxa were added to the analysis; they are a visual aid for the distribution.

Each PCA was then used for a MANOVA. The Principal Component Scores of each test were used as dependent variables for two pairs of MANOVAs: one for incisor biting and molar biting each for the dataset where the **ADM** is compared to the **IOZM**, and for the dataset where the **ADM** is compared to the **DM** and the **IOZM** data is removed from the PCA completely. I chose to compare the **ADM** and **IOZM** because they are both anterior differentiations of the masseter which are characteristic of specific morphotypes; by comparing them, all taxa and all muscles can be included in a single PCA, rather than having to remove sections of the data. The possibility of comparing these two muscles was mentioned in the Discussion of Chapter 2, and can be explored here. The two subdivisions will be compared alongside comparisons between homologous muscles, contextualising the extent of potential differences between their mechanics. These create a quantitative value as a reference point for the patterns identified using the PC plots, highlighting which analyses show a statistically significant difference between the means of the morphotype categories' PC scores. These MANOVAs' results tables are included in the relevant subheadings on the results of the PCAs.

As the 'individual muscle' MANOVAs perform multiple analyses on the same sets of dependent variables (mechanical advantage at the selected bite point), a Bonferroni correction was applied to the initial p-value of 0.05. This set of MANOVAs performs 10 analyses for each bite point, resulting in an adjusted p-value of 0.005. The incisor and molar analyses on the PC scores only conduct one MANOVA on each bite point, and so require no correction and retain a p-value of 0.05.

3.2.4 – Head Size Correlation Testing

To test for a correlation between head size and mechanical advantage, one measure of head size is required from the several possible options. Different measurements of size can be better suited to specific aims (Jungers, Falsetti and Wall, 1995), and several factors were considered when selecting the measure of head size for this analysis.

For comparison with head size, the data of mechanical advantage needs to be reduced in dimensionality to a more convenient scale than the thousands of mechanical advantage datapoints can present as raw data. I resolved this issue by testing for a correlation between head size and the PC scores of mechanical advantage produced in the PCAs outlined above, as these scores already reduce the dimensionality without losing the variation from their contributing factors. As for head size itself, an individual dimension does not account for variation in proportions; for example, using head length as a measure of head size would not reflect the fact that some specimens are proportionally long for their height (such as *L. aenigmamus*) while others are comparatively tall for their head length (such as *Thomomys umbrinus*), and could give a distorted or incomplete representation of 'size' as a result. Since only some specimen scans contained soft-tissue, head volume or mass measurements including soft-tissue were unsuitable for this study.

One option is to calculate a mean size measurement using simple measurements. I selected Geometric Mean as the size measurement for this study, and calculated it using the x-, y- and z-dimensions of the specimens as shown in Equation (7). This is not without precedent, as Geometric Mean has been applied previously in the field of biology, both for body size and for skulls, including in comparisons with other measures of size (Robinson and Redford, 1986; Jungers, Falsetti and Wall, 1995; Coleman, 2008). Since all specimens had been aligned in molar occlusion in the same way relative to the global axes, measurements could be taken in Avizo with only a small potential human error. I viewed the specimens in the XY, YZ, and XZ planes, and took measurements using the 3D measurement tool in Avizo. 'Height' was measured from the lowest point of the mandibular body (typically

somewhere directly below the molar tooth row) to the highest point of the dorsal cranium when in lateral view. 'Length' was measured from the most posterior point of the skull to the most anterior tip in lateral view (due to the shape of the nasal bones in some taxa, the anterior point was at the tip of the nasal bones, in others, it was at the bottom of the nasal opening, on the premaxilla). 'Breadth' was measured between the furthest mediolateral points of the right and left zygomatic arches, in anterior view.

$$Geometric\ Mean = \sqrt[3]{Length \times Width \times Height} \qquad (7)$$

I used these three measurements to calculate Geometric Mean using Equation (7). Functionally, this makes this measure of head size a representation of the volume of the head; even if one specimen is longer than is typical for the height of its head, as in the case of *L. aenigmamus*, this will be factored into the measurement of its volume rather than obscured by or obscuring its relative size in other dimensions.

I used these calculations of geometric mean as the dependent variable in a Multiple Linear Regression (MLR) to test for a correlation between head size and mechanical advantage. Every muscle attachment centroid is a variable that affects the mechanical advantage of each muscle in the raw results. When conducting a PCA to reduce the dimensionality of the data, the mechanical advantage of each muscle within each taxon is a variable that affects the PC score of that taxon. Gape angle is also a variable in these results, itself affecting the in-lever of each muscle individually. The active tooth of the simulated bite (molar or incisor) is also a variable in the overall results of mechanical advantage for each muscle, within each taxon. By running a multiple regression of the PC scores of mechanical advantage for a given bite point, I can test if the geometric mean of head size correlates with the variation in mechanical advantage as affected by these variables. If it does correlate, then head size may be a significant component in the variance of the results.

This regression was conducted separately for each bite point, using their corresponding tables of PC scores, and conducted on both the PCA

datasets discussed prior. The equations were assumed to include a constant, as size cannot equal zero in a real physical specimen, and the regression was performed using PAST 4. I compiled the outputted statistics in results tables, of which the most relevant are the F-statistic and its corresponding p-value.

This analysis could not include all Principal Components in the PC score table. An MLR cannot be conducted if the number of rows and columns are equal in the input table. As such, a single PC was removed from this analysis (PC 26), and the MLR was conducted for PCs 1 to 25. Since PC 26 itself accounts for 0.00016% of the total variance in incisor biting and 0.00003% of the total variance in molar biting for the **IOZM** v **ADM** PCA and for 0.00003% and 0.00001% respectively in the **ADM** v **DM** PCA, I believe its absence will not have a notable effect on the results of this analysis.

3.3 – Results

3.3.1 – Comparing Morphotypes

As outlined in the Introduction, these data and analyses can be used to answer two primary key questions: does incorporating gape allow the mechanical advantage data to differentiate between morphotype categories, and does comparing the mechanical advantage data for incisor and molar biting reveal differences between the morphotype categories? Both of these will be addressed in this section.

3.3.1.1 – A brief overview of observable trends in the raw data

The raw mechanical advantage data is included in the supplementary materials of the thesis. These results will not be discussed in detail as patterns of morphotypes—the focus of this chapter—are not identifiable on so many graphs. The 54 raw data graphs themselves are too numerous, noisy and complex to clearly identify patterns between the morphotypes using the graphs alone, or to reasonably show at a readable scale in this chapter, hence the use of PCAs and MANOVAs in subsequent sections to assess my hypotheses by reducing the dimensionality of the data and evaluating patterns. A few key trends are notable and identifiable and will be discussed here. Of all of the data collected, I will only discuss the broad visually obvious patterns: that muscles can increase, decrease, or inflect their trends in mechanical advantage with gape, and that some muscles are consistently high or low compared to others. Some muscles will be discussed less than others, as they lack easily identifiable visual patterns.

As would be expected, mechanical advantage is higher in molar biting than incisor biting. This is due to the molar out-lever (the denominator in the formula for mechanical advantage) being shorter than the incisor out-lever. This does not apply evenly to all muscles due to their different positions—anterior muscles like the **ADM** and **Superficial Masseter (SM)** typically

display a mechanical advantage greater than 1.0 during biting with the first molar at lower gape, as the muscle origin on the skull is anterior to the cheek teeth and so the in-lever is longer than the out-lever. However, since muscles are affected differently, the relationship between their mechanical advantages can sometimes change when comparing molar and incisor biting within a specimen, particularly among muscles that have similar mechanical advantages. The patterns observed will be discussed in separate paragraphs: incisor data first, molar data second.

Functionally, a graph of a muscle's mechanical advantage against gape will always be like a cosine graph except all negative values are flipped to positive; mechanical advantage cannot be negative, the type of lever simply changes when the in-lever reaches zero and force is therefore passing 'behind' the pivot. If one were to mathematically continue opening the jaws until the mandible completes a full circle through the head, back to its starting position at occlusion, there would be two gape angles where a given muscle has a mechanical advantage of zero, because the muscle's line of action will point directly to or directly away from the TMJ, resulting in an in-level of zero at this gape angle. The closer a muscle's line of action is to the TMJ when the teeth are at occlusion, the sooner in the opening of the jaws that the in-lever will reach zero; this can be observed occurring in the studied gape range in certain posterior muscles (e.g. the **PZM** in *C. porcellus* between 5° and 10° during incisor biting, and in *H. hydrochaeris* in both incisor and molar biting in this gape range; the **IP** in *L. aenigmamus* between 10° and 15° in incisor and molar biting, and between 5° and 10° degrees in incisor biting in *H. cristata*; and in the **EP** in *E. dorsatum* between 30° and 35° in incisor biting, and between 35 and 40 in incisor biting in both *H. hydrochaeris* and *M. coypus;* this occurs because these muscles' origins and insertions are so posterior on the specimen relative to the position of the TMJ). Across the graphs, "anterior" muscles tend to have higher mechanical advantage than "posterior" ones (for example the **IOZM** being higher than the **AZM**, which is itself higher than the **PZM**). However, the shallower the inclination of the line of action of a muscle at occlusion (and thus the shorter its initial in-lever

compared to a different muscle with an origin in a similar position) the sooner it will reach a mechanical advantage of zero as gape increases; this is why the **SM**'s mechanical advantage drops off relatively sharply as gape increases, whereas muscles like the **IOZM** tend to see an increase with gape. Due to the variations in the initial in-lever at occlusion, and the associated inclination of the muscle's line of action in 2D, each muscle's mechanical advantage is thus a cosine graph with a different amplitude (i.e. peak mechanical advantage) and a different phase-shift (i.e. a different offset from zero degrees gape). The differences in these variables, especially the phase shift, can cause muscles to 'cross' over each other on these graphs as gape increases. This can cause muscles one might think of as "anterior" based on their skull origins to drop below the mechanical advantage of relatively "posterior" muscles at higher gape angles, such as the **SM** starting with a higher mechanical advantage than **AZM**, then dropping below it as gape increases, in many studied taxa.

There is simply too much data to list the pattern of every single line, but a couple of particular points of contrast stand out to me, observing all 54 graphs together. *A. rufa* possesses an especially high mechanical advantage in the **AZM**, noticeably much more similar to that of its **ADM** than in other taxa with an **ADM**; typically, the **AZM** has a higher mechanical advantage than the **DM** in hystricomorphs, but substantially lower than the **ADM** in myomorphs and sciuromorphs. The **SM** consistently decreases with increasing gape, often showing the steepest change with gape on many graphs; this is because its relatively anterior origin and posterior insertion give it an especially shallow line of action. The **IOZM** is typically the highest mechanical advantage muscle when present, especially in *E. dorsatum*, but is closely matched by the **ADM** in *R. norvegicus*, exceeded by the **ADM** at all gape angles in *A. cahirinus*, and sometimes exceeded by the **SM** at low gape in *G. capensis*, *H. hydrochaeris*, and *L. maximus*. **IP**, **EP**, and **T** typically have low mechanical advantage relative to most masseter subdivisions, and often show their peak mechanical advantage in the tested gape range, with other muscles more rarely showing a peak in this range (e.g. the **ADM** in *T.*

umbrinus). **EP** is typically the lowest mechanical advantage muscle, sometimes similar to the **T** or **PZM**, but *B. suillus* is an odd outlier for having an **IP** that starts with a high mechanical advantage than the **EP** and then decreases below that of the **EP** as gape increases to almost reach zero at 40°, forming a similar slope to the **SM** in this taxon; usually when the **IP** exhibits a greater change with gape than other low mechanical advantage muscles, that is usually a positive trend as gape increases in this sample and often peaks at higher gape.

For clarity, only one visual example will be shown here, in Figure 3.2. This is to illustrate some of these patterns, and incisor biting in *R. norvegicus* was selected in continuity with its use as an illustrative example previously in this chapter. It can be observed that the **SM** and **PDM** decrease in mechanical advantage with increasing gape, with the **SM** decreasing most steeply. Meanwhile, the **ADM**, **IOZM**, **AZM**, **PZM**, and **T** increase with gape, and the

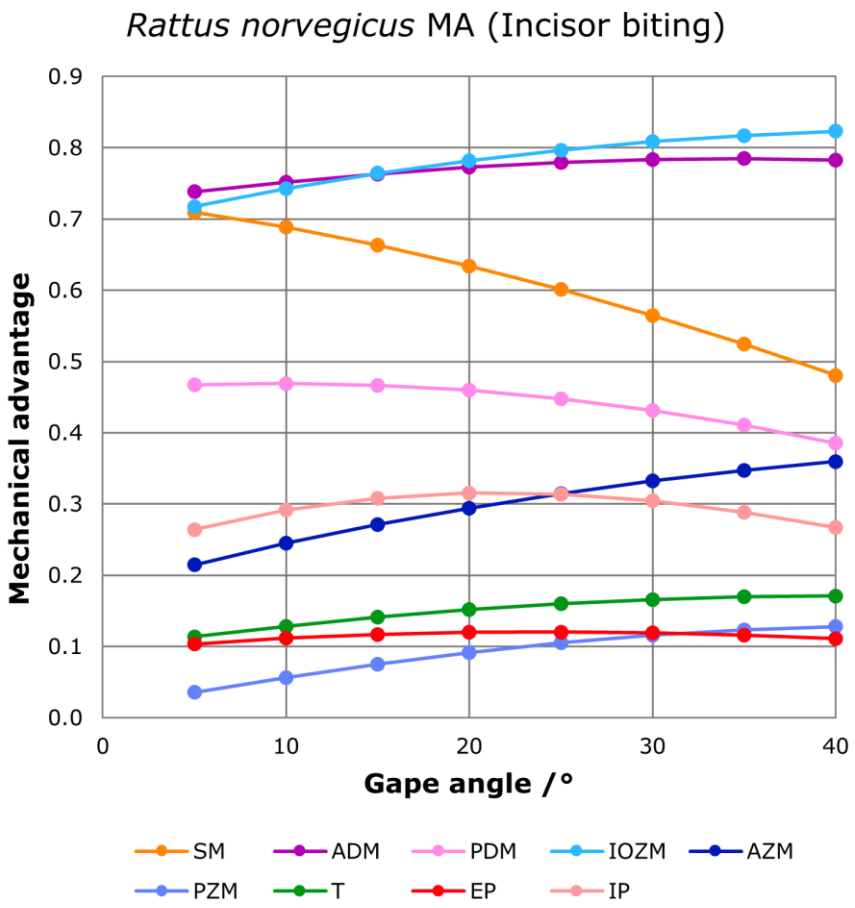

Figure 3.2: Raw mechanical advantage data for *R. norvegicus* during biting with the incisors. Each muscle is shown at the full range of studied gape angles.

IOZM and **ADM** can be observed to 'cross' as gape increases between 10° and 15°; the **IP** and **EP** both have an inflected pattern, peaking around 20° then decreasing as gape increases.

The exact patterns and trends vary depending on taxon, and identifying trends by morphotype is not especially feasible with the number and complexity of the graphs. The variation in trends and patterns is reflective of the intricate arrangement of each subdivision of the muscular system within individual taxa, let alone between them.

3.3.1.2 – Individual muscle MANOVA results

The results of the individual muscle MANOVAs are compiled in Table 3.1, below. I conducted 20 MANOVAs in total, divided into two groups by the bite point in question: incisor biting or molar biting. The significant results (p-value below 0.005 due to the Bonferroni correction) are highlighted for clarity using bold green text.

According to these MANOVAs, only one muscle has mechanical advantage that significantly correlates with morphotype category in either bite point: the test that compares the **ADM** and **DM**. The implications of this are complex. Since these analyses compare both the **ADM** and the **PDM** with the undifferentiated **DM** of the hystricomorphs the results of the **ADM** and **PDM** should be considered in relation to one another and the **DM**. The variance in mechanical advantage for the **PDM** and the **DM** are not significantly correlated with the morphotype categories. However, the variation among the **ADM** and **DM** when combined is significantly correlated with the morphotypes in incisor biting: i.e. the **ADM** and the **DM** have significantly different mechanical advantage while the **PDM** and the **DM** do not. In effect, this mathematically represents the difference in mechanical advantage of the masticatory system due to the differentiation of the **DM** complex and its anterior expansion onto a zygomatic plate to form the **ADM**. This is in line with prior interpretations on the mechanical function of the **ADM** (Druzinsky, 2010).

Bite	Muscle	df1	df2	Pillai's Trace	F	p
Incisor	SM	24	54	1.028	1.173	0.307
	ADM & IOZM	24	54	1.164	1.426	0.140
	ADM & DM	24	54	**1.554**	**2.419**	**0.004**
	PDM & DM	24	54	0.873	0.932	0.573
	IOZM & ADM	24	54	1.141	1.381	0.162
	AZM	24	54	0.732	0.726	0.803
	PZM	24	54	1.061	1.231	0.259
	T	24	54	1.036	1.186	0.295
	EP	24	54	0.824	0.852	0.659
	IP	24	54	1.103	1.309	0.204
Molar	SM	24	54	1.056	1.222	0.266
	ADM & IOZM	24	54	1.121	1.342	0.184
	ADM & DM	24	54	**1.555**	**2.420**	**0.004**
	PDM & DM	24	54	1.321	1.769	0.042
	IOZM & ADM	24	54	1.366	1.881	0.028
	AZM	24	54	0.747	0.746	0.781
	PZM	24	54	1.288	1.692	0.055
	T	24	54	1.026	1.170	0.309
	EP	24	54	1.124	1.349	0.180
	IP	24	54	0.762	0.767	0.759

Table 3.1: This table displays the results of the MANOVAs conducted on the raw data. Significant values are bolded and coloured in green; the corrected p-value is 0.005. The row '**ADM** & **IOZM**' compares all **ADM** results with the **IOZM** of taxa that lack an **ADM** (the hystricomorphs and bathyergids), whereas the '**IOZM** & **ADM**' results compared all **IOZM** results with the **ADM** of taxa that lack an **IOZM** (the sciuromorphs and *A rufa*). This has to be split because the myomorphs possess both muscle subdivisions.

3.3.1.3 – Principal Components Analyses results

3.3.1.3.1 – Analysis with all muscles

The comparisons made in this PCA were discussed at length in the Materials and Methods section, but as a reminder, the **IOZM** and **ADM** are compared, and the **DM** is compared with the **PDM**, allowing all taxa and all muscles to be included in a single PCA. Of the 26 PCs generated by this analysis, only the first four will be displayed as PC plots; from PC 5 onwards the components are responsible for ever decreasing proportions of the variance, which is insufficient to draw significant interpretations from them.

The variance accounted for by each PC from 1 to 4 for each bite point analysis is displayed in Table 3.2. Of the remaining PCs, no PC accounts for more than 5% of the variance in the sample in incisor biting, and only PC 5 does in molar biting, at 6.09%.

Analysis	PC 1	PC 2	PC 3	PC 4	Total % of variance
Incisor bite	44.84	16.86	12.47	8.82	82.99
Molar bite	39.04	21.10	10.59	8.79	79.54

Table 3.2: This table displays the percentage of the total variance accounted for by PCs 1–4 in each of the PCAs for the analysis comparing the **IOZM** and **ADM**. All values are rounded to two decimal places.

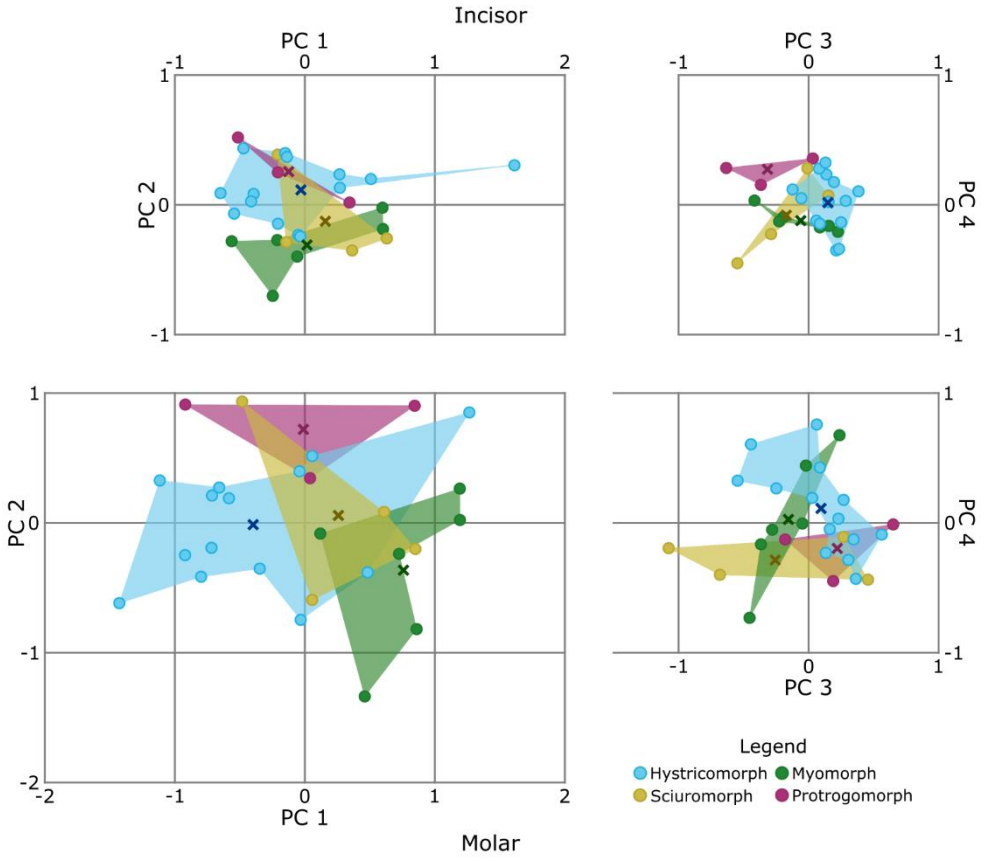

Figure 3.3: PC Plots for mechanical advantage data across all muscles, where the **IOZM** and **ADM** are compared. All graphs are at the same scale, displaying PC 1 vs 2 and PC 3 vs 4 for incisor and molar biting. Means for morphotypes are marked with an x-mark.

Figure 3.3 displays the results of the incisor and molar PCAs in the form of four PC plots. These plots have axes of PC 1 against PC 2, and PC 3 against PC 4. Several key trends are observable. Firstly, the incisor PC plots cluster around the mean (0,0) more tightly than their molar counterparts. In

incisor biting for PC 1 v 2 (44.84% v 16.86% variance), the groups roughly divide on PC 2 into two groups, with the myomorphs and most sciuromorphs (except for *C. canadensis*) and *A. rufa* occupying the negative PC 2 space, with most hystricomorphs and the bathyergids in the positive PC 2 space. Among the hystricomorphs, *P. capensis* is a major outlier on PC 1, and in incisor biting is far not only from its morphotype but from all other rodents, being the only hystricomorph with a PC score greater than one on PC 1 in both incisor and molar biting. On molar PC 1 v 2 (39.04% v 21.10%), the hystricomorphs mostly separate from the other rodents, with several taxa forming a cluster in the negative PC 1 space. For molar PC 3 v 4 (10.59% v 8.79%), most of the hystricomorphs cluster closely with the other morphotypes.

Of the protrogomorphs, *G. capensis* is the most consistently similar to hystricomorphs across multiple plots, and the group is mostly distinct from the other morphotypes on incisor PC 3 v 4 (12.47% v 8.82%) and molar PC 1 v 2, but overlaps entirely with hystricomorphs and sciuromorphs on incisor PC 1 v 2 and molar PC 3 v 4; curiously, the protrogomorphs are most similar to *C. canadensis* among the hystricomorphs on both PC 1 v 2 plots, but most similar to *S. carolinensis* and *P. petaurista* on molar PC 3 v 4. Among the sciuromorphs, except for *C. canadensis* they group with the myomorphs on both PC 1 v 2 plots, but are split on the PC 3 v PC 4 plots—*S. carolinensis* and *P. petaurista* group closely with hystricomorphs and protrogomorphs, while *T. umbrinus* and *C. canadensis* are outliers to this grouping on both PC 3 v 4 plots. The myomorphs are distinct from the hystricomorphs on the PC 1 v 2 plots, with *G. watersi* and *C. gambianus* typically being the most similar to hystricomorphs, and they form narrow inclined spreads across the PC 3 v 4 plots, with most taxa being close to those of other morphotypes except for *R. norvegicus*, which has the most negative PC 4 score of any taxon on molar PC 3 v 4.

Since PCs 1–4 account for decreasing proportions of the variance, the most significant visual results listed above are likely those of the PC 1 v 2 plots: the separation of *P. capensis* from other hystricomorphs on PC 1, the rough separation of myomorphs from hystricomorphs, the differentiation of

protrogomorphs in molar biting, and the difference between *C. canadensis* and the other sciuromorphs. These are the most notable differences between morphotypes in these data, but no plot can fully differentiate one morphotype grouping from all of the others without exception; there is always overlap with at least one other on one or both of the axes of that plot, and individual taxa (such as *C. canadensis*, for example) can sometimes be more similar to those of a different morphotype than to taxa of their own.

By examining the loading plots (Figure 3.4a and 3.4b), one can see which specific muscles are responsible for the variance on each PC, and how gape angle affects this contribution. In other words, which gape angles and muscles have the greatest disparity within the sample, in decreasing order of the PCs' contribution to variance. On these loading plots, bars that exceed the translucent grey region are contributing to the total positive or negative variance on that PC more than would be expected if all loadings contributed equally to positive or negative variance. The bars that extend beyond the grey region are those that contribute notably to the variance. I used a simple calculation to determine the value represented by the grey region; one is divided by the number of loadings. The figure is split across two pages to keep the bars at a readable scale in this thesis, but shall be discussed together. For readability, the analyses that have multiple muscles are not given complex or split colours to represent this, but the x-axis clarifies the comparisons.

Several trends can be observed. Each muscle's contribution to variance on a given PC tends to increase or decrease as gape increases, and it is relatively rare for a muscle's contribution to positive or negative variance to be consistent as gape increases (e.g. the **IOZM** on molar PC 1). Across most muscles and PCs, the high or low ends of the studied gape range are responsible for the majority of the variance.

For the incisor biting analysis, PC 1 (44.84% variance) has no muscles that overall contribute to negative variance, so these values may be most reflective of the distinction of *P. capensis*. The largest contribution to the variance is from the **AZM**, then the **IOZM** vs sciuromorphs **ADM** and **ADM**

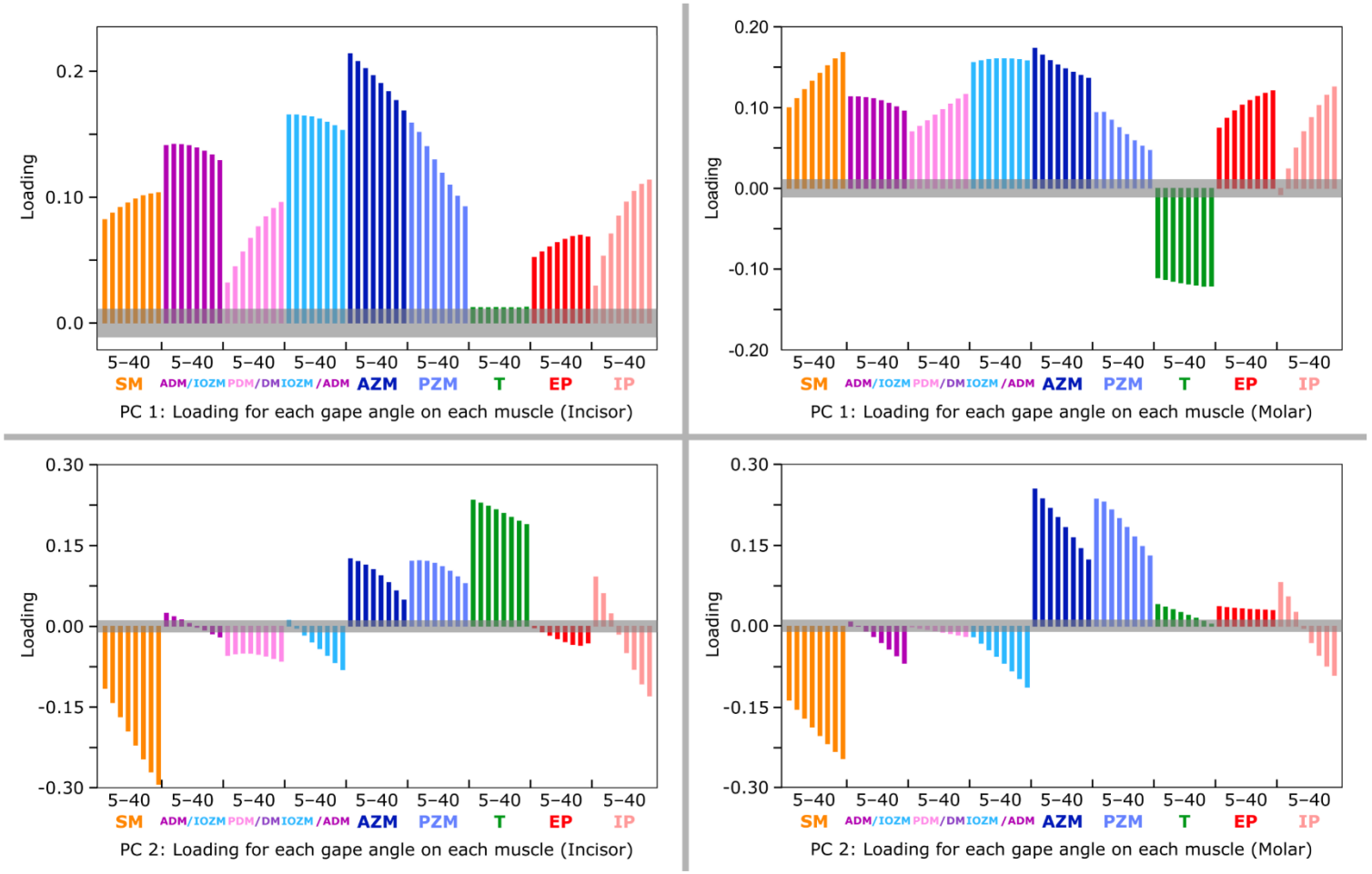

Figure 3.4a: Panel figure displaying the Loading Plots for PCs 1–2 in both incisor (left plots) and molar (right plots) biting with the **IOZM** and **ADM** compared to each other. Bars that extent beyond the grey area are significant.

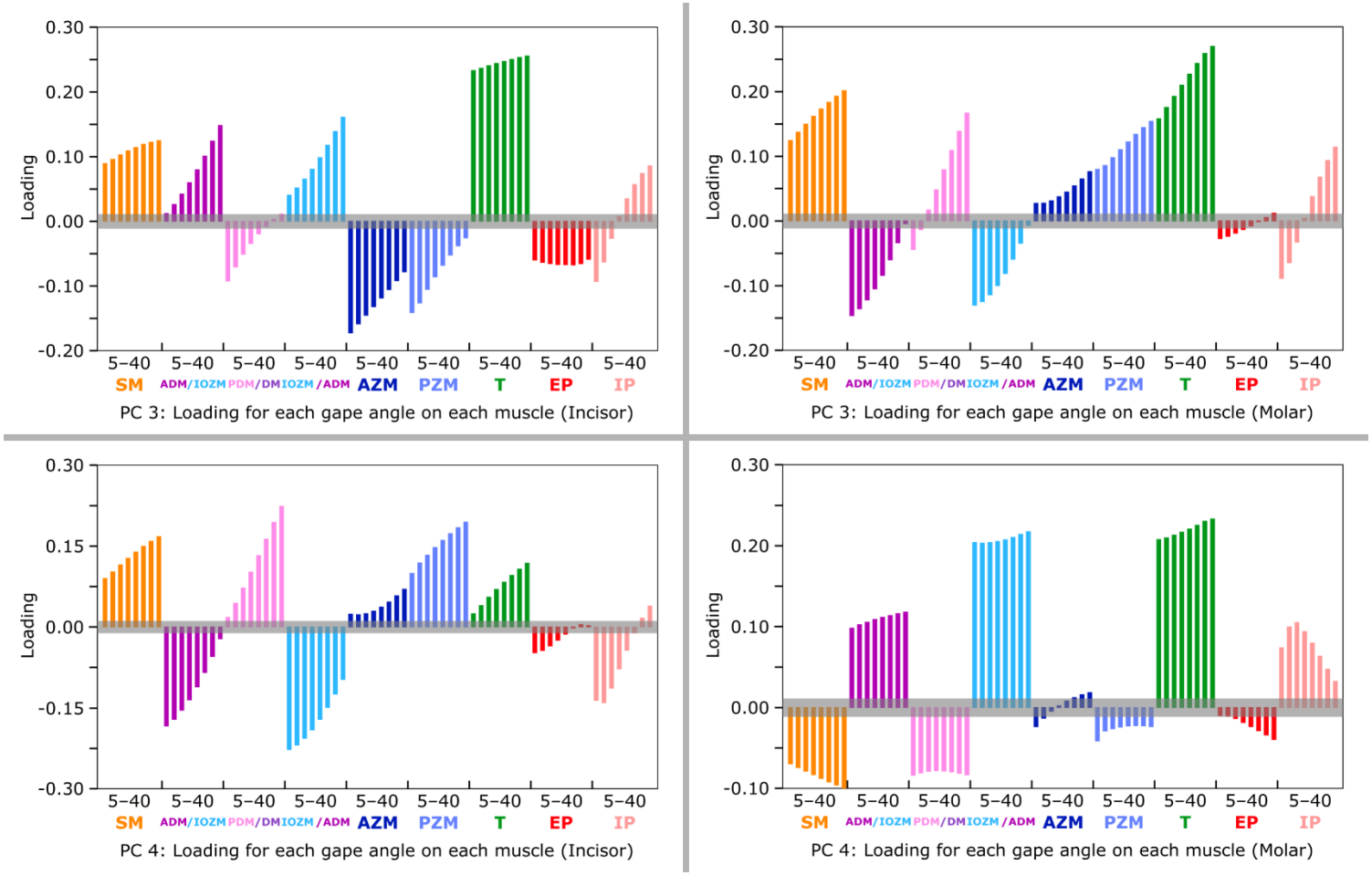

Figure 3.4b: Panel figure displaying the Loading Plots for PCs 3–4 in both incisor (left plots) and molar (right plots) biting with the **IOZM** and **ADM** compared to each other. Bars that extent beyond the grey area are significant.

vs hystricomorph/bathyergid IOZM, then the PZM; all of these muscles decrease in their contribution to the positive variance as gape increases, i.e. they trend towards negative values. The SM, IP, PDM vs DM, and EP all contribute less, with the T being the smallest contributor to the variance. For PC 2 (16.86% variance), the T contributes the most to the positive variance, while the SM contributes the most to the negative variance. The other muscles all contribute less to the either the positive (AZM, PZM) or negative (most other muscles) variance. The IP contributes to the positive variance at low gape, but to the negative variance at high gape. In most of these muscles, they trend towards the negative as gape increases. On the incisor PC 3 (12.47% variance) plot, the largest positive contribution is once again from T. Smaller positive contributions come from the SM, IOZM and ADM comparisons, and the IP at high gape. The largest contributions to the negative variance come from AZM and PZM, with smaller contributions from the PDM vs DM, the EP, and the IP at low gape. All muscles on this PC trend positive with increasing gape, except for the EP, which is consistent as gape increases. And finally, on PC 4 (8.83%), the largest positive contributions come from the SM, PDM vs DM, and PZM. Smaller contributions to the positive variance come from the AZM and T. The largest negative contributors are the IOZM v ADM analyses, and the IP at low gape. All muscles trend towards the positive direction with increasing gape.

In molar biting, there are substantial differences. On PC 1 (39.04%), the T contributes significantly to the negative variance, and trends slightly more negative as gape increases. Otherwise, the muscles all contribute positively to the variance in incisor biting, with the largest contributions from the SM at high gape, the AZM, and the IOZM vs sciuromorph ADM. The ADM vs hystricomorph/bathyergid IOZM, PDM vs DM, PZM, EP, and IP all contribute slightly less to the variance. The SM, PDM vs DM, EP, and IP become increasingly positive with gape, while the IOZM vs sciuromorph ADM is consistent, and the other muscles trend negative as gape increases. On the PC 2 (21.10%) plot, the AZM and PZM are the largest contributors to the positive variance, with small contributions from the T, EP, and low gape

IP; compared to incisor biting, the T contributes less and the AZM and PZM contribute more. The biggest contributor to the negative variance is SM, with contributions to the negative variance at high gape from the ADM vs hystricomorph IOZM and IOZM vs sciuromorph ADM analyses, and the IP. All muscles on this PC trend negative as gape increases. On PC 3 (10.59%), the largest positive contribution is from T, with smaller contributions from the SM, PZM, PDM vs DM, and AZM. All the muscles on PC 3 trend positive as gape increases, and compared with incisor biting, the deep and zygomaticomandibularis subdivisions have all flipped from negative variance to positive variance, or vice versa. Finally, on the PC 4 molar plot (8.79% variance), the largest positive contributions come from the IOZM vs sciuromorph ADM, and T, with smaller contributions from the ADM vs hystricomorph IOZM, and IP. The largest contributions to the negative variance come from the SM and PDM vs DM, with smaller negative contributions from the PZM and EP. The positive muscles tend to trend slightly positive as gape increases, while the negative muscles tend to trend slightly more negative, but IP is a notable outlier to most of these trends in both incisor and molar biting; its contribution to negative/positive variance peaks around 10–15° before trending towards zero.

In summary, all muscles contribute significantly to the variance on at least one PC, but some muscles contribute notably across all plots (e.g. SM), while others only contribute on a few (e.g. EP, which is most notable on PC 1 and less so on PCs 2–4). Interestingly, despite the fact that some of these comparisons are between separate muscle subdivisions (ADM vs IOZM, PDM vs DM), they do not dominate the loading plots; these muscles are distinct, but not out of line with the variation in, say, the SM and the T across the sample. Bite point affects the contribution of some muscles to the variance, but others are loosely consistent between the two bite points.

Finally, the PC scores for mechanical advantage across the full sample were also compared using a MANOVA, to statistically test for significant difference between means of the morphotype categories. In order to produce a valid result due to the number of PCs, only PCs 1–23 were included in this

MANOVA; this accounts for 99.99954% of the variance in incisor biting and 99.99971% of the variance in molar biting. The p-value for this analysis is 0.05, and the results are shown in Table 3.3. The morphotypes are statistically significantly different during incisor biting (p-value of 0.04076), and molar biting (p-value 0.04424). This provides a statistical confirmation that the observed qualitative differences on the PC plots are significant and not solely visual.

Analysis	Incisor	Molar
df1	69	
df2	9	
Pillai's Trace	**2.873**	**2.870**
F	**2.961**	**2.887**
p	**0.041**	**0.044**

Table 3.3: This table displays the statistical results of the MANOVA conducted on PC scores for the full sample. Statistically significant values are bold and coloured in green.

3.3.1.3.2 – Analysis without IOZM

This PCA removed the **IOZM** from the data and instead compared the **DM** with the **ADM**, as well as with the **PDM**. The resulting PCA plots are displayed in Figure 3.5. As in Figure 3.3, the plots are at the same visual scale for ease of comparison between them. In addition, a table displaying the variance accounted for by each PC in this analysis, Table 3.4, from PC 1 to PC 4. Compared with the previous PCA, PC 4 accounts for less of the total variance, and PC 1 in particular accounts for substantially more of the total.

Analysis	PC 1	PC 2	PC 3	PC 4	Total % of variance
Incisor bite	48.21	23.39	10.80	4.53	86.92
Molar bite	55.58	15.88	10.60	4.76	86.82

Table 3.4: This table displays the percentage of the total variance accounted for by PCs 1–4 in each of the PCAs for the analysis comparing the **ADM** and **DM**.

Examining the PC plots in Figure 3.5, it can be observed that incisor biting displays a tighter clustering around the mean, while molar biting displays higher disparity in PC score. The rough split between myomorphs and hystricomorphs has been made much more sharp in this PCA.

On PC 1 v PC 2 in both incisor (48.21% v 23.39% variance) and molar biting (55.58% v 15.88% variance), the hystricomorphs group with the bathyergid protrogomorphs in the negative PC 1 space, with *P. capensis* once again being an outlier from other taxa of its morphotype. The myomorphs and sciuromorphs group together in the positive PC 1 space, along with *A. rufa*, the non-bathyergid protrogomorph, creating a split on the PC 1 v 2 plots and cleaving the sample into these two groupings. On the PC 3 v PC 4 plots (10.80% v 4.53% incisor; 10.60% v 4.76% molar), meanwhile, most taxa cluster much closer to the mean, with the hystricomorphs overlapping with

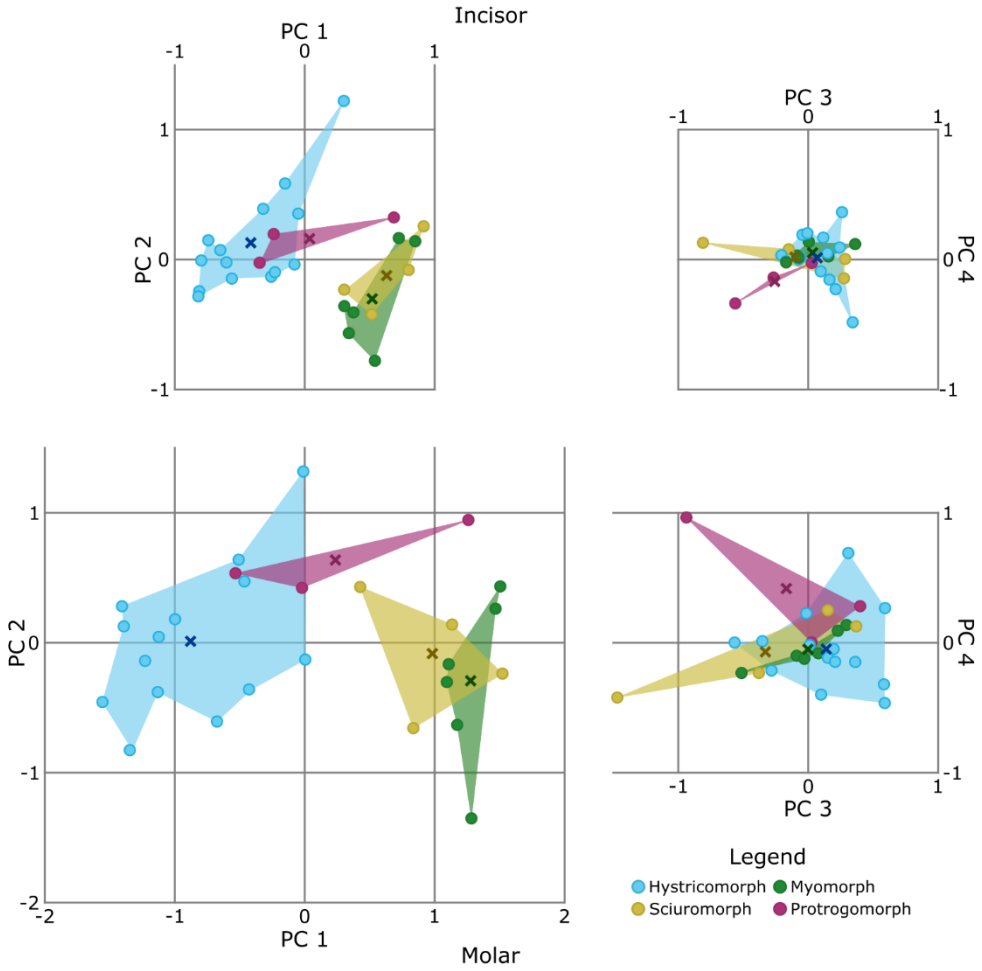

Figure 3.5: PC Plots for mechanical advantage data where the **IOZM** is absent and the **ADM** and **DM** are compared. All graphs are at the same scale, displaying PC 1 vs 2 and PC 3 vs 4 for incisor and molar biting.

most other taxa. Not dissimilar to the PC 3 v 4 molar plot in the previous analysis, *R. norvegicus* is relatively separate from other myomorphs on molar PC 2, having the most negative PC score of any rodent on PC 2 in both incisor and molar biting. Among the protrogomorphs, *A. rufa* is an outlier on PC 1, and on incisor PC 3 v 4, with the bathyergids (which, as a reminder, have an undifferentiated **DM**) being more similar to hystricomorphs on PC 1 v 2 plots. Curiously, *B. suillus* is an outlier on molar PC 3 v 4, not only to protrogomorphs but to the rest of the sample entire, occurring alone near (-1,1). The sciuromorphs mostly overlap with the myomorphs and hystricomorphs on PC 3 v 4 plots, but *C. canadensis* is once again an outlier to the group on most plots, being the most negative taxon on PC 3 in both bite points. Since PC 1 accounts for around half of the total variance in both bite points, the most significant result on these plots is undoubtedly the splitting of the same into two groupings: one with an undifferentiated **DM**, and one group of the taxa with the differentiation into the **ADM** and **PDM**. This is reflected strongly in the PC 1 loading plots, where the **ADM** vs **DM** comparison is the largest contributor to the positive variance in both bite points by far. However, other muscles still contribute noticeably to the variance on this PC and others.

On incisor PC 1 (48.21% variance), small positive contributions to the variance can be observed from most muscles, with a substantial contribution to the negative variance from the **T**. The **PDM** vs **DM** and **T** are consistent in their contribution to variance as gape increases, the **ADM** vs **DM**, **IP**, **SM** and **EP** become more positive with gape, and the **AZM** and **PZM** become trend negative with increasing gape. On incisor PC 2 (23.39% variance), the largest positive contribution comes from **AZM**, with a smaller contribution from the **PZM**, then the **T**, then the other muscles. The only significant contribution to the negative variance comes from the **ADM** vs **DM**. The **ADM** vs **DM**, **PDM** vs **DM**, and **IP** trend positive with increasing gape, the **SM**, **AZM**, and **PZM** trend negative, and the other muscles are consistent across gapes. On PC 3 (10.80%, the largest contribution to the positive variance comes from **SM**,

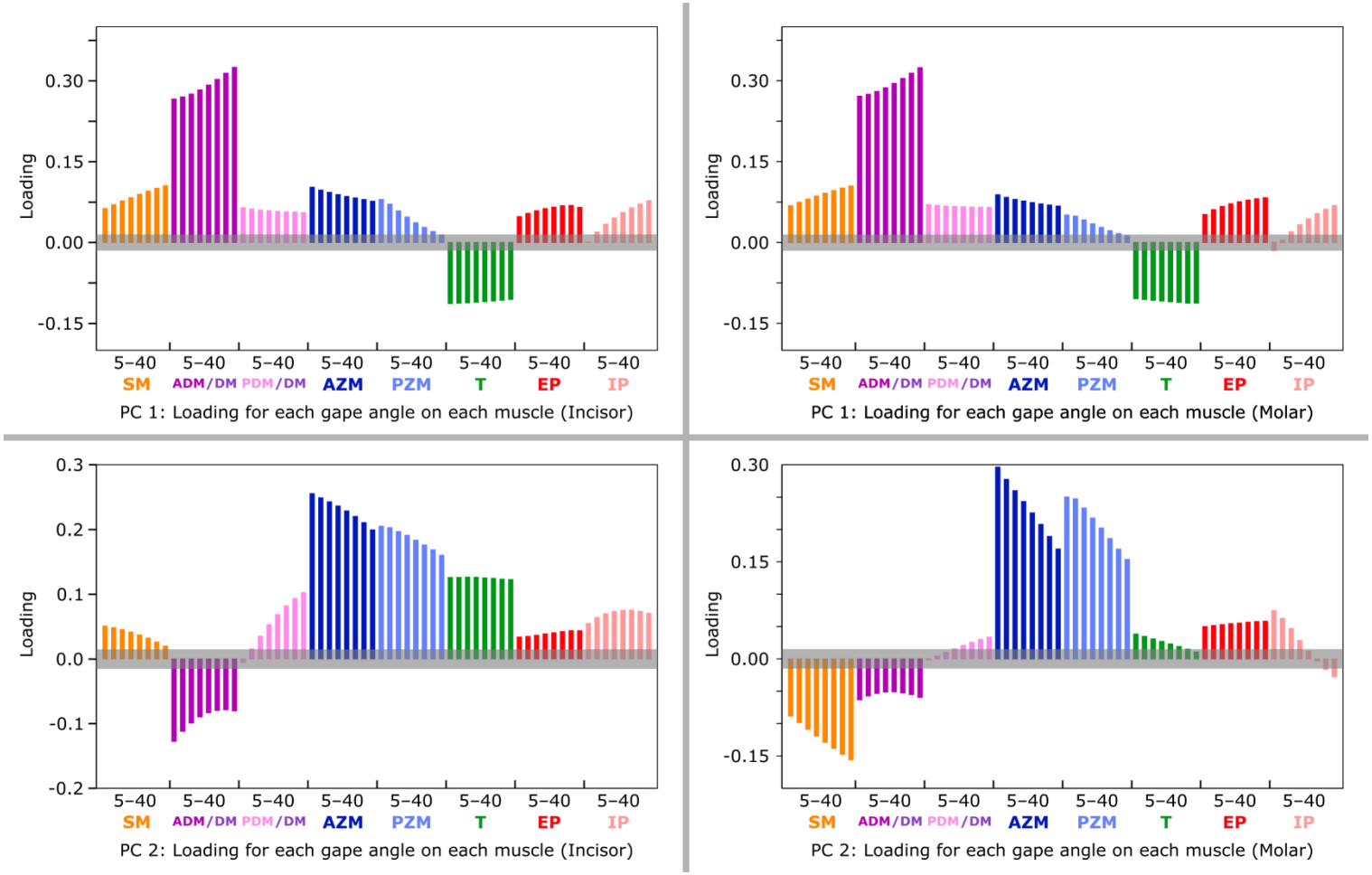

Figure 3.6a: Panel figure displaying the Loading Plots for PCs 1–2 in both incisor (left plots) and molar (right plots) biting when the **ADM** and **DM** are compared and the **IOZM** is absent. Bars that extent beyond the grey area are significant.

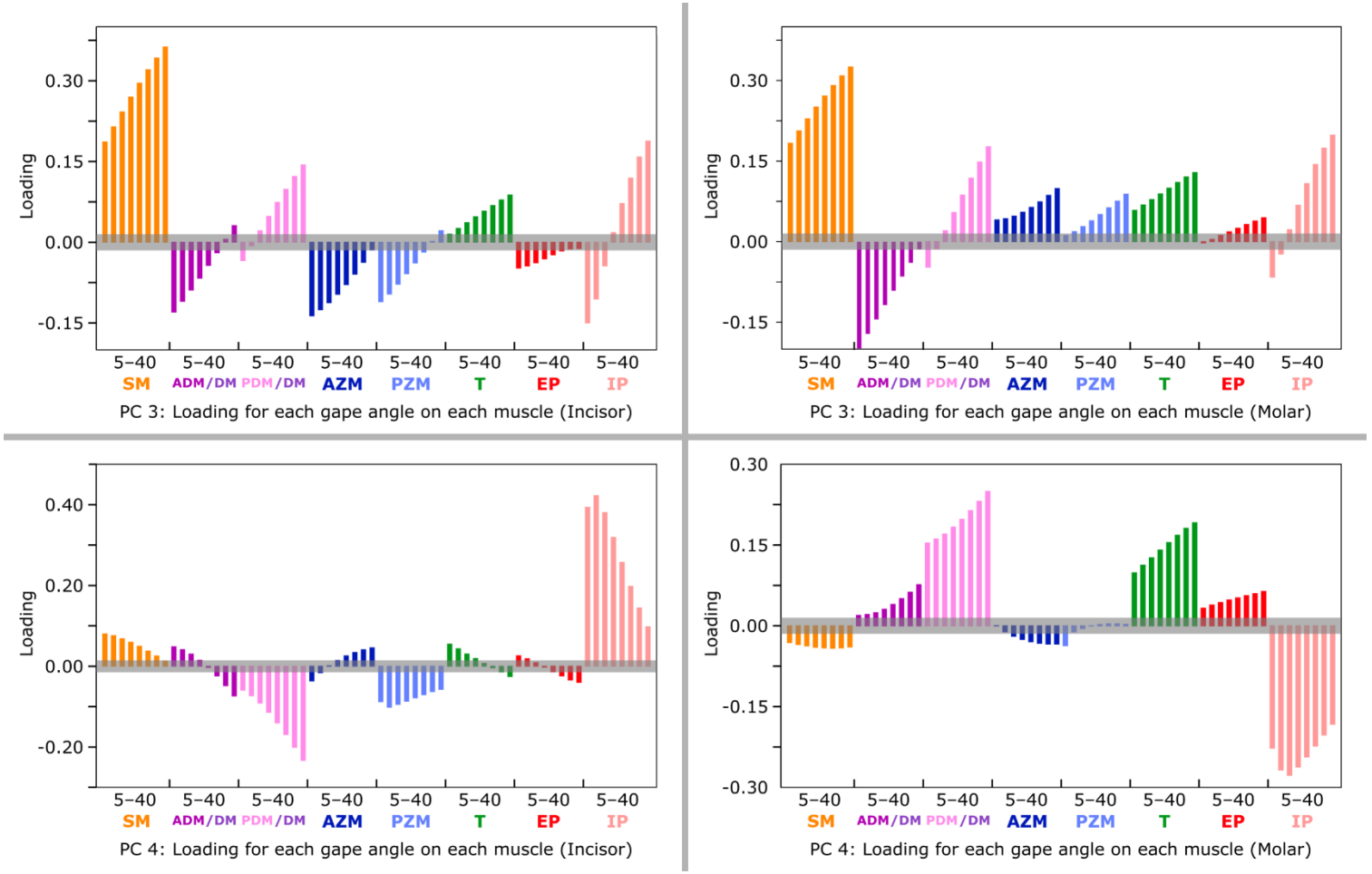

Figure 3.6b: Panel figure displaying the Loading Plots for PCs 3–4 in both incisor (left plots) and molar (right plots) biting when the **ADM** and **DM** are compared and the **IOZM** is absent Bars that extent beyond the grey area are significant.

with smaller contributions from T, and from PDM vs DM and IP above 20° gape, all of which trend positive with gape. ADM vs DM, AZM, PZM, and IP below 15° gape all contribute similarly to the negative variance, All muscles on this PC trend positive with increasing gape. Finally, on incisor PC 4 (4.53%), the only major contributor to the positive variance is IP, peaking at 10° gape before trending negative as gape increases further. The largest contributor to the negative variance is PDM vs DM, with smaller contributions from PZM, and AZM above 30° gape. Most noteworthy muscles trend negative with increasing gape, but the PZM trends positive as gape increases above 10°.

Meanwhile, on molar PC 1 (55.58%), the loadings are mostly the same as those of incisor biting, with marginally smaller contributions from the AZM and PZM, and slightly larger contributions from EP. PC 2 (15.88%) is more different, with SM now being the largest contributor to the negative variance. T, PDM vs DM, and IP all contribute less to the positive variance, and the contribution from the AZM and PZM to the positive variance is even greater. SM and IP both trend negative as gape increases, but ADM vs DM now exhibits its greatest contributions to the negative variance at the ends of the gape range. In molar PC 3 (10.60%), the main difference when compared with incisor biting is that the AZM, PZM, and EP have 'flipped' from negative to positive variance, and the contribution to the negative variance is now almost entirely from the ADM vs DM. SM remains the largest contributor to positive variance, and all muscles still trend positive as gape increases.

In molar PC 4 (4.76%), the loadings are very different to those of incisor biting. The largest contributor to the positive is PDM vs DM, then T, then smaller contributions from the ADM vs DM and EP. The only major contributor to negative variance is IP, peaking at 15° gape, and the negative contributions from the SM and

Analysis	Incisor	Molar
df1	69	
df2	9	
Pillai's Trace	2.787	2.774
F	1.708	1.600
p	0.195	0.228

Table 3.5: This table displays the statistical results of the MANOVA conducted on PC scores when the ADM and DM are compared.

AZM are much smaller. All muscles trend positive with increasing gape, though in the case of **IP** this only occurs beyond 15° degrees gape.

The results of the MANOVA of PC scores is compiled in Table 3.5. This compares the group means of all four morphotypes, with the significance threshold of the p-value being 0.05. Both p-values are above this threshold, so the morphotypes do not have significantly different group means.

I conducted a second MANOVA, with the results compiled in Table 3.6, with the sample split into two groups instead of four: the group mean of the hystricomorphs and protrogomorphs was compared with the group mean of the myomorphs and sciuromorphs, testing the significance of the division on PC 1 v 2 between these groupings. This returned a p-value of 0.03851 in incisor biting and 0.00423 in molar biting, both below 0.05. Both of these MANOVAs cover PCs 1–23, accounting for 99.9998% of incisor biting variance and 99.99993% molar variance. This second MANOVA shows that the division of the morphotypes into two clusters on PC 1 v 2 observed in this dataset is significant; the taxa are divided in this PCA between those that have an **ADM** and those that do not, which is supported by the earlier individual muscle MANOVAs showing the significance of the difference between the **ADM** and **DM** in isolation.

Analysis	Incisor	Molar
df1	23	
df2	3	
Pillai's Trace	**0.988**	**0.997**
F	**10.420**	**47.770**
p	**0.039**	**0.004**

Table 3.6: This table displays the statistical results of an additional MANOVA conducted on PC scores when the **ADM** and **DM** are compared. This compares the Hystricomorphs and Protrogomorphs with the Sciuromorphs and Myomorphs, thereby testing the significance of the apparent split into two such regions for the PC 1 v 2 plots. Statistically significant values are bolded and coloured in green.

3.3.2 – Head Size Regression

Table 3.7 summarises the outputs of the multiple regressions. In all cases, the p-value is greater than 0.05, and the null hypothesis (that head size does not correlate with mechanical advantage PC scores) cannot be rejected. It is important to note that these regressions were not conducted under a phylogenetic framework. Since the PCs included in this analysis account for well over 99.9% of the total variance, these tests conclude that size does not significantly correlate with mechanical advantage in these taxa. It can be ruled out as a potential complicating factor in interpreting the rest of the results.

		IOZM v ADM		**ADM v DM**	
Model		**Incisor**	**Molar**	**Incisor**	**Molar**
R Square		0.064	0.151	0.112	0.162
Mean Squared Error		0.022	0.055	0.025	0.074
Change Statistics	Wilks' Lambda	0.0084	0.0029	0.0003	0.0195
	F	4.737	13.660	138.7	2.008
	df1	25	25	25	25
	df2	1	1	1	1
	p	0.350	0.211	0.067	0.513

Table 3.7: Summary statistics of regression of the incisor biting and molar biting mechanical advantage PC scores on PCs 1 to 25 against geometric mean of head size.

3.4 – Discussion

3.4.1 – Key Questions and Hypotheses

To recap, the key hypotheses of this study were as follows. Firstly (**H2.1**) that gape was expected to have a notable impact on the variation in mechanical advantage, with the group means of morphotypes being significantly different. Secondly (**H2.2**), that the variation seen on the incisor PC plot would be smaller than that of the molar counterpart, with rodent taxa being closer towards the mean for gnawing when compared to chewing. I also anticipated that even during molar biting, there would be at least some overlap between morphotype categories on multiple PCs, and some taxa would be more similar to those of a different morphotype than to those of their own. To summarise briefly, these hypotheses and expectations are supported by the results. The morphotypes are not mutually exclusive but their means are significantly different, and both bite point and gape angle see substantial difference in variance. Even during molar biting, morphotype categories still overlap on multiple PCs despite having distinct group means. A more detailed discussion will follow in the coming paragraphs.

When examining the results of the PCAs, the morphotypes have a visible degree of overlap between them (especially in incisor biting) on multiple PC plots, despite some notable differences. Some taxa can be more similar to those of different morphotypes than others of their own morphotype. The MANOVA analyses of the PC scores show that the means of each morphotype are significantly different despite the similarities between individual taxa of different morphotypes, confirming that the categories are distinct despite the visible overlap. This supports **H2.1**.

In particular, hystricomorphs and myomorphs are distanced from one another on PC 1 v 2 plots, especially on PC 1. Though this distinction is present in the sample with all the muscles, where the **ADM** and **IOZM** are compared, the distinction becomes even stronger when comparing the undifferentiated **DM** to the **ADM** of other groups (statistically supported by the MANOVA results of the individual muscles). This supports the

interpretation that the **ADM** functions as an expansion of the deep masseter complex to increase mechanical advantage (Druzinsky, 2010), as the mechanical advantage of the two subdivisions is very sharply different, more different than the **IOZM** and **ADM**. The **ADM** and **DM** are significantly different during incisor biting (p-value of 0.003644 for incisor biting and 0.003634 in molar biting). However, the results suggest that even outside the differentiation of the deep masseter complex, hystricomorphs seem distinct from myomorphs and sciuromorphs in general, though *C. canadensis* and the bathyergid protrogomorphs tend to be more similar to hystricomorphs. The molar PC 1 v PC 2 plots tend to distinguish the hystricomorphs from the protrogomorphs, compared to the incisor plots—this is particularly apparent in the analysis with all muscle subdivisions, where a majority of the hystricomorphs cluster in an area of the negative PC 1 space where no other morphotypes co-occur. This aligns with existing interpretations that hystricomorphs are specialised for molar chewing when compared with the other morphotypes (Cox *et al.*, 2012), but with the exception of *C. canadensis* the sciuromorphs tend to group close to the myomorphs and away from the hystricomorphs on PC 1 v 2, especially during molar biting where the disparity between the groups is broader. This aligns with how historical comparisons have often contrasted hystricomorphs specifically with sciuromorphs in their molar biting (Cox *et al.*, 2012), but may also be affected by the sampling of this thesis project and disparity within the morphotype categories. It can also be observed that sciuromorphs tend to be very distinct from protrogomorphs on the incisor PC plots, though *C. canadensis* breaks this trend; this difference on the PC plots aligns with the existing interpretation that sciuromorphs are more efficient at incisor biting than protrogomorphs (Druzinsky, 2010), as the groups are clearly distinct. Furthermore, by examining the loading plots we can observe that almost all muscles contribute substantially to the variance; this suggests that the difference between morphotypes is not limited to the differentiation of certain muscles in isolation (where most muscles' individual MANOVAs do not imply that the morphotypes are significantly different) but encompasses

the entire jaw-closure musculature and other components of the masticatory system.

Overall, I argue that my first hypothesis (**H2.1**) is sufficiently supported by these results to falsify the null hypothesis, though the full story is nuanced. The morphotypes cluster on the PC plots for incisor biting and show a broader scatter in molar biting mechanics, and the group means are different with the extremes of the studied gape range contributing the most to the variance. The difference between morphotypes appears to be, in general, smaller than the variation within each category on the PC plots, though there are notable differences such as a functional space in molar biting where only hystricomorphs are found. The differentiation of the **DM** into the **ADM** and **PDM** is such a substantial change to its mechanics that comparing them splits the sample along that line, but the loading plots show that the variation among other muscles is still very notable even then. Given these intricacies, I would argue that morphotype alone should not be used to make sweeping assertions about the assumed mechanics of an individual species, though it does have utility when discussing the wider patterns across the order.

Regarding gape, there are some particular specific observations in the raw data that should be noted here. Gape clearly affects the variance in mechanical advantage (as shown by the loading plots of the PCAs), with most muscles exhibiting the greatest variance at either the low or high extremes of the gape angles assessed. This is paired with some observable trends as gape increases, with some muscles (such as the **SM**) exhibiting high mechanical advantage at low gape and a steep drop-off in efficiency as gape increases in some taxa. Other muscles display smaller changes in mechanical advantage within the studied gape range, with some increasing in mechanical advantage as gape increases (such as the **IOZM** in many taxa). One might wonder if perhaps this could suggest the potential existence of an 'optimum gape' in certain taxa, depending on the size of the food items that it habitually eats, where multiple muscles are close to their peak mechanical advantage. Unfortunately, potential patterns at which these thresholds might

occur and the relation to real food objects are beyond the focus of this study, and the relative significance of the individual muscles in that context is currently unclear; paired with the lack of dietary information in many taxa, it is not feasible to make interpretations about potential optimum gapes using these data. That being said, the observations in the raw data fit with established observations of trends in specific taxa, such as the previously discussed paper comparing mechanical advantage at a range of gapes in six select rodent taxa within the family Bathyergidae (McIntosh and Cox, 2016b). Their studies observed a trend of decreasing mechanical advantage for certain studied muscles such as the temporalis as gape increased up to a threshold (40° gape in *B. suillus*, 90° gape in the chisel-tooth digging mole-rat taxa), after which mechanical advantage rose again (McIntosh and Cox, 2016b). This turning point is indeed observable in this sample as predicted, particularly on specific muscles (such as the **IP** and **EP**) which often have their peak within the studied range of gape angles among taxa in this analysis. Based on the extreme gape of the turning point in chisel-tooth digging rodents, it is likely that some muscles in this sample's taxa also exhibit their peak mechanical advantage above 40°, the maximum gape in this analysis, but without further analysis of more extreme gapes this cannot be determined. Identifying suitable limits for such an analysis would also require additional supporting research—it does not really matter what the hypothetical mechanical advantage of a muscle would be at a gape angle the jaw physically cannot open to. Such a study would need to account for TMJ anatomy to identify an accurate maximum gape for each taxon, which itself would be a substantial topic to research regarding the masticatory adaptations of these organisms.

As alluded to previously in this section, the mechanical advantage data also exhibit reduced scatter and smaller overall variation on the PC plots during incisor biting. Rather than taxa within each morphotype clustering closer to those of their own morphotype during incisor biting, all taxa cluster closer towards the mean regardless of their morphotype. The groupings visually overlap more closely in incisor biting while still having significantly

different means according to the MANOVAs of PC scores. This indicates that the overall similarity during incisor biting compared to molar biting does not erase the broad differences between morphotypes, though this does still fit with the established view that rodents converge towards gnawing.

Considering these factors, I argue that the second hypothesis (**H2.2**) is supported, and the null hypothesis has been sufficiently falsified. Through the comparison of the bite points, and the introduction of the molar biting analyses, the morphotypes can be differentiated when they could not in Chapter 2. The hystricomorphs occupy a particular functional space on molar PC plots as previously discussed, and the MANOVAs of PC scores identify the morphotypes as being significantly different. That said, not all PCs display this difference; for example, most hystricomorphs are quite similar to other morphotypes on the PC 3 v 4 plots. Rodents are more diverse in the mechanical advantage of their molar biting than their incisor biting, with several hystricomorphs being generally distinct, supporting existing assertions of their specialisation towards molar chewing (Cox *et al.*, 2012). I would argue that the contrast between gnawing and chewing is important for understanding the different morphotypes. These interpretations combined confirm that rodents are more similar during incisor biting and more diverse in molar biting. Clearly, the common function of gnawing is associated with common ground in the mechanical advantage of the masticatory system of rodents, but this does not completely overshadow the anatomical differences of morphotypes. All rodents gnaw, and their masticatory system is adapted to perform this function, imposing a restriction on the possible mechanical configurations. Although the absolute size of objects being bitten is not assessed as part of these analyses, gnawing of food can occur at low gape (Herrel *et al.*, 2012; Cox, Kirkham and Herrel, 2013) or at high gape (Stefen, Habersetzer and Witzel, 2016). Gnawing allows rodents to access large or hard objects for their size by biting off small pieces rather than biting the whole food object at once, so without *in-vivo* observation, assertions about physical gape during feeding should be made with caution. As the extreme lows and highs of the gape angles studied are

typically those responsible for the majority of the positive or negative variance on significant loadings for each PC, I would argue that particular muscles are therefore specialised in taxa for these ranges of gape. I loosely propose that some taxa and muscles are specialising for specific mechanical advantages at high gape, while others are specialised for performance at low gape, either due to food object size or the behaviour used to access the food; the **SM**'s common pattern of especially high mechanical advantage at low gape suggests it is often specialised for that gape range, while the shallower declines of the **ADM** and **IOZM** that often result in them having higher mechanical advantages at high gape than the **SM** may suggest the **ADM** and **IOZM** are often more mechanically efficient at a range of gapes, including higher gape.

Unfortunately, without detailed dietary information, the possible implications cannot be assessed in more detail here. Key muscle subdivisions are also occurring with observable mechanical advantage patterns, and the **ADM** of sciuromorphs, *A. rufa*, and myomorphs and the **IOZM** of hystricomorphs and bathyergids are both providing a muscle subdivision with especially high mechanical advantage. With these data alone I would argue that while these those two muscles may be fulfilling a similar role as an anterior extension of an existing portion of the masseter, the comparison between them in the 'all muscles' analyses show that they are in fact distinct in mechanical advantage. Without a zygomatic plate hystricomorphs cannot have an **ADM**, and without an enlarged infraorbital foramen there is insufficient space for such a large **IOZM** with as a high a mechanical advantage as that seen in many hystricomorphs, not only distinguishing the **ADM** from the **IOZM**, but also distinguishing the myomorphs' **IOZM** from the hystricomorphs' **IOZM**.

In the introduction it was briefly noted that head size would need to be assessed to determine if it needed to be included as an additional factor in these analyses. As the results of the regression show, head size does not have a statistically significant correlation to the variation in mechanical advantage. Since mechanical advantage is a ratio (and therefore the number

is size-independent) it was not unexpected that head size did not correlate, and the alternate hypothesis—that head size is a significant factor in the mechanical advantage variation—can be rejected. Size is not significant noise in these data, and not likely to distort the interpretations of these results discussed in this section.

3.4.2 – Potential limitations

These interpretations are stated with a few caveats that should be reiterated here. The fact that hystricomorphs are the most represented group in this study, and that sciuromorphs and protrogomorphs only have four and three representatives respectively, is a limitation on what can be inferred from these data, and should be kept in mind when interpreting the results. Other extant sciuromorphs and myomorphs not represented here (as certain families are especially speciose) could potentially affect this observed difference across the whole extant order. With respect to the subsample, *B. suillus* and *G. capensis* both have disputed classifications between protrogomorphy and hystricomorphy, though this analysis categories them as protrogomorphs due to their lack of two critical hystricomorph characteristics (a large infraorbital foramen, and a large **IOZM** passing through it).

Since only a few taxa have a differentiated deep masseter, including that muscle in the analysis and assessing its relevance requires comparing it to other muscles (the **IOZM** in the 'all muscles' PCA, and the undifferentiated **DM** of hystricomorphs in the second PCA) in order to assess the full sample at once without losing several key muscles or removing taxa from the sample. Because the two subdivisions of the deep masseter complex are often physically inseparable in taxa that possess a differentiated deep masseter, and several muscles aside from the comparative categories (**ADM** vs **IOZM**, **ADM** vs **DM**, **PDM** vs **DM**) contribute to the variance in the PCAs, these comparative differences are not likely to be solely responsible for the differentiation of hystricomorphs from other groups in these results, even in

the **ADM** vs **DM** PCA. I argue that comparing these subdivisions in this way was sound for the purpose of these analyses, though it should be kept in mind. Furthermore, this is used to the advantage of this study, providing a clear quantitative confirmation that the differentiation of the deep masseter complex has a substantial impact on the mechanical advantage of the system, significant enough to be noteworthy in the analysis of a masticatory system as a whole, and demonstrating that the **ADM** and the **IOZM** are not mechanically homologous as anterior muscle subdivisions; they are not simply different solution to the same goal, they are distinct in their own right. Together, these observations help to illuminate the nuances of the mechanical distinctions between the morphotypes, and as the loading plots show, there are homologous muscles of noteworthy contribution to the variance too (especially the **SM**, **T**, **AZM**, and **PZM**).

Once again, I wish to emphasise that high mechanical advantage is not necessarily advantageous. "Advantage" is a term that implies a value judgement, but these results should not be taken to imply a value judgement. Anatomical constraints can prevent increasing mechanical advantage, and other functional characteristics (such as jaw closing speed) can also conflict with adaptations that increase mechanical advantage; there is an anatomical and functional opportunity cost to adapting for it. 'Low' mechanical advantage can be functionally overcome by simply having larger muscles, or pennation, or other soft-tissue characteristics to apply more force during contraction. Depending on the hardness of the food object being bitten, and where on the tooth row it is bitten, the jaw can operate as a second-class lever, potentially increasing downward force at the TMJ and increasing the risk of dislocation of the jaw; this requires additional mechanical compensation to keep the jaw joint occluded properly, or reduced bite force to offset this effect. This is, in fact, represented in this study; *P. capensis* is established in the literature as having a jaw that operates a second-class lever during biting with the third molar (Cox, 2017), and here exhibits some of the highest mechanical advantage on the **IOZM** of any muscle or taxon in the sample (exceeded only by the **IOZM** of *C. gambianus*), being so unusual in

its overall configuration that it is distinct from all other hystricomorphs on PC 1, especially during incisor biting where it is distinct from all other rodents. This is not necessarily an 'advantage' for this taxon. Being a term from engineering and mechanical design, 'mechanical advantage' does come with linguistic baggage that can be misleading in the context of biology.

As well as the previously mentioned avenues for further study, there are additional relevant topics that could be assessed, although some of them cannot be assessed with the data and body of knowledge available at present. With the lack of detailed wild dietary information for so many taxa across the order, the interaction between anatomy, behaviour, and diet cannot be fully explored yet. Most rodents are primarily herbivorous, with some that incorporate insects into that diet, and with others having a more varied omnivorous diet known in varying degrees of specificity (Wilson, Lacher and Mittermeier, 2016, 2017). Food size and the material properties and hardness of food have not been assessed in extensive detail in the wild for most taxa; understandably so, given that many taxa are very small or remote, making such data difficult to gather. Dietary differences could have a correlation with the mechanical variation in this sample, and this could be evaluated in detail in the event of substantial new information on wild diets across the tree.

In addition, this is a purely mechanical analysis. Muscular characteristics like muscle mass, pennation and pennation angle, muscle stretch, and cross-sectional area are not estimated or compared. Potentially, this could be used to further evaluate the similarities and differences between the function of, for example, the **ADM** and the **IOZM**, perhaps supported further by *in vivo* data and measurements. For many rodent taxa such soft-tissue information was not published as of the data gathering stage of this PhD. With detailed physical or digital dissection data across the order, future analyses could incorporate such information, as these are major components of the *in vivo* performance of a muscular system. Other anatomical characteristics like tooth crown morphology and its performance for the organism's diet are also not accounted for here, but are important

components of the masticatory system as a whole. Furthermore, this is a simplified biting model in 2D, as opposed to the complex movements of mastication. Other quantitative results such as measurements or estimates of bite force, or stress and strain partitioning of the skull and the impact of skull shape, are also a part of the functional story that is beyond the scope of these analyses or requires new data being gathered. All-in-all, it must be stressed that this is a comparison of the 2D mechanical efficiency of the arrangement of muscles to compare morphotypes using a sample of 27 taxa, and that other factors could significantly affect the conclusions drawn. Feeding is a complex behaviour, and models must remove some of that complexity in order to assess their hypotheses, resulting in inherent limitations.

The analyses conducted in this study do not have outgroups; this is not so much an issue as a potential avenue towards a different question. Comparing outgroups on homologous muscles would be difficult since many of the subdivisions of the masseter present in rodents are not present in other taxa that are distant outgroups. If multiple outgroups could be compared, however, that could contrast the difference between morphotypes with the difference between rodents as an order and other groups. This could compare rodent mechanics with the mechanics of other organisms, extant or extinct, including those with potential or proposed common ground. Chapter 4 shall explore this in relation to select multituberculate fossils.

In summary, these results do provide support to existing interpretations of the differences between morphotypes, and illuminate the variation introduced by gape and bite point when examining the functional significance of morphotypes. Despite the broad variation in feeding mechanics within each morphotype, these analyses identify the group means as significantly different. The anatomy of individual taxa can cause them to be similar to taxa of different morphotypes, but according to these analyses there is a degree of functional significant difference between the groups. The observed morphological differences between the morphotype categories do reflect functional differences in mechanical advantage. Rodents possess multiple anatomical solutions for a shared function of gnawing, with broad

variation in their group and granular variation on a smaller scale, and these solutions are distinct. There are especially significant differences between the **ADM** and **DM**, though not within other individual muscles in isolation, but the comparisons including all the muscle show the overall difference between the categories. There are individual specialisations for the variation in molar chewing mechanics, especially among many hystricomorphs which occupy regions of the PC plots where no other morphotypes are present, but the morphotypes still have overlap between them. In contrast to Chapter 2, comparisons involving molar biting have identified the morphotypes as significantly different.

3.5 – Conclusions

Morphotypes are anatomically distinct, but share mechanical similarities for the function of gnawing. Greater variation is observed in mechanical advantage during molar biting, with hystricomorphs occupying particular functional spaces in which other morphotypes are not present, but overall hystricomorphs tend to be more similar to protrogomorphs than they are to myomorphs or sciuromorphs. Myomorphs and sciuromorphs tend to group together, though individual taxa are outlier to their morphotype (often consistently so, especially *C. canadensis* and *P. capensis*). There is broad variation within morphotypes, and notable similarity between them for certain muscles and gape angles. Despite their similarities, the means of the groups are significantly different in most analyses performed, indicating that morphotypes are significantly different categories to one another. The extremes of high and low gape are responsible for the bulk of the variance in mechanical advantage across the sample, suggesting species-specific and muscle-specific adaptations at particularly high or low gapes. The introduction of gape angle and bite point does differentiate the morphotypes when a simpler analysis did not.

I would argue that morphotypes are broad categories of nuanced functional approaches, and the anatomy of individual taxa is more relevant to understanding their mechanical advantage than a generalised assertion based on the mean of a morphotype. Where possible, specific and detailed anatomical data are critical to identifying these granular differences. I conclude that morphotypes have functional differences from one another, yet share broad similarity across Rodentia for the function of gnawing.

Furthermore, the comparison between the conclusions of Chapters 2 and 3 supports existing practices of incorporating a range of gapes or bite points into an analysis of feeding performance, in that a static bite at incisor occlusion failed to identify the significant patterns in the groups that introducing these variables revealed. Lever-arm mechanics analyses at a single tooth without testing other bite points, or at one gape angle only, are

likely to be too specific and limited when attempting to compare performance in taxa. When conducting study of mechanical advantage in groups of organisms or individual taxa, I would argue that analyses at more than one bite point and at a range of gapes is likely to be of critical importance.

Bibliography

Anapol, F. and Lee, S. (1994) 'Morphological adaptation to diet in platyrrhine primates', *American Journal of Physical Anthropology*, 94(2), pp. 239–261. Available at: https://doi.org/10.1002/ajpa.1330940208.

Ball, S.S. and Roth, V.L. (1995) 'Jaw muscles of new world squirrels', *Journal of Morphology*, 224(3), pp. 265–291. Available at: https://doi.org/10.1002/jmor.1052240303.

Basu, C. and Hutchinson, J.R. (2022) 'Low effective mechanical advantage of giraffes' limbs during walking reveals trade-off between limb length and locomotor performance', *Proceedings of the National Academy of Sciences of the United States of America*, 119(28: e2108471119). Available at: https://doi.org/10.1073/pnas.2108471119.

Becerra, F., Echeverría, A.I., Casinos, A. and Vassallo, A.I. (2014) 'Another one bites the dust: Bite force and ecology in three caviomorph rodents (Rodentia, Hystricognathi)', *Journal of Experimental Zoology Part A: Ecological Genetics and Physiology*, 321(4), pp. 220–232. Available at: https://doi.org/10.1002/jez.1853.

Becht, G. (1953) 'Comparative biologic-anatomical researches on mastication in some mammals', *Proc. Koninklijke Nederlandse Akademie van Wetenschappen, Ser C*, 56, pp. 508–527.

Biewener, A.A., Farley, C.T., Roberts, T.J. and Temaner, M. (2004) 'Muscle mechanical advantage of human walking and running: implications for energy cost', *Journal of Applied Physiology*, 97, pp. 2266–2274. Available at: https://doi.org/10.1152/japplphysiol.00003.2004.

Bourke, J., Wroe, S., Moreno, K., McHenry, C. and Clausen, P. (2008) 'Effects of gape and tooth position on bite force and skull stress in the dingo (*Canis lupus dingo*) using a 3-dimensional finite element approach', *PLOS One*, 3(5). Available at: https://doi.org/10.1371/journal.pone.0002200.

Brandt, J.F. (1855) *Beiträge zur nähern Kenntniss der Säugethiere Russlands*.

Casanovas-Vilar, I. and Van Dam, J. (2013) 'Conservatism and adaptability during squirrel radiation: what is mandible shape telling us?', *PLOS One*, 8(4:e61298). Available at: https://doi.org/10.1371/journal.pone.0061298.

Christiansen, P. (2008) 'Evolution of skull and mandible shape in cats (Carnivora: *Felidae*)', *PLOS One*, 3(7). Available at: https://doi.org/10.1371/journal.pone.0002807.

Christiansen, P. and Adolfssen, J.S. (2005) 'Bite forces, canine strength and skull allometry in carnivores (Mammalia, Carnivora)', *Journal of Zoology*, 266(2), pp. 133–151. Available at: https://doi.org/10.1017/S0952836905006643.

Coleman, M.N. (2008) 'What does geometric mean, mean geometrically? Assessing the utility of geometric mean and other size variables in studies of skull allometry', *American Journal of Physical Anthropology*, 135, pp. 404–415. Available at: https://doi.org/10.1002/ajpa.20761.

Cox, P.G. (2017) 'The jaw is a second-class lever in *Pedetes capensis* (Rodentia: Pedetidae)', *PeerJ*, 5:e3741. Available at: https://doi.org/10.7717/peerj.3741.

Cox, P.G. and Baverstock, H. (2016) 'Masticatory muscle anatomy and feeding efficiency of the American beaver, *Castor canadensis* (Rodentia, Castoridae)', *Journal of Mammalian Evolution*, 23, pp. 191–200. Available at: https://doi.org/10.1007/s10914-015-9306-9.

Cox, P.G., Faulkes, C.G. and Bennett, N.C. (2020) 'Masticatory musculature of the African mole-rats (Rodentia: Bathyergidae)', *PeerJ*, 8:e8847. Available at: https://doi.org/10.7717/peerj.8847.

Cox, P.G. and Hautier, L. (2015) *Evolution of the Rodents: Advances in Phylogeny, Functional Morphology and Development*. Edited by P. G. Cox and L. Hautier. Cambridge University Press (Cambridge Studies in Morphology and Molecules: New Paradigms in Evolutionary Bio, 5). Available at: https://doi.org/10.1017/CBO9781107360150.

Cox, P.G. and Jeffery, N. (2011) 'Reviewing the morphology of the jaw-closing musculature in squirrels, rats, and guinea pigs with Contrast-Enhanced MicroCT', *The Anatomical Record*, 294, pp. 915–928. Available at: https://doi.org/10.1111/j.1469-7580.2011.01436.x.

Cox, P.G., Kirkham, J. and Herrel, A. (2013) 'Masticatory biomechanics of the Laotian rock rat, *Laonastes aenigmamus*, and the function of the zygomaticomandibularis muscle', *PeerJ*, 1:e160. Available at: https://doi.org/10.7717/peerj.160.

Cox, P.G., Morris, P.J.R., Hennekam, J.J. and Kitchener, A.C. (2020) 'Morphological and functional variation between isolated populations of British red squirrels (*Sciurus vulgaris*)', *Journal of Zoology*. Edited by N. Bennett, 312(4), pp. 271–283. Available at: https://doi.org/10.1111/jzo.12829.

Cox, P.G., Rayfield, E.J., Fagan, M.J., Herrel, A., Pataky, T.C. and Jeffery, N. (2012) 'Functional evolution of the feeding system in rodents', *PLOS One*, 7(4). Available at: https://doi.org/10.1371/journal.pone.0036299.

Dechow, P.C. and Carlson, D.S. (1990) 'Occlusal force and craniofacial biomechanics during growth in rhesus monkeys', *American Journal of Physical Anthropology*, 83(2), pp. 219–237. Available at: https://doi.org/10.1002/ajpa.1330830211.

Devlin, H. and Wastell, D.G. (1986) 'The mechanical advantage of biting with the posterior teeth', *Journal of Oral Rehabilitation*, 13(6), pp. 607–610. Available at: https://doi.org/10.1111/j.1365-2842.1986.tb00684.x.

Druzinsky, R.E. (1995) 'Incisal biting in the mountain beaver (*Aplodontia rufa*) and woodchuck (*Marmota monax*)', *Journal of Morphology*, 226(1), pp. 79–101. Available at: https://doi.org/10.1002/jmor.1052260106.

Druzinsky, R.E. (2010) 'Functional anatomy of incisal biting in *Aplodontia rufa* and sciuromorph rodents – Part 1: Masticatory muscles, skull shape and digging', *Cells Tissues Organs*, 191(6), pp. 510–522. Available at: https://doi.org/10.1159/000284931.

Druzinsky, R.E. (2015) 'Chapter 12 – The oral apparatus of rodents: variations on the theme of a gnawing machine', in P.G. Cox and L. Hautier (eds) *Evolution of the*

Rodents: Advances in Phylogeny, Functional Morphology and Development. Cambridge University Press (Cambridge Studies in Morphology and Molecules: New Paradigms in Evolutionary Bio, 5), pp. 323–349. Available at: https://doi.org/10.1017/CBO9781107360150.

Dumont, E.R. and Herrel, A. (2003) 'The effects of gape angle and bite point on bite force in bats', *Journal of Experimental Biology*, 206(13), pp. 2117–2123. Available at: https://doi.org/10.1242/jeb.00375.

Dumont, E.R., Herrel, A., Medellín, R.A., Vargas-Contreras, J.A. and Santana, S.E. (2009) 'Built to bite: Cranial design and function in the wrinkle-faced bat', *Journal of Zoology*, 279(4), pp. 329–337. Available at: https://doi.org/10.1111/j.1469-7998.2009.00618.x.

Echeverría, A.I., Becerra, F., Buezas, G.N. and Vassallo, A.I. (2017) 'Bite it forward … bite it better? Incisor procumbency and mechanical advantage in the chisel-tooth and scratch-digger genus *Ctenomys* (Caviomorpha, Rodentia)', *Zoology*, 125, pp. 53–68. Available at: https://doi.org/10.1016/j.zool.2017.08.003.

van Eijden, T.M.G.J., Klok, E.M., Weijs, W.A. and Koolstra, J.H. (1988) 'Mechanical capabilities of the human jaw muscles studied with a mathematical model', *Archives of Oral Biology*, 33(11), pp. 819–826. Available at: https://doi.org/10.1016/0003-9969(88)90106-9.

Elner, R.W. and Campbell, A. (1981) 'Force, function and mechanical advantage in the chelae of the American lobster *Homarus americanus* (Decapoda: Crustacea)', *Journal of Zoology*, 193, pp. 269–286. Available at: https://doi.org/10.1111/j.1469-7998.1981.tb03444.x.

Emry, R.J. and Thorington, Richard.W. (1984) 'The tree squirrel *Sciurus* (Sciuridae, Rodentia) as a living fossil.', in N. Eldredge and S.M. Stanley (eds) *Living Fossils*. New York: Springer US (Casebooks in Earth Sciences), pp. 23–31. Available at: https://doi.org/10.1007/978-1-4613-8271-3_3.

Eng, C.M., Ward, S.R., Vinyard, C.J. and Taylor, A.B. (2009) 'The morphology of the masticatory apparatus facilitates muscle force production at wide jaw gapes in tree-gouging common marmosets (*Callithrix jacchus*)', *Journal of Experimental Biology*, 212(24), pp. 4040–4055. Available at: https://doi.org/10.1242/jeb.029983.

Fabre, P., Hautier, L., Dimitrov, D. and Douzery, E.J.P. (2012) 'A glimpse on the pattern of rodent diversification: a phylogenetic approach', *BMC Evolutionary Biology*, 12(88). Available at: https://doi.org/10.1186/1471-2148-12-88.

Fricano, E.E.I. and Perry, J.M.G. (2019) 'Maximum bony gape in primates', *Anatomical Record*, 302(2), pp. 215–225. Available at: https://doi.org/10.1002/ar.23897.

García-Morales, P., Buschang, P.H., Throckmorton, G.S. and English, J.D. (2003) 'Maximum bite force, muscle efficiency and mechanical advantage in children with vertical growth patterns', *European Journal of Orthodontics*, 25, pp. 265–272. Available at: https://doi.org/10.1093/ejo/25.3.265.

Ginot, S., Herrel, A., Claude, J. and Hautier, L. (2019) 'Morphometric models for estimating bite force in *Mus* and *Rattus*: Mandible shape and size perform better

than lever-arm ratios', *Journal of Experimental Biology*, 222(12). Available at: https://doi.org/10.1242/jeb.204867.

Godinho, R.M., Fitton, L.C., Toro-Ibacache, V., Stringer, C.B., Lacruz, R.S., Bromage, T.G. and O'Higgins, P. (2018) 'The biting performance of *Homo sapiens* and *Homo heidelbergensis*', *Journal of Human Evolution*, 118, pp. 56–71. Available at: https://doi.org/10.1016/j.jhevol.2018.02.010.

Gomes Rodrigues, H., Šumbera, R. and Hautier, L. (2016) 'Life in burrows channelled the morphological evolution of the skull in rodents: the case of African mole-rats (Bathyergidae, Rodentia)', *Journal of Mammalian Evolution*, 23, pp. 175–189. Available at: https://doi.org/10.1007/s10914-015-9305-x.

Greaves, W.S. (1985) 'The generalised carnivore jaw', *Zoological Journal of the Linnean Society*, 85(3), pp. 267–274. Available at: https://doi.org/10.1111/j.1096-3642.1985.tb01506.x.

Grossnickle, D.M. (2020) 'Feeding ecology has a stronger evolutionary influence on functional morphology than on body mass in mammals', *Evolution*, 74(3), pp. 610–628. Available at: https://doi.org/10.1111/evo.13929.

Grubich, J.R., Rice, A.N. and Westneat, M.W. (2008) 'Functional morphology of bite mechanics in the great barracuda (*Sphyraena barracuda*)', *Zoology*, 111(1), pp. 16–29. Available at: https://doi.org/10.1016/j.zool.2007.05.003.

Hammer, Ø., Harper, D.A.T. and Ryan, P.D. (2001) 'Past: Paleontological Statistics software package for education and data analysis', *Palaeontologia Electronica*, 4(1), pp. 0–9.

Hampton, P.M. and Moon, B.R. (2013) 'Gape size, its morphological basis, and the validity of gape indices in western diamond-backed rattlesnakes (*Crotalus atrox*)', *Journal of Morphology*, 274(2), pp. 194–202. Available at: https://doi.org/10.1002/jmor.20087.

Hanson, T.R., Newmark, W.D. and Stanley, W.T. (2007) 'Forest fragmentation and predation on artificial nests in the Usambara Mountains, Tanzania', *African Journal of Ecology*, 45(4), pp. 499–507. Available at: https://doi.org/10.1111/j.1365-2028.2007.00760.x.

Harkness-Armstrong, C., Debelle, H.A., Maganaris, C.N., Walton, R., Wright, D.M., Bass, A., Baltzopoulos, V. and O'Brien, T.D. (2020) 'Effective mechanical advantage about the ankle joint and the effect of achilles tendon curvature during toe-walking', *Frontiers in Physiology*, 11(407). Available at: https://doi.org/10.3389/fphys.2020.00407.

Hartstone-Rose, A., Perry, J.M.G. and Morrow, C.J. (2012) 'Bite force estimation and the fiber architecture of felid masticatory muscles', *Anatomical Record*, 295(8), pp. 1336–1351. Available at: https://doi.org/10.1002/ar.22518.

Hautier, L., Cox, P.G. and Lebrun, R. (2015) 'Chapter 10 – Grades and clades among rodents: the promise of geometric morphometrics', in *Evolution of the Rodents: Advances in Phylogeny, Functional Morphology and Development*. (Cambridge Studies in Morphology and Molecules: New Paradigms in Evolutionary Bio, 5), pp. 277–299. Available at: https://doi.org/10.1017/CBO9781107360150.

Helfman, G.S. and Clark, J.B. (1986) 'Rotational feeding: overcoming gape-limited foraging in anguillid eels', *Copeia*, 1986(3), pp. 679–685. Available at: https://doi.org/10.2307/1444949.

Herrel, A., Fabre, A., Hugot, J., Keovichit, K., Adriaens, D., Brabant, L., Van Hoorebeke, L. and Cornette, R. (2012) 'Ontogeny of the cranial system in *Laonastes aenigmamus*', *Journal of Anatomy*, 221(2), pp. 128–137. Available at: https://doi.org/10.1111/j.1469-7580.2012.01519.x.

Herrel, A., Podos, J., Huber, S.K. and Hendry, A.P. (2005) 'Evolution of bite force in Darwin's finches: A key role for head width', *Journal of Evolutionary Biology*, 18(3), pp. 669–675. Available at: https://doi.org/10.1111/j.1420-9101.2004.00857.x.

Herring, S.W. (1980) 'Functional design of cranial muscles: comparative and physiological studies in pigs', *American Zoology*, 20, pp. 283–293.

Herring, S.W., Grimm, A.F. and Grimm, B.R. (1979) 'Functional heterogeneity in a multipinnate muscle', *American Journal of Anatomy*, 154(4), pp. 563–575. Available at: https://doi.org/10.1002/aja.1001540410.

Herring, S.W. and Herring, S.E. (1974) 'The superficial masseter and gape in mammals', *The American Naturalist*, 108(962), pp. 561–576. Available at: https://doi.org/10.1086/282934.

Hiiemae, K. and Ardran, G.M. (1968) 'A cinefluorographic study of mandibular movement during feeding in the rat (*Rattus norvegicus*)', *Journal of Zoology*, 154, pp. 139–154. Available at: https://doi.org/10.1111/j.1469-7998.1968.tb01654.x.

Hildebrand, M., Bramble, D.M., Liem, K.F. and Wake, D.B. (eds) (1985) *Funcitonal Vertebrate Morphology*. Cambridge, MA and London, UK: Harvard University Press. Available at: https://doi.org/10.4159/harvard.9780674184404.

Hirakawa, H. (2001) 'Coprophagy in leporids and other mammalian herbivores', *Mammal Review*, 31(1), pp. 61–80. Available at: https://doi.org/10.1046/j.1365-2907.2002.00105.x.

Huby, A., Lowie, A., Herrel, A., Vigouroux, R., Frédérich, B., Raick, X., Kurchevski, G., Godinho, A.L. and Parmentier, E. (2019) 'Functional diversity in biters: the evolutionary morphology of the oral jaw system in pacus, piranhas and relatives (Teleostei: Serrasalmidae)', *Biological Journal of the Linnean Society*, 127, pp. 722–741. Available at: https://doi.org/10.1093/BIOLINNEAN%2FBLZ048.

Hulme, P.E. and Benkman, C.W. (2002) 'Granivory', in C.M. Herrera and O. Pellmyr (eds) *Plant-Animal Interactions: An Evolutionary Approach*. Wiley-Blackwell, pp. 132–156.

Jones, K. and Law, C.J. (2018) 'Differentiation of craniomandibular morphology in two sympatric *Peromyscus* mice (Cricetidae: Rodentia)', *Mammal Research*, 63, pp. 277–283. Available at: https://doi.org/10.1007/s13364-018-0364-2.

Jungers, W.L., Falsetti, A.B. and Wall, C.E. (1995) 'Shape, relative size, and size-adjustments in morphometrics', *American Journal of Physical Anthropology*, 38, pp. 137–161. Available at: https://doi.org/10.1002/ajpa.1330380608.

Kunz, C. and Sakamoto, M. (2024) 'Elevated evolutionary rates of biting biomechanics reveal patterns of extraordinary craniodental adaptations in some herbivorous dinosaurs', *Palaeontology*, 67(e12689). Available at: https://doi.org/10.1111/pala.12689.

Laird, M.F., Kanno, C.M., Yoakum, C.B., Fogaça, M.D., Taylor, A.B., Ross, C.F., Chalk-Wilayto, J., Holmes, M.A., Terhune, C.E. and de Oliveira, J.A. (2023) 'Ontogenetic changes in bite force and gape in tufted capuchins', *Journal of Experimental Biology*, 226(jeb245972). Available at: https://doi.org/10.1242/jeb.245972.

Ledogar, J.A., Luk, T.H.Y., Perry, J.M.G., Neaux, D. and Wroe, S. (2018) 'Biting mechanics and niche separation in a specialized clade of primate seed predators', *PLOS One*, 13(1: e0190689). Available at: https://doi.org/10.1371/journal.pone.0190689.

McIntosh, A.F. and Cox, P.G. (2016a) 'Functional implications of craniomandibular morphology in African mole-rats (Rodentia: Bathyergidae)', *Biological Journal of the Linnean Society*, 117(3), pp. 447–462. Available at: https://doi.org/10.1111/bij.12691.

McIntosh, A.F. and Cox, P.G. (2016b) 'The impact of gape on the performance of the skull in chisel-tooth digging and scratch digging mole-rats (Rodentia: Bathyergidae)', *Royal Society Open Science*, 3(10). Available at: https://doi.org/10.1098/rsos.160568.

Morales-García, N.M., Gill, P.G., Janis, C.M. and Rayfield, E.J. (2021) 'Jaw shape and mechanical advantage are indicative of diet in Mesozoic mammals', *Communications Biology*, 4(242). Available at: https://doi.org/10.1038/s42003-021-01757-3.

Nabavizadeh, A. (2016) 'Evolutionary trends in the jaw adductor mechanics of ornithischian dinosaurs', *Anatomical Record*, 299, pp. 271–294. Available at: https://doi.org/10.1002/ar.23306.

Navalón, G., Bright, J.A., Marugán-Lobón, J. and Rayfield, E.J. (2019) 'The evolutionary relationship among beak shape, mechanical advantage, and feeding ecology in modern birds', *Evolution*, 73(3), pp. 422–435. Available at: https://doi.org/10.1111/evo.13655.

Nogueira, M.R., Peracchi, A.L. and Monteiro, L.R. (2009) 'Morphological correlates of bite force and diet in the skull and mandible of phyllostomid bats', *Functional Ecology*, 23(4), pp. 715–723. Available at: https://doi.org/10.1111/j.1365-2435.2009.01549.x.

Olberding, J.P., Deban, S.M., Rosario, M.V. and Azizi, E. (2019) 'Modelling the determinants of mechanical advantage during jumping: Consequences for spring- and muscle-driven movement', in *Integrative and Comparative Biology*. Oxford University Press, pp. 1515–1524. Available at: https://doi.org/10.1093/icb/icz139.

Osborn, J.W. (1996) 'Features of human jaw design which maximise the bite force', *Journal of Biomechanics*, 29(5), pp. 589–595. Available at: https://doi.org/10.1016/0021-9290(95)00117-4.

Pillai, K.C.S. (1955) 'Some new test criteria in Multivariate Analysis', *The Annals of Mathematical Statistics*, 26(1), pp. 117–121. Available at: https://doi.org/10.1214/aoms/1177728599.

Pröschel, P.A., Jamal, T. and Morneburg, T.R. (2008) 'Motor control of jaw muscles in chewing and in isometric biting with graded narrowing of jaw gape', *Journal of Oral Rehabilitation*, 35(10), pp. 722–728. Available at: https://doi.org/10.1111/j.1365-2842.2008.01871.x.

Renaud, S., Gomes Rodrigues, H., Ledevin, R., Pisanu, B., Chapuis, J.-L. and Hardouin, E.A. (2015) 'Fast evolutionary response of house mice to anthropogenic disturbance on a Sub-Antarctic island', *Biological Journal of the Linnean Society*, 114, pp. 513–526. Available at: https://doi.org/10.1111/bij.12454.

Robinson, J.G. and Redford, K.H. (1986) 'Body size, diet, and population density of neotropical forest mammals', *The American Naturalist*, 128(5), pp. 665–680. Available at: https://www.jstor.org/stable/2461950.

Rodríguez-Robles, J.A., Bell, C.J. and Greene, H.W. (1999) 'Gape size and evolution of diet in snakes: feeding ecology of erycine boas', *Journal of Zoology*, 248(1), pp. 49–58. Available at: https://doi.org/10.1111/j.1469-7998.1999.tb01021.x.

Ross, C.F., Baden, A.L., Georgi, J., Herrel, A., Metzger, K.A., Reed, D.A., Schaerlaeken, V. and Wolff, M.S. (2010) 'Chewing variation in lepidosaurs and primates', *Journal of Experimental Biology*, 213(4), pp. 572–584. Available at: https://doi.org/10.1242/jeb.036822.

Ross, C.F. and Iriarte-Diaz, J. (2014) 'What does feeding system morphology tell us about feeding?', *Evolutionary Anthropology*, 23(3), pp. 105–120. Available at: https://doi.org/10.1002/evan.21410.

Sakamoto, M. (2010) 'Jaw biomechanics and the evolution of biting performance in theropod dinosaurs', *Proceedings of the Royal Society B: Biological Sciences*, 277(1698), pp. 3327–3333. Available at: https://doi.org/10.1098/rspb.2010.0794.

Samuels, J.X. (2009) 'Cranial morphology and dietary habits of rodents', *Zoological Journal of the Linnean Society*, 156, pp. 864–888. Available at: https://doi.org/10.1111/j.1096-3642.2009.00502.x.

Santana, S.E., Dumont, E.R. and Davis, J.L. (2010) 'Mechanics of bite force production and its relationship to diet in bats', *Functional Ecology*, 24(4), pp. 776–784. Available at: https://doi.org/10.1111/j.1365-2435.2010.01703.x.

Santana, S.E., Grosse, I.R. and Dumont, E.R. (2012) 'Dietary hardness, loading behaviour, and the evolution of skull form in bats', *Evolution*, 66(8), pp. 2587–2598. Available at: https://doi.org/10.5061/dryad.d548646j.

Satoh, K. (1999) 'Mechanical advantage of area of origin for the external pterygoid muscle in two murid rodents, *Apodemus speciosus* and *Clethrionomys rufocanus*', *Journal of Morphology*, 240, pp. 1–14. Available at: https://doi.org/10.1002/(sici)1097-4687(199904)240:1%3C1::aid-jmor1%3E3.0.co;2-d.

Schultz, J.A., Krause, D.W., Von Koenigswald, W. and Dumont, E.R. (2014) 'Dental function and diet of *Vintana sertichi* (Mammalia, Gondwanatheria) from the late cretaceous of Madagascar', *Journal of Vertebrate Paleontology*, 34(6), pp. 182–202. Available at: https://doi.org/10.1080/02724634.2014.965778.

Scott, W.B., Jepsen, G.L. and Wood, A.E. (1937) 'The mammalian fauna of the White River Oligocene: Part II. Rodentia', *Transactions of the American Philosophical Society*, 28(2), pp. 155–269.

Stefen, C., Habersetzer, J. and Witzel, U. (2016) 'Biomechanical aspects of incisor action of beavers (*Castor fiber* L.)', *Journal of Mammalogy*, 97(2), pp. 619–630. Available at: https://doi.org/10.1093/jmammal/gyv209.

Sun, Z., Liu, Z.-J. and Herring, S.W. (2002) 'Movement of temporomandibular joint tissues during mastication and passive manipulation in miniature pigs', *Archives of Oral Biology*, 47, pp. 293–305. Available at: https://doi.org/10.1016/s0003-9969(02)00004-3.

Swiderski, D.L. and Zelditch, M.L. (2010) 'Morphological diversity despite isometric scaling of lever arms', *Evolutionary Biology*, 37, pp. 1–18. Available at: https://doi.org/10.1007/s11692-010-9081-8.

Tanner, J.B., Zelditch, M.L., Lundrigan, B.L. and Holekamp, K.E. (2010) 'Ontogenetic change in skull morphology and mechanical advantage in the Spotted Hyena (*Crocuta crocuta*)', *Journal of Morphology*, 271, pp. 353–365. Available at: https://doi.org/10.1002/jmor.10802.

Taylor, A.B. and Vinyard, C.J. (2005) 'The relationship between jaw-muscle architecture and feeding behavior in primates: Tree-gouging and non-gouging gummivorous Callitrichids as a natural experiment.', in C.J. Vinyard, M.J. Ravosa, and C. Wall (eds) *Primate Craniofacial Function and Biology*. Springer, Boston, MA (Developments in Primatology: Progress and Prospects), pp. 241–262. Available at: https://doi.org/10.1007/978-0-387-76585-3_12.

Taylor, A.B. and Vinyard, C.J. (2009) 'Jaw-muscle fiber architecture in tufted capuchins favors generating relatively large muscle forces without compromising jaw gape', *Journal of Human Evolution*, 57(6), pp. 710–720. Available at: https://doi.org/10.1016/j.jhevol.2009.06.001.

Terhune, C.E., Hylander, W.L., Vinyard, C.J. and Taylor, A.B. (2015) 'Jaw-muscle architecture and mandibular morphology influence relative maximum jaw gapes in the sexually dimorphic *Macaca fascicularis*', *Journal of Human Evolution*, 82, pp. 145–158. Available at: https://doi.org/10.1016/j.jhevol.2015.02.006.

Throckmorton, G.S. and Dean, J.S. (1994) 'The relationship between jaw-muscle mechanical advantage and activity levels during isometric bites in humans', *Archives of Oral Biology*, 39(5), pp. 429–437. Available at: https://doi.org/10.1016/0003-9969(94)90174-0.

Troyer, A., Legrand, A., Gevenois, P.-A. and Wilson, T.A. (1998) 'Mechanical advantage of the human parasternal intercostal and triangularis sterni muscles', *The Journal of Physiology*, 513(3), pp. 915–925. Available at: https://doi.org/10.1111/j.1469-7793.1998.915ba.x.

Turnbull, W.D. (1970) *Mammalian Masticatory Apparatus*. Chicago: Field Museum Press (Fieldiana (Geology)). Available at: https://doi.org/10.5962/bhl.title.5442.

Van Wassenbergh, S., Heindryckx, S. and Adriaens, D. (2017) 'Kinematics of chisel-tooth digging by African mole-rats', *Journal of Experimental Biology*, 220(23), pp. 4479–4485. Available at: https://doi.org/10.1242/jeb.164061.

Vander Wall, S.B. (2001) 'The Evolutionary Ecology of Nut Dispersal', *The Botanical Review*, 67(1), pp. 74–117. Available at: https://www.jstor.org/stable/4354385.

Velhagen, W.A. and Roth, V.L. (1997) 'Scaling of the mandible in squirrels', *Journal of Morphology*, 232, pp. 107–132. Available at: https://doi.org/10.1002/(SICI)1097-4687(199705)232:2<107::AID-JMOR1>3.0.CO;2-7.

Verwaijen, D., Van Damme, R. and Herrel, A. (2002) 'Relationships between head size, bite force, prey handling efficiency and diet in two sympatric lacertid lizards', *Functional Ecology*, 16(6), pp. 842–850. Available at: https://doi.org/10.1046/j.1365-2435.2002.00696.x.

Vinyard, C.J., Wall, C.E., Williams, S.H. and Hylander, W.L. (2003) 'Comparative functional analysis of skull morphology of tree-gouging primates', *American Journal of Physical Anthropology*, 120(2), pp. 153–170. Available at: https://doi.org/10.1002/ajpa.10129.

Wang, K., Lobbezoo, F., Svensson, P. and Arendt-Nielsen, L. (2007) 'Influence of jaw gape on EMG of jaw muscles and jaw-stretch reflexes', *Archives of Oral Biology*, 52(6), pp. 562–570. Available at: https://doi.org/10.1016/j.archoralbio.2006.12.004.

Weijs, W.A. (1994) 'Chapter 9: Evolutionary Approach of Masticatory Motor Patterns in Mammals', in V.L. Bels, M. Chardon, and P. Vandewalle (eds) *Biomechanics of Feeding in Vertebrates*. Springer, Berlin, Heidelberg (Advances in Comparative and Environmental Physiology, 18), pp. 281–320. Available at: https://doi.org/10.1007/978-3-642-57906-6_10.

Weijs, W.A., Brugman, P. and Klok, E.M. (1987) 'The growth of the skull and jaw muscles and its functional consequences in the New Zealand rabbit (*Oryctolagus cuniculus*)', *Journal of Morphology*, 194(2), pp. 143–161. Available at: https://doi.org/10.1002/jmor.1051940204.

West, A.G. and King, C.M. (2018) 'Variation in mandible shape and body size of house mice *Mus musculus* in five separate New Zealand forest habitats', *New Zealand Journal of Zoology*, 45(2), pp. 136–153. Available at: https://doi.org/10.1080/03014223.2017.1411955.

Westneat, M.W. (2003) 'A biomechanical model for analysis of muscle force, power output and lower jaw motion in fishes', *Journal of Theoretical Biology*, 223(3), pp. 269–281. Available at: https://doi.org/10.1016/S0022-5193(03)00058-4.

Wheelwright, N.T. (1985) 'Fruit-size, gape width, and the diets of fruit-eating birds', *Ecology*, 66(3), pp. 808–818. Available at: https://doi.org/10.2307/1940542.

Wilks, S.S. (1932) 'Certain generalizations in the analysis of variance', *Biometrika*, 24(3), pp. 471–494. Available at: https://doi.org/10.2307/2331979.

Williams, S.H., Peiffer, E. and Ford, S. (2009) 'Gape and bite force in the rodents *Onychomys leucogaster* and *Peromyscus maniculatus*: Does jaw-muscle anatomy predict performance?', *Journal of Morphology*, 270(11), pp. 1338–1347. Available at: https://doi.org/10.1002/jmor.10761.

Wilson, D.E., Lacher, T.E. and Mittermeier, R.A. (eds) (2016) *Handbook of the Mammals of the World, Volume 6: Lagomorphs and Rodents I*. Lynx Edicions (Handbook of the Mammals of the World (HMW)).

Wilson, D.E., Lacher, T.E. and Mittermeier, R.A. (eds) (2017) *Handbook of the Mammals of the World, Volume 7: Rodents II*. Lynx Edicions (Handbook of the Mammals of the World (HMW)).

Wood, A.E. (1955) 'A revised classification of the rodents', *Journal of Mammalogy*, 36(2), pp. 165–187. Available at: https://doi.org/10.2307/1375874.

Wood, A.E. (1965) 'Grades and clades among rodents', *Society for the Study of Evolution*, 19(1), pp. 115–130. Available at: https://doi.org/10.2307/2406300.

Wroe, S., Huber, D.R., Lowry, M., McHenry, C., Moreno, K., Clausen, P., Ferrara, T.L., Cunningham, E., Dean, M.N. and Summers, A.P. (2008) 'Three-dimensional computer analysis of white shark jaw mechanics: How hard can a great white bite?', *Journal of Zoology*, 276(4), pp. 336–342. Available at: https://doi.org/10.1111/j.1469-7998.2008.00494.x.

Young, J.W. (2006) 'Ontogeny of muscle mechanical advantage in capuchin monkeys (*Cebus albifrons* and *Cebus apella*)', *Journal of Zoology*, 267(4), pp. 351–362. Available at: https://doi.org/10.1017/S0952836905007521.

Chapter 4 – Comparing the mechanical advantage and jaw-closing musculature among rodent morphotypes and Djadochtatherioid multituberculates

4.1. – Introduction

4.1.1 – A brief summary

Extinct multituberculates have historically been compared with rodents due to their shared characteristics such as paired incisors for gnawing, a primarily insectivorous-herbivorous diet, and similar size (Ostrander, 1984; Gambaryan and Kielan-Jaworowska, 1995; Adams *et al.*, 2019). During the Eocene and Oligocene, multituberculates and rodents co-existed in the same areas, with rodents radiating throughout and beyond the multituberculates' decline; though there is dispute, it has been proposed that rodents contributed to the extinction of multituberculates via competitive exclusion (Valen and Sloan, 1966; Krause, 1986; Adams *et al.*, 2019). I reconstructed three digitised fossil multituberculates for this chapter, and compared them with the sample of rodents used in Chapter 3 via the same methods as before. The mechanical efficiency of individual homologous muscles can be assessed for both incisor gnawing and biting with the multituberculates' distinctive premolars, and compared to assess the potential similarities or differences in mechanical advantage between fossil multituberculates and extant rodents. This chapter provides a framework for future expansion assessing the potential role of feeding in competitive exclusion during the extinction of multituberculates.

4.1.2 – Multituberculates: a point of comparison

In Chapter 3, building on the data of Chapter 2, I concluded that morphotypes are broad generalised categories of nuanced functional approaches, and that the anatomy of the individual taxa being studied may supersede their morphotype category when making predictions about individual mechanical advantage. Despite their differences, rodents share similarity across their order in their cranial anatomy and muscle subdivisions, as one might expect given their degree of homoplasy. This is a principle that can potentially be expanded to compare extant rodents with other taxa and groups that share some of their cranial traits or possess homologous muscles to compare; one such group are the extinct multituberculates. The sample of rodents, and studied characteristics of feeding (individual muscles, morphotypes, bite points, and gape angles) were discussed extensively in Chapters 2 and 3 and will not be restated here.

Multituberculata (Cope, 1884) is an extinct order of mammals that branched from the synapsid lineage after monotremes, but before the evolution of Metatheria or Eutheria (Kielan-Jaworowska, Cifelli and Luo, 2004; Weaver *et al.*, 2022). They, and the loosely-similar order Haramiyida, are primarily united by the morphology of their molars, which possess distinctive longitudinal rows of cusps for which the 'multituberculates' themselves are named, and also by their relative lack of transverse jaw movement (compared with other mammals) during chewing (Butler, 2000; Kielan-Jaworowska, Cifelli and Luo, 2004). They possessed large, paired, diprotodont incisors, were capable of gnawing, could not occlude their incisors and cheek teeth simultaneously, trended from insectivory to increasing herbivory throughout their evolution, are thought to have possessed a large subdivided masseter complex, and most were physically small and the order was widely distributed across the world over tens of millions of years (Kielan-Jaworowska, 1974; Kielan-Jaworowoska, Presley and Poplin, 1986; Gambaryan and Kielan-Jaworowska, 1995; Kielan-Jaworowska, Cifelli and Luo, 2004; Wilson *et al.*, 2012; Grossnickle and Polly, 2013; Adams *et al.*, 2019; Grossnickle, Smith and Wilson, 2019; Weaver and Wilson, 2021); these are traits they share with

modern rodents, which fill some of the ecological niches once occupied by multituberculates.

Multituberculates originated in the Middle Jurassic, with fossils occurring in Laurasia in the Bathonian, 165–168 Ma, (Butler and Hooker, 2005; Averianov *et al.*, 2021), and several Early Cretaceous fossils and one Early/Middle Jurassic fossil of uncertain age in Gondwanaland (Kielan-Jaworowoska *et al.*, 2007; Rich *et al.*, 2009, 2022; Parmar, Prasad and Kumar, 2013; Krause, Hoffmann and Werning, 2017). Much of these early records consist of isolated or fragmented teeth or bones. Multituberculata radiated through the Mesozoic (Grossnickle, Smith and Wilson, 2019), declined in distribution following the Palaeocene (Wilson *et al.*, 2012) and went extinct in the Eocene. Specifically, the latest known multituberculates occur in modern-day North America in the Late Eocene (though the rocks are sometimes stated as Early Oligocene, particularly in older papers) (Krishtalka *et al.*, 1982; Ostrander, 1984; Schumaker and Kihm, 2006), in Europe during the Ypresian (early Eocene) (Smith and Smith, 2003; Hooker, 2010; Marandat *et al.*, 2012), and in Mongolia in the Thanetian (Late Palaeocene) (Matthew and Granger, 1925, 1928; Lopatin, 2020). Rodents are regionally present during the extinction of multituberculates in these areas during their respective time periods (Ostrander, 1984; Smith and Smith, 2003; Hooker, 2010; Emry and Korth, 2012; Marandat *et al.*, 2012; Samuels and Hopkins, 2017; Li, Mao and Wang, 2018; Lopatin, 2020; Lopatin and Averianov, 2004a, 2004b).

For decades, it has been discussed whether their extinction is a case of competitive exclusion, a result of environmental changes in climate or habitat, or an adaptive radiation of rodents to fill the ecological niche left by the ongoing decline of multituberculates (Matthew, 1897; Jepsen, 1949; Wilson, 1951; Simpson, 1953; McKenna, 1961; Wood, 1962, 2010; Landry, 1965; Valen and Sloan, 1966; Hopson, 1967; Clemens, Kielan-Jaworowska and Lillegraven, 1979; Ostrander, 1984; Krause, 1986; Benton, 1987; Jablonski, 2008; Adams *et al.*, 2019). Given their similar size, overlapping geographical distributions, proposed diets, limited number of homologous anatomical

characteristics, and that both groups perform gnawing with their large, paired incisors and diverse chewing behaviours with their cheek teeth, the two orders would likely have been competing during the decline and extinction of multituberculates.

Order Multituberculata is large and divided into two suborders: Plagiaulacida, and Cimolodonta (Kielan-Jaworowska, Cifelli and Luo, 2004). Suborder Plagiaulacida (Ameghino, 1889) originated in the late Jurassic and persisted until the early Cretaceous and is a paraphyletic group based on a set of dental plesiomorphies (Kielan-Jaworowska and Hurum, 2001; Kielan-Jaworowska, Cifelli and Luo, 2004). It can be further subdivided into: the Allodontid line (Kielan-Jaworowska and Hurum, 2001; Kielan-Jaworowska, Cifelli and Luo, 2004), comprising two families and one *incertae sedis* taxon, all of which are Jurassic; the Paulchoffatiid line (Kielan-Jaworowska and Hurum, 2001; Kielan-Jaworowska, Cifelli and Luo, 2004), comprising three families, one Jurassic, two Cretaceous; and the Plagiaulacid line (Kielan-Jaworowska and Hurum, 2001; Kielan-Jaworowska, Cifelli and Luo, 2004), comprising three families from the Late Jurassic to Early Cretaceous (Kielan-Jaworowska, Cifelli and Luo, 2004). Arginbaataridae (Hahn and Hahn, 1983) is *incertae sedis* and associated with Plagiaulacida (Kielan-Jaworowska and Hurum, 2001; Kielan-Jaworowska, Cifelli and Luo, 2004), and is not grouped into any of the three lineages due to its unique fourth lower premolar shape among the clade (Kielan-Jaworowska, Cifelli and Luo, 2004). The lower fourth premolars of most plagiaulacid multituberculates are not especially enlarged compared to those of many cimolodont multituberculates, and the first, second, and third premolars are still present and functional (Kielan-Jaworowska, Cifelli and Luo, 2004).

Suborder Cimolodonta (McKenna, 1975) first evolved in the Early Cretaceous and persisted until the Eocene. Though they lack the pattern of 'lineages' defined in Plagiaulacida, they are arranged into a set of superfamilies with *incertae sedis* taxa within and outside of these groupings (Kielan-Jaworowska, Cifelli and Luo, 2004). The three superfamilies are: Djadochtatherioidea (Late Cretaceous) (Kielan-Jaworowska and Hurum, 2001;

Kielan-Jaworowska, Cifelli and Luo, 2004), containing two families and three *incertae sedis* taxa; Taeniolabidoidea (Late Cretaceous to Palaeocene) (Sloan and Van Valen, 1965), containing two families and one isolated taxon with no assigned family; and Ptilodontoidea (Late Cretaceous to Eocene) (Sloan and Van Valen, 1965), containing three families (Kielan-Jaworowska, Cifelli and Luo, 2004). A family and four genera form an unnamed superfamily *incertae sedis* between Taeniolabidoidea and Ptilodontoidea, and three families are *incertae sedis* between Djadochtatherioidea and Taeniolabidoidea (Kielan-Jaworowska, Cifelli and Luo, 2004). Whereas plagiaulacid multituberculates retain their first and second lower premolars, cimolodont multituberculates lost those teeth completely, and their third premolar became reduced substantially while the fourth premolar remained; in some taxa, this fourth lower premolar is enlarged and ridged (referred to as a "plagiaulacoid" form, despite not occurring within suborder Plagiaulacida), but in other taxa it is relatively small (Kielan-Jaworowska, Cifelli and Luo, 2004). Subsequent phylogenetic trees, when made, have added newly discovered taxa but broadly agree with this overall arrangement.

Figure 4.1 displays a rough diagrammatic tree of the multituberculate suborders and their respective lineages and superfamilies. This is based on the early-2000s systematics (Kielan-Jaworowska and Hurum, 2001; Kielan-Jaworowska, Cifelli and Luo, 2004), with three genera shown and marked with an asterisk, and their branching order shown (with *Nemegtbaatar* splitting off first within Djadochtatherioidea, then *Chulsanbaatar* and then *Kryptobaatar*) matches two recent

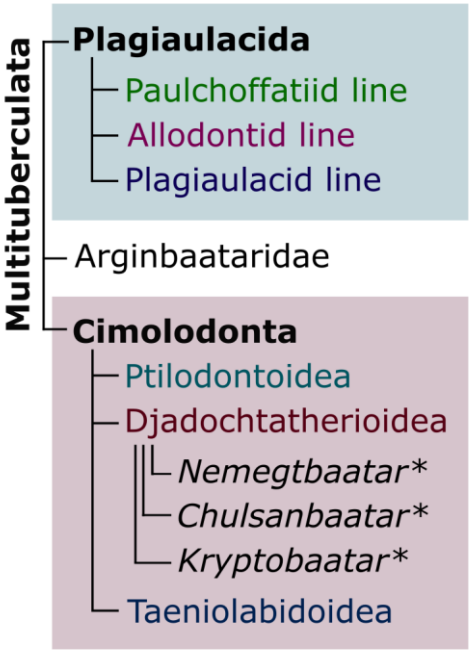

Figure 4.1: A simplified diagrammatic tree of order Multituberculata, showing the arrangement of lineages and superfamilies of each suborder, and three select genera.

papers that included them in their phylogenetic trees generated via parsimony analysis, which independently found this same arrangement of these taxa (Smith *et al.*, 2022; Jin *et al.*, 2023).

There are more detailed genera-level phylogenies of Multituberculata than the simplified Figure 4.1, including those based on different datasets or including newly discovered taxa, though such detail is beyond the scope of this thesis (Parmar, Prasad and Kumar, 2013; Yuan *et al.*, 2013; Xu *et al.*, 2015; Mao, Wang and Meng, 2016; Williamson *et al.*, 2016; King and Beck, 2020; Smith *et al.*, 2022; Jin *et al.*, 2023). Unfortunately, there is no new phylogenetic tree that includes all known multituberculate taxa; given the fact that so many are known through fragments and isolated teeth and distributed around the world in collections spanning decades of research, creating a more complete tip-dated phylogeny using modern methods would be a substantial collaborative project.

The enlarged plagiaulacoid premolar of certain cimolodont multituberculates is one of the most distinctive features of their toothrows. For some species or genera, the molars or premolars can be all that is preserved in the fossil record, but there are a number of well-preserved skulls and mandibles in Cimolodonta, some of which have been used in mechanical analyses (Wall and Krause, 1992; Gambaryan and Kielan-Jaworowska, 1995; Adams *et al.*, 2019); several taxa within Djadochtatherioidea in particular, from the Late Cretaceous Djadochta Formation in what is now Central Asia, are among these. These include the three genera shown in Figure 4.1. With this current—and hopefully ongoing—growth in the digitised sample of multituberculates, there is an opportunity to compare multituberculates with rodents using modern methods such as Finite Element Modelling, metal 3D-printed physical testing, or in this case of this thesis project, lever-arm mechanics. In the case of lever-arm mechanics, the muscles of these fossil taxa need to be digitised, and this thesis developed a workflow applied to rodents in earlier chapters.

During existing muscle reconstructions of the group, rodents have been used as a point of comparison due to their size, gnawing, and

immediately observable similarities such as a clearly complex and subdivided masseter based on muscle scars on the fossilised bones (Simpson, 1926; Gambaryan and Kielan-Jaworowska, 1995). However, functional propositions (Wall and Krause, 1992; Gambaryan and Kielan-Jaworowska, 1995) have not been tested using modern quantitative methods on a sample of multiple digitised multituberculates, and the group has not been quantitatively compared with a large sample of rodent species such as the one evaluated during this thesis project. Functional anatomical interpretations observed in extant taxa, including those regarding gape, can be applied to similar unrelated taxa to assess feeding mechanics (Herring, 1980; Ross and Iriarte-Diaz, 2014), a principle that can be applied here. Though these three studied taxa are Cretaceous and pre-date Rodentia, the example set by, and conclusions drawn from, the following analyses can provide a foundation for future expansion using more fossil multituberculates and fossil rodents as they are scanned and digitised in the coming years. This would deepen our understanding of potential similarity and competition in feeding between these two orders.

4.1.3 – Key questions and hypotheses

By using the previous two chapters as a foundation, this chapter aims to compare the mechanical advantage of homologous muscles of rodents and multituberculates. Once again, I must reiterate that the term 'mechanical advantage' is not a value judgement, and "higher" does not mean "better". The rodent morphotype categories will still be differentiated from one another in the results, and the multituberculates can be compared with them individually or with the full sample across Rodentia.

To do this, the multituberculate specimens must be digitised. The skull and mandible of *K. dashzevegi* were scanned together, and segmentation and alignment were trivial. In *C. vulgaris*, only one side of the head was well-preserved and unbroken, and was mirrored for figures but muscle mapped unilaterally. For *N. gobiensis* the degree of fracturing and

brittle deformation via crushing and displacement necessitated a reconstruction of the skull. This provides a point of comparison with older reconstructions using this specimen, which lacked such digitisation methods at the time of their production. A Key Question here is; are there notable differences between my new reconstruction using the µCT scans, and the older reconstructions of the specimen/taxon?

I hypothesise (**H3.1**) that several muscle attachments homologous to those of rodents will be identifiable in multituberculates; the masseter in particular will be subdivided into layers which have further subdivisions. To assess this, I will identify possible homologous muscle attachments on the fossil multituberculates, which can be compared with existing papers that did muscle reconstructions based on examination of the specimens and supported by photography. A Key Question arises from this comparison; are there proposed muscle attachment sites described in older papers that I cannot identify, or any new ones I propose here based on these scans?

I hypothesise (**H3.2**) that multituberculates will group together in the mechanical advantage results, closer to each other on the PCAs than to the rodents. Given the phylogenetic distance between Djadochtatherioidea and Rodentia, and the temporal difference between the Late Cretaceous and the present day, and the distinctive anatomical and mechanical traits of multituberculates (such as their laterally offset jaw joints and palinal power stroke), one would expect their masticatory musculature to be distinctive despite possessing homologous subdivisions. This can be assessed by examining the PC plots from the analyses of mechanical advantage data, and using MANOVAs to compare the group means and identify significant differences or a lack thereof.

I hypothesise (**H3.3**) that multituberculates will be mechanically similar to individual rodent taxa in these analyses, and that the disparity within rodents will be greater than that of the multituberculates. Partly, I propose this due to the difference in sample size, with only 3 multituberculates and 27 rodents. However, since this study uses two-dimensional lever-arm mechanics, I anticipate that some of the known

differences between the two groups (such as their palinal power stroke and laterally offset jaw joint, as mentioned previously) are not accounted for in this method. Despite expecting the multituberculates to group on the PC plots, I expect there to be rodents that are similar to them, since Chapter 3 displayed that the disparity among the rodent morphotypes is quite broad. The MANOVA analyses will be key to quantifying whether or not to accept this hypothesis, but visual examination of the PC plots can aid in it even if visual differences are not significant.

I hypothesise (**H3.4**) that, as in the results of Chapter 3, gape will affect the variance of mechanical advantage among the sample, and that in most muscles contribution to variance will be highest at the high or low extremes of the gape range studied. Certain muscles will exhibit lower variance at certain gape ranges, while others will exhibit higher variance at certain gape ranges. This can be confirmed or disputed using the loading plots produced during the PCAs of mechanical advantage, identifying which muscles and gape ranges are contributing the most to the total variance.

And finally, I anticipate that (as with rodents alone), mechanical advantage will not correlate with head size. This can be tested using a Multiple Regression, and if confirmed, head size can be dismissed as a potential source of noise in these data.

4.2 – Materials & Methods

4.2.1 – Sample Preparation

4.2.1.1 – General Sample Preparation

This sample consists of 27 rodent species from 20 families across Rodentia, and 3 multituberculate taxa, one from family Djadochtatheriidae (*K. dashzevegi*), two *incertae sedis* within superfamily Djadochtatherioidea (*C. vulgaris* and *N. gobiensis*). All of these were digitised using µCT scanning. The scans for rodent taxa are all available on MorphoSource (www.morphosource.org), and *K. dashzevegi* was accessed on Digimorph (www.digimorph.org), though a new CT scan of a different specimen has been published on MorphoSource in March 2024. The other multituberculate scans are novel and were produced concurrently with the research for this project, by Łucja Fostowicz-Frelik of the Institute of Paleobiology at the Polish Academy of Sciences, Warsaw, and Ian Corfe of the University of Helsinki. These two novel scans are not currently on databases such as MorphoSource and are not previously published. All three multituberculate scans are stated in Table 4.1, including the catalogue number of each specimen. The rodent sample information is not repeated here, and can instead be found in Chapter 2, Table 2.1.

Kryptobaatar dashzevegi, Djadochtatheriidae (Kielan-Jaworowska, 1970; Kielan-Jaworowska and Hurum, 1997; Kielan-Jaworowska, Cifelli and Luo, 2004) was CT scanned and digitised in the early 2000s, and has been used in recent functional research comparing it with extant rodent taxa (Adams *et al.*, 2019). The two newly scanned specimens *Nemegtbaatar gobiensis* (Kielan-Jaworowska, 1974) and *Chulsanbaatar vulgaris* (Kielan-Jaworowska, 1974) are both taxa within Djadochtatherioidea (Kielan-Jaworowska and Hurum, 2001; Kielan-Jaworowska, Cifelli and Luo, 2004) that were studied in previous mechanical research (Gambaryan and Kielan-Jaworowska, 1995).

As shall be discussed in the following subheading, the mandible for *N. gobiensis* that was scanned is not the original I/82 that was paired with the

skull it is catalogued with. As such, Table 4.1 states the label as I/82* instead of I/82. The analysis of *N. gobiensis* uses the scanned skull and mandible available, but unfortunately these are not from the same individual.

Species	Family	From	Specimen	Scanned
C. vulgaris	Djadochtatherioidea	ZPAL	MgM-I/108	Warsaw
K. dashzevegi	Djadochtatherioidea	AMNH	PSS-MAE 101	Austin
N. gobiensis	Djadochtatherioidea	ZPAL	MgM-I/81 & MgM-I/82*	Warsaw

Table 4.1: This table displays information about the multituberculate taxa in the sample. Institution acronyms are as follows: American Museum of Natural History, New York (AMNH), Institute of Paleobiology, Polish Academy of Sciences, Warsaw (ZPAL).

I segmented the µCT scans in Avizo version 9.2 (Thermo Fisher Scientific, Waltham, MA, USA) and in the case of *N. gobiensis* individual bones were isolated. In the case of rodents and *K. dashzevegi*, this was sufficient segmentation; however, in the cases of *C. vulgaris* and especially *N. gobiensis*, further processing was necessary, as outlined in the following subheadings. Once a specimen was segmented or reconstructed as required, I aligned it relative to the global axes in a uniform orientation across the sample: the x-axis is parallel with the mediolateral axis of the head, the y-axis is parallel to the dorsoventral axis, and the z-axis is parallel with the anteroposterior axis, with the specimens positioned in the positive space of all three axes. With these aligned and the mandible or hemimandible articulated, I landmarked the tips of the incisors, the contact points of the lower fourth premolar and the upper premolar row, and the articular surfaces of the temporomandibular joint (TMJ).

I identified and mapped the attachment sites of muscles in these taxa according to my own interpretations, exported them as .stl files and recorded the coordinates of their centroids in Blender (www.blender.org), as in the rodents. I used my prior study of rodents to identify and name homologous muscles on the fossil multituberculates where present.

4.2.1.2 – Multituberculate Fossil Reconstructions

4.2.1.2.1 – Nemegtbaatar gobiensis

Due to *N. gobiensis*' exceptional surface preservation and high scan resolution, muscle attachment sites were clearest on this specimen of the three, and I used it to guide the reconstruction and muscle identification of the multituberculate taxa with poorer surface detail (*C. vulgaris*) and lower scan resolution (*K. dashzevegi*). Individual bones were also easiest to identify in this specimen, and its historical importance in existing reconstructions of multituberculate taxa made it of particular interest as a point of potential comparison with older methods and conclusions (Kielan-Jaworowska, 1974).

The skull and hemimandible were scanned separately. The mandible is fractured but not distorted, and had been glued along fractures to preserve it, whereas the skull experienced substantial crushing in multiple directions during fossilisation that require extensive reconstruction to correct. The left side was more severely damaged than the right, so I mostly conducted the reconstruction on the more-intact right side of the head, and mirrored for a 'full' skull reconstruction. The right upper incisor was broken off, but the left upper incisor was intact and I incorporated it into the reconstruction using mirroring of the left premaxilla.

I segmented the skull CT scan in Avizo. I initially removed the external matrix with a rough threshold, revealing sections of bone that were otherwise obscured. Bones were fractured, shattered, and misaligned but there was no observable ductile or plastic deformation of the bone; all observed deformation in this specimen is brittle. The specimen had been crushed dorsoventrally, flattening it slightly, the left side of the skull had been displaced posteriorly relative to the right along the broken sagittal midline. The front of the skull had been anteroposteriorly bent to the right side, and the left premaxilla had been dislocated and rotated out of place. As all deformation was brittle, the specimen could be reconstructed by isolating the individual bones and bone fragments, then manually reconstructing the head using translation and rotation of the pieces. I segmented the bones

individually beginning at the dorsal front of the head (the nasal bones), before working back along the dorsal cranium, then along the ventral skull's surface, and finally down the lateral surfaces that remained unsegmented. I initially assigned the bones a letter at first and different colours, since some fragments were not easily identifiable as specific bones; I assigned bone names once the reconstruction was complete, using the modern established names in mammals. The interior of the head was entirely replaced with matrix material, so the resulting reconstruction is only of the identifiable surface bones due to the lack of preservation of deep internal structures.

I created a flat plate as a surface file in Avizo and aligned it on what was to be the reconstructed sagittal midline. This plate was perpendicular to the y-z plane of the global axes and parallel with the z-axis, so that the resulting head would be aligned similarly to the rodent specimens studied prior. Since many of the sutures between bones—or contact surfaces that were sutures prior to disarticulation—were intact and undeformed, I used these as guides to align the edges of the bones. Some sections were especially affected by replacement with matrix material, but where surfaces of matrix material connected between bones in an anatomically plausible way (such as the orbital margin of the dorsal surface of the anterior zygomatic root, a slightly convex surface replacing the lacrimal bone and connecting the frontal and parietal bones to a visible suture surface on the zygomatic root) I segmented them to aid in realignment of the bones during reconstruction. I removed some of these segmented matrix sections after this alignment was complete, whilst some appeared accurate enough that I left them in to approximate the surface of the skull in that region. Other areas were more severely replaced and the accuracy of the matrix material to the original bone was more difficult to guess, such as the orbital wall. For the purpose of jaw mechanics analyses these regions are not of critical importance, and I accepted the imperfect shape of the matrix material where necessary for reconstruction to be practical. The figures shown in the Results sections show these uncertain areas clearly as well as other holes and gaps.

I conducted the alignment of bones beginning with the nasal bone and working backwards using the sutures, shapes, and topography of bones to align them correctly relative to one another, along the sagittal midline plate. I did this because the sutures and bone surfaces were especially well preserved in this region of the head, and the shapes were simple compared to the more complex shapes of the posterior cranial region. I fine-tuned segmented matrix regions when aligning them, trimming their edges as necessary once bones were brought back into alignment. I used the zygomatic arch to ensure that the posterior and anterior skull were correctly aligned relative to one another. Due to the minor fracturing of the zygomatic arch and the lack of plastic deformation, and that the shape of the zygomatic would have strongly resisted any potential plastic deformation that was dorsoventral (as the majority of brittle compression of the specimen is), I considered the zygomatic arch to be an especially reliable piece to ensure correct alignment across the length of the head. In particular, since so many of the key muscle origins are on the zygomatic arch, I wanted to avoid altering its shape during reconstruction.

Once the reconstruction of the dorsal cranium was complete and the zygomatic arch was used to ensure accuracy, the reconstruction of the posterior cranium was straightforward. Once all bones were realigned, the cranial reconstruction of the specimen was complete. A number of holes, both small and large, remained where the accuracy of matrix replacement was ambiguous, and I patched them for the final, mirrored "full skull" surfaces used for certain figures. For those final figures, I imported the reconstructed right side of the skull into Blender as individual bone surface files, and then exported them as a single surface file. I imported this new surface back into Avizo and converted it into a label field, then patched the holes and cracks using the segmentation editor, although larger gaps where no material indicated the original surface shape of the bone were left untouched and open. This produced a final, mostly-complete surface file of a reconstruction of the skull. Finally, I imported this new right side back into Blender and

mirrored it to complete the full head surface used for the anatomical diagrams in the final figures.

With the skull reconstruction complete, I imported the hemimandible and aligned it relative to the skull; it was at this point that I identified the scanned hemimandible as not being the original mandible for this specimen, as it was approximately 15% too short for the incisors to occlude even if the incisor tip was complete on the hemimandible. By examining the plates from an existing paper with new photographs of this specimen, I confirmed that it is a different hemimandible, and notably the original specimen did possess an intact incisor (Kielan-Jaworowska, 1974; Gambaryan and Kielan-Jaworowska, 1995). Based on these photographs of the skull and original hemimandible, and the measurements of dimensions listed in the paper, I rescaled the scanned hemimandible to bring it close to the original dimensions of the original mandible. The measurements of both mandibles are recorded in Table 4.2 and were used to calculate rescaled measurements for the hemimandible surface, with a resulting scale factor of 1.168 applied in the x-dimension, 1.147 in the y-dimension, and 1.188 in the-z-dimension.

	Measurement /mm		
	Scanned	**Real I/82**	**Rescaled surface**
Length	22.43	26.65	26.65
Height (below p4)	4.67	5.20	5.36
Height (below m1)	5.93	7.00	6.80
Width (at p4)	3.05	3.75	3.56
Width (at incisor root)	3.03	3.35	3.54

Table 4.2: Measurements of the scanned hemimandible, the original hemimandible (Kielan-Jaworowska, 1974), and the rescaled version of the scanned mandible.

I notified the Museum of Natural History, Warsaw, of this cataloguing error (as the specimens had been mistakenly switched at some point prior to 2019 when they were photographed by Jesse Hennekam early in this project), but the correct original mandible has not been scanned to date. Since the muscle attachments surfaces of the scanned specimen were well preserved

and the hemimandible had suffered little deformation, the rescaling allowed the scanned mandible to be brought to roughly the right size, within around 0.2mm according to these measurements. Since it is not from the original mandible, and the broken incisor prevents precise verification of alignment accuracy, the lever-arm mechanics analyses of this specimen should be treated with relative caution. They are less likely to be accurately representative of the taxon than the other multituberculates in this analysis, and future analyses with the original mandible may result in changes to the results obtained. With the intact muscle attachment surfaces and excellent preservation of the articular surface and cheek teeth, and the rescaling resulting in differences of around 0.2mm in measurements due to differences in shape, I argue that this hemimandible specimen is still suitable for the analyses, and I used it to aid in identifying the jaw-closing muscles present in *N. gobiensis*.

For the muscle mapping and lever-arm mechanics calculations, I mapped the specimen's muscle attachments unilaterally on the reconstructed right side. I identified the muscle attachments by examination of the surface shape of the bones of the skull, and the rescaled hemimandible. I applied the nomenclature from Rodentia to name homologous muscles. I then compared this with the existing muscle reconstruction of this taxon (Kielan-Jaworowska, 1974; Gambaryan and Kielan-Jaworowska, 1995).

I articulated copies of the hemimandible at both premolar occlusion and incisor occlusion, and identified its alignment for incisor biting using the photographs of the original mandible and skull, and images taken in Avizo using the rescaled hemimandible. With the broken incisor tip, this cannot be confirmed with absolute certainty, but with the good quality of the original photographs and the careful translation of the hemimandible, I reached an arrangement where the jaw joint was articulated, the mandible and skull did not intersect, and the mediolateral orientation of the mandible aligned so that the intact incisor would have occluded if present and the same length as that of the original. For the premolar bite, I aligned the molar cusp rows and

brought the plagiaulacoid lower fourth premolar (p4) into contact with the upper premolar row. With the existing scans, this is as close as can be realistically reconstructed, and I estimate the accuracy to be within a few millimetres, as the required translations after rescaling were approximately 1–2 millimetres, with no rotation of the jaw required. Initially, the muscles were mapped at premolar occlusion since the intact teeth aided in alignment, and then re-mapped on the incisor-occlusion hemimandible.

4.2.1.2.2 – Chulsanbaatar vulgaris

The skull of *C. vulgaris* was comparatively simple to prepare for muscle mapping. I imported the CT scan and segmented the skull and hemimandible in separate files. For the mandible, a simple thresholding and removal of islands was sufficient, with some filling of fractures and repair of damaged surfaces in areas that are not relevant to these analyses. The skull surface was in relatively poor condition due to extensive replacement of bone with matrix material. In *N. gobiensis*, bones were often identifiable with clear sutures and internal architecture, but much of the skull surface—particularly the dorsal cranium—was completely replaced in *C. vulgaris*. Thankfully, most muscle attachment surfaces were in good condition and identifiable.

I segmented the skull using thresholding, and the lack of brittle or ductile deformation meant further reconstruction was not required for the left side. The damage to the right side, particularly its zygomatic arch, made it less suitable for identifying and mapping muscle attachments. However, with the presence of only one hemimandible, I decided to mirror the left side and hemimandible for the full anatomical figures presented in this thesis, rather than patching the right side in sections. With the replacement of bones in the dorsal cranium and slight asymmetry, mirroring was more involved than *N. gobiensis*; an accurate sagittal midline was not easily identifiable with the lack of bone detail and internal architecture. I imported the hemimandible and aligned it with the skull. After some trial and error using mirroring of the hemimandible and occlusion of the cheek teeth, incisors, and

articular surfaces, I adjusted the 'midline' of the reconstructed skull until both sides of the head were positioned for articulation with both hemimandibles at incisor occlusion with a small symphysis between the hemimandibles rather than a larger gap, and no gap in the middle of the skull between the two sides. This was sufficient to produce an undeformed head and mandibles for the production of the finalised figures in this thesis.

I conducted the muscle identification and mapping unilaterally on the articulated skull and hemimandible, comparing it with *N. gobiensis* and rodents to aid in identification. Due to the surface damage and replacement, some of the origins on the skull were substantially more difficult to identify than in *N. gobiensis*. I mapped the insertion attachments with a hemimandible at premolar inclusion, and I applied the translation matrices that produced the incisor-occlusion hemimandible position to these muscle attachment surfaces, translating them into their incisor-occlusion positions. Due to extensive replacement, the upper incisors are heavily obscured, but I treated the existing material as accurate to the tooth length due to the lack of alternatives to replace the upper incisors. With a specimen that has better preserved upper incisors, this occlusion could be modelled more robustly. As such, this study may result in a slight undercutting of the gape angle during the incisor biting modelling (i.e. that with the upper incisor intact the mandible may have been positioned at a larger gape to occlude the incisor tips). Based on the shape of the incisors in their current state of presentation, I believe this is unlikely to be more than a couple of degrees of error in gape.

4.2.1.2.3 – Kryptobaatar dashzevegi

Of the three multituberculate taxa, *K. dashzevegi* was the simplest to prepare for analysis. The method was no more complex than the segmentation of rodent taxa. I imported the CT scan into Avizo and used thresholding to isolate the skull and mandibles (which were scanned together, at occlusion). I segmented the skull and mandibles into separate materials to produce two surface files. Due to the low scan resolution—compared with the other multituberculates—and the unimportance of molar

cusp morphology to these analyses, I did not accurately separate the upper and lower molar teeth to preserve the fine details of their cusp morphology. I took greater care to cleanly and accurately separate the upper and lower premolars, as they are to be landmarked for these analyses.

I duplicated the mandible, and produced the two bite points by translating one mandible into premolar occlusion, and the other into incisor occlusion. The muscle attachment surfaces were identified using the rodent taxa and both previously mapped multituberculate taxa as guides. The fossae were less prominent than on *N. gobiensis*, partly due to the larger voxel dimensions, but were mostly clear, in good condition, and easily identified. I used the transformation matrices for mandible occlusion to translate my mapped muscle insertions into their incisor-occlusion position. As no additional reconstruction was required, the Results section for *K. dashzevegi* omits the figures of the unreconstructed surfaces in Avizo displayed for *N. gobiensis* and *C. vulgaris*, as the outline figures are sufficient for the relevant observations and results.

4.2.2 – Lever-arm mechanics modelling

The individual steps for the lever-arm mechanics calculations are discussed in detail in Chapters 2 and 3. The same framework and equations from Chapter 3, subheading 3.2.2 were applied here with only one difference; I had duplicated the multituberculate mandibles and identified their attachment centroid coordinates at both incisor biting and biting with p4. As a result, the equations used in Chapter 2 and 3 to simulate protraction of the mandible for gnawing were not required for these three taxa. I mapped both the incisor and premolar configurations together rather than allowing potential error from delay between mapping sessions. In the early years of this project, the aims were focussed specifically on molar biting, which is why the original rodent taxa were not aligned and mapped in incisor and molar configurations during the preparation of those specimens. In the case of the multituberculates, the scans arrived late in the project and were mapped after incisor biting had become part of the study.

In *N. gobiensis* and *C. vulgaris*, all these muscle attachments were mapped unilaterally on the reconstructed or better-preserved side of the head. In *K. dashzevegi* and all rodent taxa, they were mapped bilaterally and the left and right sides were averaged. In *N. gobiensis*, the fact that the lower incisor in the scanned specimen is snapped off meant that the lower incisor tip could not be landmarked; instead, since the incisor tips of specimens are landmarked at incisor occlusion, the lower incisor tip landmark was placed on the upper incisor tip as if the two were in contact, potentially resulting in a small source of error. This simulated lower incisor tip landmark was then rotated as normal for gape simulation.

As in Chapter 3, a zero-gape analysis is not included as tooth tips are not in contact with one-another when biting a real food object, and 40° was maintained as the upper gape limit. This limit is likely to be at or past the limit of gape for multituberculate taxa according to older analyses, which determined that some multituberculate taxa (not those in this study) would dislocate their jaw joint if they bit at a gape of 40° (Gambaryan and Kielan-Jaworowska, 1995). I calculated the mechanical advantage of each muscle at each gape angle using the equations presented in Chapter 3, subheading 3.2.2.

4.2.3 – Statistical Analyses

The methodology for the MANOVA analyses was also discussed in detail in Chapter 3's Materials and Methods, but will be briefly reiterated here. A MANOVA (Wilks, 1932) tests the significance of the difference between the means of group categories, and how strongly the independent variable accounts for that difference. For all analyses, Pillai's Trace (Pillai, 1955) is presented along with its associated F statistic and p-value. Unlike Chapter 3, these analyses are comparing the multituberculates with the rodent taxa. For most analyses, the multituberculates are treated as a fifth group and contrasted with the four rodent morphotypes together; in these tests, the MANOVA compares the means for all five of these groups simultaneously, so

that variation between the morphotypes is not ignored in the context of these new comparisons.

I conducted four sets of MANOVAs in PAST version 4 (Hammer, Harper and Ryan, 2001) for this Chapter's analyses. First, a set of MANOVAs on the raw mechanical advantage data. Due to the limitations of a MANOVA, the raw data cannot include multiple muscles in a single MANOVA, and I conducted them for each muscle separately for all studied gape angles, at each bite point; nine muscle comparisons and two bite points makes for a total of eighteen tests. As in Chapter 3, I compared the **Infraorbital ZygomaticoMandibularis (IOZM)** with the **Anterior Deep Masseter (ADM)** in taxa that lack one of those muscles, and compared the **Deep Masseter (DM)** of hystricomorphs with both the **ADM** and the **Posterior Deep Masseter (PDM)**.

I conducted the remaining three sets of MANOVAs on the PC scores of each of the Principal Components Analyses (PCAs), as the reduced dimensionality produced by the PCAs allows all muscles and gape angles to be included in a single analysis. As in Chapter 3, the raw data are difficult to interpret visually, and statistical tests are limited when dealing with so many variables—hence the separation of raw mechanical advantage data MANOVAs into individual muscles. A PCA reduces the dimensionality of the data, allowing for easier visualisation of patterns and trends, and testing of the variance among the full masticatory muscle systems rather than individual muscles alone. All uses of muscle names and acronyms will share their text colour with the figures, following the same colour scheme in previous chapters. Notably, I could not identify the **Superficial Masseter (SM)** in the multituberculate taxa studied, with no identifiable origin on the skulls or identifiable insertion on the mandible. Its data among the rodents will be removed from the analyses in this chapter, but I did identify the other muscle subdivisions observed frequently among rodents in these multituberculate taxa. As before, some taxa lack the **IOZM** (namely the sciuromorphs and *A. rufa*), so two PCAs were conducted: one contains the full sample of muscles and compares the mechanical advantage of the **IOZM**

with the **ADM** with taxa that lack either muscle, and the other omits the **IOZM** data and compares the hystricomorph **DM** with both the **ADM** and the **PDM**. This allows for the full sample to be run in both PCA while removing as few muscles as possible.

Each muscle sample has two PCAs: one for the incisor biting data, and one for the molar biting data. I conducted the PCAs in PAST 4. I recorded the loading of all PCs recorded, and their contributions to the total variance, but have only included results for PCs 1 to 4, as they account for the majority of the variance. I produced PC plots to aid in the visual identification of patterns and trends, as in Chapter 3. For the purpose of these analyses and comparisons of group means, the 'groups' as defined are the four rodent morphotypes, plus the multituberculates, for a total of five groups.

Two of remaining MANOVA sets are of the PC scores which compare the multituberculates against all the included rodents (one set for the **ADM** v **IOZM** PCA, and the second for the **ADM** v **DM** PCA). The last is a set of MANOVAs conducted comparing the PC scores of the multituberculate taxa against each individual morphotype in isolation, and against the distinct groupings identified in Chapter 3, to compare the significance of the difference between the multituberculates and each individual morphotype.

Since the MANOVAs in the raw data tests share dependent variables, I applied the Bonferroni correction to the initial 0.05 p-values when necessary (Dunn, 1961). For the individual muscle MANOVAs on the raw data, the adjusted p-value is 0.0055. For the comparison between multituberculates and individual morphotypes, this results in an adjusted p-value of 0.0125 for the **ADM** v **IOZM** PCA and 0.0083• for the **ADM** v **DM** PCA. In the other MANOVAs conducted, no adjustment is required as each one uses different dependent variables.

4.2.4 – Head size correlation testing

As discussed in Chapter 3, subheading 3.2.4, head size could be a potential source of noise in the data. I again applied geometric mean (Robinson and Redford, 1986; Jungers, Falsetti and Wall, 1995; Coleman, 2008) to calculate a measure of head size using measurements of length, width, and height. I measured zygomatic-to-zygomatic width on the mirrored reconstructions in the case of *C. vulgaris* and *N. gobiensis*; different reconstructions might result in a different measurement. As before, I used the geometric mean as the dependent variable in a pair of Multiple Linear Regression (MLR) tests. These MLRs test whether the geometric mean of head size correlates with the variation across the mechanical advantage in the sample. In Chapter 3, no correlation was identified, and the addition of only three new taxa to this sample's analyses are unlikely to affect this result. But the potential impact of size should still be tested, and I argue this test is sufficient.

4.3 – Results

4.3.1 – Anatomy and fossil reconstructions

4.3.1.1 – Nemegtbaatar gobiensis

Photographs of the skull and mandible that were scanned for this taxon are displayed in Figure 4.2. These photographs are included to show the state of surface preservation and damage in each specimen, in colour.

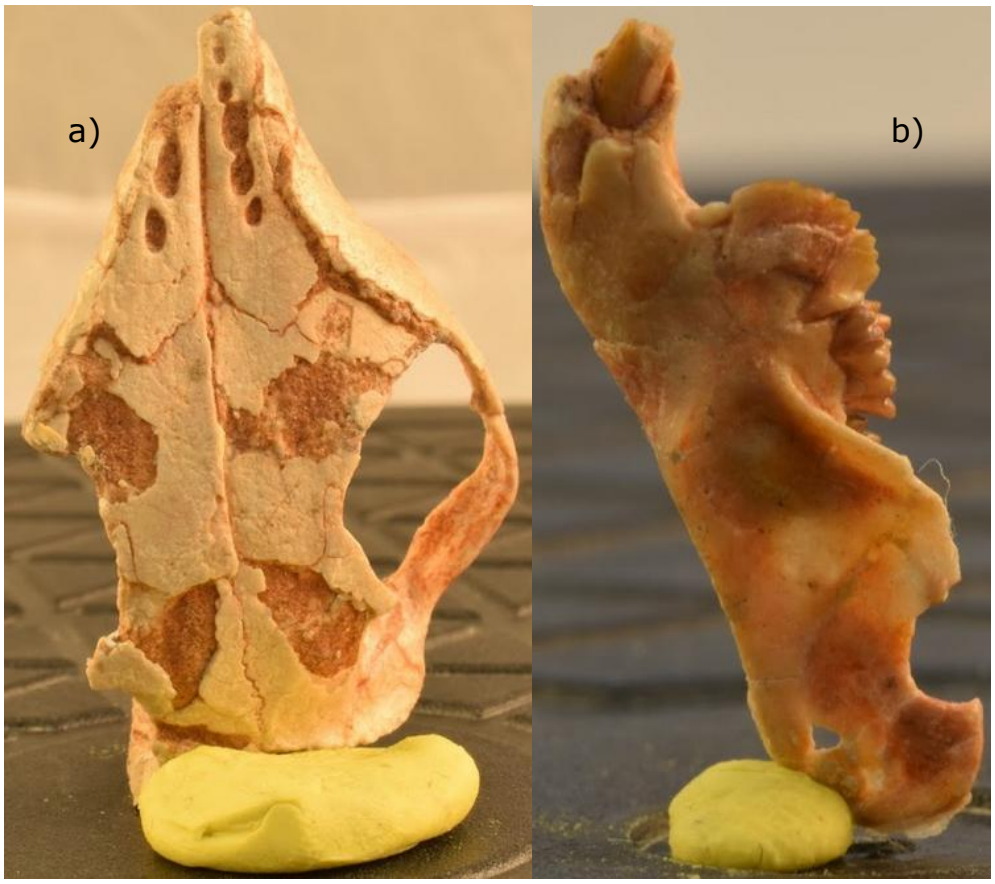

Figure 4.2: Photographs of fossil specimens of *N. gobiensis* that were later scanned: a) skull I/81, b) the hemimandible incorrectly labelled as I/82. These photographs are not at the same scale.

As can be observed, many sections of the bone (lighter material) are fully replaced by the reddish-brown matrix material. This distinction is also clear in the CT scans to follow. Figures 4.3 and 4.4 display the initial volume renders prior to reconstruction. It can be observed that the hemimandible is mostly intact aside from some small holes and that the coronoid process is broken and lacks its tip, leaving its exact shape unclear. In all scans, the teeth

and intact bone surfaces are in excellent condition (exempting the snapped lower incisor), and all deformation is brittle.

The right maxilla in particular is in excellent condition, with good preservation of the teeth and no evidence of substantial deformation; the dorsal cranium and the crushing primarily displacing the left-hand side has left the right maxilla especially protected from damage, providing a well-preserved tooth row that could be used in future masticatory analyses, or analyses of tooth morphology. The posterior basicranial region is perhaps the worst preserved of the ventral surfaces, but the right pterygoid plate and its muscle attachment are intact. The right zygomatic arch has some fractures but is not noticeably deformed. Between all of these surfaces, those critical to these analyses are all well-preserved and have suffered little damage.

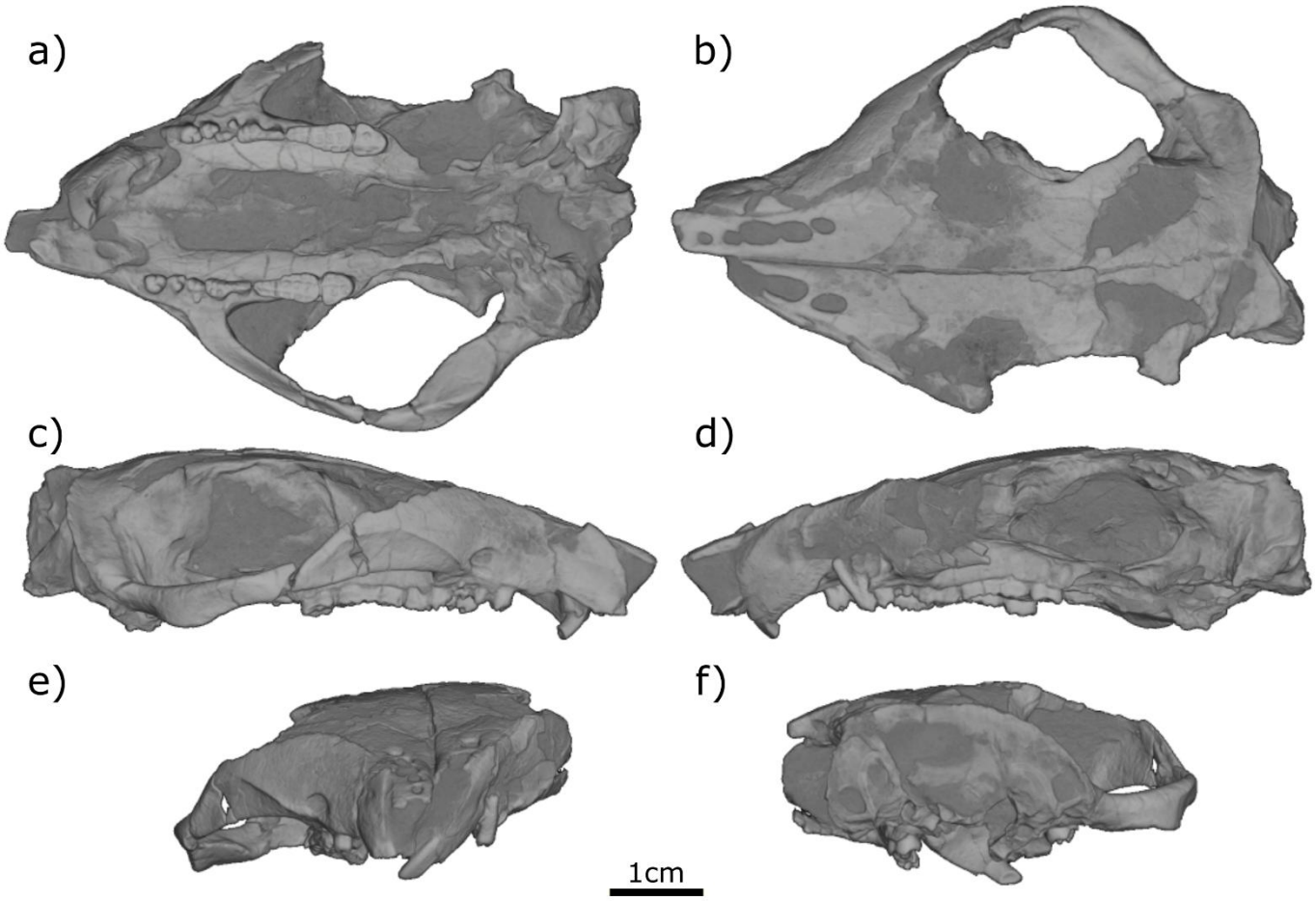

Figure 4.3: a) Ventral, b) dorsal, c) right lateral, d) left lateral, e) frontal, and f) rear views of a volume render of the scanned skull of *N. gobiensis*.

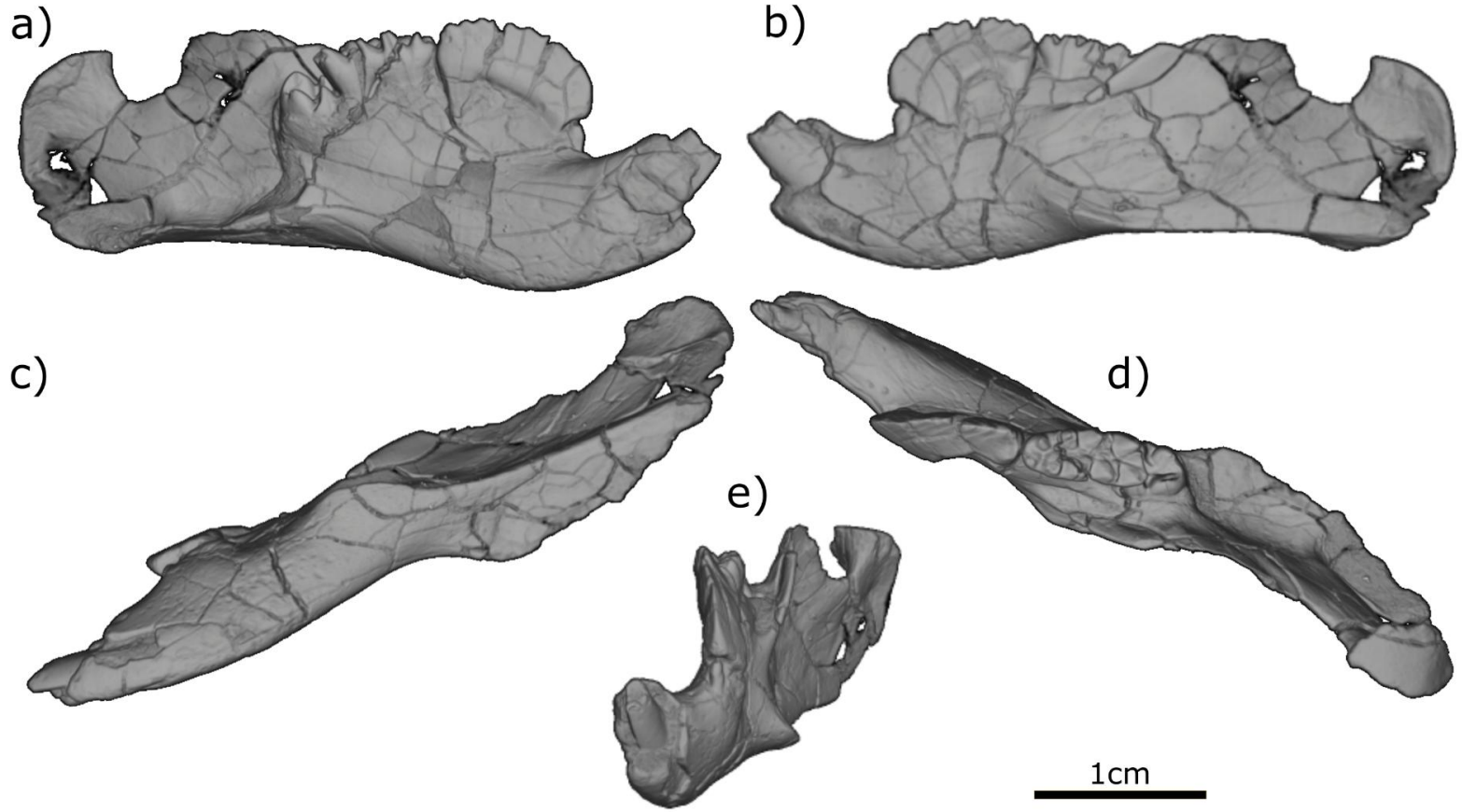

Figure 4.4: A panel figure showing a) lingual, b) labial, c) ventral, d) dorsal, and e) frontal views of a volume render of the scanned hemimandible of *N. gobiensis* prior to segmentation.

4.3.1.1.1 – Skull reconstruction

Figure 4.5 displays the initial segmentation of the bones in Avizo during the first stage of reconstruction. Each separate bone or bone fragment is segmented in a distinct colour, with a key shown. With only one half of the head segmented (except for the left premaxilla for its intact incisor) the mediolateral bending of the specimen is clear, but I did not identify any evidence that the bones underwent plastic deformation during the segmentation. The deformation appears brittle, with displacement primarily coinciding with regions where bone has been replaced with matrix material and its structure is not preserved; once I assembled the bone fragments along a midline, this became clear as no 'bending' of pieces was required to position them plausibly.

The light pastel green region of the lateral face of the alisphenoid/orbitosphenoid region was completely replaced with matrix material and the original surface was often quite unclear, leaving large white gaps where I chose not to segment it; this is one of the 'segmented matrix' regions of relative uncertainty in the reconstruction, and is not of particular importance to the mechanical analyses later conducted. Similarly, the grey region connecting the frontal bone to the dorsal root of the anterior zygomatic arch on the maxilla is reconstructed matrix. There were small fragments of bone in this region, and a relatively distinct margin along its posterolateral edge, forming a bridge between the frontal and the zygomatic root. This would be the lacrimal in the previous existing reconstructions of this specimen (Kielan-Jaworowoska, Presley and Poplin, 1986; Kielan-Jaworowska, Cifelli and Luo, 2004), and despite not being clear and intact bone, is included in the segmentation with relative confidence compared to the orbitosphenoid 'patch'. The nasal foramina on the nasal bone (segmented in bright neon pink) are among the only openings in this reconstruction that are not simply replacement of bone with matrix material (as in the posterior parietals or along the ventral midline of the skull); existing reconstructions proposed five openings, but these are not reconstructed in detail here. It appears that the third and fourth foramina (proceeding from

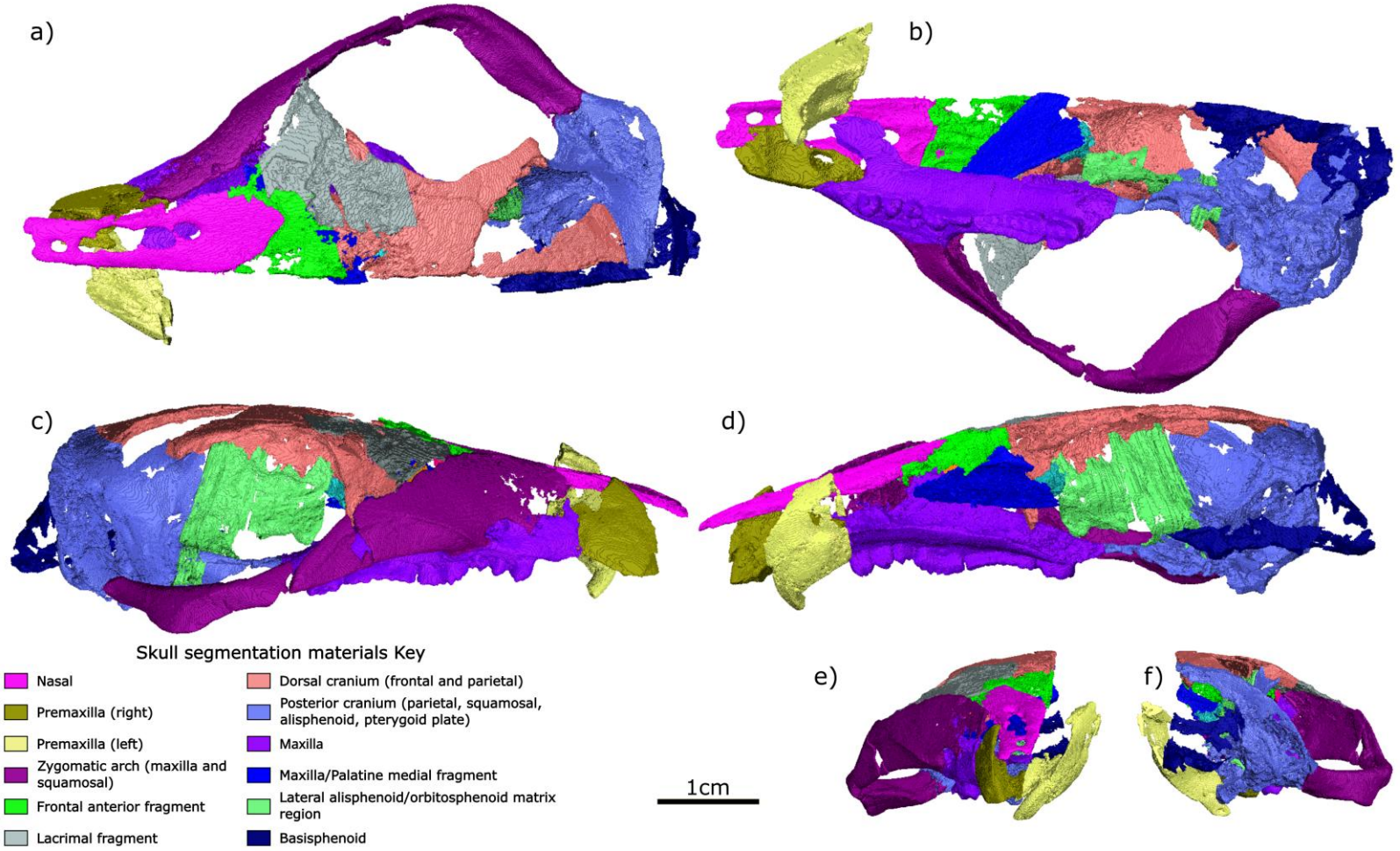

Figure 4.5:
Panels: a) dorsal, b) ventral, c) lateral, d) medial, e) frontal and f) rear views of the segmented bones of the skull of *N. gobiensis*. A key shows what bones/segmented regions are each colour.

the anterior to the posterior) may be the largest assuming bone around the edges is not replaced to expand them, which does fit with the previous reconstruction of this specimen (Kielan-Jaworowoska, Presley and Poplin, 1986; Kielan-Jaworowska, Cifelli and Luo, 2004).

Figure 4.6 shows the bones reassembled using the midline plate. The snapped palatine/maxilla region (royal blue) that was displaced up into the snout was positioned using the maxilla. The damage to its margins makes the palatal vacuity's shape unclear, and the ventral skull posterior to this region is very poorly preserved along the midline in the vomer and basisphenoid and basioccipital regions (the latter bone partially preserved in navy blue). Based on this reconstruction and its sutures, a major difference in shape is clear compared to existing reconstructions. The nasal bone does not exhibit evidence of plastic deformation or internal fractures that could 'straighten' it and 'bend' its anterior region away from the premaxilla. Along the lateral face of the nasal a trough-like suture surface is visible, and existing reconstructions seem to have treated this as having originally been in direct contact with the curved antero-medial margin of the premaxilla. This would require major plastic deformation of the bone without leaving any visible trace of damage on the CT scans from such bending; this would require the nasal bone to have overlapped with and blocked the incisors in life, which is anatomically implausible. The older reconstructions would also require plastic deformation of the well-preserved maxilla, the tooth row, and the zygomatic arch to accommodate this and create the older proposed head shape in lateral view; there is no superficial or internal structural deformation identifiable in the new CT scans that supports such an interpretation, and indeed this would require substantial bending in opposing directions only millimetres apart on the skull.

As such, my new reconstruction has a larger nasal opening than the older reconstructions would have implied with such a bent nasal bone, and results in an overall flatter and shallower skull shape in lateral view. Some rodents also possess a similar divergence of the nasal and premaxilla, with a large nasal opening, and often have a cartilaginous segment bridging some

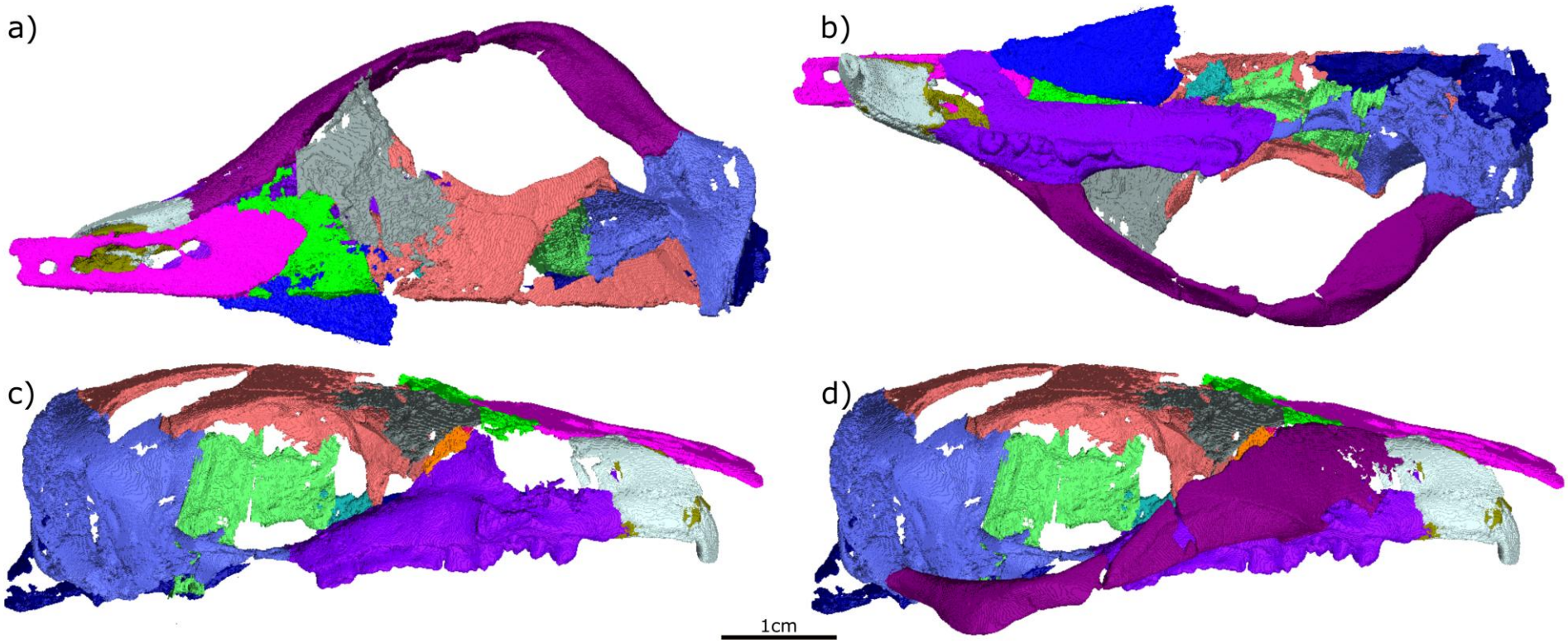

Figure 4.6: A panel figure showing the reconstructed right side of *N. gobiensis* using the midline plate, in a) dorsal, b) ventral, c) lateral with the zygomatic arch hidden, and d) lateral with the zygomatic arch shown.

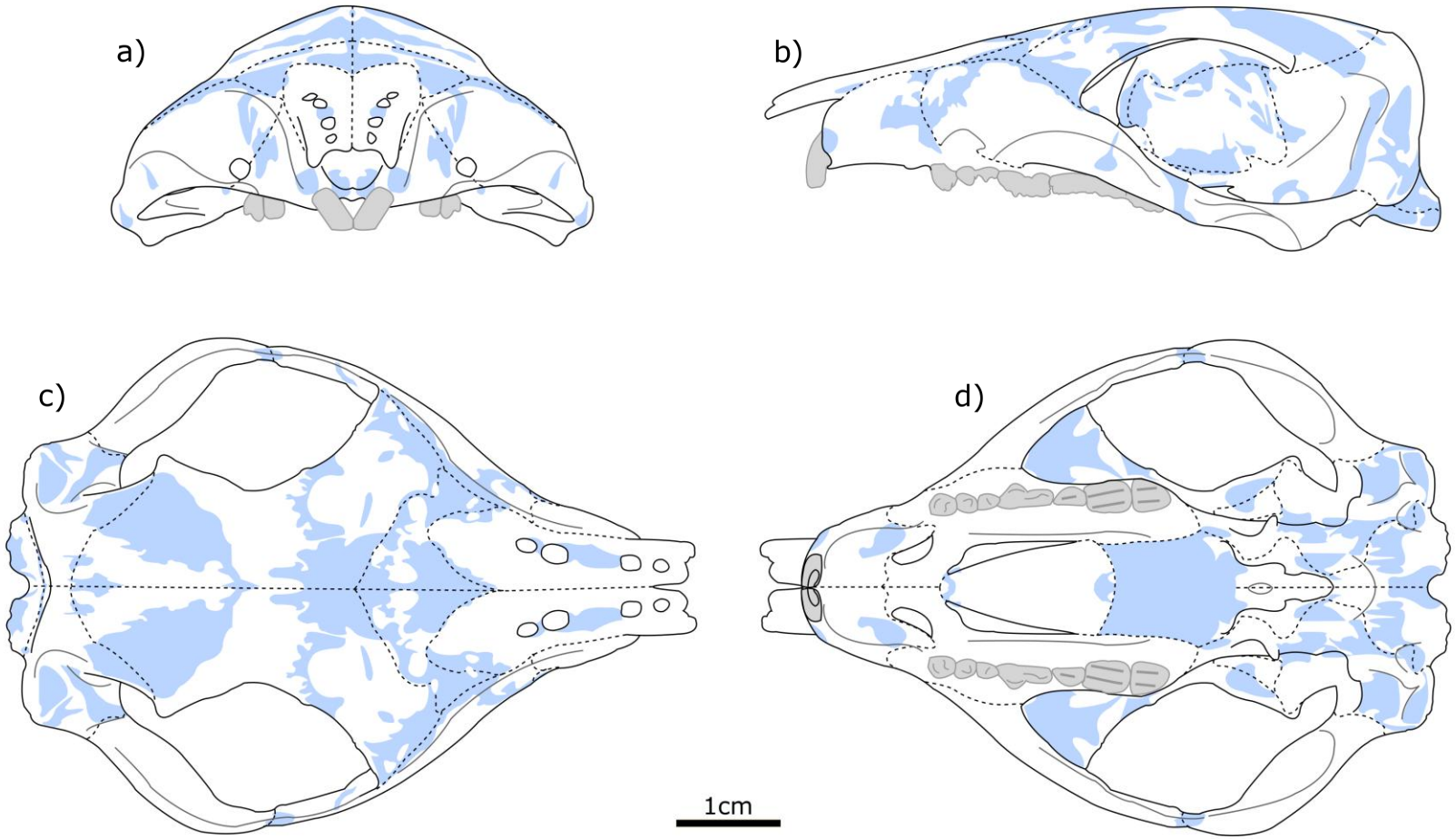

Figure 4.7: A panel figure showing line diagrams of the skull of *N. gobiensis* in a) frontal, b) lateral, c) dorsal, and d) ventral views. Pale blue represents areas where the bone surface is not preserved, and proposed/identified sutures are illustrated with dashed lines.

of the gap between the two bones for support; I propose that the observable suture-like depressions on the lateral margin of nasal mark the anterior extent of a cartilaginous support region between the bones. All muscle attachment identification and mapping for the lever-arm mechanics was conducted on this segmented and reconstructed right-side of the skull as outlined in the Materials and Methods. From this, I produced a mirrored 'full skull' surface to illustrate simplified anatomical diagrams as shown in Figure 4.7.

4.3.1.1.2 – Hemimandible reconstruction

Whereas the skull experienced substantial crushing and deformation, the scanned mandible is almost completely intact. The incisor is snapped, and the coronoid process is broken leaving its original shape dorsal to this damage unclear. No extensive reconstruction was required, but I patched the cracks and damaged regions. Since there was no reconstruction from fragments required, the hemimandible is shown below in the form of a line diagram rather than screenshots of the 3D surface, for improved visual clarity. Aside from the damaged incisor, the teeth are well-preserved, and the muscle attachments surfaces are clearly identifiable. Figure 4.8 displays the hemimandible diagrammatically from different orientations.

As alluded to in the Materials and Methods, once the hemimandible surface was translated into the same coordinate system as the skull and the two were aligned, it became clear that the scanned hemimandible is not the original from this organism, as it is too small; even if the incisor was intact, incisor occlusion would dislocate this lower jaw. Comparison with photographs published in previous papers studying MgM-I/81 and I/82 further supports this conclusion. Even lower quality photographs clearly show that the incisor and coronoid process on the original I/82 hemimandible were intact (Kielan-Jaworowska, 1974). However, higher quality photographs published in a later paper reconstructing the musculature of *N. gobiensis* allow for clearer comparisons with the scanned hemimandible (Gambaryan and Kielan-Jaworowska, 1995). At some point prior to 2019 when the

photographs shown in Figure 4.2 were taken, the original hemimandible must have been accidentally switched with the hemimandible that is scanned. Due to the degree of similarity between the two specimens, I believe that the scanned hemimandible is indeed of *N. gobiensis*. On the scan data provided with the CT scan, the specimen is referred to as ZPAL MgM-I/182, but searching their available collections information reveals that this classification

Figure 4.8: Panels showing line diagrams of the scanned hemimandible of *N. gobiensis* in a) lingual, b) labial, c) dorsal, and d) ventral views.

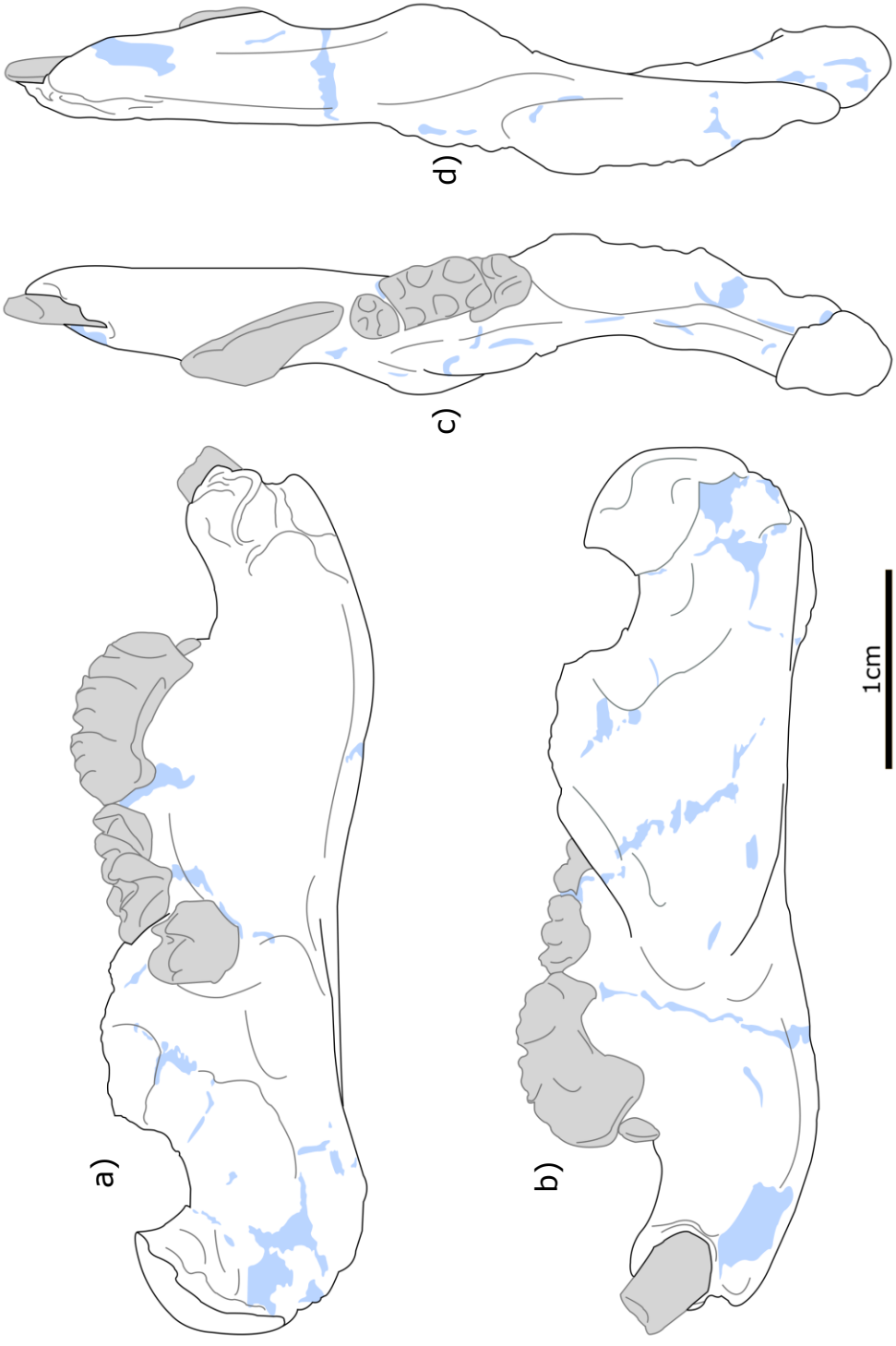

only goes up to I/166, and there is no I/182; this is most likely a typographical error during the scanning, I do not believe that this specimen is I/182, and as of the time of writing, the true specimen number of the scanned hemimandible has not been identified.

Using the scan, the good quality lateral view photograph from the 1995 paper, and the measurements of the specimen provided in the 1974 paper, I rescaled the scanned hemimandible in three dimensions, increasing its size by approximately 15–19%, with the original and rescaled measurements shown in Table 4.2 in the Materials and Methods. Figure 4.9 displays the photograph of the original I/82 published in 1995, the 3D model of the scanned specimen at its original scale (in pastel pink for the bone and lime green for the filled fractures and chipped areas) and the 3D model of the scanned specimen after rescaling (in cyan and orange).

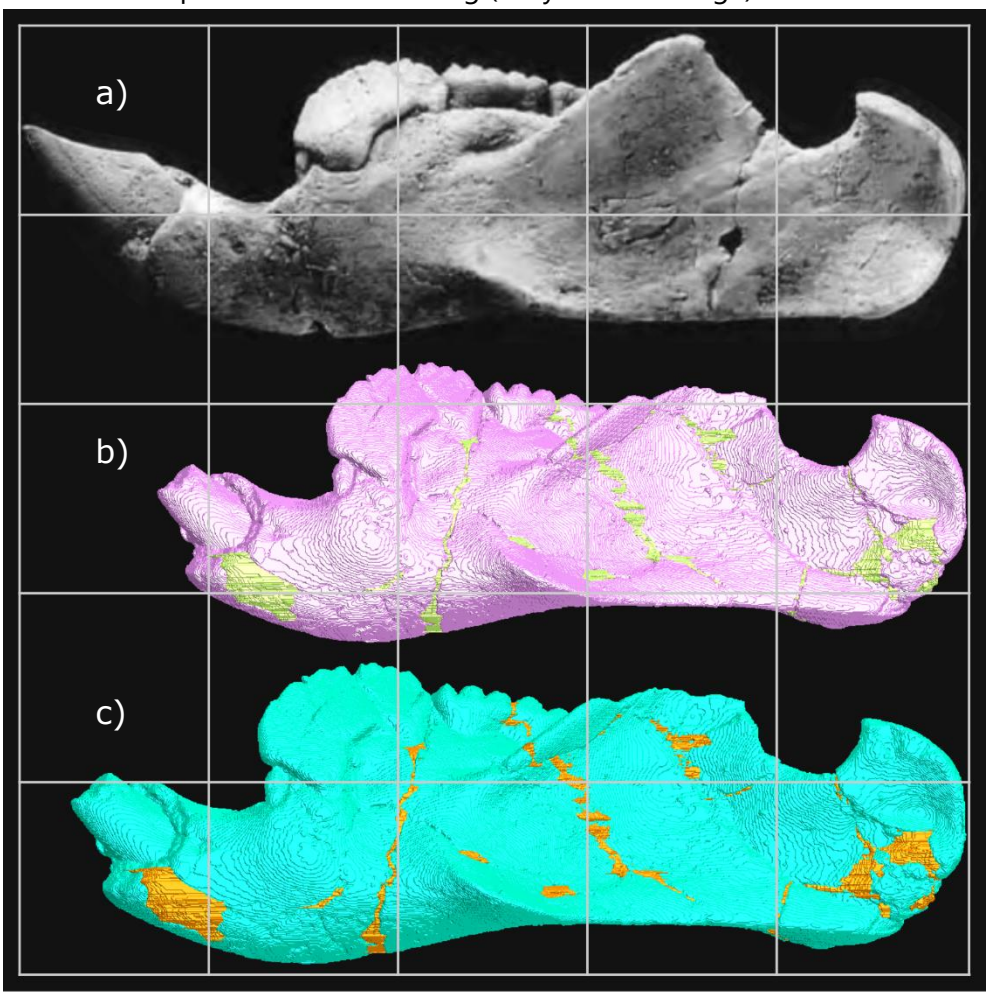

Figure 4.9: Lateral views of a) the original I/82 left hemimandible as photographed in Gambaryan and Kielan-Jaworowska, 1995, b) the scanned left hemimandible of *N. gobiensis* prior to rescaling, and c) the rescaled hemimandible that was mapped. A grey grid helps compare proportions.

Once the mandible had been rescaled by the scale factors estimated using the existing measurements and the lateral photograph, it could be duplicated and positioned at incisor and premolar occlusion.

4.3.1.1.3 – Mandible position during incisor and molar biting

I first aligned the rescaled mandible at molar occlusion, as the orientation of the upper and lower molar tooth rows aided in correct alignment. Since the hemimandible is from a different individual the tooth cusp shapes may differ, but I performed the alignment using the teeth on the scanned specimen rather than estimating from photographs of the original. Then I translated the hemimandible forwards so that the TMJ was articulated in a middle position and the lower fourth premolar was brought into occlusion with the upper premolars; at this occlusion, the cusps of the lower and upper molars did not touch and the hemimandible had to shift posteriorly and open slightly to bring them closer together, but this will likely differ from the original tooth shapes and be an inaccurate interpretation.

Using the photographs of the original hemimandible and lateral views of the reconstructed skull in Avizo, the protraction required to bring the incisor tips together was estimated at 1.294 mm anterior movement and 0.879 mm dorsal movement. Unlike with many rodent taxa, the jaw does not appear to need to open very much to bring the incisor tips into alignment. Rather than translating the hemimandible surface by eye or constructing a 'synthetic' incisor using the limited photographs, I translated the hemimandible by these distances. When mirrored, the two hemimandibles are close enough to be similar to a symphysis along the sagittal midline, and no mediolateral rotation of the hemimandible is required to align them or to align the hemimandible so that the broken incisor tip of the scanned specimen points directly towards the upper incisors, implying that the rotation around the y-axis and the z-axis are sufficiently accurate.

Figure 4.10 displays line diagrams of the two mandible positions, traced over screenshots of lateral views of the specimen in Avizo and

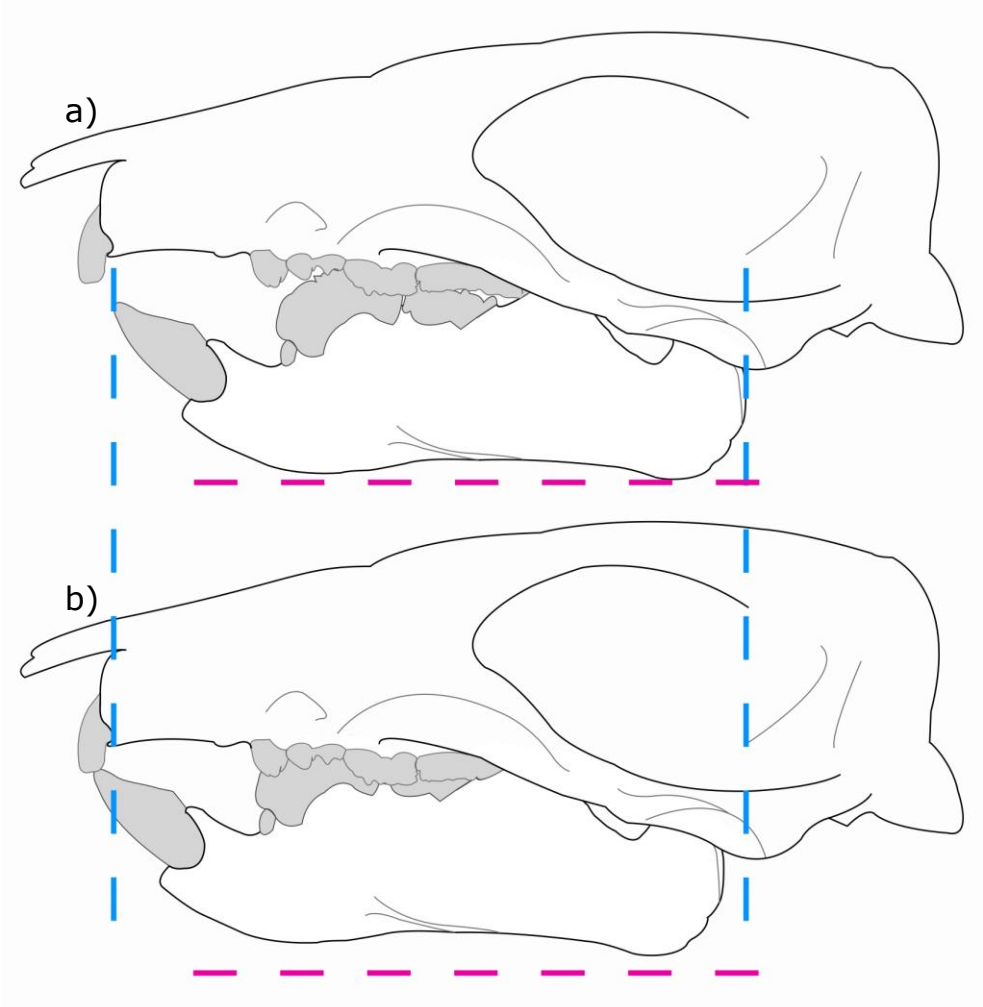

Figure 4.10: Outline diagrams of the reconstructed *N. gobiensis*, with the scanned mandible and original incisor tip. In a) premolar occlusion, and b) incisor occlusion. The dashed blue lines provide a line of reference for the horizontal movement, and the pink lines provide a line of reference for the vertical movement.

simplified for clarity. The incisor tip of the original scanned specimen is placed on this specimen, to aid in visual clarity of the simulated occlusion.

Using the reconstructed, mirrored skull and screenshots of the 3D surfaces in Avizo, and the photographs of the original I/82 left hemimandible, I produced additional diagrams. Figure 4.11 shows the reconstructed head with the mandible in incisor occlusion, and Figure 4.12 shows the mandible where the left fourth premolar is in occlusion with the upper premolars. This diagrammatic hemimandible uses the shape of the rescaled, scanned hemimandible where intact, with the intact incisor and coronoid process 'transplanted' onto the specimen for the illustration. The original specimen's photographs lack a ventral view of the hemimandible, so the incisor is not

replaced in the ventral view in either case, leaving a gap where the intact incisor would proceed further forwards into occlusion in the incisor biting configuration.

At incisor occlusion, the mandible is positioned far forwards in the TMJ, and the cheek teeth are not occluded. The sloping surface of the jaw's upper condylar surface is inclined so that the anterior margin is higher up than the posterior margin, accommodating the dorsal movement of the mandible as it protracts for incisor occlusion.

At premolar occlusion, the lower premolars cannot occlude bilaterally in this reconstruction. With the original specimen, this may hypothetically be achievable if the teeth are shaped or inclined differently than the cheek teeth of the scanned specimen, or if the full mandible is wider relative to the skull. However, based on these teeth and this specimen, the illustrated occlusion is unilateral. Historically, multituberculates have been thought to perform bilateral occlusion of their cheek teeth (Kielan-Jaworowska, Cifelli and Luo, 2004). But if correct, unilateral occlusion during premolar biting would not be strange given the proposed shearing action of these teeth in cimolodont multituberculates, allowing lateral physical pressure to support the shearing (Krause, 1982; Gambaryan and Kielan-Jaworowska, 1995).

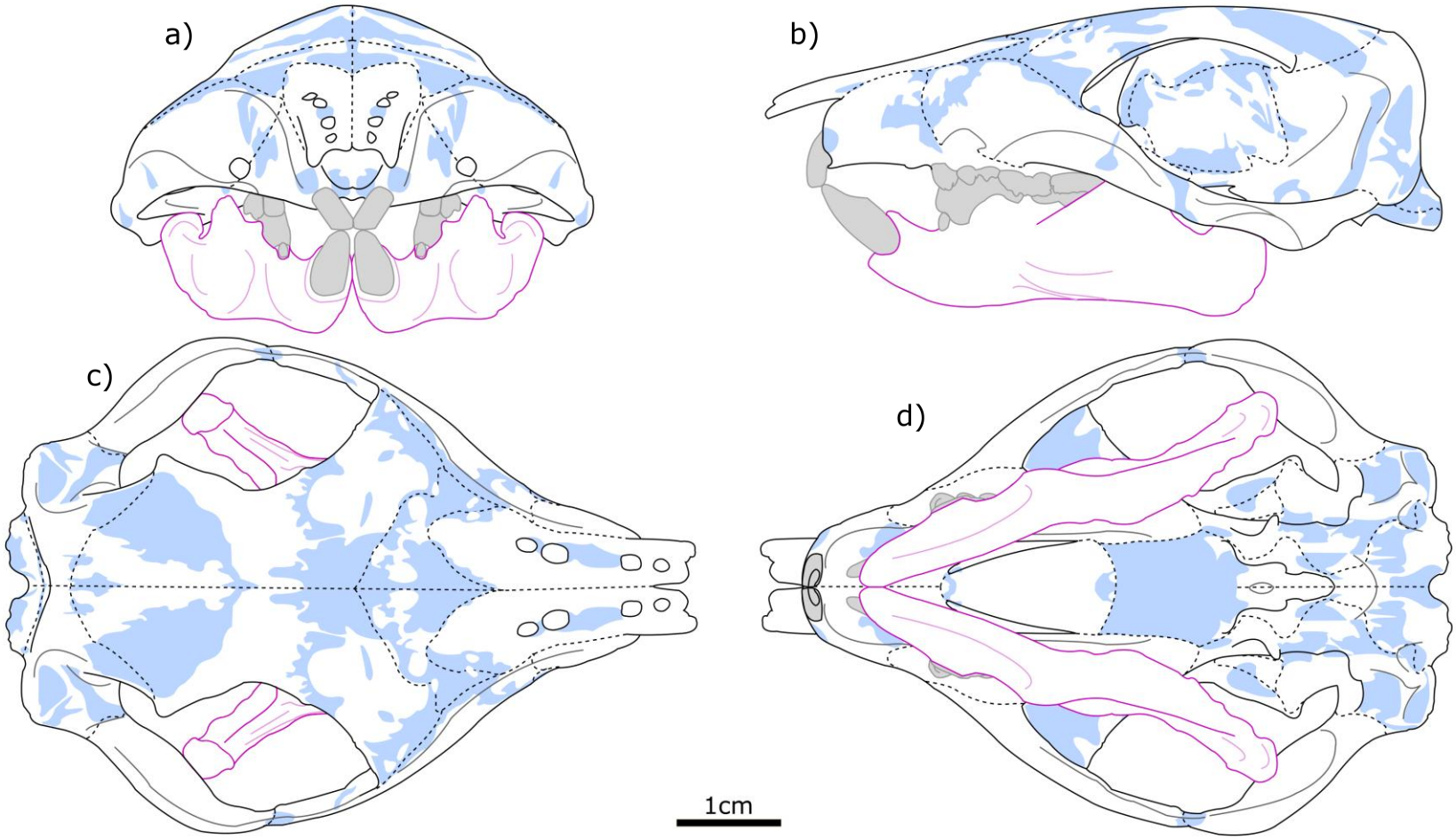

Figure 4.11: Outline diagrams of *N. gobiensis*, at incisor occlusion. The mandible is outlined in pink for clarity. These are shown in a) frontal, b) left lateral, c) dorsal and d) ventral views

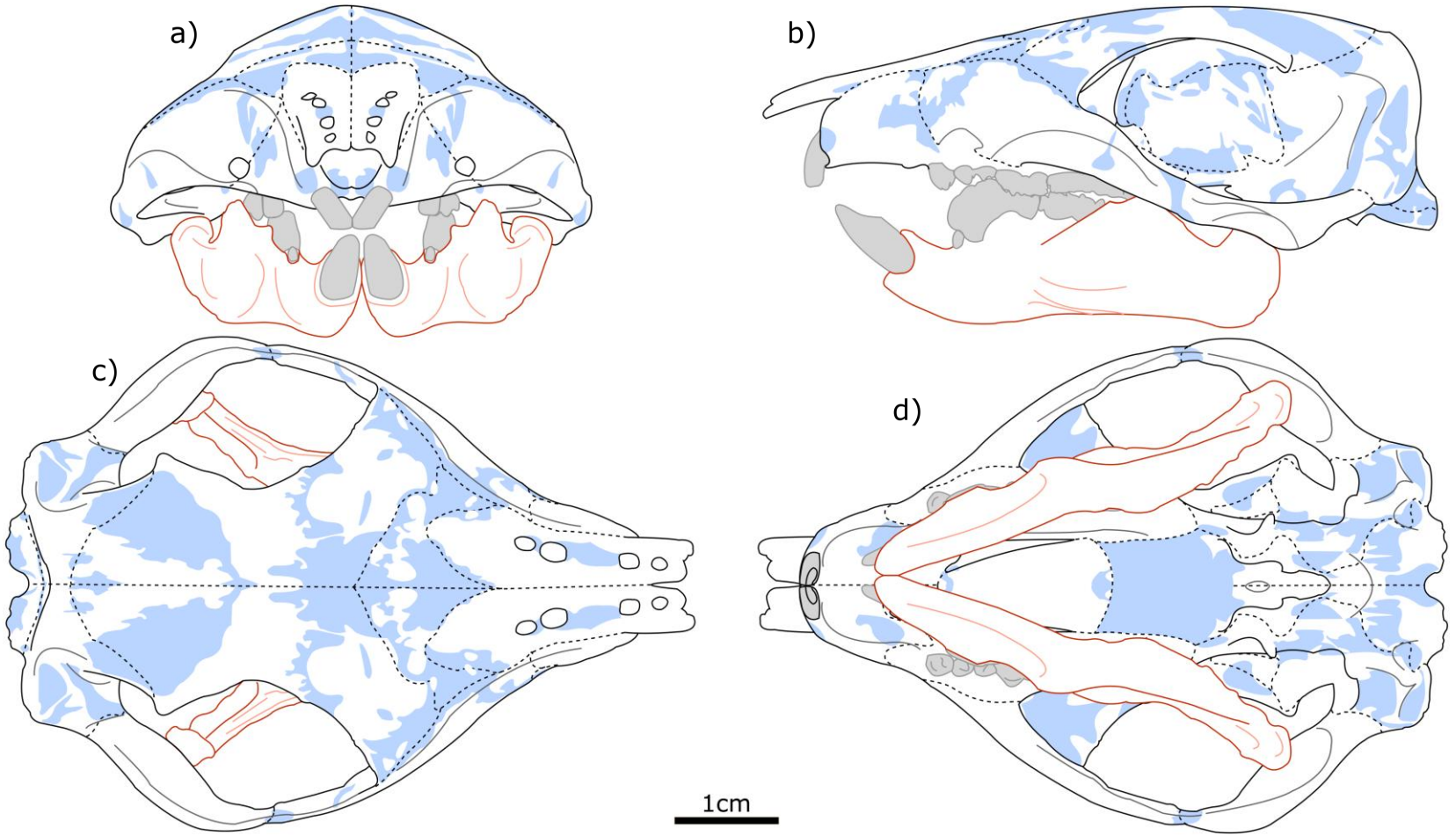

Figure 4.12: Outline diagrams of *N. gobiensis*, with the premolar at occlusion. The mandible is outlined orange for clarity. These are shown in a) frontal, b) left lateral, c) dorsal and d) ventral views.

4.3.1.1.4 – Muscle attachments

I identified and mapped the muscle attachments on the 3D surfaces. I identified and recorded the centroid coordinates in Blender as in the rodent taxa, for use in the lever-arm mechanics calculations, and I named the identified muscles in accordance with the rodent specimens. There are several muscles proposed based on older analyses of *N. gobiensis* (Kielan-Jaworowska, 1974; Gambaryan and Kielan-Jaworowska, 1995) that I could not identify, and left absent due to the lack of support for their potential presence. Of particular note when comparing with the rodent sample, an origin surface of a muscle homologous to the **Superficial Masseter (SM)**, a major subdivision of the masseter in rodents, was not identifiable on this skull; all other major rodent subdivisions have seemingly homologous muscle subdivisions that are clear and well-defined on this skull, though the origin of the **IOZM** is the least clear.

Figure 4.13 displays diagrams of the identified muscle attachment surfaces on the mirrored, reconstructed skull of *N. gobiensis*. Some sections of bone are treated as translucent to allow attachments to be visualised when partially or fully obscured from a certain view. Figure 4.14 is a similar diagram of the scanned hemimandible with the mapped muscle attachment surfaces displayed in colour. This is the rescaled hemimandible, without the outlines of the original specimen's incisor and coronoid process. Due to the damage of this specimen, the insertion of the **Temporalis (T)** cannot be identified in full on the damaged coronoid process. It was mapped on the intact bone surface, and the shape shown on this diagram is based on the intact surface; in the original specimen, this attachment surface will likely extend further dorsally on the coronoid process. Rather than discussing Figures 4.13 and 4.14 individually, they will be discussed together on a muscle-by-muscle basis, identified on the reconstructed right side of the head in isolation.

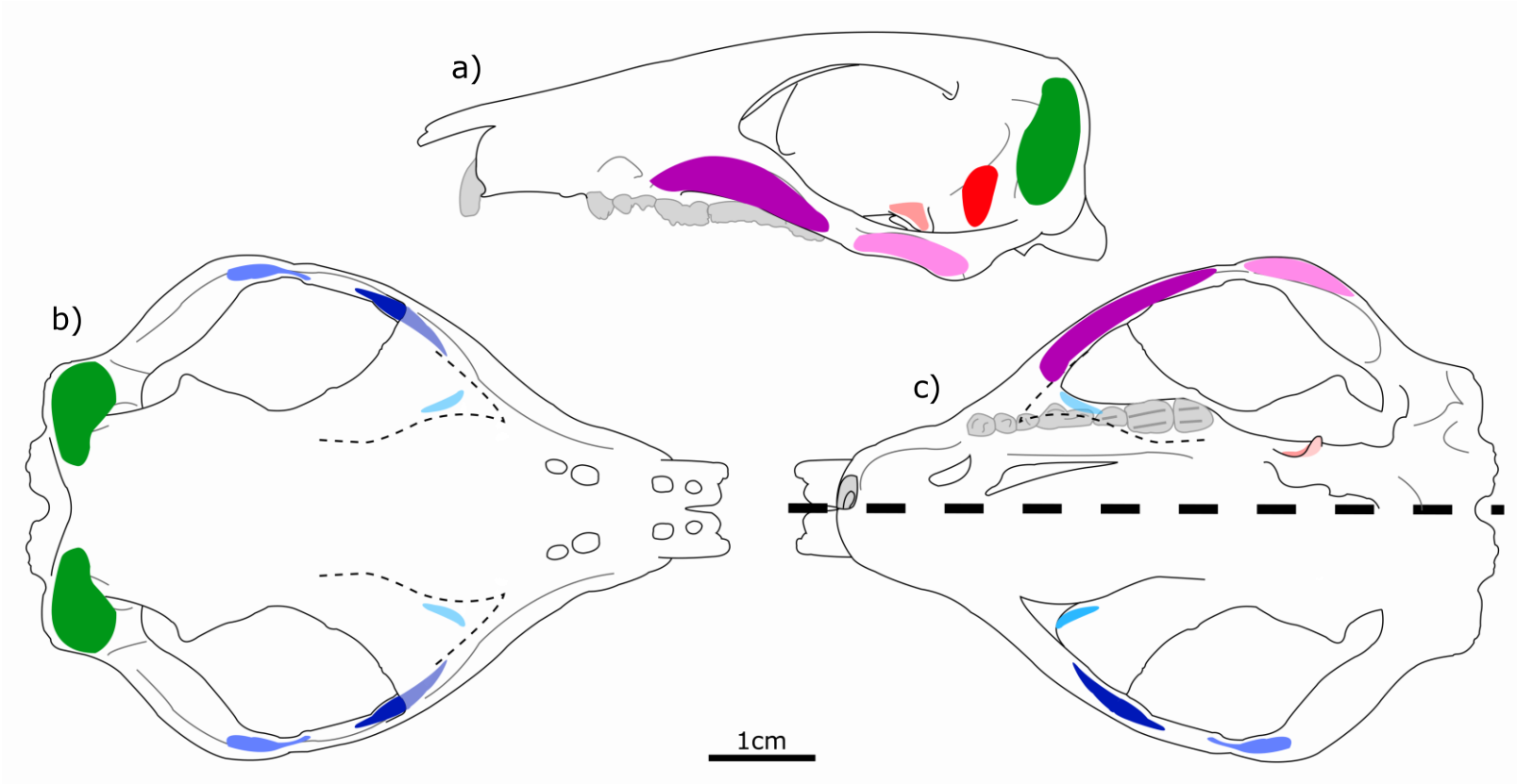

Figure 4.13: Diagrams of the muscle attachment surfaces in *N. gobiensis*. Thin dashed lines show the shape of the ventral anterior zygomatic root and maxilla. In ventral view, a thick black dashed line divides the diagram: on one side of the line, the deep masseter subdivision origins and internal pterygoid are shown, on the other, the ventral skull is blanked out and the ZM subdivision origins are shown. The specimen is shown in a) left lateral, b) dorsal and

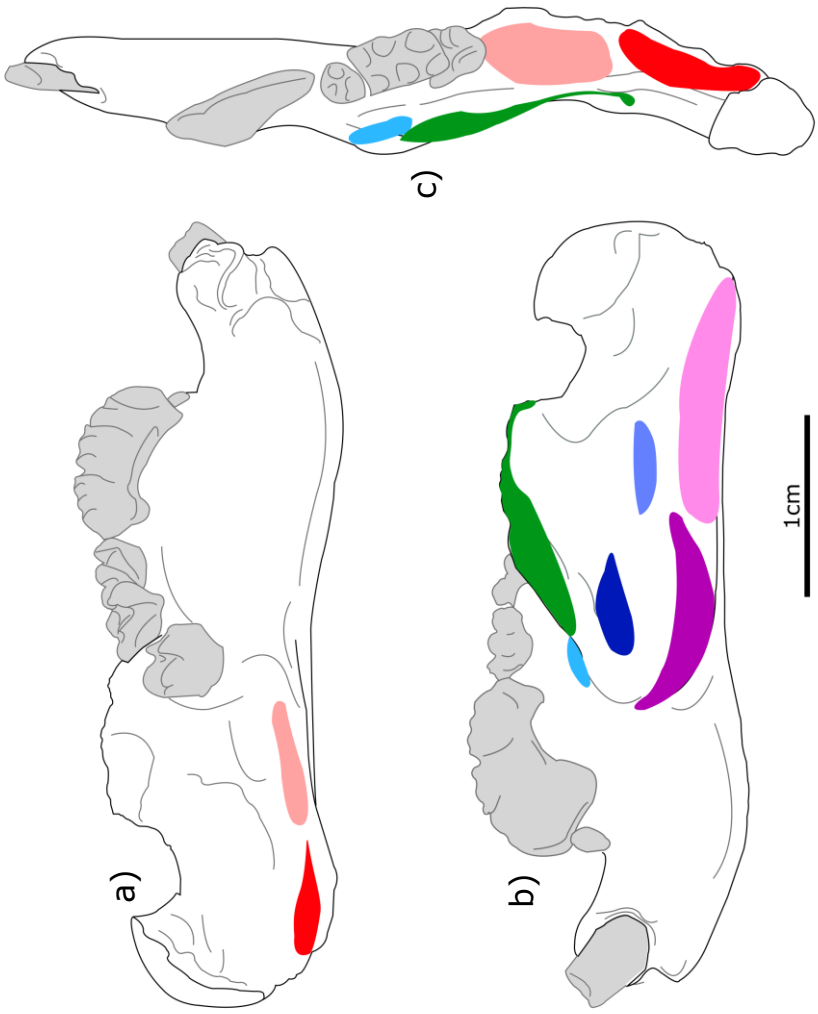

Figure 4.14: Outline diagrams of the scanned *N. gobiensis* hemimandible with proposed muscle attachment surfaces coloured in accordance with the main text. The hemimandible is shown in a) lingual, b) labial and c) dorsal views.

On the lateral zygomatic arch, there are two curved fossae clearly bordered by a prominent crest along their dorsal margins. There is no zygomatic plate as in myomorphs or sciuromorphs, but with the shape of the upper cheek teeth and the tooth row's extension anteriorly to the dorsal zygomatic root, there was no identifiable attachment site for a potential **SM** as in rodents. Of the two lateral muscle attachments surfaces, the anterior origin is larger and extends along the lateral and ventral surface almost to where the anterior zygomatic root attaches to the rostrum. As this is a muscle attachment surface on the ventrolateral face of the anterior maxillary zygomatic arch, I propose this to be homologous with the rodent **ADM** and will use the same name. On the scanned hemimandible, the body of the mandible flares out labially along the ventral margin of the mandibular angle, and attachments sites are identifiable by changes in topography along its lateral face. Along this area, two proposed fossae are separated by a narrow

region with an inclined shift in surface shape. The anterior of the two is a fossa that curves along posterior to the masseteric ridge and then seemingly curves dorsally along the aforementioned change in topography; since this is an attachment surface close to the masseteric ridge on the lateral face of the mandibular angle, I identify this as the insertion of the **ADM**.

The two muscle attachments surfaces posterior to the identified **ADM** attachments are referred to here as the **PDM**. The **PDM** origin is smaller than the **ADM** origin with a less defined crest along its upper margin, and extends along the ventrolateral side of the zygomatic arch across the suture between the maxilla and the squamosal, terminating posteriorly above the jaw joint's surface on the squamosal. The **PDM** insertion is posterior to the **ADM** insertion and separated by the region where the shape of the surface changes, and extends along the posterior extent of the ventral margin of the mandibular angle. It terminates dorsally and posteriorly along a sharp change in shape as the mandible begins to bend up towards the condylar process. Unlike rodents, there is no defined angular process separate from the condylar process.

On the medial surfaces of the zygomatic arch—which are inclined so that they face slightly dorsally—there are two apparent fossae bordered by changes in surface shape. One occurs anteriorly to and is larger than the other. The anterior fossa has a curved upper boundary, and seemingly extends down to the ventral margin of the zygomatic arch. In this specimen, this passes across the region where the zygomatic arch is fractured and glued, obscuring part of the attachment. Its anterior margin appears to terminate roughly in line with the back of the upper fourth premolar (P4), and its posterior margin terminates roughly level with the back of the upper first molar (M1). As this is a muscle attachment on the medial surface of the maxillary zygomatic arch, anterior to a smaller attachment surface, I identify it here as the **AZM**. On the hemimandible, in the masseteric region, there is a notable change in the shape and curvature of the lateral bone surface below the anterior end of the root of the coronoid process. This is long and relatively narrow, and inclined almost horizontally. Since it is a muscle

attachment site on the masseteric region, ventral to the coronoid process, and almost directly below the **AZM** origin when the jaw is articulated and the teeth are occluded, I identified it as the **AZM** insertion.

As was the case for the **ADM** and **PDM**, attachment surfaces are observable posterior to the **AZM** origin and insertion. On the skull, there is a muscle attachment on the medial surface of the maxillary zygomatic arch, extending posteriorly almost to the suture between the maxilla and squamosal. It terminates anteriorly behind the origin of the **AZM**, and extends from the dorsal margin of the zygomatic to its ventral margin in this area. I identify this as the **PZM** origin. On the masseteric region of the mandible's lateral face, posterior and ventral to the **AZM** insertion with an apparent gap between them, there is a thin near-horizontal change in topography on the bone surface smaller than the proposed **AZM** insertion. Due to its placement relative to the **AZM** insertion, the tip of the coronoid process, and the **PZM** origin, I identified it as the **PZM** insertion.

I propose an **IOZM** is present in this organism, but the limited preservation makes mapping the margins of the origin difficult. Below the lacrimal and medial to the anterior zygomatic root, there is a deep 'pocket' above the small infraorbital foramen where the maxilla meets the anterior extent of the frontal; in existing papers, this is referred to as the "orbital pocket" (Kielan-Jaworowska, 1974; Kielan-Jaworowska, Cifelli and Luo, 2004). Within this pocket, medial to the zygomatic root and ventral to the lacrimal bone, there is an observable change in topography along what appears to be the suture between the maxilla and frontal. When the jaw is articulated at incisor occlusion, this occurs almost directly above a clear fossa medial to the anterior tip of the root of the coronoid process and medial to the lower first molar (m1). By comparing these two and examining the orbital process, I identified an origin as well as I could with the preservation in the area, though this is the least certain of all the muscle attachments on this specimen in terms of accuracy due to the ambiguous margins of the proposed attachment surface. As this originates dorsal to the infraorbital foramen and posterior to the anterior zygomatic root's attachment to the skull, and inserts

medially to the coronoid process and anterodorsal to the **AZM** insertion, I here propose it to be homologous to the **IOZM**. In most rodents that possess it, this muscle extends through an expanded (relative to sciuromorphs which lack this muscle subdivision) infraorbital foramen, but in two studied rodent taxa it occurs posterodorsal to the infraorbital foramen, according to Chapter 2's muscle mapping of rodents. The taxa in question are *B. suillus* and *G. capensis*, which lack the expanded infraorbital foramen seen in other rodents that possess this muscle subdivision. As a result, the proposed position for this muscle's origin in this reconstruction and the older one (Gambaryan and Kielan-Jaworowska, 1995) is not unprecedented within the context of rodents, at least in Bathyergidae (Cox, Faulkes and Bennett, 2020).

Along the posterior margin of the dorsal cranium, there is a large, prominent fossa anterior to the lambdoidal crest; this extends across the parietal bone and outwards toward the squamosal, posterior relative to the level of the TMJ surface on the squamosal, and apparently terminates lateral to the sagittal midline. Its lateral extent terminates medial to the posterior zygomatic root. Due to its position along the dorsal cranium and margin clearly marked by the lambdoidal crest, I identified this as the **Temporalis (T)**. The anterodorsal surface of the coronoid process is well preserved up until the broken edge, and an apparent muscle attachment surface is clear on the intact surfaces. I mapped the insertion in the preserved region under the assumption that this attachment surface would continue up towards the tip to the coronoid process rather than terminating arbitrarily where the tip was snapped off.

On what is likely the alisphenoid, there is a large, roughly triangular region bordered by sharp changes in the angle of the bone surface, terminating around the ventral margin of the alisphenoid and approximately level to the TMJ surface. Due to its placement anteroventral to the **T**, medial to the TMJ, and posterior to the pterygoid bone, I propose this apparent muscle attachment surface to be the origin of the **External Pterygoid (EP)**. On the lingual face of the mandibular angle, a prominent shelf extends medially where the mandible inflects substantially, which has been referred

to previously as the 'pterygoideus shelf' (Gambaryan and Kielan-Jaworowska, 1995; Kielan-Jaworowska, Cifelli and Luo, 2004). On this shelf's dorsal surface, there are two large, prominent fossae separated by a thin area where the surface shape changes. Of the two, the posterior attachment occurs ventral to the condyle, extending from the posterior margin of the angle to around level with the anterior extent of the mandibular notch, posterior to the coronoid process. This is here proposed to be the attachment surface of the **EP**, but if one were to identify a potential origin of the **SM** in this taxon, this might be interpreted as the insertion of that muscle as its placement is similar in rodents. Either way this contrasts with the existing reconstruction's placement of the **EP** insertion (Gambaryan and Kielan-Jaworowska, 1995).

Anterior to this **EP** insertion is a wider but otherwise similarly large fossa that extends anteriorly ventral to the coronoid process and terminates where the pterygoideus shelf terminates and curves up towards the root of the lower second molar (m2). Due to its position, I propose this to be the insertion of the **Internal Pterygoid (IP)**. On the ventral skull, the pterygoid plate curves laterally outwards towards its tip, and is well preserved. Its lateral face possesses a clear and well-defined fossa on the pterygoid plate, ventral to the sharp ridge on the lateral face of the pterygoid bone. As this is a muscle origin on the pterygoid plate, I identified this as the origin of the **IP**.

None of the additional muscle attachments proposed in existing literature based on photography and the fossil, and not discussed in these results, were identified in this analysis (Gambaryan and Kielan-Jaworowska, 1995). This will be explored in detail in the Discussion of this chapter.

Figure 4.15 displays the configuration of these identified muscles in lateral view, similarly to the diagrams of the rodent taxa in Chapter 2. The deep masseter muscles (**ADM** and **PDM**) and ZM complex (**IOZM**, **AZM**, and **PZM**) can be observed to be inclined steeply in their lines of action. The **T** is long and shallowly inclined due to the length of the head and mandible posterior to the coronoid process, and the pterygoid muscles are steeply

inclined, with the **EP** having to curve slightly due to the shape of the alisphenoid.

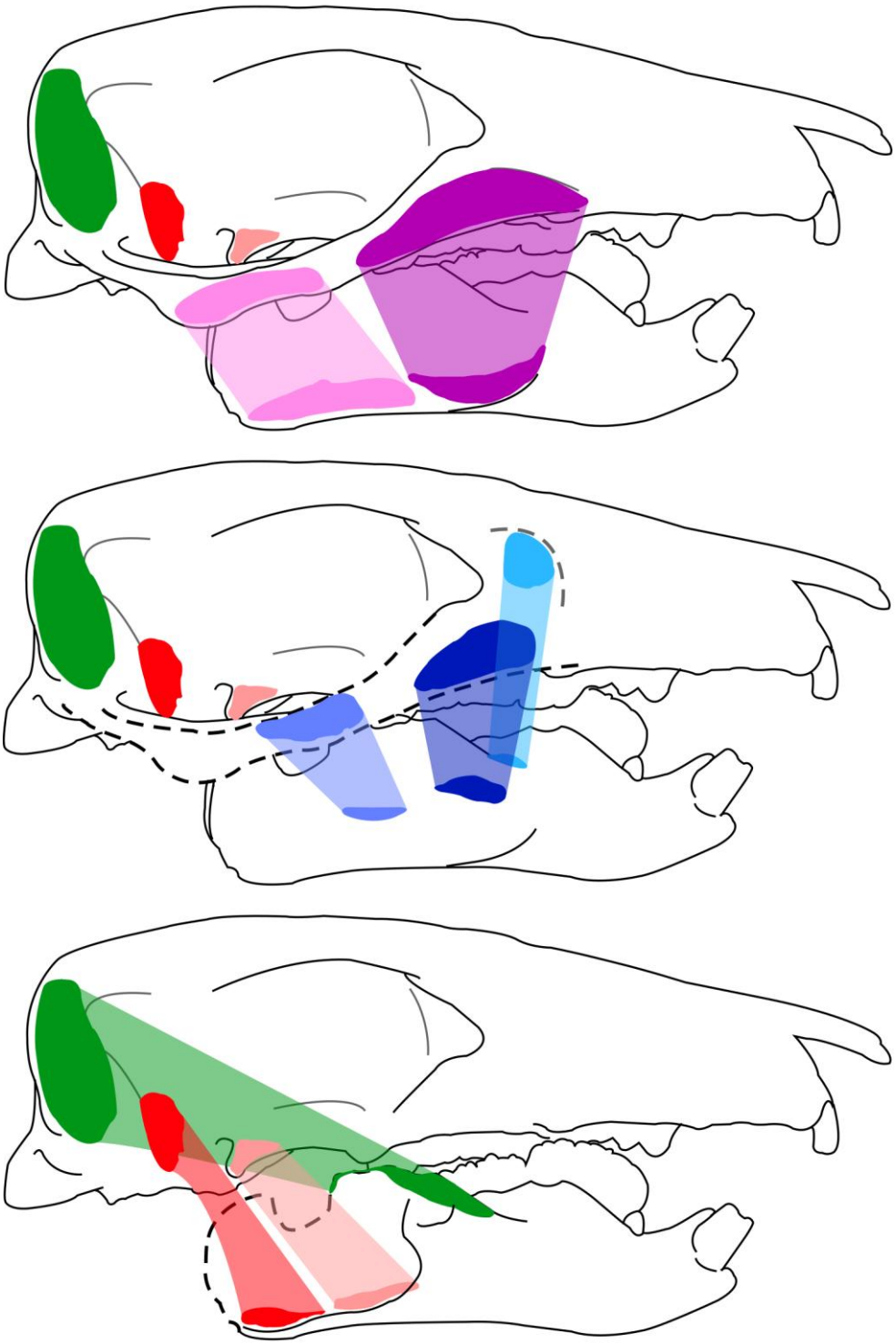

Figure 4.15: Simplified lateral view diagrams showing the origins and insertions of each of the identified jaw-closing muscle subdivisions. Translucent shapes connect the origins and insertions to illustrate the rough position of the muscles. These progress from superficial muscles to deep muscles, with dashed lines indicating that the attachments are on the medial surface of a bone.

4.3.1.2 – Chulsanbaatar vulgaris

Figure 4.16 shows the initial rough segmentation of the scanned skull of *C. vulgaris*. As can be observed, the left side of the head is displaced posteriorly along the midline due to brittle deformation, and the dorsal cranium is extensively replaced, giving it a rough and poorly-defined surface. The basicranial region, however, is much better preserved than in *N. gobiensis*, though this region is not of particular interest to this study outside the pterygoid plates. The incisors are partly replaced and packed around with matrix material that obscures their shape, but the cheek teeth have clean cusps. The orbital pocket is also packed with matrix material, obscuring potential muscle attachment surfaces. I removed the damaged left side of the skull, and mirrored the intact right side of the skull to create a full skull. I duplicated and articulated the scanned hemimandible in molar and incisor occlusion, and mirrored it at the symphysis to approximate a full head. I aligned this relative to the global axes, and mapped the skull's muscle attachments unilaterally on the right side.

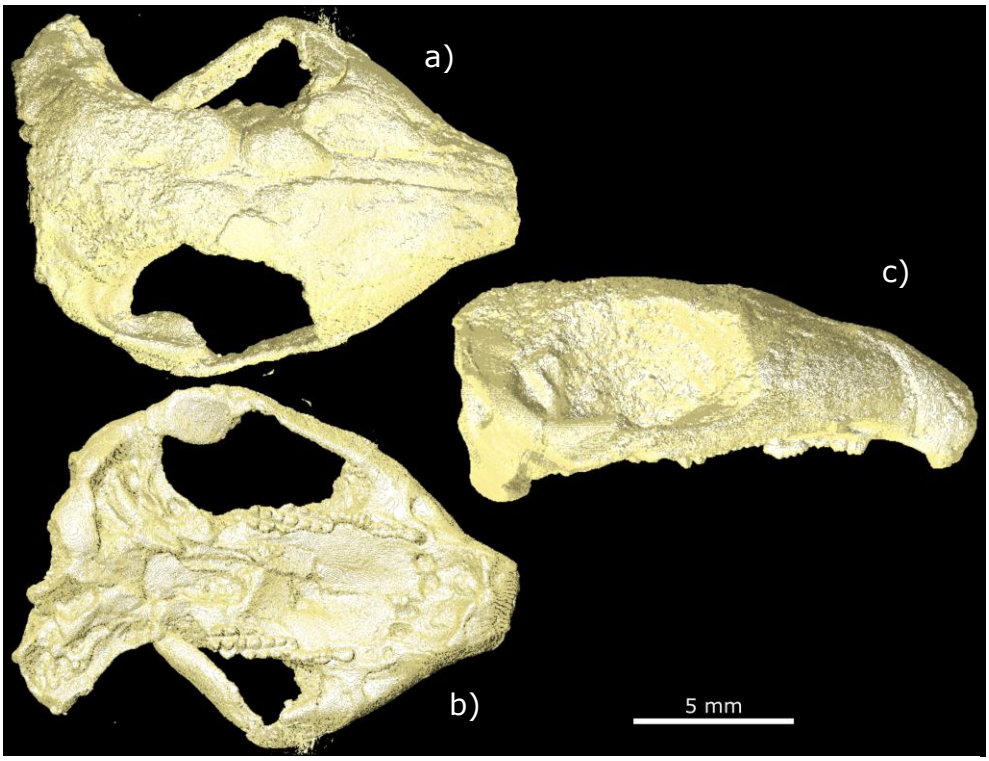

Figure 4.16: Dorsal (a), ventral (b), and lateral (c) views of the rough segmentation of the scanned skull of *C. vulgaris*.

Figure 4.17 shows the scanned hemimandible. The teeth are all intact and well-preserved, as is the condylar process. Unfortunately, as can be observed, the coronoid process is broken, with an uncertain portion of its upper region missing in this specimen. In shape and structure, it is broadly similar to the hemimandible of *N. gobiensis*, but the plagiaulacoid p4 is proportionally smaller. Aside from the damage to the coronoid process, the attachment surfaces of all studied muscles are preserved. As the hemimandible scan was conducted at a much smaller voxel size, after being imported into the skull's coordinate space in Avizo, I had to rescale the surface using measurements taken of the skull and hemimandible in 2019 for this project in order to articulate it. This resulted in a rescaled hemimandible length of 10.07 mm, 0.055 mm longer than the physical measurement taken on the specimen, which I believe is an acceptable degree of error given the innate imperfection of human-conducted measurements and photographs.

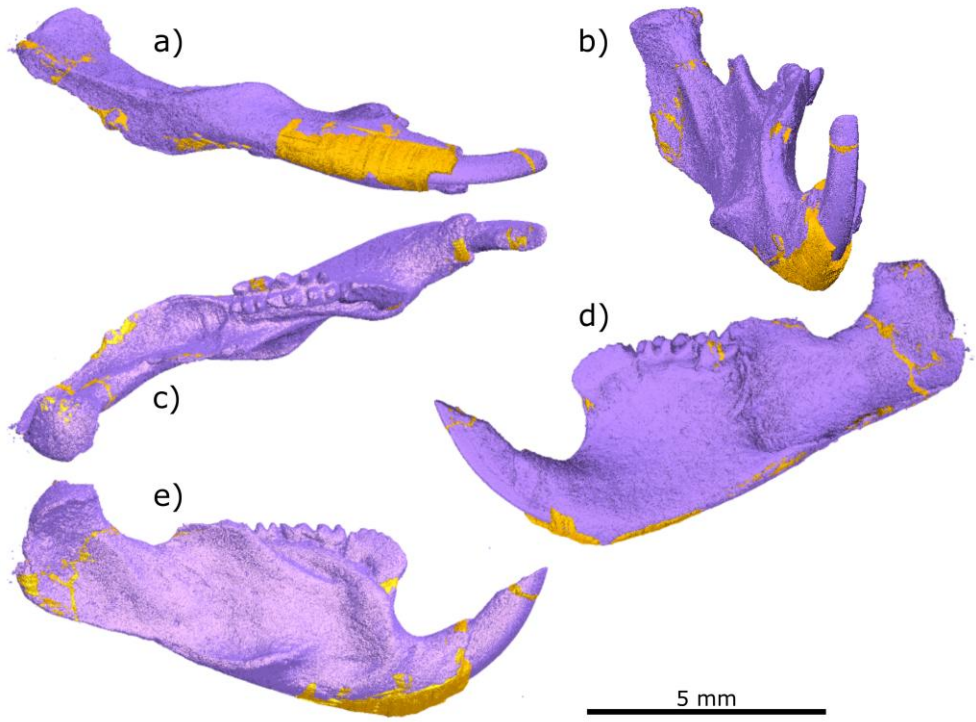

Figure 4.17: Ventral (a), frontal (b), dorsal (c), lingual (d) and labial (e) views of the segmented hemimandible of *C. vulgaris*. The bone and teeth are in purple, and the patches made for damaged, fractured, or missing sections are orange.

As for *N. gobiensis*, I produced simplified line diagrams of the skull (Figure 4.18) and hemimandible (Figure 4.19), and the skull with the mandible in incisor (Figure 4.20) and premolar (Figure 4.21) occlusion.

I was able to identify the same muscles in *C. vulgaris* as in *N. gobiensis*, with similar anatomical positions although their margins are less strongly defined. The muscle attachment surfaces are shown on the skull and hemimandible in simplified line diagrams in Figures 4.22 and 4.23. The surface replacement makes some difficult to see (especially the origin of the

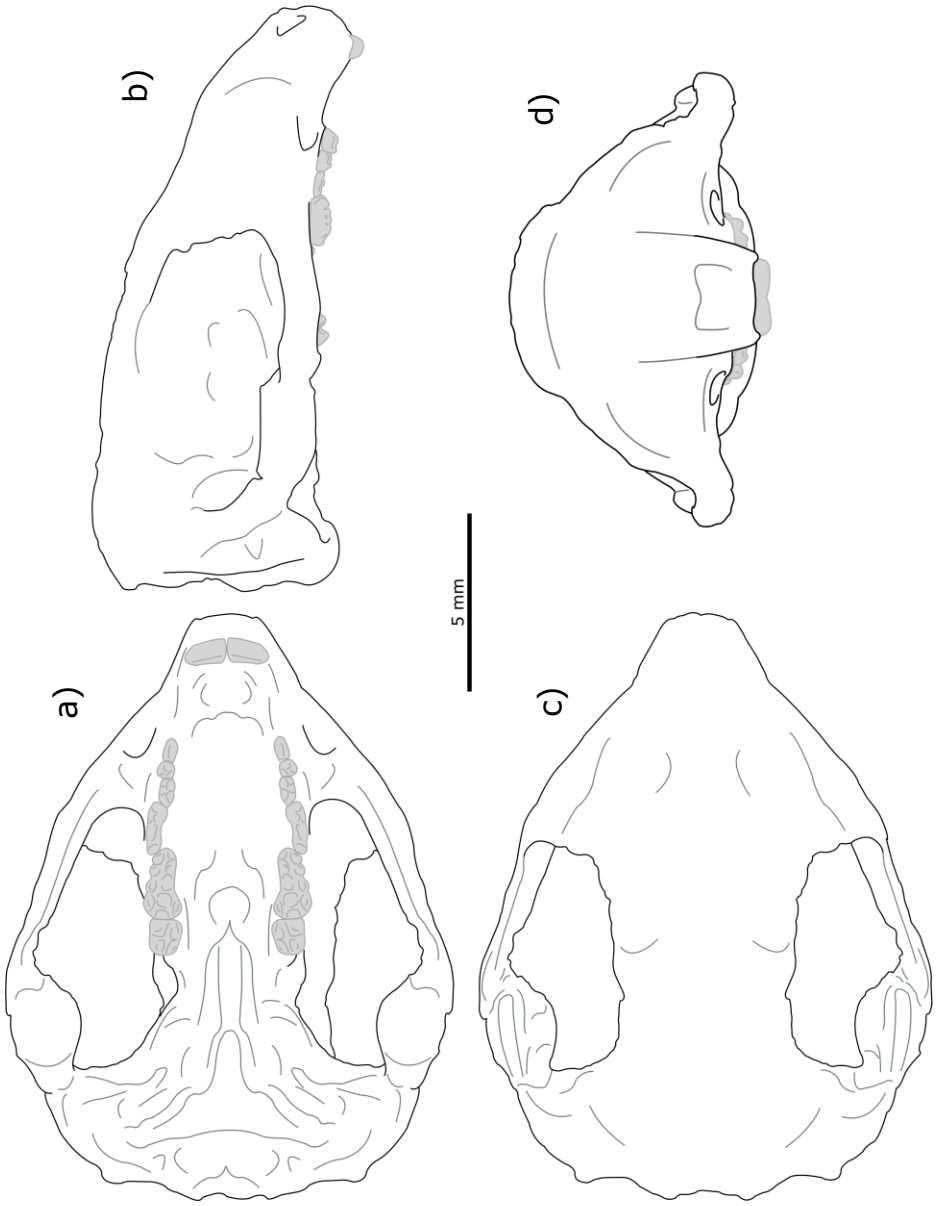

Figure 4.18: Simplified line diagrams of the mirrored right side of the head of *C. vulgaris*, shown in: a) ventral view, b) lateral view, c) dorsal view, and d) frontal view.

IOZM, and to a lesser degree, the PZM). On the ventral surface of the anterior zygomatic root, there is a small flat-ish region anterior to where I identified the ADM. This occurs lateral to the second and third upper premolars (P2

and P3), around the teeth's width away on the zygomatic root, but is small and ambiguous; I did not consider it to be an origin for a **SM**, and I consider that muscle absent in *C. vulgaris* as in both other multituberculate taxa studied. Most origin attachment surfaces (with the uncertain exception of **T**) seem proportionally smaller on the skull than they were on *N. gobiensis*, as can be seen in Figure 4.22. The **ADM** and **PDM** originate from two fossae with curved upper margins on the lateral face of the zygomatic arch with the **PDM** spreading across the maxilla-squamosal suture; the **IOZM** (present

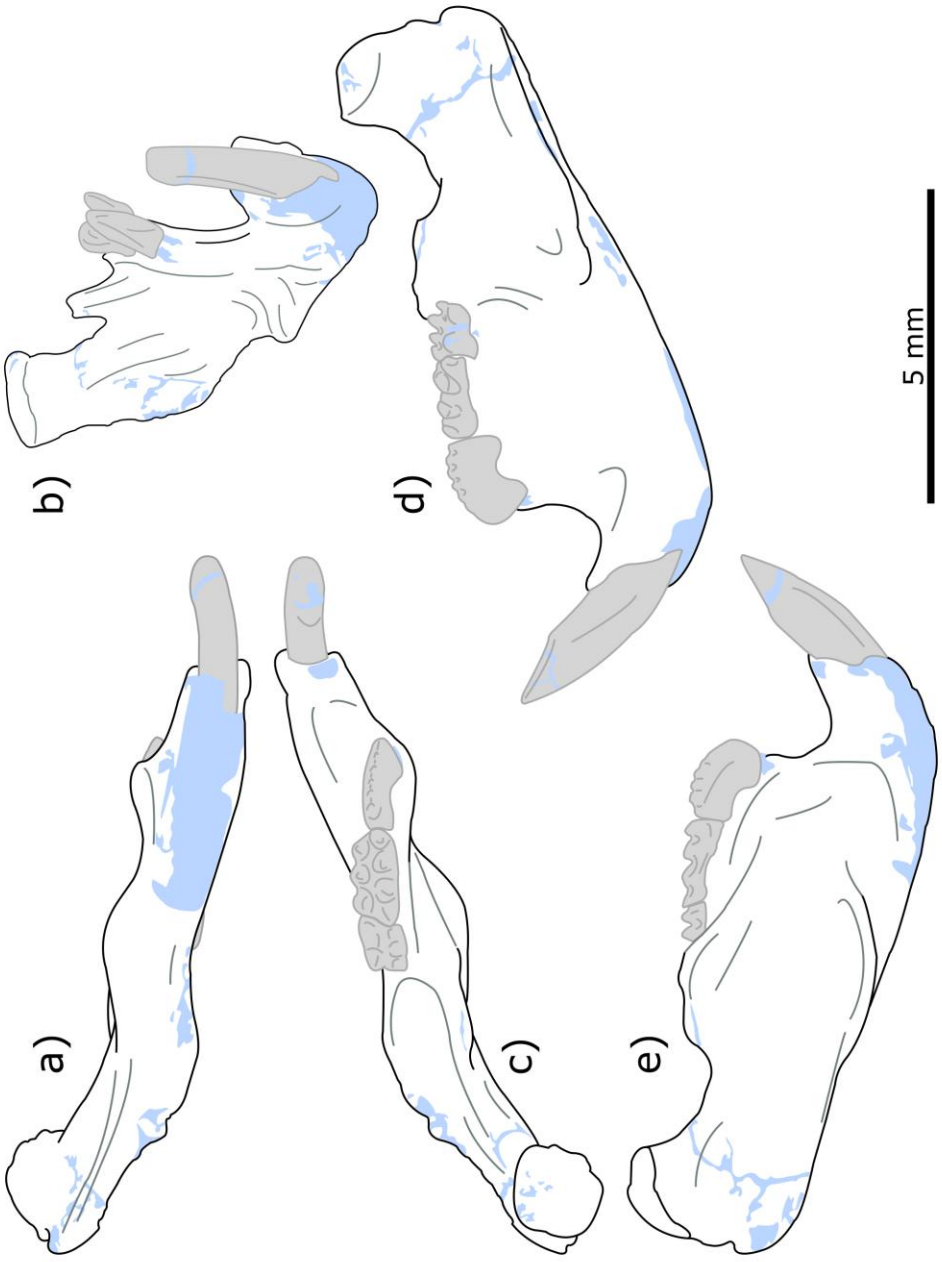

Figure 4.19: Simplified line diagrams of the right hemimandible of *C. vulgaris*, shown in: a) ventral view, b) frontal view, c) dorsal view, d) lingual view, and e) labial view. Pale blue represents damaged areas that are patched.

based on the trench-like attachment surface medial to the anterior region of the root of the coronoid process) was mapped on the matrix material partially filling the orbital pocket since the bone surfaces are completely lost in this region (again making it the most uncertain origin surface); the **AZM** and **PZM** originate from a pair of fossae on the medial surface of the zygomatic arch, on the maxilla; the **T** originates from a fossa on the posterior dorsal cranium, anterior to the lambdoidal crest, and the damage to the skull surface makes the margins identified uncertain; the **EP** originates on from a roughly-triangular fossa on what may be the alisphenoid; and the **IP** originates on the

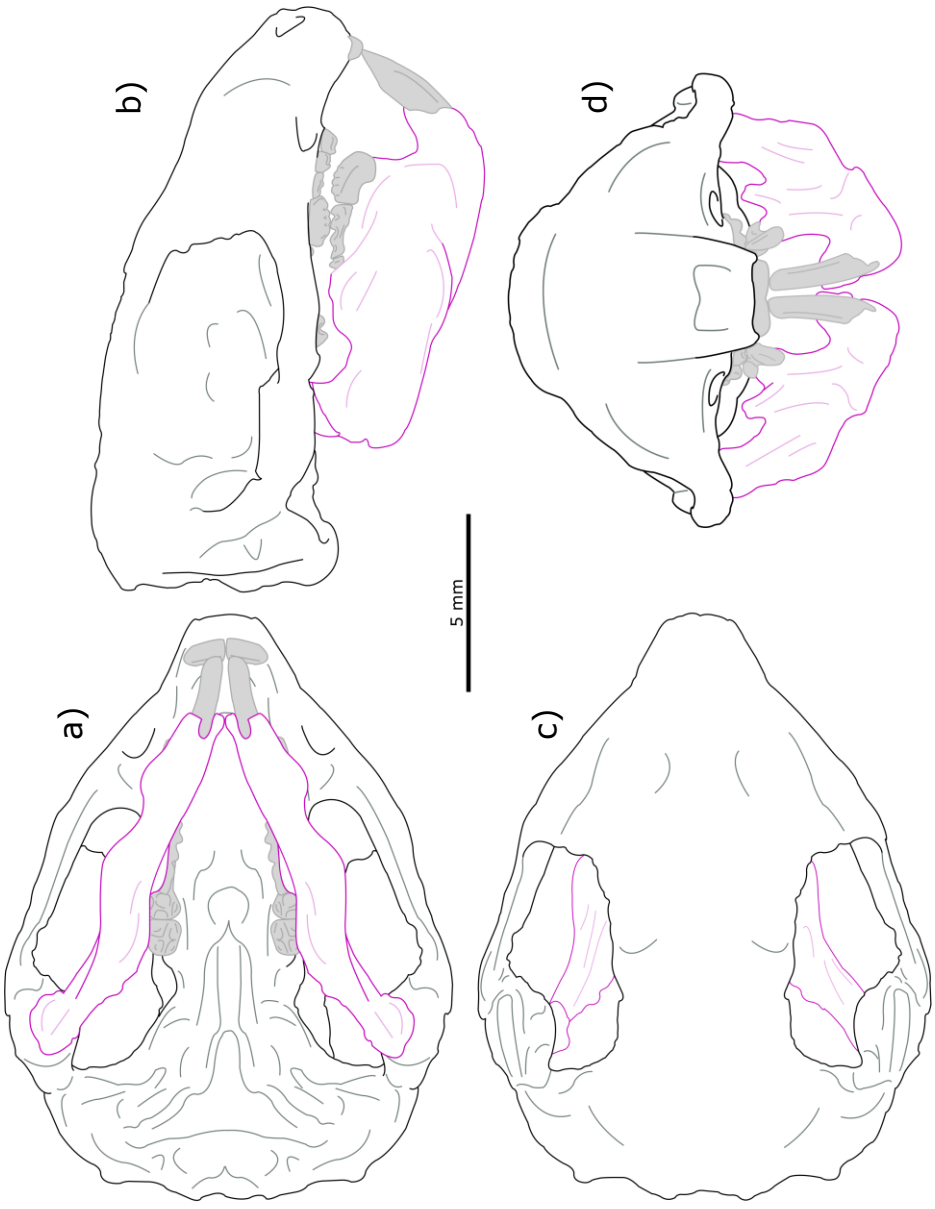

Figure 4.20: Simplified line diagrams of the mirrored skull and mandible of *C. vulgaris* in incisor occlusion shown in: a) ventral view, b) lateral view, c) dorsal view, and d) frontal view.

lateral face of the pterygoid plate. The pterygoid plate of *C. vulgaris* is less prominent and isolated than in *N. gobiensis*, and is connected with the skull at its posterior end.

The insertions of the muscles are also similar to *N. gobiensis*. The **ADM** and **PDM** insert along the ventral margin of the mandibular angle's

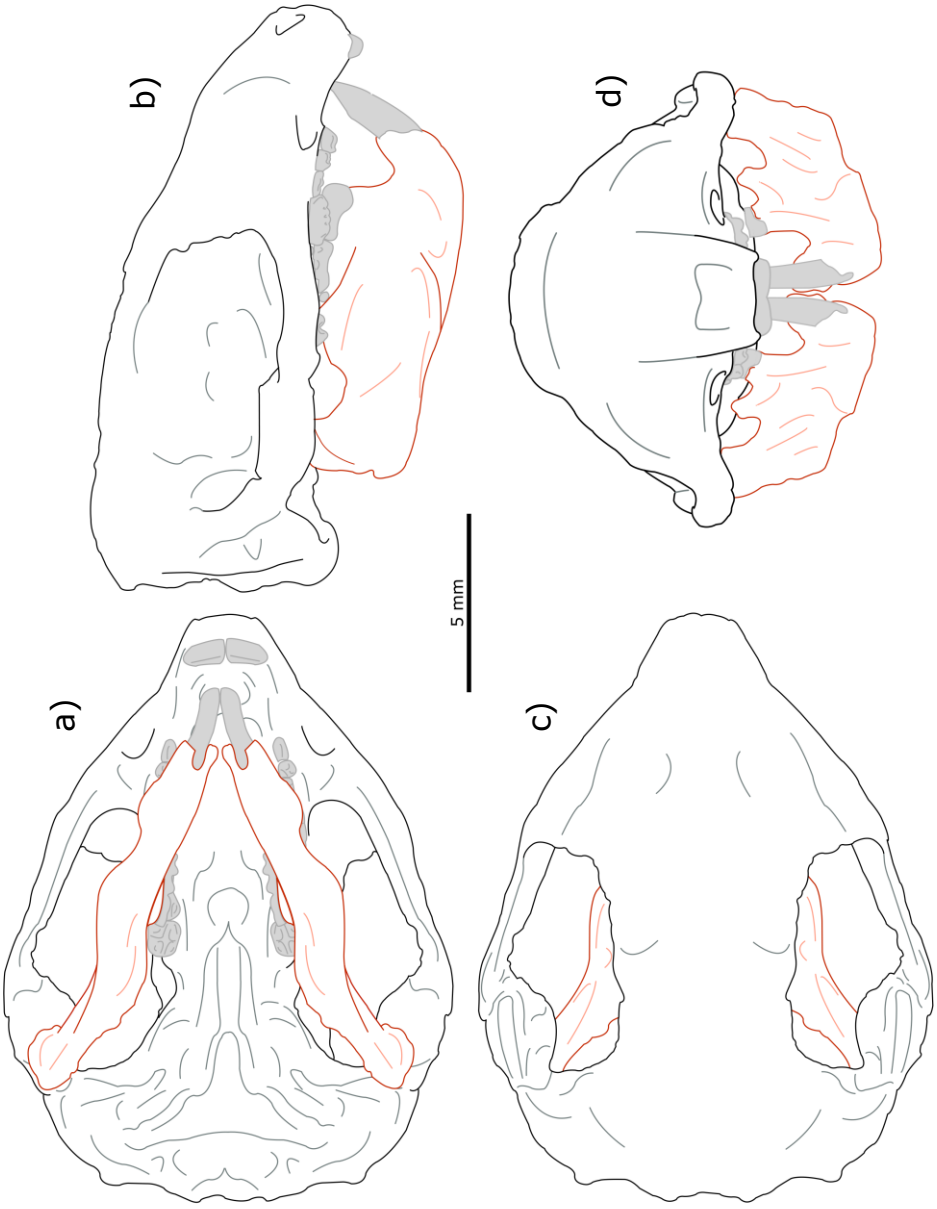

Figure 4.21: Simplified line diagrams of the mirrored skull and mandible of *C. vulgaris* in premolar occlusion shown in: a) ventral view, b) lateral view, c) dorsal view, and d) frontal view. Note that this occlusion is unilateral, occurring on the right side.

lateral face, with the former posterior to the masseteric ridge and the latter fossa separated from the former by a narrow change in surface shape; the **IOZM** inserts in a troughlike fossa medial to the coronoid process and lateral

to the cheek teeth, adjacent to m1; the **AZM** and **PZM** insert in two narrow, small fossae on the lateral face of the mandible, in the masseteric region, with the **AZM** inserting ventral to the root of the coronoid process and the **PZM** inserting posteroventral to the **AZM**; the **T** inserts on the dorsal coronoid process, but the severity of the damage causes only the ventral extent of the attachment to be identifiable (as in *N. gobiensis*, it was mapped up to the broken edge of the coronoid process); the **EP** inserts in a large fossa in the posterior region of the pterygoideus shelf, ventral to the condylar process; and the **IP** inserts in a fossa on the pterygoideus shelf anterior to the **EP** insertion and posterior to the m2 in dorsal or lateral view.

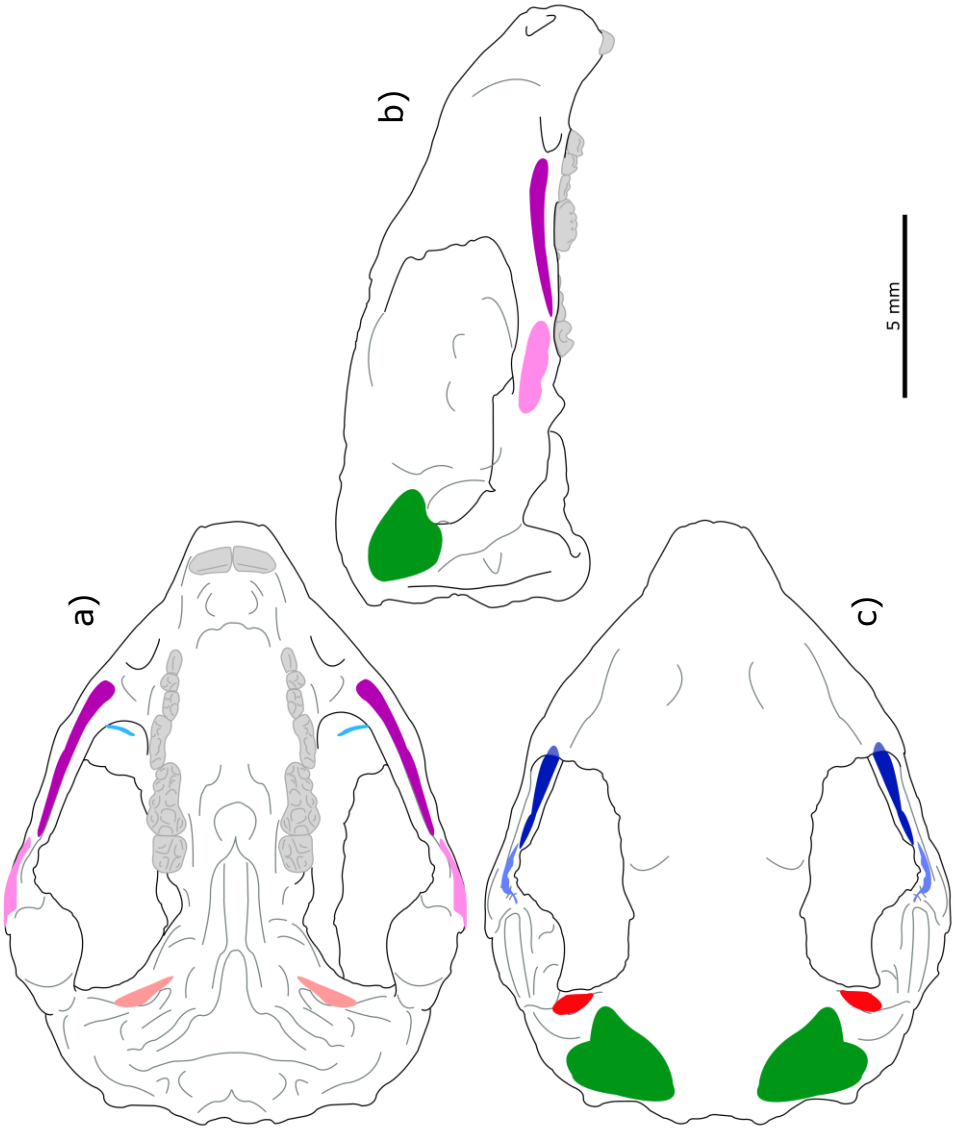

Figure 4.22: Outline diagrams of the reconstructed *C. vulgaris* skull with proposed muscle attachment surfaces shown in a) ventral, b) right lateral and c) dorsal views.

Figure 4.24 shows the muscle attachments and rough shapes in lateral view, as in the figure for *N. gobiensis*, and the rodents in Chapter 2.

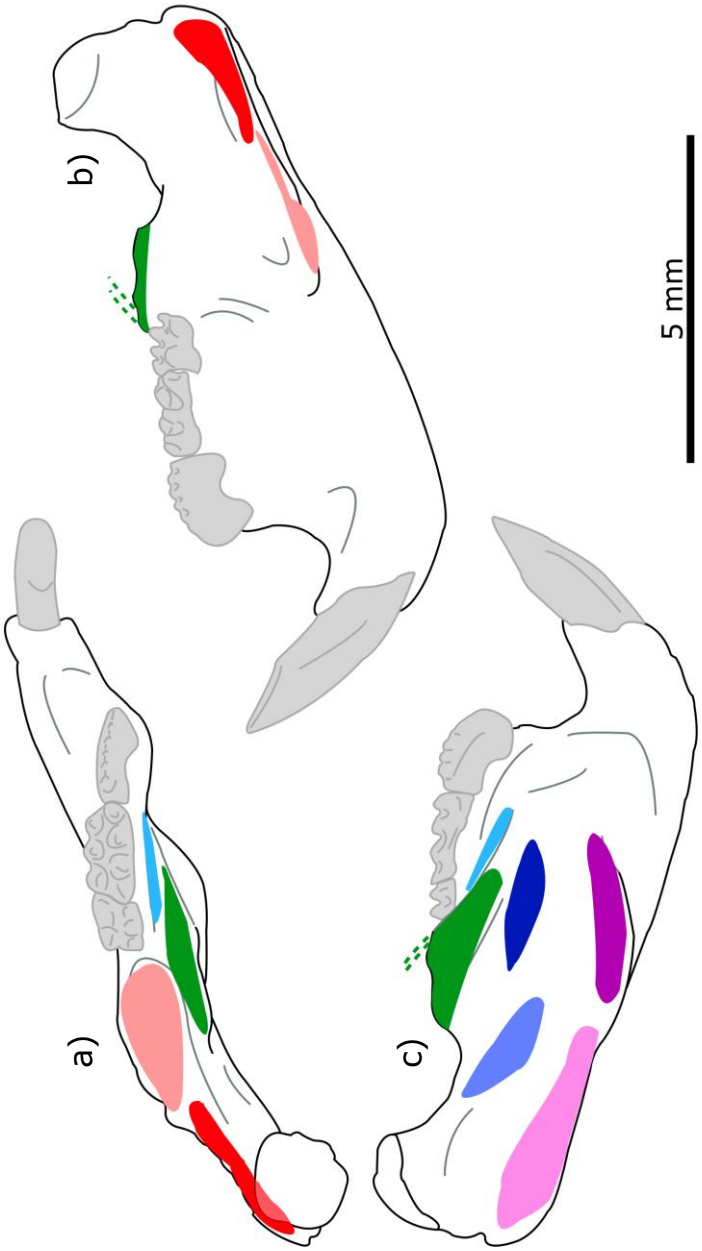

Figure 4.23: Outline diagrams of the *C. vulgaris* hemimandible with proposed muscle attachment surfaces shown in a) dorsal, b) lingual and c) labial views.

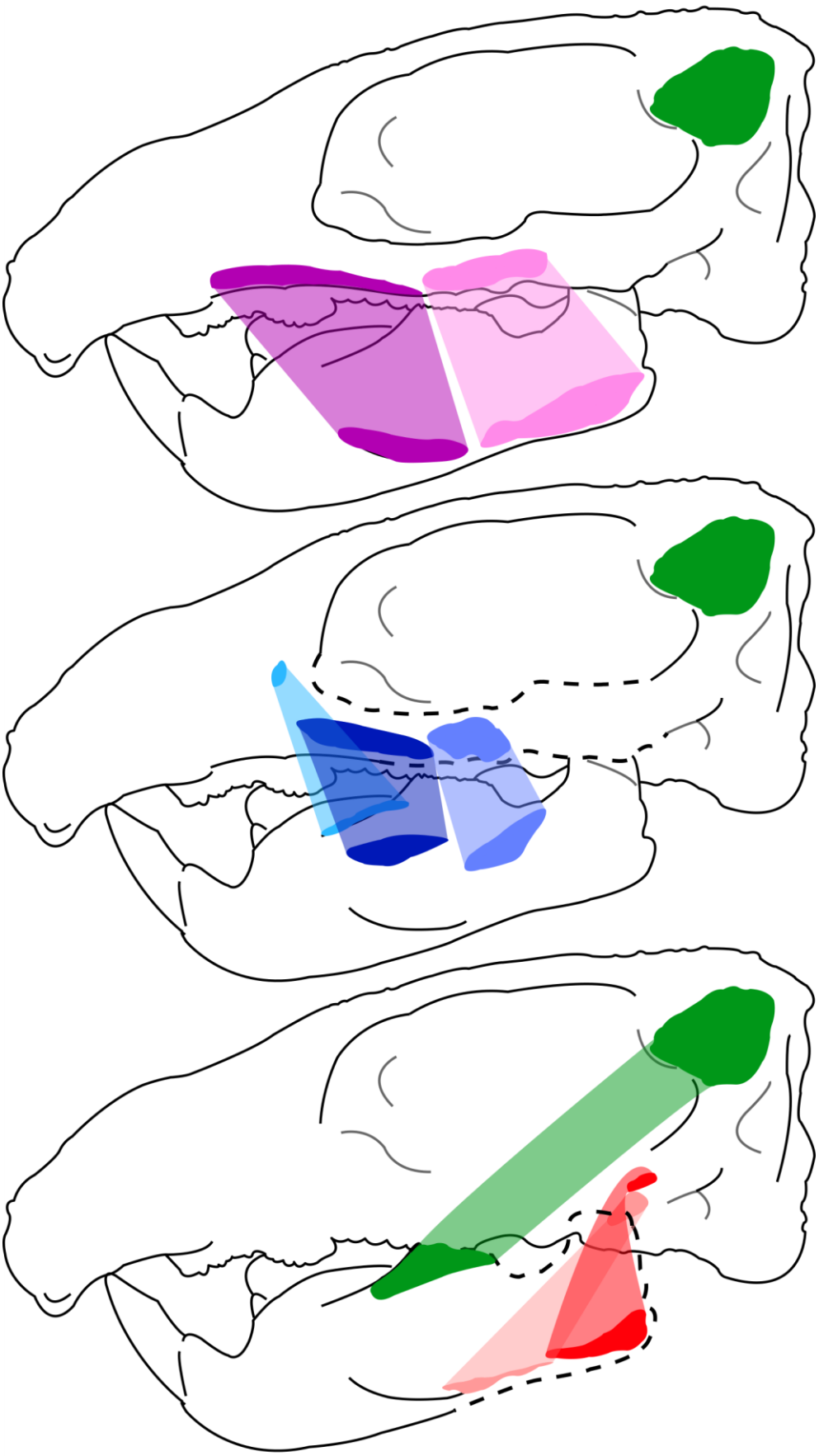

Figure 4.24: Simplified lateral view diagrams showing the origins and insertions of each of the identified jaw-closing muscle subdivisions. Translucent shapes connect the origins and insertions to illustrate the rough position of the muscles. Dashed lines indicate that the attachments are on the medial surface of a bone.

4.3.1.3 – Kryptobaatar dashzevegi

Of the three studied multituberculates, *K. dashzevegi* required the least preparation before muscle mapping. The skull and mandible were scanned together but I segmented them into separate surfaces, and duplicated and articulated the mandible in both premolar and incisor occlusion. Rather than showing surfaces in Avizo, since there was no reconstruction or mirroring required, the specimen is represented here using

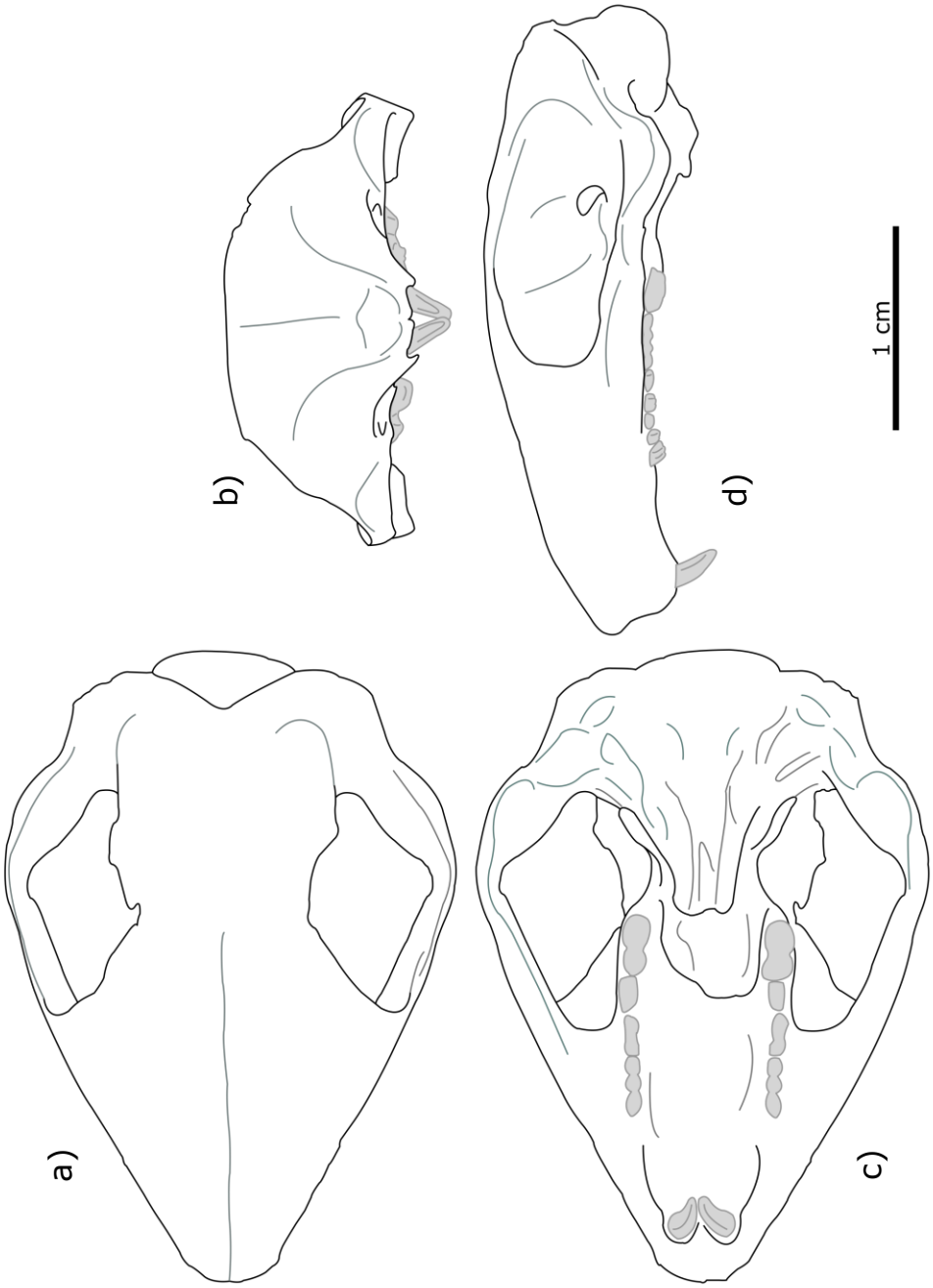

Figure 4.25: Simplified line diagrams of the scanned skull of *K. dashzevegi*, in a) dorsal, b) frontal, c) ventral, and d) lateral view.

line diagrams. Figure 4.25 shows a line diagram of the skull, and Figure 4.26 shows a line diagram of the mandible.

The skull and mandible are both quite asymmetric, as can be seen in the ventral skull in particular, and throughout the hemimandibles. However, the surface preservation is good despite the larger voxel size/lower resolution of the scans compared to the newly scanned multituberculates, and the coronoid processes are almost fully intact. The muscle attachment surfaces are clear and well-defined, though less prominent than *N. gobiensis* (which

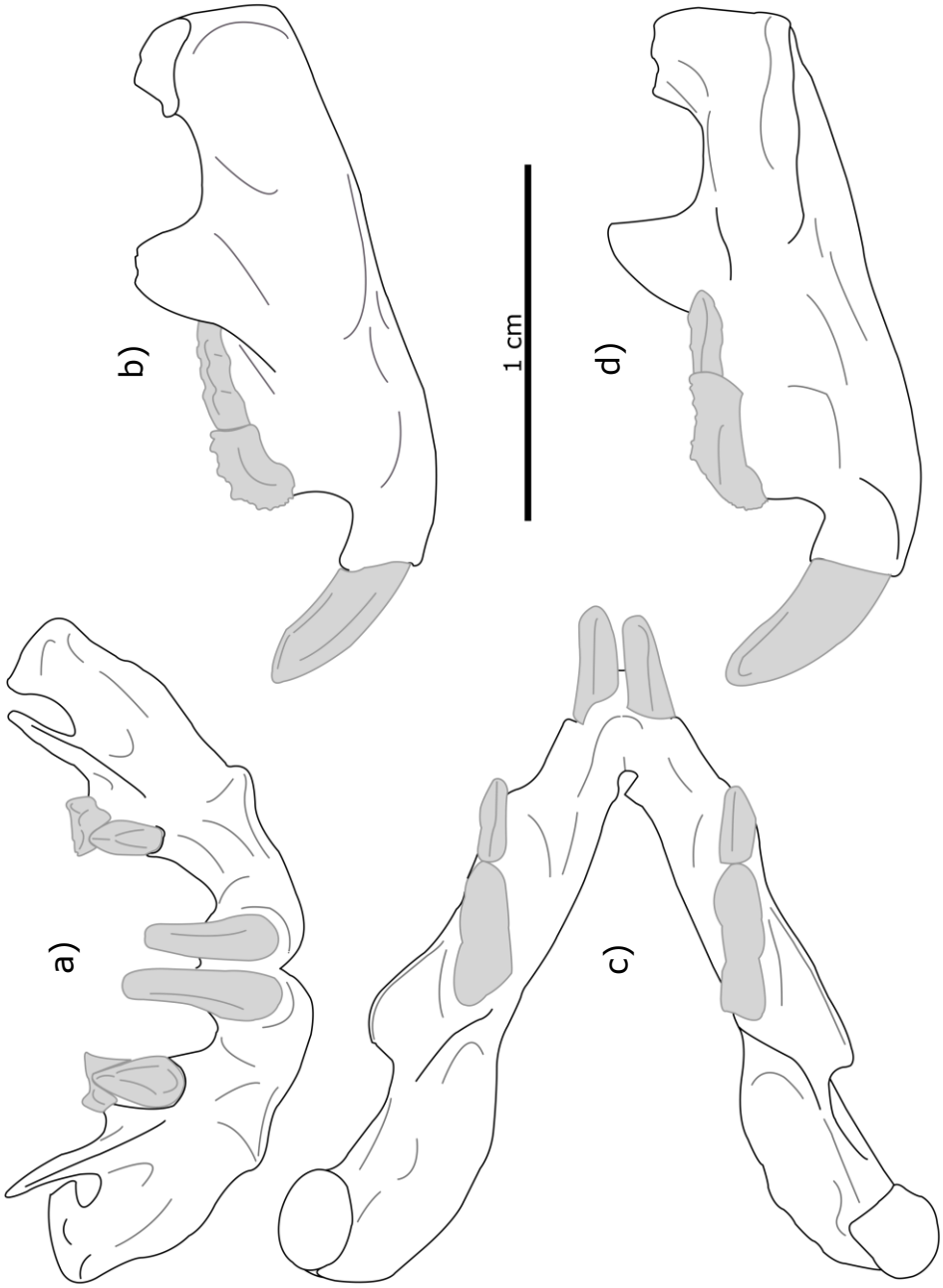

Figure 4.26: Simplified line diagrams of the scanned mandible of *K. dashzevegi*, in a) frontal, b) labial, c) dorsal, and d) lingual view.

may be partially affected by the voxel size of this scan), and the only muscle attachment that is relatively difficult to reliably define is the insertion of the **AZM**. All the muscles identified in *N. gobiensis* are observed here, and no additional ones could be identified.

As in both other multituberculate taxa, the mandible protracts to move from premolar to incisor occlusion, but whereas the *N. gobiensis* specimen with the incorrect mandible did not require rotation of the mandible for incisor occlusion in these analyses, *K. dashzevegi* does require some opening of the jaws to occlude the incisor tips. Figures 4.27 and 4.28

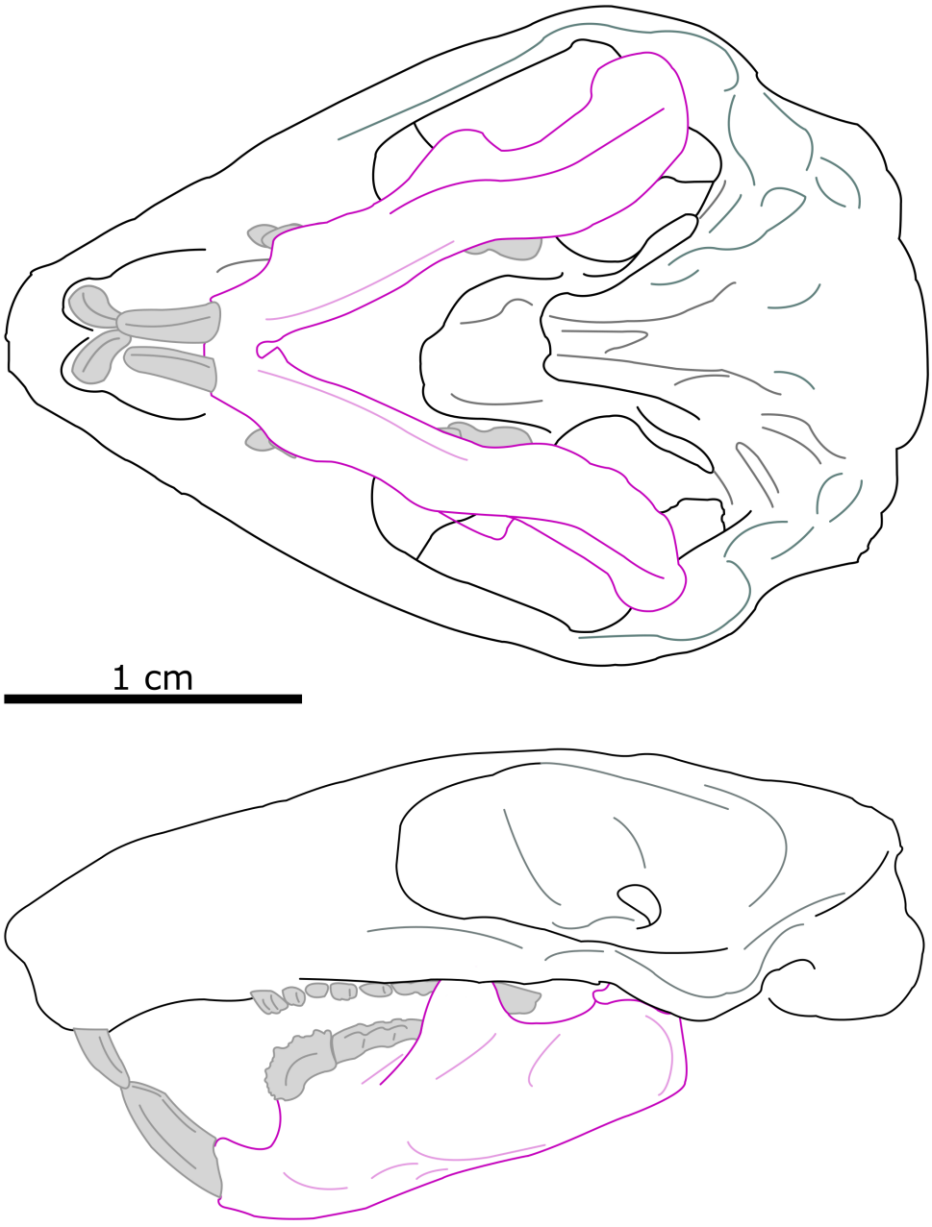

Figure 4.27: Simplified line diagrams of the skull and mandible of *K. dashzevegi* in incisor occlusion, shown in ventral and lateral view.

show the jaw position for incisor and left premolar occlusion, and the mandibles are not displaced mediolaterally as much as in the other taxa; this may be affected by the high degree of asymmetry in this specimen, as opposed to the mirrored hemimandibles of the other specimens.

The muscles originate from and attach to the same bones and surfaces as *N. gobiensis* and *C. vulgaris*, though the good preservation of the orbital pocket allows for a more reliable surface of the **IOZM**'s origin. The surface of the orbital pocket on which it attaches is smooth and slopes steeply, with a clear rounded fossa within its central region. In *N. gobiensis*,

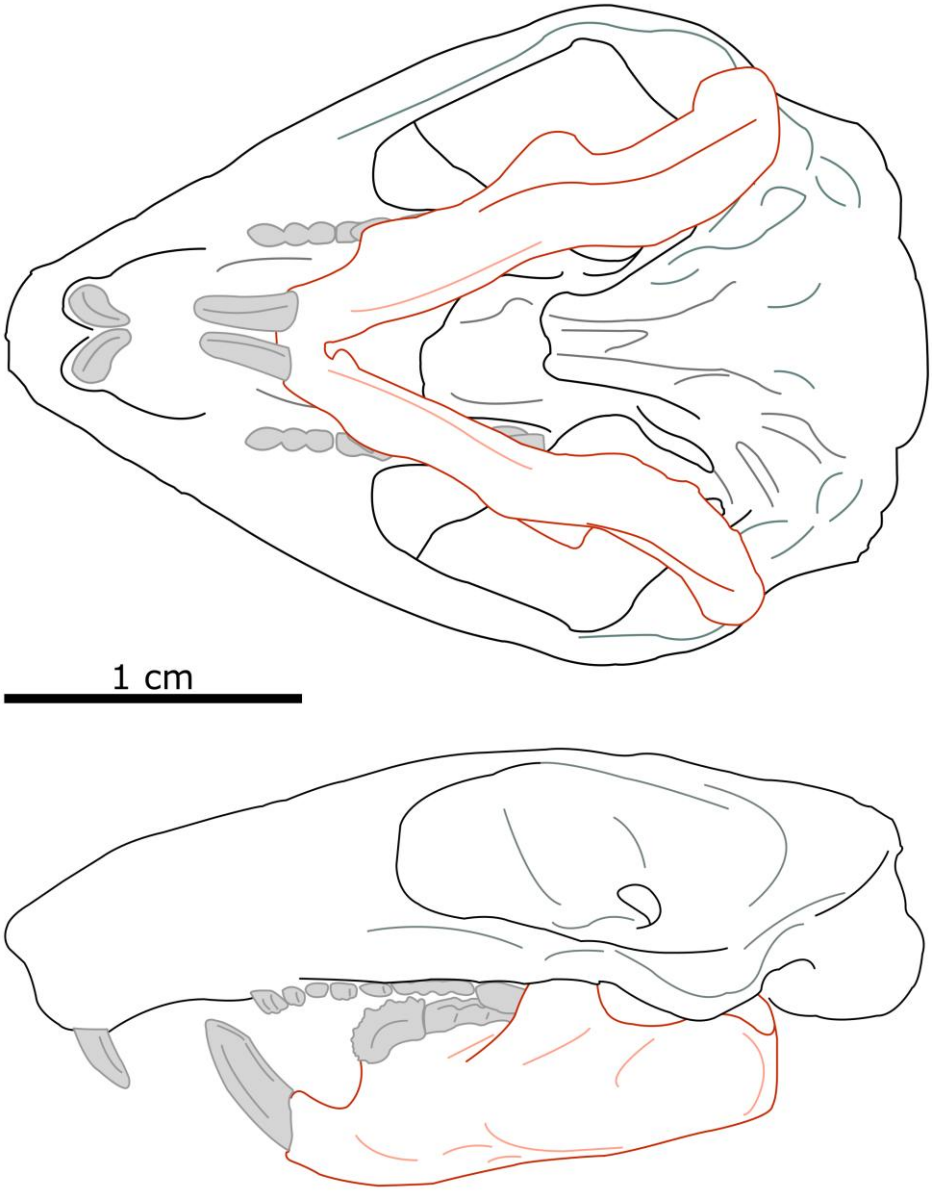

Figure 4.28: Simplified line diagrams of the skull and mandible of *K. dashzevegi* in premolar occlusion, shown in ventral and lateral view.

there was no preservation of such a steeply sloping wall of the orbital pocket, and in *C. vulgaris* the matrix replacement in the area was too severe to reliably identify the bone surface; in *K. dashzevegi*, the attachment can be mapped more confidently. Since the full skull and mandible are preserved and intact in this specimen, and no mirroring was required, I identified the specimen's muscle attachments and mapped them on both sides of the head and mandible, and averaged the two sides' centroid coordinates as in the rodent taxa.

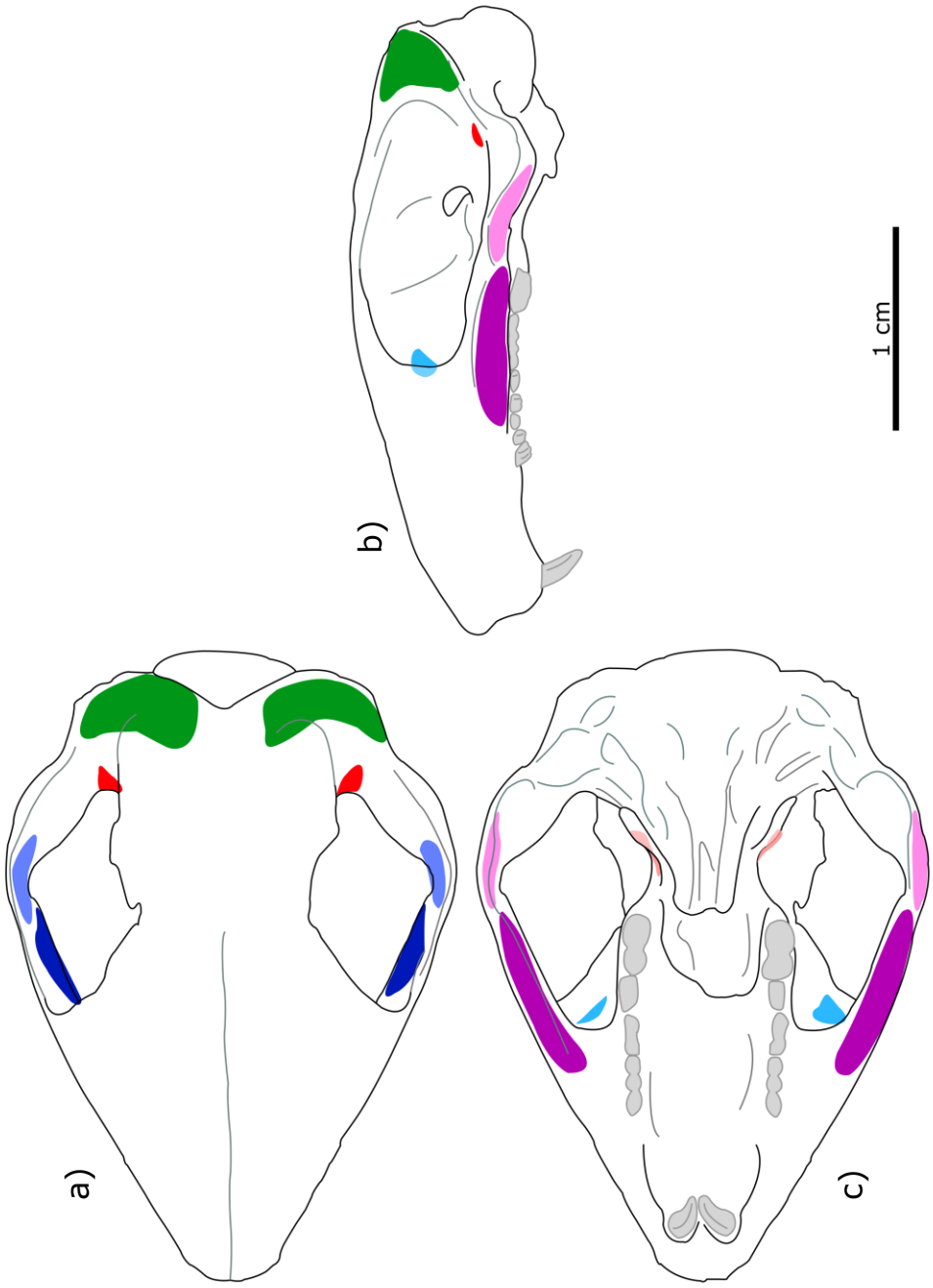

Figure 4.29: Outline diagrams of the skull of *K. dashzevegi* with proposed muscle attachment surfaces shown in a) dorsal, b) left lateral and c) ventral views.

rough muscles in lateral view, as in *N. gobiensis* and *C. vulgaris*, in layers from lateral to medial to the zygomatic arch, with dashed outlines of bones showing when an attachment is on the medial surface.

The attachment surfaces are shown in Figure 4.29 for the skull and Figure 4.30 for the mandible. As in both other taxa, the **ADM** and **PDM** originate from two fossae with curved upper margins on the lateral face of the zygomatic arch with the **PDM** spreading across the maxilla-squamosal

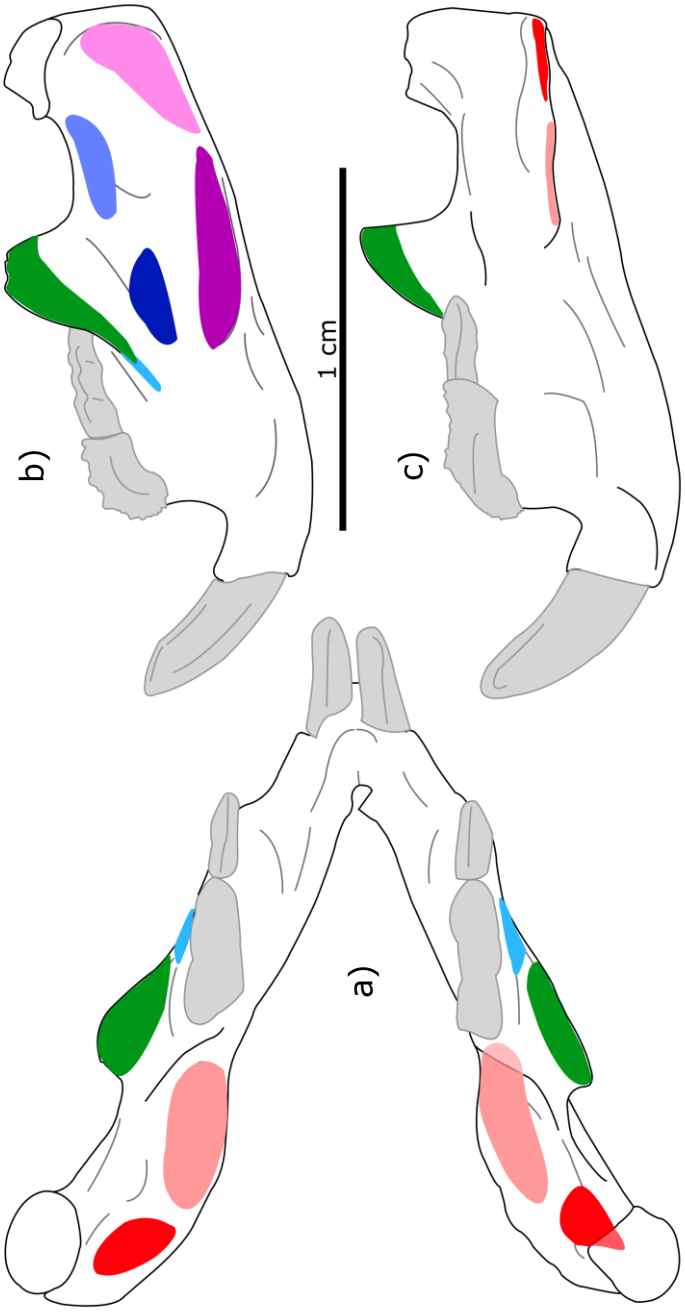

Figure 4.30: Outline diagrams of the mandible of *K. dashzevegi* with proposed muscle attachment surfaces shown in a) dorsal view, b) labial view of the left hemimandible, and c) lingual view of the right hemimandible.

suture, and insert along the ventral margin of the mandibular angle's lateral face, with the former posterior to the masseteric ridge and the latter fossa separated from the former by a narrow change in surface shape. The **IOZM** originates from the anterior wall of the orbital pocket and inserts in a trench-like fossa medial to the anterior region of the root of the coronoid process. The **AZM** and **PZM** originate from a pair of fossae on the medial surface of the zygomatic arch, on the maxilla, and insert on two narrow, small fossae on the lateral face of the mandible, in the masseteric region, with the **AZM** inserting anteroventral to the root of the coronoid process and the **PZM** inserting posteroventral to the **AZM**. The **T** originates from a fossa on the posterior dorsal cranium, anterior to the lambdoidal crest, and inserts on the dorsal margin of the coronoid process, which is preserved well in this specimen. The **EP** originates on from a rounded fossa on what may be the alisphenoid and inserts in a large fossa in the posterior region of the pterygoideus shelf, ventral to the condylar process. The **IP** originates in a clear fossa on the lateral face of the pterygoid plate and inserts in a fossa on the pterygoideus shelf anterior to the **EP** insertion and posterior to the m2 in dorsal or lateral view. There is a notable ridge between the insertions of the pterygoid muscles.

Figure 4.31 shows the rough muscles in lateral view, as in *N. gobiensis* and *C. vulgaris*, in layers from lateral to medial to the zygomatic arch, with dashed outlines of bones showing when an attachment is on the medial surface.

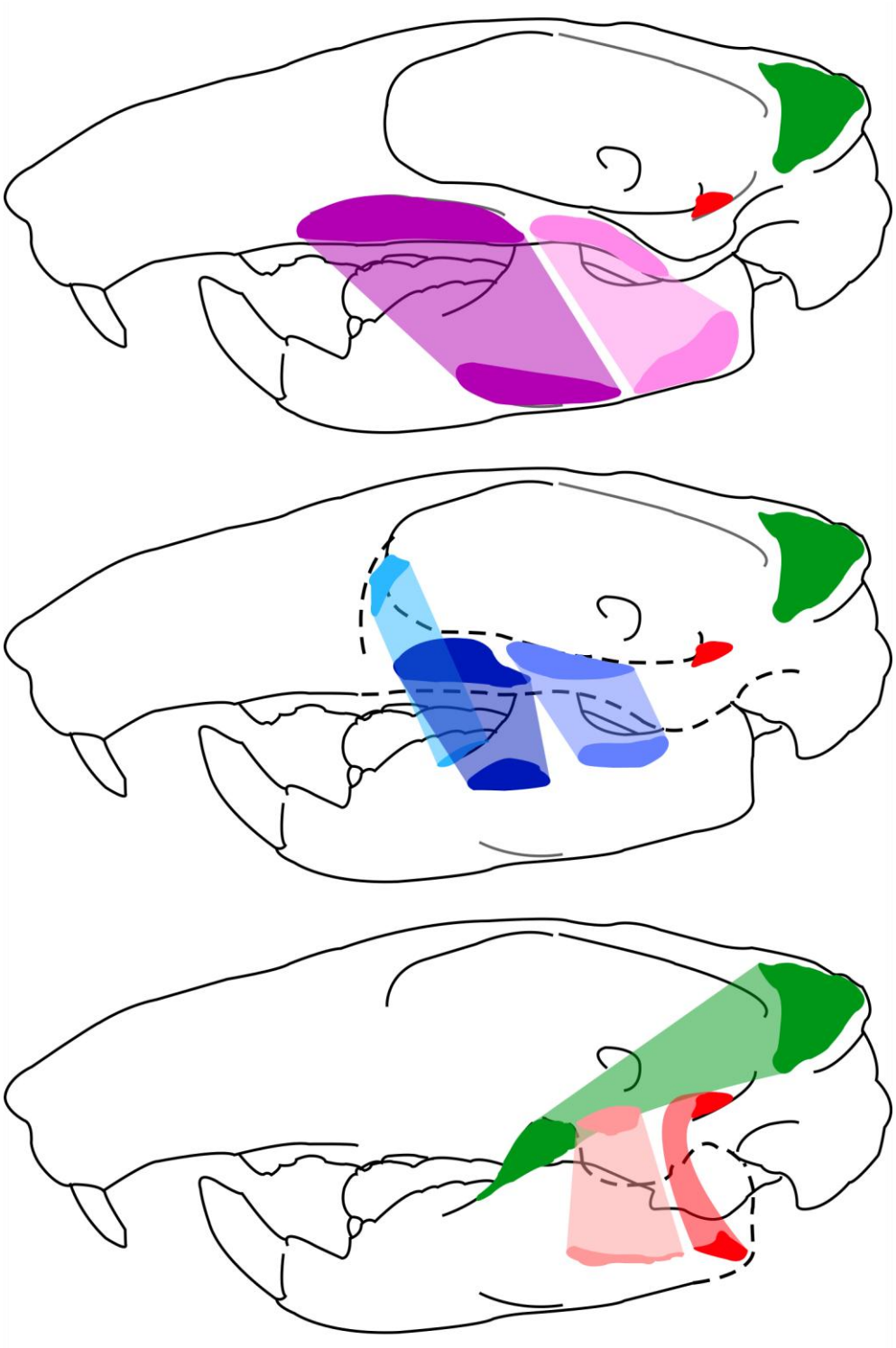

Figure 4.31: Simplified lateral view diagrams showing the origins and insertions of each of the identified jaw-closing muscle subdivisions. Translucent shapes connect the origins and insertions to illustrate the rough position of the muscles. These progress from superficial muscles to deep muscles, with dashed lines indicating that the attachments are on the medial surface of a bone.

4.3.2 – Lever-arm mechanics

4.3.2.1 – Individual muscle MANOVAs

In Table 4.3, the results of the individual muscle MANOVA analyses are compiled, including relevant statistics such as Pillai's Trace and its associated F statistic and p-value. As outlined in the Materials and Methods, Bonferroni correction adjusted their threshold p-value for significance to 0.0055. The 18 analyses are divided into two groups: one for incisor biting, and one for molar biting. The **IOZM** of hystricomorphs is compared with the **ADM** of sciuromorphs and *A. rufa*, and the **ADM** of myomorphs, sciuromorphs, and *A. rufa* are compared with the **IOZM** of hystricomorphs, allowing all muscles to be included in the analysis of all taxa as in Chapter 3. The independent variable is the group (multituberculates, or one of the four rodent morphotypes) and the dependent variables are the raw mechanical advantage data for the studied gape angles of a specific muscle. It can be clearly observed that on a muscle-by-muscle basis only the **ADM** v **DM** (incisor $p = 0.00095$, molar $p = 0.0017$) at both bite points, and the **IOZM** v sciuromorph **ADM** data in molar biting ($p = 0.00016$) show statistically significant differences between the morphotype categories and multituberculates. In all significant cases, the F-statistic and Pillai's Trace are both greater than 1. As in Chapter 3's analyses, the differentiation of the **DM** is a characteristic of specific morphotypes despite its inferred presence in the multituberculate taxa. To include the full sample when using as much of the muscle data as possible, the subdivisions of the **DM** are compared with the **DM** data too. Combined, these results indicate that the **DM** and **ADM** remain significantly different when multituberculates are added to the sample, causing significant differences in mechanics between organisms/groups that possess them and those that don't. The results here fit with established interpretations on the mechanical function of the **ADM** (Druzinsky, 2010). Furthermore, these results suggest that, among these two muscles in isolation, there are significant differences between the mean of each group of organisms, and that the **IOZM** and **ADM** are significantly different also, despite both being anterior expansions of the masseter onto the rostrum.

Further evaluation through the PCAs and their subsequent MANOVAs and PC scores can identify the variation across the masticatory systems as a whole.

Analysis	Muscle	df1	df2	Pillai's Trace	F	p
Incisor	ADM & IOZM	32	84	1.510	1.592	0.047
	ADM & DM	32	84	**1.893**	**2.358**	**0.001**
	PDM & DM	32	84	1.515	2.007	0.046
	IOZM & ADM	32	84	1.733	2.007	0.006
	AZM	32	84	1.155	1.066	0.397
	PZM	32	84	1.248	1.190	0.261
	T	32	84	1.447	1.488	0.077
	EP	32	84	1.498	1.572	0.052
	IP	32	84	1.563	1.683	0.031
Molar	ADM & IOZM	32	84	1.370	1.367	0.130
	ADM & DM	32	84	**2.026**	**2.693**	**0.0002**
	PDM & DM	32	84	1.703	1.946	0.008
	IOZM & ADM	32	84	**1.846**	**2.250**	**0.002**
	AZM	32	84	1.242	1.182	0.269
	PZM	32	84	1.553	1.667	0.033
	T	32	84	1.476	1.535	0.062
	EP	32	84	1.430	1.461	0.087
	IP	32	84	1.323	1.297	0.173

Table 4.3: The results of eighteen MANOVA analyses for data simulating incisor biting, and molar biting, for an individual muscle. In each, the mechanical advantage data for multituberculates and all four rodent morphotypes are compared simultaneously. Critical threshold = 0.0055

4.3.2.2 – PCA results

4.3.2.2.1 – ADM v IOZM

This PCA compares the IOZM with the ADM as outlined above. It includes all muscles I identified that are homologous to those in rodents, so the SM discussed in Chapters 2 and 3 is absent. Further detail on the muscles identified was discussed in the Materials & Methods and Anatomy and Fossil Reconstruction Results subheadings earlier in this Chapter. Of the 29 Principal Components generated in these analyses, only the first four will be discussed in depth and included in figures; combined, they account for more than 80% of the total variance in the data. Table 4.4 contains the individual contribution

to the total variance from each of PCs 1 to 4. PCs 5 and beyond individually account for less of the variance, and are not discussed as part of these results.

Analysis	PC 1	PC 2	PC 3	PC 4	Total % of variance
Incisor bite	50.66	13.87	11.59	8.11	84.22
Molar bite	47.35	16.33	10.96	6.78	81.43

Table 4.4: This table displays the percentage of the total variance accounted for by PCs 1–4 in each analysis for the full sample of studied muscles, with the **ADM** and **IOZM** compared.

Figure 4.32 displays a set of four PC plots in the same format as the figures in Chapter 3. All four of these plots are at the same visual scale to aid comparisons between them. Several key results can be observed on this panel figure. As in the results of Chapter 2, the PC scores of taxa cluster more closely around the mean of the data (coordinates (0,0)) in incisor biting than in molar biting. All groups have at least some overlap with other taxa on at least one of the axes shown. On PC 1 in incisor (50.66% variance) and molar

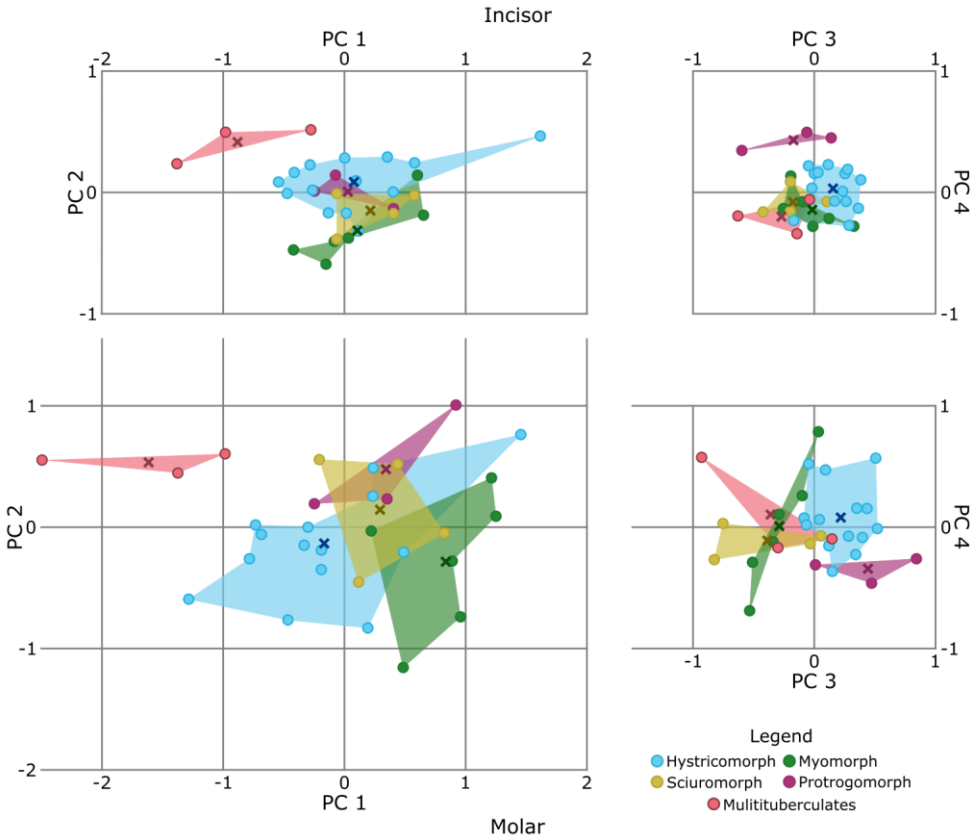

Figure 4.32: PC plots of mechanical advantage data across the sample when the **ADM** and **IOZM** are compared. All plots are at the same scale, displaying PC 1 v 2 and PC 3 v 4 for both incisor and molar biting.

biting (47.35%), multituberculates occupy a region in the PC space where no rodent taxa are present, closer on the plot to the hystricomorphs than to other rodents. *N. gobiensis* is the most negative taxon on PC 1, occurring furthest from any rodents, and furthest from the mean in molar biting. On PC 1 v 2, the rodents most similar to multituberculates are *D. punctata*, *H. cristata*, *L. maximus*, and *M. coypus* during incisor biting (50.66% v 13.87% variance), and *L. maximus*, *M. coypus*, *B. suillus* and C. *canadensis* during molar biting (47.35% v 16.33% variance). As in Chapter 3, *P. capensis* is an outlier on the positive PC 1 space in incisor biting, even further from the mean than the multituberculates.

On the PC 3 v 4 plots, multituberculates are much closer to the rodents, closer to the mean than the protrogomorphs in incisor biting and more similar to the myomorphs an sciuromorphs than the other morphotypes. On PC 3 v 4 in molar biting (10.96% v 6.78% variance), *N. gobiensis* is once again furthest far from the mean and from other rodents; *C. vulgaris* and *K. dashzevegi* are more similar to rodents than to *N. gobiensis* on PC3 v 4 plots. In incisor biting (11.59% v 8.11% variance), *C. vulgaris* is most similar to *D. sagitta* and *C. badius*, while *K. dashzevegi* is most similar to *G. watersi* and *P. capensis*, and *N. gobiensis* is most similar to *C. canadensis*; in molar biting, *C. vulgaris* is most similar to *H. cristata* and *S. carolinensis*, *K. dashzevegi* is most similar to *C. badius*.

Regarding the rodent morphotypes themselves, all four plots have overlap between the groups, but the hystricomorphs and myomorphs are the most different rodent groups on PC 1 v 2. Protrogomorphs are more different to other rodents than multituberculates in incisor PC 3 v 4 and mostly distinct during molar PC 3 v 4. Sciuromorphs are, as in Chapter 3, split between those similar to myomorphs and those similar to hystricomorphs/protrogomorphs (*C. canadensis* on PC 1 v 2), with a split across the myomorph space on PC 3 v 4 (*C. canadensis* and *T. umbrinus* more negative on PC 3, *P. petaurista* and *S. carolinensis* close to the origin).

As in Chapter 3, the spread of the data is much broader in the molar plots. It is difficult to identify what anatomical or mechanical feature may be responsible for *N. gobiensis* being so dissimilar to other taxa, especially on

PC 1 v 2. In molar biting for PC 1 v 2, *N. gobiensis* is further from the other multituberculates than the nearest rodent taxa are, clearly distinct from its multituberculate relatives in molar/p4 mechanical advantage in particular.

Despite all of these observed similarities and differences, the multituberculates are not occurring exclusively on multiple PCs simultaneously. For example, they are differentiated by PC 1 in molar biting, but are still within the positive range of several rodents on PC 2. With the observable spread of rodents on PC 1 v 2 during molar biting in particular, the rodent morphotype categories can be comparably different to one another as they are to the multituberculates, indicating that the variance among Rodentia is still significant when comparing them to multituberculates.

By examining the loading plots for PCs 1 to 4 at both bite points—which are compiled in the two-part panel figure, Figure 4.33a and 4.33b—the muscles and gape angle ranges that are significantly responsible for the variance on each PC can be identified. In the loading plots (as in Chapter 3) the grey region helps to identify which datapoints are significant. It is simple to calculate the relative contribution that would be assumed under Brownian motion; if all variables contributed equally, they would have the same value on the loading plot. Therefore, if a bar extends beyond the grey region, this indicates that it contributes to the total variance more than would be expected if all were equal; loadings in the grey region can be dismissed as insignificant to the positive and negative variance on that PC.

By observing these plots, one can identify which muscles are contributing to the patterns identified on the PC plots, and which gape angles are responsible. In broad terms, Figure 4.33a and 4.33b shows that all muscles contribute significantly to the variance of at least one PC in both incisor and molar biting. When comparing the bite points and plots, further details can be identified.

On PC 1 (50.66% variance in incisor biting, 47.35% variance in molar biting), the **ADM** v **IOZM**, **PDM** v **DM**, **IOZM** v **ADM**, **AZM**, **PZM**, and **IP** all contribute significantly to the positive variance at both bite points. During

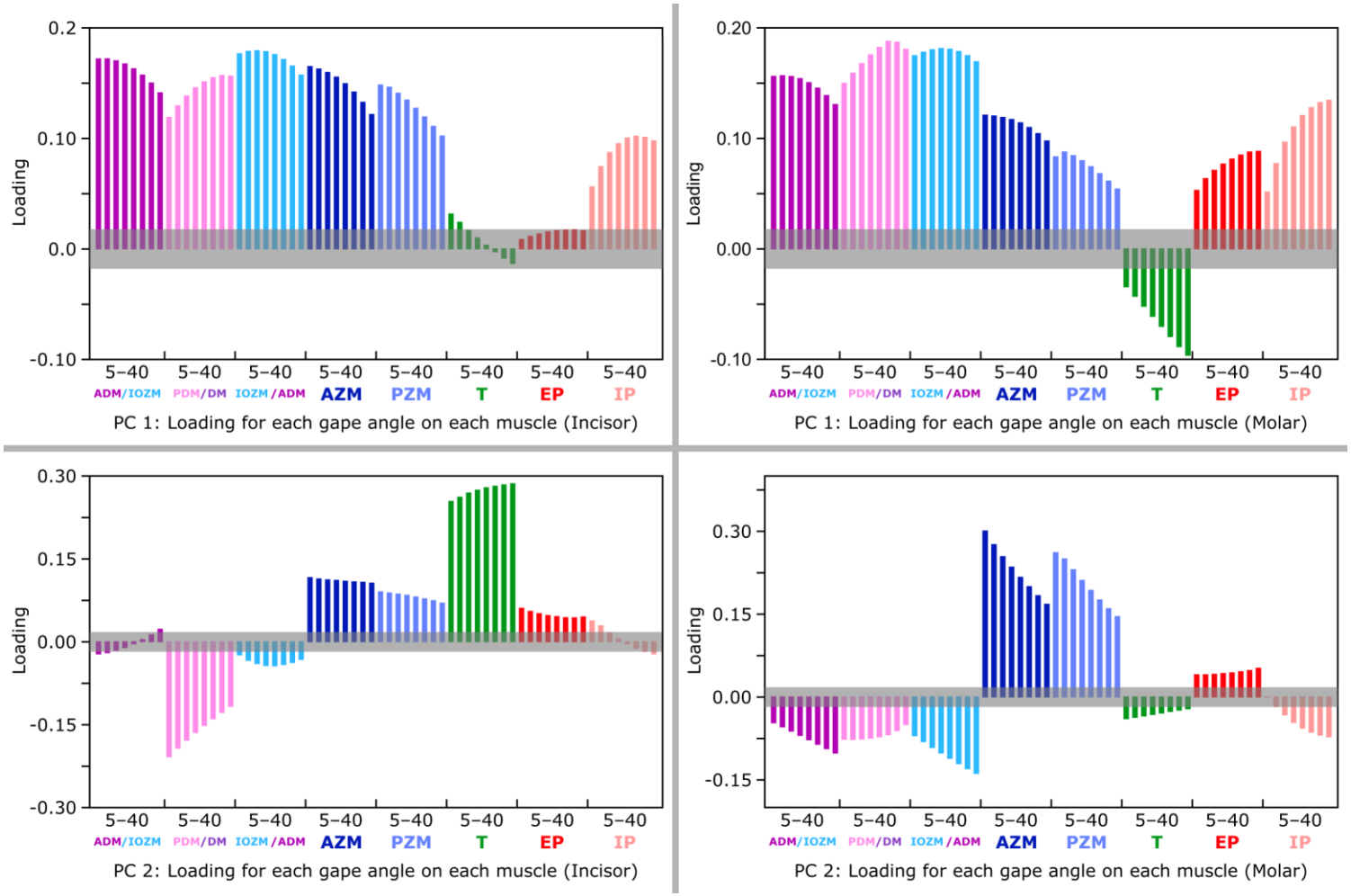

Figure 4.33a: Panel figure displaying the Loading Plots for PCs 1v2 in both incisor (left) and molar (right) biting when the **ADM** and **IOZM** are compared. Bars that extend beyond the grey region contribute beyond what would be expected under Brownian motion.

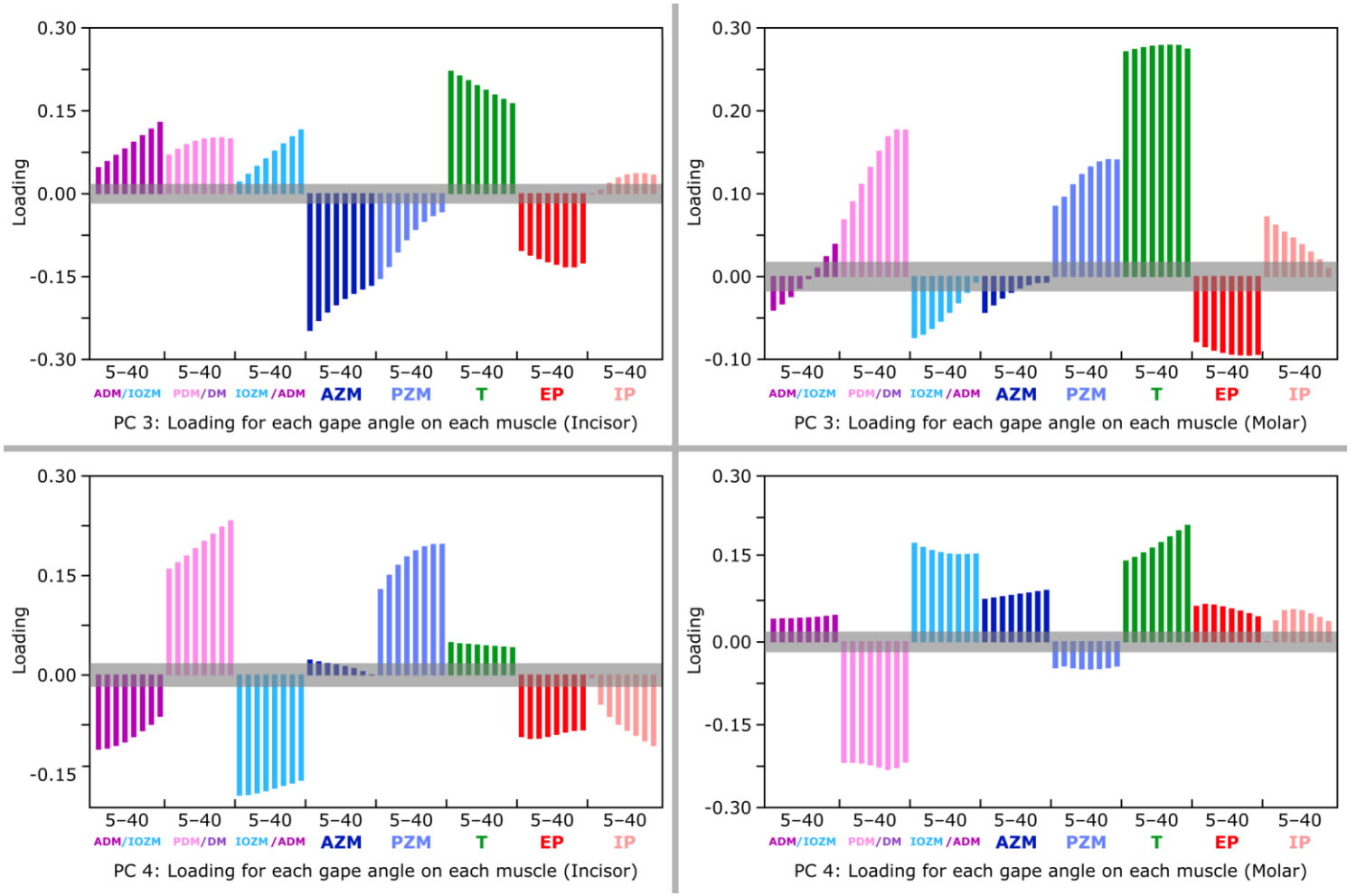

Figure 4.33b: Panel figure displaying the Loading Plots for PCs 3v4 in both incisor (left) and molar (right) biting when the **ADM** and **IOZM** are compared. Bars that extend beyond the grey region contribute beyond what would be expected under Brownian motion.

incisor biting, the contribution of the masseter subdivisions is similar to one another, and most muscles show a decreasing positive contribution as gape increases, and the PDM v DM and IP showing an increasing contribution as gape rises. In molar biting, EP also has a positive contribution to the variance (also increasing with rising gape) and T has a substantial contribution to the negative variance; furthermore, the contribution to the variance from the AZM and PZM is relatively lower, and IOZM increases in its contribution to positive variance until gape passes 20°, then decreases.

For PC 2 (13.87% incisor variance, 16.33% molar variance), the bite points are much more different. During incisor biting, the largest positive contribution comes from T (increasing with gape), with smaller positive contributions from the AZM and PZM, then the EP. The largest negative contribution comes from the PDM v DM, contributing less as gape increases, with a smaller contribution from the IOZM v ADM. In molar biting, the largest contributions to the positive variance come from the AZM and PZM, both decreasing as gape increases, then the EP. The ADM v IOZM, PDM v DM, and IOZM v ADM now contribution similarly to the negative variance, with the PDM v DM decreasing its contribution as gape increases and the others increasing; smaller contributions to the negative variance are observable from the IP and T.

On PC 3 (11.59% incisor variance, 10.97% molar variance), during incisor biting the largest positive contribution comes from T, with smaller positive contributions from the ADM v IOZM, PDM v DM, and IOZM v ADM and an even smaller contribution from the IP above 15°; the contribution from T decreases as gape increases, and the other aforementioned muscles increase with gape. The largest contribution to the negative variance is the AZM, with smaller contributions from the PZM and EP, with the EP increasing its contribution with gape until 30°, and the AZM and PZM both decreasing their contributions as gape increases. On the molar biting plot, the largest positive contribution is again from T, but this time with smaller contributions from the PDM v DM, PZM, low-gape IP, and ADM v IOZM above 35°. In contrast to the incisor plot, the largest contributor to the negative variance

is **EP**, with smaller contributions from the **IOZM** v **ADM**, and the **ADM** v **IOZM** and **AZM** below 20° gape.

On the PC 4 (8.11% incisor variance, 6.78% molar variance) loading plots, during incisor biting the largest contribution to the positive variance is the **PDM** v **DM**, with a smaller contribution from **PZM**, and much smaller contribution from the **T**; the latter decreases slightly gape increases, while the former two muscles increase their contribution with increasing gape. The largest contribution to the negative variance comes from the **IOZM** v **ADM**, with smaller contributions from the **ADM** v **IOZM**, **EP**, and **IP**. The **IOZM** v **ADM**, **ADM** v **IOZM**, and **EP** all decrease their contributions are gape increases, while the **IP** increases. For molar biting, the contributions are once again different. The largest contributors to the positive variance are the **T** and **IOZM** v **ADM**, the former increasing with gape and the latter decreasing, with smaller contributions from the **AZM**, **EP**, **ADM** v **IOZM**, and **IP** —the **ADM** v **IOZM** and **AZM** both increase with gape, the **EP** and **IP** both peak (at 10° and 15° respectively) before decreasing as gape increases further. The biggest contributor to the negative variance is the **PDM** v **DM**, with a small contribution from the **PZM**; both fluctuate with increasing gape.

Taken together, the masseter subdivisions and **T** in particular are consistently large contributors to the variance in the sample, with the **IP** and **EP** both typically contributing less to the variance on most PCs. Despite the **ADM** v **IOZM** and **IOZM** v **ADM** datasets only differing by six taxa (the myomorphs), the two categories often contribute quite differently to the variance. The **PDM** v **DM** often exhibits similar or greater contributions to the variance, as does the **T**. The fact that the **AZM**, **PZM**, and **T** show such high contributions to the variance on several PCs despite being strictly homologous muscles (as opposed to the mixed categories referred to above) shows how broad the variation can be even on homologous muscles. Despite the individual muscle MANOVAs mostly not showing significant differences between the group means on each individual muscle, in aggregate their contribution to the variance can be observed here. The extremes of the studied gape angle range are typically responsible for the highest contributions to the variance from each muscle that is significant, though the

pterygoids in particular tend to break this pattern. The variation within Rodentia and between them and multituberculates when comparing homologous muscles is observable on all muscles, and is typically greatest when biting objects that are relatively small or relatively large. Especially beyond PC 1, incisor and molar biting present notable divergences in which muscles are the primary contributors to variance.

Further statistical analyses can evaluate these comparisons. Table 4.5 displays the results of two MANOVAs of PC scores, with incisor biting and molar biting tested separately. In both analyses, the group means of all five categories are all compared against each other. In this table, PCs 1–25 were used for both analyses, meaning that the inputs for the MANOVAs consist of over 99.9% of the total variance. In molar biting, the p-value is below the critical threshold of 0.05; according to this test, the means of the five groups are significantly different in molar biting, but not during incisor biting. This implies that the lower disparity (especially among rodents) observable in the incisor PC plots results in the morphotypes and multituberculates not being significantly different. However, this MANOVA does include the differences between rodent morphotypes in its input, and testing the significance of comparisons between multituberculates and individual rodent morphotypes could illuminate the specifics of these potential differences.

Analysis	Incisor	Molar
df1	100	
df2	16	
Pillai's Trace	3.696	**3.781**
F	1.944	**2.764**
p	0.0657	**0.012**

Table 4.5: The results of two MANOVA analyses of PC scores when simulating incisor biting, and molar biting when the **ADM** and **IOZM** are compared. In each test, multituberculates and all four rodent morphotypes are compared.

As can be observed in Table 4.6, the MANOVAs comparing the multituberculate taxa with each individual morphotype by their PC scores identify significant differences between the group means of multituberculates and certain morphotypes in particular. The Bonferroni correction adjusted threshold p-value for significance is 0.0125. The

	Incisor				Molar			
	vs H	**vs M**	**vs P**	**vs S**	**vs H**	**vs M**	**vs P**	**vs S**
df1	4	4	4	4	4	4	4	4
df2	12	4	1	2	12	4	1	2
Pillai's Trace	**0.83**	**0.96**	0.99	**0.995**	**0.80**	**0.98**	0.94	0.94
F	**14.33**	**21.14**	182.5	**100.8**	**11.72**	**49.39**	4.197	7.645
p	**0.0002**	**0.006**	0.06	**0.0098**	**0.0004**	**0.001**	0.35	0.12

Table 4.6: The results of eight MANOVA analyses for data simulating incisor biting, and molar biting when the **ADM** and **IOZM** are compared. In each test, multituberculates are compared against one rodent morphotype and the significance of the difference between the means of the two groups in question is evaluated. For the page size, the morphotypes are abbreviated using capital letters. 'H' for hystricomorphs, 'M' for myomorphs, 'P' for protrogomorphs, and 'S' for sciuromorphs.

protrogomorphs are not significantly different from the multituberculates at either bite, but the sciuromorphs are significantly different from the multituberculates during incisor biting only. The hystricomorphs and myomorphs are significantly different to the multituberculates at both bite points; however, it must be noted that they are the most speciose categories in this analysis (14 hystricomorphs, 6 myomorphs), so the lack of significant difference between multituberculates and protrogomorphs/molar sciuromorphs may be a result of the sampling. Future analyses with more multituberculates and more rodent taxa of those morphotypes could perhaps identify further significant differences. With that caveat, the most significant difference between multituberculates and rodents is when they are compared with those rodents that possess an expanded infraorbital foramen. Together, these current data suggest that the observed significant result of the individual **IOZM** v **ADM** MANOVA for molar biting in Table 4.3 may be primarily representing the significance of the difference between multituberculates and the hystricomorphs and myomorphs specifically.

4.3.2.2.2 – ADM v DM

In this PCA, the **IOZM** is absent from the data and the **ADM** and **PDM** are both compared with the **DM**. As in the previous analysis, only PCs 1 to 4

will be shown. This accounts for 87.04% of the total variance in the incisor biting data and 85.59% of the total variance in molar data, with Table 4.7 showing a breakdown of each PC's contribution to this value.

Analysis	PC 1	PC 2	PC 3	PC 4	Total % of variance
Incisor bite	44.26	25.19	11.44	6.15	87.04

Table 4.7: This table displays the percentage of the total variance accounted for by PCs 1–4 in each analysis for the PCA that removes the **IOZM** and compares the **ADM** and **DM**.

These PCs are displayed as PC plots in Figure 4.34. As in the previous analyses, the taxa are more closely clustered around the mean in incisor biting than during molar biting. Key patterns can be identified, some of which contrast with those in the preceding analysis. On PC 1 vs PC 2, the multituberculates occur in a region not occupied by any rodents, this time in

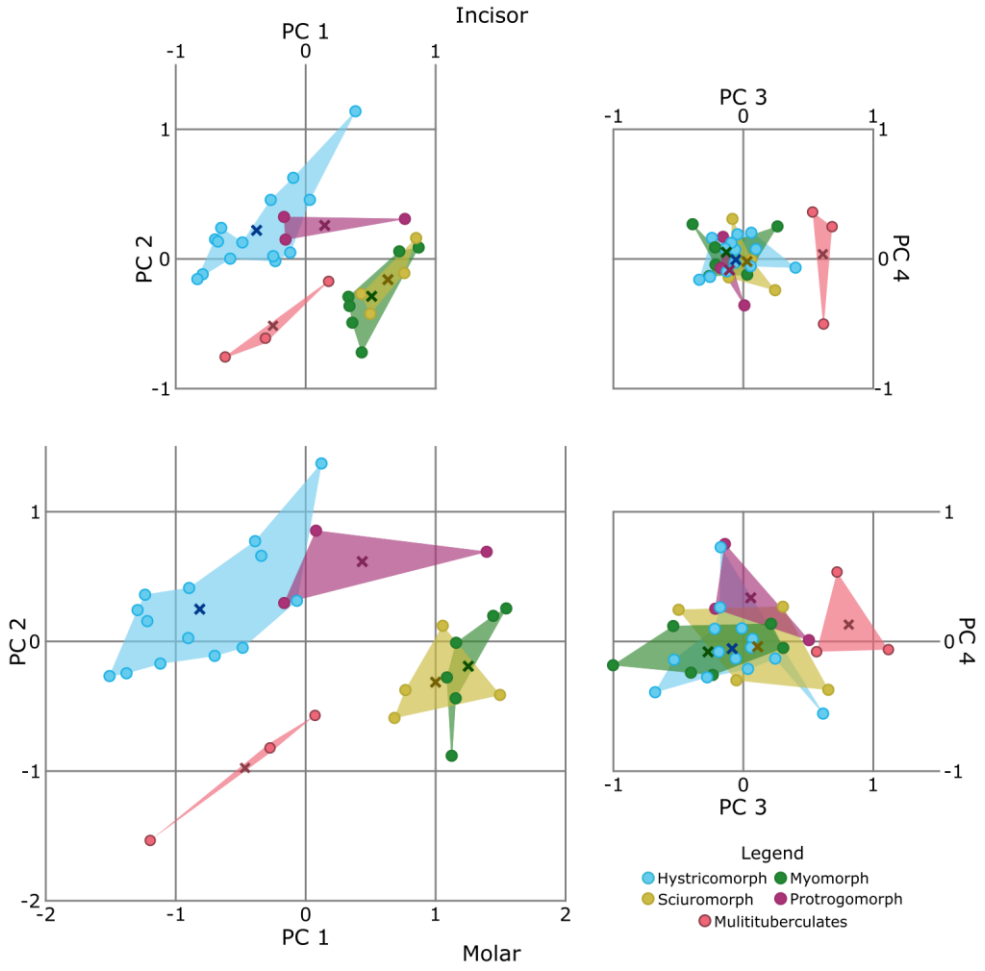

Figure 4.34: PC plots for mechanical advantage data for the PCA that removes the **IOZM** and compares the **ADM** and **DM**. All plots are at the same scale, displaying PC 1 vs 2 and PC 3 vs 4 for both incisor and molar biting.

the negative PC 1 v 2 space. As in the rodents-only analysis of Chapter 3, the rodents are split into two groups by the differentiation of the **DM**, showing that despite the differentiation being present in multituberculates, they are still distinct from rodents. *C. vulgaris* is the closest to the mean and to rodents, occurring between the hystricomorph-protrogomorph and myomorph-sciuromorph clusters, visibly closer to the latter grouping; the two closest rodents to *C. vulgaris* on the incisor PC 1 v 2 plot (44.26% v 25.19% variance) are *C. badius* and *C. gambianus*, both myomorphs, but the closest in molar biting (52.49% v 17.47% variance) are sciuromorphs, namely *C. canadensis* and *S. carolinensis*. As in the **ADM** v **IOZM** PCA, *N. gobiensis* is the furthest multituberculate from the mean. Patterns among the rodents are as expected based on Chapter 3, with *A. rufa* being closer to the myomorph-sciuromorph cluster than it is to the other protrogomorphs, which group closely with the hystricomorphs' space, and *P. capensis* maintaining its position as an outside to hystricomorphs on both plots.

In the incisor PC 3 v 4 plot (11.44% v 6.15% variance), the rodents form an overlapping cluster around the mean, with the multituberculates being separated into the positive PC 3 space. *N. gobiensis* is once again the outlier, being more similar to *C. canadensis* and *P. capensis* than it is to the other multituberculates. *C. vulgaris* and *K. dashzevegi* are closest to *G. watersi* and *P. capensis*, with *C. vulgaris* being the closest to the rodents. In the molar PC 3 v 4 plot (10.86% v 4.77% variance), the rodents are more spread out, with the protrogomorphs being mostly separated from the sciuromorphs and myomorphs across the origin, and the multituberculates again being separated into the positive PC 3 space. This time, *K. dashzevegi* is the closest multituberculate to the rodents, with *N. gobiensis* being distinct from it on PC 3 and *C. vulgaris* being separated from both other multituberculates into the positive PC 4 space. The closest rodent to *K. dashzevegi* on this plot is *A. rufa*. *P. capensis* and *C. canadensis* occur near *K. dashzevegi* on PC 3, but are further down in the negative PC 4 space. The means of hystricomorphs, myomorphs, sciuromorphs, and multituberculates can be observed to be roughly arranged in a line across this plot, with the mean of the

protrogomorphs being notably displaced from this rough line, as the protrogomorphs are distinguished from most other rodents on molar PC 4.

In summary, the multituberculates often distinguish themselves from the rodents on these PC plots, and have variation within their group (as do the rodent morphotypes). Sometimes, *C. vulgaris* and *K. dashzevegi* in particular are more similar to rodent taxa than to *N. gobiensis* or even to each other, depending on the plot and bite point in question, with specific rodent taxa (especially *C. canadensis*) reoccurring as similar to multituberculates.

The loading plots of this PCA are shown in Figure 4.35a and 4.35b as before. All muscles contribute notably to the variance on at least one PC, but the **ADM** v **DM** results are particularly important to the variance on PCs 1 and 2 at both bite points.

Comparing by bite point, the incisor and molar loading plots for PC 1 (44.26% incisor variance, 52.49% molar variance) are very similar, with **ADM** v **DM** the contributing the most to the positive variance and increasing in its contribution as gape increases. **T** is the only significant contributor to the negative variance, and also increases with gape. All other muscles contribute similar amounts to the positive variance, with the pterygoids increasing with gape and the remaining masseter subdivisions decreasing as gape increases.

PC 2 is more different between the bite points. In incisor biting (25.19% variance), the largest contributions to positive variance come from the **AZM**, **PZM**, and high-gape **PDM** v **DM**. Smaller contributions come from the **PDM** v **DM** at low-gape, the **T**, and **IP**. The **PZM** and **IP** both peak around 20° before decreasing as gape increases, the **AZM** and **T** both decrease with increasing gape, and the **PDM** v **DM** increases its contribution with increasing gape. The only significant negative contribution to the variance is from the **ADM** v **DM**, which decreases its contribution until around 20° before increasing to peak at 40°. In molar biting on PC 2 (17.47% variance), there are some differences: the **AZM**, **PZM**, and **T** all contribute less, with the

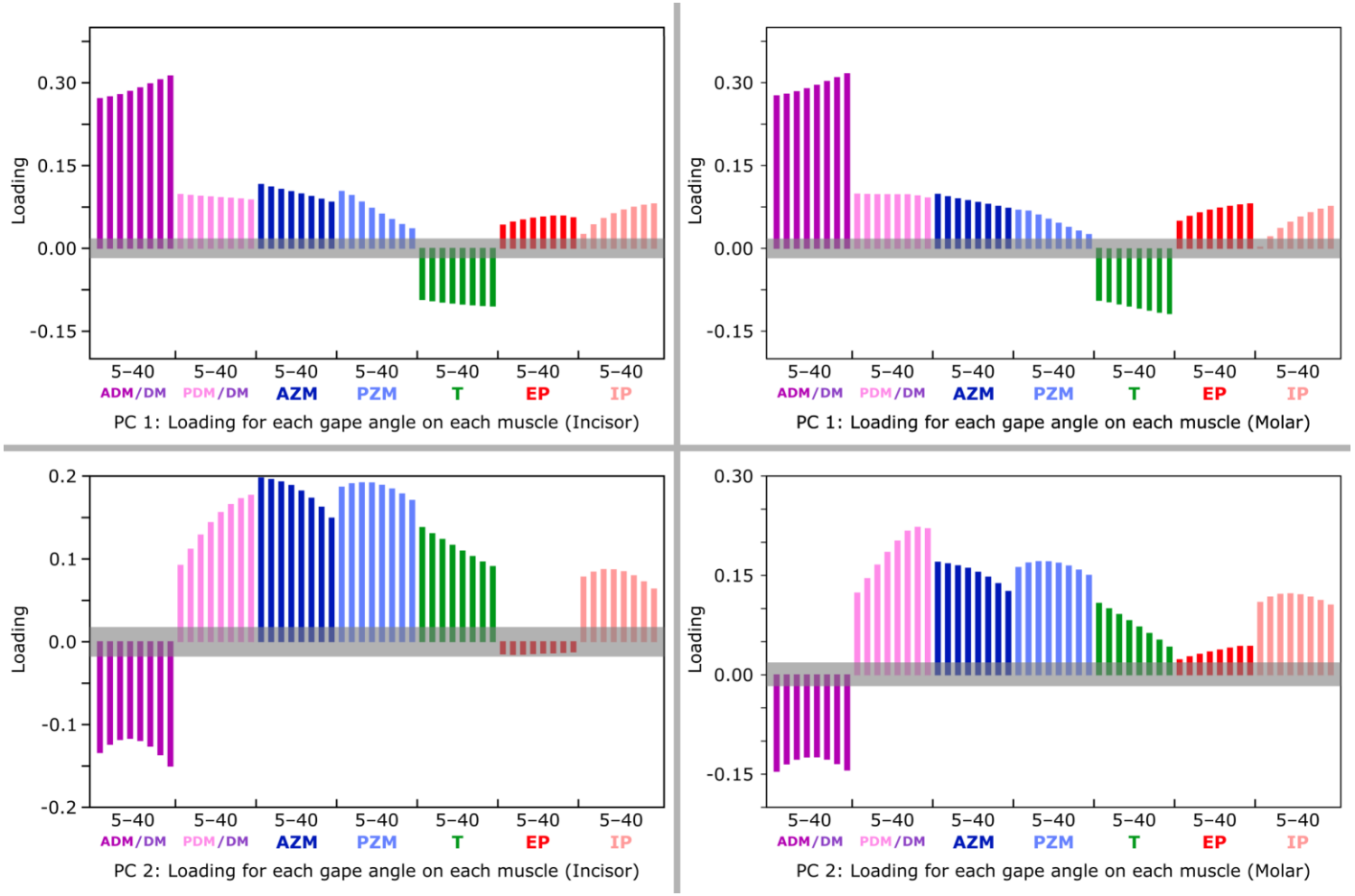

Figure 4.35a: Panel figure displaying the Loading Plots for PCs 1v2 in both incisor (left) and molar (right) biting for the **ADM** v **DM** PCA. Bars that extend beyond the grey region contribute beyond what would be expected under Brownian motion.

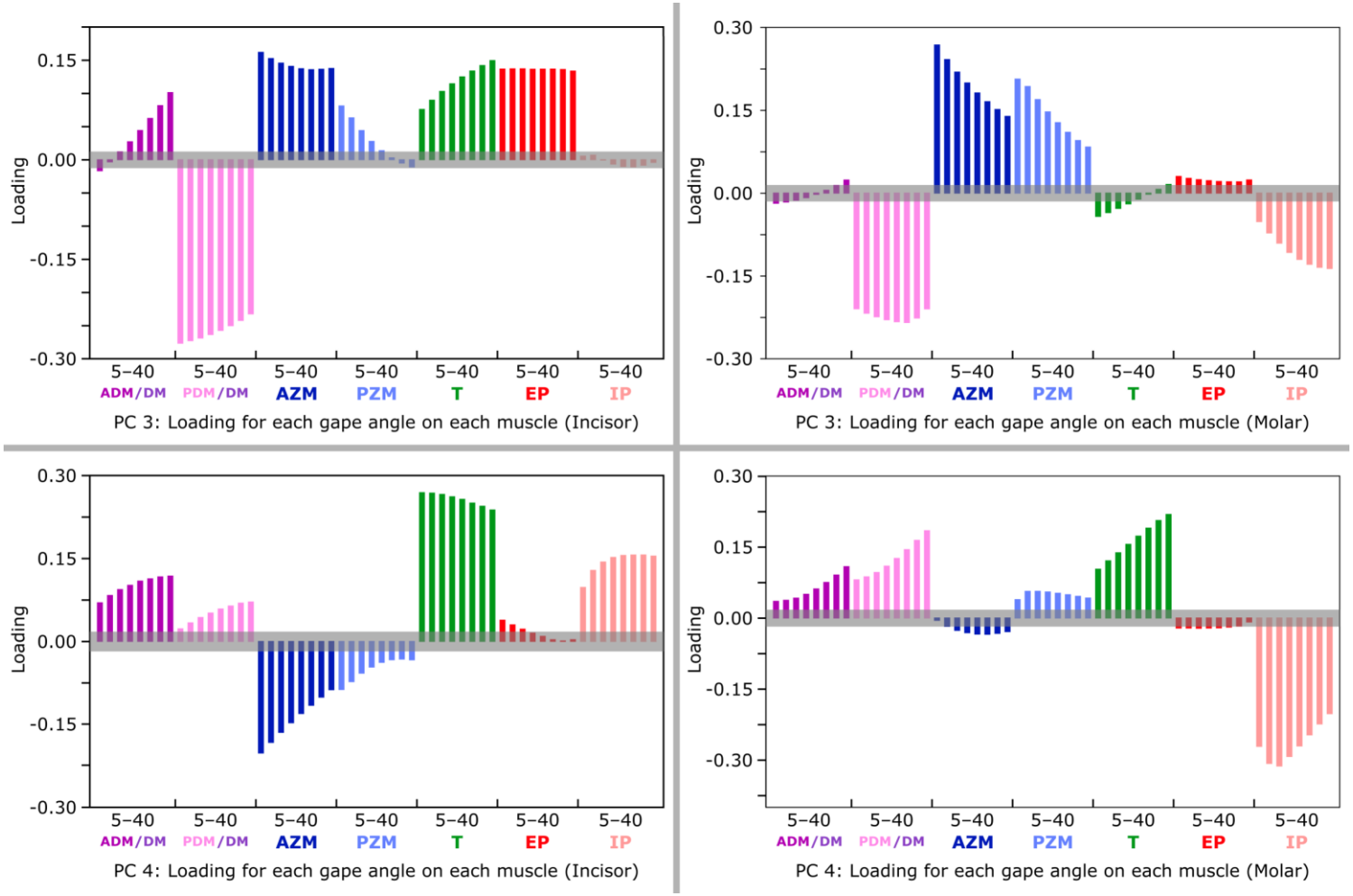

Figure 4.35b: Panel figure displaying the Loading Plots for PCs 3v4 in both incisor (left) and molar (right) biting for the **ADM** v **DM** PCA. Bars that extend beyond the grey region contribute beyond what would be expected under Brownian motion.

PDM v DM now being the largest contributor to the positive variance and peaking at 35° gape; the ADM v DM's contribution is now symmetrical, being similar at the low and high ends of the gape range; and the EP is now slightly contributing to the positive variance, increasing its contribution with gape.

Taken together, PC 1 and PC 2 combined imply that the ADM v DM is responsible for a large portion of the variance on the PC 1 v 2 plots, as expected given Chapter 3's results. Despite this, the multituberculates are separated from the myomorphs and sciuromorphs on these PC plots, so the difference between the multituberculates and the rodents is still clear even when comparing the ADM and DM.

Reaching PC 3, the two bite points are more different in their loadings. In incisor biting (11.44% variance) the largest contributions to the positive variance come from the AZM, T at high gape, and EP. Smaller contributions come from the ADM above 15° gape and the PZM below 20° gape, with the ADM v DM and T increasing their contributions with gape, the AZM decreasing before rising again above 25° gape, the PZM decreasing into insignificance, and the EP being stable with increasing gape. The only significant contributor to the negative variance is the PDM v DM, decreasing its contribution with increasing gape. In molar biting (10.86% variance), the only major contributors to the positive variance are the AZM and PZM, both decreasing their contribution with gape; the EP at all gapes and ADM v DM at 40° have contributions to the positive variance that are barely significant. The largest contributor to the negative variance is the PDM v DM, increasing with gape to peak around 30° gape, with a smaller contribution from the IP that increases with gape.

On incisor PC 4 (6.15% variance), the T is the largest contributor to the positive variance and decreases with increasing gape, with smaller contributions from the IP, ADM v DM and PDM v DM, all increasing with gape. The EP has a small contribution below 20°. The largest contributor to the negative variance is the AZM, with a smaller contribution from the PZM, both decreasing as gape increases. For molar biting (4.77% variance), the largest contributors to the positive variance are T, PDM v DM, and ADM v

DM, all increasing with gape, with a smaller contribution from PZM that peaks at 5–10°. The largest contributor to the negative variance is the IP, peaking at 15°, with very small contributions from the AZM above 10° and the EP.

In summary, the bulk of the distribution on the PC 1 v 2 plots is affected by the ADM v DM, but other muscles are still substantially contributing to the variance on these plots. The observable distributions on the PC 3 v 4 plots are affected by all studied muscles, with the PDM v DM and AZM being especially important for the PC 3 axes and the ADM v DM, PDM v DM and T being most responsible for the aforementioned position of the protrogomorphs out of 'alignment' with the distribution formed by the other groups on molar PC 3 v 4. Once again, the high and low ends of the studied gape angles are contributing the most to the variance in most muscles. As in the previous PCA, the difference in bite points illuminates observable divergences in which muscles are contributing the most to the variance, with the bite points being most similar on PCs 1 and 2. This further supports the proposed mechanical differences between these two bite points, despite the differentiation of the DM complex being the largest contributor to the variance in this PCA. However, these PC plots and loading plots do not identify if the difference between the group means of the organisms are significantly different.

Table 4.8 contains the results of the MANOVA analyses of PC scores for each bite point analysis, comparing the group means of multituberculates and rodent taxa. PCs 1–25 are included in the inputs for these MANOVAs, accounting for over 99.999% of the total variance at both bite points. In incisor biting, the p-value is below 0.05, indicating that there is a

Analysis	Incisor	Molar
df1	100	
df2	16	
Pillai's Trace	3.81	3.71
F	2.97	2.05
p	0.008	0.052

Table 4.8: The results of two MANOVA analyses of PC scores when simulating incisor biting and molar biting when the ADM and DM are compared. In each test, multituberculates and all four rodent morphotypes are compared.

	Incisor				Molar			
	vs H	**vs M**	**vs P**	**vs S**	**vs H**	**vs M**	**vs P**	**vs S**
df1	4	4	4	4	4	4	4	4
df2	12	4	1	2	12	4	1	2
Pillai's Trace	**0.02**	0.93	0.98	0.98	**0.95**	0.93	0.89	0.81
F	**129.8**	12.52	13.4	19.73	**54.44**	12.83	2.07	2.12
p	**9.14E-10**	0.02	0.20	0.05	**1.36E-7**	0.01	0.48	0.35

Table 4.9: The results of eight MANOVA analyses of PC scores when simulating incisor biting and molar biting when the **ADM** and **DM** are compared. In each test, multituberculates are compared to each individual morphotype. The p-value is 0.0083•.

significant difference between the group means in incisor biting, but not molar biting; this may be due to the broader disparity in the molar plots, potentially overshadowing the difference between the group means as in Chapter 3. As in the previous subheading, the multituberculates were also compared individually with each morphotype, with the results in Table 4.9.

With a p-value of 0.0083, these results suggest that the multituberculates are significantly different to the hystricomorphs, but not to the other morphotypes individually, which may be affected by the sample size of each group and how the morphotypes are divided into two clusters by the differentiation of the **DM** complex. As in Chapter 3, I now compare

	Incisor		Molar	
	Mu v H&P	**Mu v M&S**	**Mu v H&P**	**Mu v M&S**
df1	4	4	4	4
df2	15	8	15	8
Pillai's Trace	**0.95**	**0.92**	**0.87**	**0.84**
F	**72.49**	**21.73**	**25.32**	**10.27**
p	**1.26E-09**	**2.35E-04**	**1.61E-06**	**3.07E-03**

Table 4.10: The results of four MANOVA analyses of PC scores when simulating incisor biting and molar biting when the **ADM** and **DM** are compared. In each test, multituberculates are compared to a pair of morphotypes. The p-value is 0.0083•.

the multituberculates with each of these clusters of rodents (the hystricomorphs and protrogomorphs, and the myomorphs and sciuromorphs). The results of these MANOVAs are shown in Table 4.10. All are below 0.05, so the multituberculates are significantly different to each of the two groups of rodents visible on the PC 1 v 2 plots.

The results of these MANOVAs should be kept in mind when interpreting the results of this subsection. As before in rodents alone in Chapter 3, the comparison of the **ADM** and **DM** divides the sample of rodents into two clusters. However, the multituberculates are distinct from both groups despite possessing a differentiated **ADM** and **PDM** according to my reconstruction here; the variation on homologous muscles remains significant despite the common differentiation of the **DM** complex.

4.3.2.3 – Head size regression

Table 4.11 compiles the results of the multiple regressions of head size against PC scores. In both analyses, PCs 1–28 were included, accounting for over 99.99% of the total variance at both bite points. As in Chapter 3, these regressions were not conducted under a phylogenetic framework. In all cases, the p-value is greater than 0.05, and there is no statistically

		ADM v IOZM		ADM v DM	
Model		**Incisor**	**Molar**	**Incisor**	**Molar**
R Square		0.025	0.059	0.089	0.119
Mean Squared Error		0.022	0.057	0.022	0.065
Change Statistics	Wilks' Lambda	0.0628	0.0006	0.0017	0.0143
	F	0.533	58.25	21.6	2.462
	df1	28	28	28	28
	df2	1	1	1	1
	p	0.818	0.103	0.169	0.471

Table 4.11: Summary statistics of regression of the incisor biting and molar biting mechanical advantage PC scores on PCs 1 to 28 against geometric mean of head size among rodents and multituberculates.

significant correlation between head size and mechanical advantage in these data. Size can be ruled out as a potential contributor or complicating factor in the variance in mechanical advantage identified in these results.

4.4 – Discussion

4.4.1 – Returning to the hypotheses

To briefly recap, this study aimed to reconstruct the musculature of select fossil multituberculates and compare the mechanical advantage of potentially homologous muscles during incisor and molar biting with a range of extant rodent taxa.

I hypothesised (**H3.1**) that multituberculates would possess multiple identifiable jaw-closing muscles which would be homologous with those of rodents: temporalis muscles, pterygoid muscles, and a complex masseter with multiple subdivisions originating from the lateral and medial faces of the zygomatic arch. This hypothesis is broadly confirmed by the reconstructions; although I could not identify attachments sites for a **Superficial Masseter (SM)**, all other muscle subdivisions mapped in the rodents appear to have homologous counterparts in the studied multituberculates.

I hypothesised (**H3.2**) that multituberculates would group together in the mechanical advantage data, occurring closer to one another on the PC plots than to the rodents, due to the notable differences in head shape and proposed mechanics (such as the palinal power stroke) in multituberculates compared to extant rodents and the related features of their muscular configuration. On the PC plots, it can be observed that *C. vulgaris* and *K. dashzevegi* often occur closer to one or more rodent taxa than they are to *N. gobiensis*, the species which is typically the furthest from the origin on the PC plots. The MANOVA analyses of the PC scores also support this hypothesis, identifying that hystricomorphs and myomorphs are significantly different in group mean from the multituberculates when all muscles are included in the PCAs, with the sciuromorphs also being significantly different from the multituberculates in incisor biting only. Between multituberculates and rodents overall, a significant difference is also identified for incisor biting when the **ADM** and **DM** are compared and the **IOZM** is not included, and the multituberculates are significantly different to both groupings on rodents

formed on the PC 1 v 2 plots for the **ADM** v **DM** analysis; perhaps the distinction between the multituberculates and the myomorph-and-sciuromorph group may be associated with the multituberculates' lack of a zygomatic plate associated with this muscle differentiation. Given the observable contributions of so many muscles in the loading plots, I would additionally argue that comparing muscles like the **ADM** and **IOZM** is not distorting or skewing the results in a way that overshadows the contributions from strictly homologous muscle comparisons. Furthermore, multituberculates do not seem significantly different to protrogomorphs according to the MANOVAs of the **ADM** v **IOZM** PCA, though it is possible that the sample sizes of the groups are at least partially responsible for this result.

I hypothesised (**H3.3**) that the variation in mechanical advantage among the rodent taxa would be greater than the difference between rodents and the three selected multituberculates (i.e. that the multituberculates would group together more closely than the rodents do), and that there would be individual rodents that are mechanically similar to the multituberculates. This is confirmed, as can be observed by comparing the spread of variation of all rodents and the trio of multituberculates. *N. gobiensis* often occurs further from the other multituberculates on the PC plots than some rodents do, with *C. canadensis* and *P capensis* (two taxa identified as outliers to their morphotypes in Chapter 3) being the taxa that are most frequently similar to *C. vulgaris* and *K. dashzevegi* on the PC plots. As stated in the Introduction (subheading 4.1.3), this is likely affected by the sampling of these taxa, with 27 rodents and only 3 scanned multituberculates suitable for these analyses. An expansion of the sample would address this limitation, and further explore the potential differences between the two orders, and variation within Multituberculata more broadly. Furthermore, mechanical characteristics of the multituberculate masticatory system such as the x-axis's potential contribution to variance in 3D lever-arm mechanics (e.g. the lateral offset of the jaw joint onto the zygomatic arch) are not incorporated into this study's analyses of mechanical variance, but may be

relevant for future research. As it is, confirming this hypothesis at least confirms that the three studied—all from one superfamily—are different to the rodents overall, but can be similar to individual taxa. The observable disparity among rodents is broad, often greater than the distance on the PC plots between them and the multituberculates, but in the PC 3 and 4 plots in particular, the rodents can cluster close to the mean; despite the variety seen in rodents, multituberculates are still distinct from them as a group, especially *N. gobiensis*.

I hypothesised (**H3.4**) that as in Chapter 3, gape would affect mechanical advantage and the variance among the sample, with certain muscles and gape angle ranges being responsible for the majority of the total variance on the PCs. This was confirmed, with all studied muscles contributing notably to the variance. The **ADM** and **DM** are significantly according to the individual muscle MANOVAs, which also identify that the **ADM** and **IOZM** are significantly different to one another during molar biting only. The high and low ends of the studied gape range typically account for the largest contributions to the variance, with most muscles either increasing their contribution to the variance on a PC as gape increases, or decreasing their contribution as gape increases. More frequently than other muscles, the **PDM** v **DM**, and **IP** can exhibit their peak contribution to variance within the studied gape range, and decrease as gape continues to rise.

Though it is not formally a 'hypothesis', as with the rodents alone I expected that mechanical advantage would not correlate significantly with head size, and it could be discounted as a potential source of noise in the data. This was confirmed, as the regressions did not identify any correlation between geometric mean of head size and PC scores of mechanical advantage.

4.4.2 – Comparisons with older reconstructions

During the reconstructions of the multituberculate taxa, I could not identify some characteristics proposed in earlier reconstructions, especially

in *N. gobiensis*. The lack of plastic deformation and the internal preservation of bones and sutures in *N. gobiensis* suggests a much less 'domed' cranium than was previously thought (Kielan-Jaworowska, 1974; Kielan-Jaworowska, Cifelli and Luo, 2004). According to these scans and my reconstruction, the nasal bones are quite flat in lateral view and diverge from the premaxillae towards their anterior tip, resulting in an apparently large nasal opening and a distinct gap between the nasals and premaxilla along the anterior region of their suture. The older interpretation would require plastic bending of the entire rostrum, of which there is no indication in the scans. This anterior divergence between the two bones is not dissimilar to a number of extant rodent taxa, such as *A. cahirinus* or *L. aenigmamus* in particular. I suggest that the skull is flatter and shallower than previously thought, longer in proportion to its height, and lacks the curved palate-region and snout of older reconstructions.

I could not identify all of the muscles proposed in older papers. Early reconstructions of multituberculates were based on Jurassic plagiaulacid taxa (Simpson, 1926), not Cretaceous cimolodonts such as those in this study. Later papers used tooth cusps and wear facets to propose a palinal power stroke (Gingerich, 1977), but the anatomical and mechanical comparisons to rodents have continued to the present day in spite of this masticatory difference. There were a number of reconstructions in the latter 20th century of individual multituberculate taxa or multiple taxa (Landry, 1970; Sloan, 1979; Krause, 1982) including mechanical analyses (Wall and Krause, 1992), but the most significant to this study is a paper that examined the same specimen of *C. vulgaris* and the same skull of *N. gobiensis* as this study, although their analyses used the original ZPAL MgM-I/82 mandible that has since been misplaced (Gambaryan and Kielan-Jaworowska, 1995). Specimen to specimen, these results can be compared. Gambaryan and Kielan-Jaworowska proposed a buccinator based on identified muscle scars on the rostrum (Gambaryan and Kielan-Jaworowska, 1995), but this study's focus on masticatory muscles meant that this was not examined in this study. Though the nomenclature used in older papers differs to the nomenclature used here,

some of the same muscles were identified in both their paper and my analysis. Their reconstructions were based primarily on a small selection of extant rodents as a reference point, and on an existing reconstruction of *Catopsbaatar catopsaloides* (Kielan-Jaworowska, 1974), a well-preserved specimen which unfortunately was not able to be scanned for these analyses due to the disruptive impact of the Covid-19 pandemic.

Gambaryan and Kielan-Jaworowska's paper identified three ridges on the lateral face of the zygomatic arch, which they termed the anterior, intermediate, and posterior zygomatic ridges (Gambaryan and Kielan-Jaworowska, 1995); the anterior ridge is identified in my study as the dorsal margin of the **ADM**'s origin, and the intermediate ridge is identified as the dorsal margin of the **PDM**'s origin, but I did not identify their proposed posterior zygomatic ridge in these three taxa, nor its associated muscle they proposed (Gambaryan and Kielan-Jaworowska, 1995). The paper also identified a weakly pronounced medial zygomatic ridge (Gambaryan and Kielan-Jaworowska, 1995) that I suspect may be the dorsal margin of the **AZM**'s origin as identified here, but it is not figured in the original paper and with this lack of visual confirmation I may be incorrect in drawing this comparison. In the orbital pocket, they identified an 'orbitonasal fossa' (Gambaryan and Kielan-Jaworowska, 1995) that corresponds with my proposed attachment surface for the **IOZM**'s origin, so I am confident in the identification of this muscle's presence despite the poor or incomplete surface preservation of this area in *N. gobiensis* and *C. vulgaris* due to partial replacement or obstruction of the bone surfaces. They also identified a lambdoidal crest and proposed a **T** attachment anterior to this crest (Gambaryan and Kielan-Jaworowska, 1995) with which my reconstruction agrees. In their paper, the **EP** and **IP** are interpreted as both originating on a 'channel' between the pterygoid and alisphenoid (Gambaryan and Kielan-Jaworowska, 1995), which differs substantially from my interpretation; what they suggest as the origin of both, I believe is the **IP** origin, with the **EP** originating in a similar position to that of rodents, where there is an identifiable fossa. Of all the muscle origin identifications I make in this study,

the **EP** is perhaps the most likely to be disputed on the basis of older reconstructions.

On the mandible, the **EP** was interpreted as inserting onto a fossa on the 'pterygoid fovea' (Gambaryan and Kielan-Jaworowska, 1995) ventral to the condylar process and similarly to extant rodents. I could not identify an attachment site there on the scanned mandibles; I interpreted the muscle as inserting on the dorsal face of the pterygoideus shelf instead, in the more-clearly defined fossa there. The **IP** was previously suggested to insert on a 'pterygoid fossa' posteroventral to the rear of the tooth row that largely occurs on the medial face of the mandible (Gambaryan and Kielan-Jaworowska, 1995), but I disagree with this reconstruction and place it instead on the dorsal face of the pterygoideus shelf, where the margins of a fossa are more clearly defined. They identified a convexity lateroventral to the p4 named the 'lunule' (Gambaryan and Kielan-Jaworowska, 1995), which I did not identify, and propose that this is where the buccinator inserts. They identified a 'masseteric fovea', clearest in *C. vulgaris* (Gambaryan and Kielan-Jaworowska, 1995), which is observable in my reconstructions and which they identify as the insertion of the masseter medialis pars anterior, the **IOZM** in the nomenclature of my study (Gambaryan and Kielan-Jaworowska, 1995). They propose that there is an anterior portion of the **T** that inserts on the temporal groove (Gambaryan and Kielan-Jaworowska, 1995), but I interpret this as the insertion of the **IOZM**, as opposed to their proposed insertion on the masseteric fovea, which would differ substantially from its range of known insertions in rodents if correct. They also interpret muscle attachments posterodorsal to the 'masseteric crest', and dorsal to the 'masseteric line' (Gambaryan and Kielan-Jaworowska, 1995), which are attachment surfaces that align with my interpretations for the insertions of the **ADM** and **PDM** respectively. On the lateral face of the mandible, they identify three weakly pronounced regions ventral to the coronoid process (Gambaryan and Kielan-Jaworowska, 1995), of which only the posterodorsal and posteroventral elevations are identified in my analysis, as the **AZM** and **PZM** insertions. They also propose a differentiated **T** with three subdivisions (of which the posterior

portion is equivalent to the **T** I identified) and an additional posterior portion of the deep masseter complex that originates from the aforementioned faint fossa associated with the posterior zygomatic ridge, posterior to the **PDM** origin and with an insertion ventral to the insertion of the **PZM** (Gambaryan and Kielan-Jaworowska, 1995); this would be similar to the posterior masseter of *A. rufa* and *G. nagtglasii* if correct, but I do not identify these additional **T** subdivisions or 'posterior masseter' muscle attachments on these specimens. In *C. vulgaris*, the proposed subdivided temporalis was not reconstructed in this study either.

In summary, the **ADM** and **PDM**, **IOZM** origin, **AZM** and **PZM**, and **T** reconstructions of this study largely agree with the older reconstruction, but the **EP** origin, **IP** origin, and **IOZM**, **EP** and **IP** insertion reconstructions differ. Their proposed additional subdivision of the deep masseter, a sheet-like masseter lateralis originating on the ventral zygomatic arch, and subdivided temporalis were not identified by me on these taxa. The combination of matrix replacement and surface damage, voxel-resolution, and the absence of the original *N. gobiensis* mandible for a one-to-one comparison may contribute to these differences of interpretation.

This configuration is broadly similar to the muscle subdivisions of rodents, with the orbital pocket and **IOZM** origin occurring dorsal to the small infraorbital foramen, similar to bathyergids (an interpretation also noted in the older reconstruction (Gambaryan and Kielan-Jaworowska, 1995)). Since the MANOVA analyses and loading plots suggest that the **IOZM** contributes to the distinct difference in group means between multituberculates and hystricomorphs, this difference between the hystricomorphs system of 'enlarged infraorbital foramen with an attachment on the rostrum and a posteriorly inclined line of action' and the multituberculate's system of 'origin in the orbital pocket and a vertical or steeply-posterior line of action' appears to be one of the most immediately noteworthy differences in mechanics. The configuration of the anterior zygomatic root and **IOZM** origin seen in *P capensis* may be the reason why

it is often similar to the multituberculates on the PC plots here, possessing a similarly steep line of action for this muscle.

I would be interested to see if protrogomorphous fossil rodents, which lack a hystricomorphous enlarged infraorbital foramen, exhibit signs of a similar IOZM origin to the bathyergids and multituberculates; this would require further analyses with a sample of scanned fossil rodents. As the line of action of this muscle is nearly vertical or slightly posterior in this analysis, and even more posteriorly-inclined in the older reconstruction (Gambaryan and Kielan-Jaworowska, 1995), this muscle may be a substantial component in the difference between the palinal stroke of multituberculates and proal stroke of rodents.

4.4.3 – Limitations and avenues for further study

Rather than assessing and making predictions about the masticatory cycle as reconstructed in older papers (Wall and Krause, 1992; Gambaryan and Kielan-Jaworowska, 1995), this study instead simulated simplified incisor and premolar biting and calculated the mechanical advantage of each muscle at a range of gape angles. Though the palinal power stroke and distinctive tooth rows may differentiate multituberculate feeding from other mammals, the quantitative results of this study do find significant differences in mechanical advantage when comparing multituberculates and extant rodents. As can be observed on the PC plots, multituberculate taxa can be more similar to rodents than to one another, and certain rodents (such as *C. badius*, *C. canadensis*, *C. gambianus*, *D. punctata*, *D. sagitta*, *G. watersi*, *H. cristata*, *L. maximus*, *M. coypus*, *P. capensis,* and *S. carolinensis*) can be similar to multituberculates on the plots, though the group means of multituberculates and rodent morphotypes are often significantly different. The morphotypes within Rodentia are also similarly distinct from each other as the multituberculates are from the rodents, grouping closer to the mean because they form the vast majority of the sample; a larger sample of multituberculates will be key to evaluating this further. As in the rodent-only

analyses of Chapter 3, the PC plots with the multituberculates show a tighter grouping around the mean in incisor biting and broader variance in molar biting, implying that both groups are adapted to facilitate gnawing specifically (which has less diverse mechanical configurations) and are more broadly differentiated in the use of their cheek teeth. Despite their specialised premolars, multituberculates only seem especially distinct on the PC 1 v 2 plots for the analysis with all muscles (Figure 4.32), and are less distinct on the PC 3 v 4 plots, though this pattern is broken when removing the **IOZM** and comparing the **ADM** and **DM**, where the multituberculates are distinct on PC 3 v 4 plots also (Figure 4.34). On Figure 4.32, even when looking at the bite point I would expect to have the most difference between the groups based on tooth shape (premolar biting) the variance of mechanical advantage among rodents is broad enough that the multituberculates are not more dramatically distinct from some rodents than other rodents themselves are; it is possible that the mechanics of the masticatory cycle and the performance of the tooth shapes, and not the muscular anatomy itself, may illuminate greater disparity between the two groups.

If not for the impact the Covid-19 pandemic had upon the data collection of this project, that could have been assessed. Several more multituberculate taxa were sought, but travel to scan in the AMNH was cancelled in the planning stage, and only two multituberculate taxa were able to be CT scanned for this project, from a shortlist of several specimens with excellent preservation. No new fossil rodent scans could be acquired as hoped. With the knock-on effect on the time available, the potential expansion of the project into physical testing using metal 3D-printed jaws was also scrapped (although a metal print of *K. dashzevegi* was produced early in the project). Physical testing remains a potential avenue for future research. The taxa that I would consider particularly good to acquire for future scanning (some of which were planned to be scanned prior to the pandemic's disruption) are well-preserved skulls with mandibles such as *Catopsbaatar* PM 120/107, *Kamptobaatar* ZPAL MgM-I/33, *Sloanbaatar* ZPAL MgM-I/20, *Ectypodus* AMNH 35536, and the recently discovered

Erythrobaatar GM30516 (Jin *et al.*, 2023). Comparison with fossil rodents, especially those from around when multituberculates went extinct, could provide further evaluation of proposed competitive exclusion extinction hypotheses for multituberculates; with such a small sample and no fossils in this study, such a topic cannot be assessed. Furthermore, since this project uses 2D methods and a ratio of muscle vectors, variation in the mediolateral dimension or from anatomical characteristics that are not preserved in the fossils may be lost, and could major contributors to the true variance between the two groups as a whole. Muscle mass, pennation and pennation angle, the material properties of food objects, and more factors not preserved in the fossil record would require extensive extrapolations and comparisons with extant taxa, and are information that has limited presence even in extant rodents at the time of the data gathering for this study. Mechanical advantage can be quantified and analysed using the bones alone, fitting with the inherent limitations of the sample available, but this limitation should be kept in mind with respect to this study's conclusions as a comparison of feeding.

Overall, it seems that multituberculates and rodents can be compared. In terms of mechanical advantage, the performance of multituberculates and rodents (especially hystricomorphs and myomorphs) is statistically different at a range of gape angles according to their group means in molar biting in particular, but specific muscles and gape angles contribute to observable variance among the sample. All studied muscles are of importance, and both rodents and multituberculates exhibit reduced mechanical disparity during gnawing than during chewing with the premolars/anterior cheek teeth. With the currently limited scanned sample from Cretaceous Djadochtatherioidea, statistically significant functional differences between the orders cannot yet be teased out in detail, but this sample of multituberculates is significantly different from the rodents. This is a promising result that hints at these potential difference, and further analysis on a larger sample could shed light on the proposed hypothesis of competitive exclusion.

4.5 – Conclusions

Multituberculates were a highly successful group prior to their extinction in the Eocene, and their ecological niche has since been filled by rodent taxa. Both groups specialised for the function of gnawing, with substantial variation in the form and function of their cheek teeth.

With new muscle reconstructions and a digital reconstruction of *N. gobiensis* (a key taxon in historical reconstructions of their anatomy and function), a small sample of three cimolodont multituberculates could be compared with extant rodents. I reconstructed the musculature of these multituberculates, identifying that most of the muscle subdivisions in rodents have homologous muscles in the multituberculates, though some homologous muscle attachments are positioned differently. These reconstructions share several similarities with the older reconstructions, but possess a few substantial differences such as a flatter, less 'domed' skull in *N. gobiensis* and the absence of certain masseter subdivisions, and different interpretations regarding specific attachments.

According to an evaluation of mechanical advantage across 27 extant rodents and 3 fossil multituberculates, all of the homologous muscle subdivisions contribute notably to the variance across the sample. The extremes of high gape (up to the calculated 40°) and low gape (down to 5°) account for the majority of the variance on most muscles. When all muscles are included in the PCA, the group means of multituberculates and rodents are significantly different during molar biting in these results, with multituberculates being significantly different to hystricomorphs and myomorphs specifically at both bite points. When the **ADM** and **DM** are compared, the multituberculates are significantly different to both groupings of rodents (those with a differentiated deep masseter complex, and those without). The variance within Rodentia overshadows the difference between the group means in this sample.

Functional comparisons between the groups seem to be a promising avenue for evaluating multituberculate mechanics, based on mechanical

advantage, though additional factors (such as chewing mechanics and the mediolateral dimension) may contribute to disparity between the groups that 2D mechanical advantage alone has missed. Future analyses can expand on the comparisons of these groups using new scans of more multituberculate taxa, scans of the original ZPAL MgM-I/82 hemimandible that has been misplaced in recent decades, an evaluation of fossil rodents contemporary to the decline of multituberculates, 3D-lever-arm mechanics analyses, or physical testing of printed toothrows.

Bibliography

Adams, N.F., Rayfield, E.J., Cox, P.G., Cobb, S.N. and Corfe, I.J. (2019) 'Functional tests of the competitive exclusion hypothesis for multituberculate extinction', *Royal Society Open Science*, 6:181536. Available at: https://doi.org/10.1098/rsos.181536.

Ameghino, F. (1889) 'Contribución al conocimiento de los mamíferos fósiles de la República Argentina', *Actas de la Academía Nacional de Ciencias de Córdoba*, 6, pp. 1–1027.

Averianov, A.O., Martin, T., Lopatin, A.V., Schultz, J.A., Schellhorn, R., Krasnolutskii, S., Skutschas, P. and Ivantsov, S. (2021) 'Multituberculate mammals from the Middle Jurassic of Western Siberia, Russia, and the origin of Multituberculata', *Papers in Palaeontology*, 7(2), pp. 769–787. Available at: https://doi.org/10.1002/spp2.1317.

Benton, M.J. (1987) 'Progress and competition in macroevolution', *Biological Reviews*, 62(3), pp. 305–338. Available at: https://doi.org/10.1111/j.1469-185X.1987.tb00666.x.

Butler, P.M. (2000) 'Review of the early allotherian mammals', *Acta Palaeontologica Polonica*, 45(4), pp. 317–342. Available at: https://bibliotekanauki.pl/articles/22584.pdf.

Butler, P.M. and Hooker, J.J. (2005) 'New teeth of allotherian mammals from the English Bathonian, including the earliest multituberculates Systematic palaeontology', *Acta Palaeontologica Polonica*, 50(2), pp. 185–207. Available at: https://agro.icm.edu.pl/agro/element/bwmeta1.element.agro-article-7436f0ce-0cd1-40d8-9278-6b28b4f78228/c/app50-185.pdf.

Clemens, W.A., Kielan-Jaworowska, Z. and Lillegraven, J.A. (eds) (1979) *Mesozoic mammals: the first two-thirds of mammalian history*. University of California Press.

Coleman, M.N. (2008) 'What does geometric mean, mean geometrically? Assessing the utility of geometric mean and other size variables in studies of skull allometry', *American Journal of Physical Anthropology*, 135, pp. 404–415. Available at: https://doi.org/10.1002/ajpa.20761.

Cope, E.D. (1884) 'The Tertiary Marsupialia', *The American Naturalist*, 18(7), pp. 686–697. Available at: https://doi.org/10.1086/273711.

Cox, P.G., Faulkes, C.G. and Bennett, N.C. (2020) 'Masticatory musculature of the African mole-rats (Rodentia: Bathyergidae)', *PeerJ*, 8:e8847. Available at: https://doi.org/10.7717/peerj.8847.

Druzinsky, R.E. (2010) 'Functional anatomy of incisal biting in *Aplodontia rufa* and sciuromorph rodents – Part 1: Masticatory muscles, skull shape and digging', *Cells Tissues Organs*, 191(6), pp. 510–522. Available at: https://doi.org/10.1159/000284931.

Dunn, O.J. (1961) 'Multiple comparisons among means', *Journal of the American Statistical Association*, 56(293), pp. 52–64. Available at: https://doi.org/10.1080%2F01621459.1961.10482090.

Emry, R.J. and Korth, W.W. (2012) 'Early Chadronian (late Eocene) rodents from the Flagstaff Rim area, central Wyoming', *Journal of Vertebrate Paleontology*, 32(2), pp. 419–432. Available at: https://doi.org/10.1080/02724634.2012.649329.

Gambaryan, P.P. and Kielan-Jaworowska, Z. (1995) 'Masticatory musculature of Asian taeniolabidoid multituberculate mammals', *Acta Palaeontologica Polonica*, 40(1), pp. 45–108. Available at: https://bibliotekanauki.pl/articles/21302.pdf.

Gingerich, P.D. (1977) 'Patterns of evolution in the mammalian fossil record', in A. Hallam (ed.) *Patterns of Evolution*. Amsterdam: Elsevier Scientific Publishing Co., pp. 469–500.

Grossnickle, D.M. and Polly, P.D. (2013) 'Mammal disparity decreases during the Cretaceous angiosperm radiation', *Proceedings of the Royal Society B*, 280(1771). Available at: https://doi.org/10.1098/rspb.2013.2110.

Grossnickle, D.M., Smith, S.M. and Wilson, G.P. (2019) 'Untangling the multiple ecological radiations of early mammals', *Trends in Ecology and Evolution*, 34(10), pp. 936–949. Available at: https://doi.org/10.1016/j.tree.2019.05.008.

Hahn, G. and Hahn, R. (1983) *Multituberculata*. Edited by F. Westphal. Amsterdam: Kugler Publications (Fossilium Catalogus, I: Animalia, Pars 127).

Hammer, Ø., Harper, D.A.T. and Ryan, P.D. (2001) 'Past: Paleontological Statistics software package for education and data analysis', *Palaeontologia Electronica*, 4(1), pp. 0–9.

Herring, S.W. (1980) 'Functional design of cranial muscles: comparative and physiological studies in pigs', *American Zoology*, 20, pp. 283–293. Available at: https://academic.oup.com/icb/article/20/1/283/1992384.

Hooker, J.J. (2010) 'The mammal fauna of the Early Eocene Blackheath Formation of Abbey Wood, London', *Monographs of the Palaeontographical Society*, 164(634), pp. 1–153. Available at: https://doi.org/10.1080/25761900.2022.12131814.

Hopson, J.A. (1967) 'Comments on the competitive inferiority of the multituberculates', *Systematic Zoology*, 16(4), pp. 352–355. Available at: https://doi.org/10.2307/2412159.

Jablonski, D. (2008) 'Biotic interactions and macroevolution: extensions and mismatches across scales and levels', *Evolution*, 62(4), pp. 715–739. Available at: https://doi.org/10.1111/j.1558-5646.2008.00317.x.

Jepsen, G.L. (1949) 'Selection, "orthogenesis," and the fossil record', *Proceedings of the American Philosophical Society*, 93(6), pp. 479–500. Available at: https://www.jstor.org/stable/3143337.

Jin, X., Mao, F., Du, T., Yang, Y. and Meng, J. (2023) 'A new multituberculate from the latest Cretaceous of central China and its implications for multituberculate tooth homologies and occlusion', *Journal of Mammalian Evolution*, 30, pp. 1–20. Available at: https://doi.org/10.1007/s10914-022-09636-2.

Jungers, W.L., Falsetti, A.B. and Wall, C.E. (1995) 'Shape, relative size, and size-adjustments in morphometrics', *American Journal of Physical Anthropology*, 38, pp. 137–161. Available at: https://doi.org/10.1002/ajpa.1330380608.

Kielan-Jaworowoska, Z., Ortiz, E., Vieytes, C., Pascual, R., Goin, F.J. and McKenna, C. (2007) 'First ?cimolodontan multituberculate mammal from South America', *Acta Palaeontologica Polonica*, 52(2), pp. 257–262. Available at: https://bibliotekanauki.pl/articles/20688.pdf.

Kielan-Jaworowoska, Z., Presley, R. and Poplin, C. (1986) 'The cranial vascular system in taeniolabidoid multituberculate mammals', *Philosophical Transactions of the Royal Society of London. B, Biological Sciences*, 313(1164), pp. 525–602. Available at: https://doi.org/10.1098/rstb.1986.0055.

Kielan-Jaworowska, Z. (1970) 'New Upper Cretaceous multituberculate genera from Bayn Dzak, Gobi Desert', *Palaeontologia Polonica*, 21, pp. 35–49. Available at: http://www.palaeontologia.pan.pl/Archive/1969-21_35-52_10-17.pdf.

Kielan-Jaworowska, Z. (1974) 'Multituberculate succession in the Late Cretaceous of the Gobi Desert (Mongolia)', *Results of the Polish-Mongolian Palaeontological Expeditions - Part V. Palaeontologia Polonica 30*, pp. 23–44. Available at: http://www.palaeontologia.pan.pl/Archive/1974_30_23-44_5-21.pdf.

Kielan-Jaworowska, Z., Cifelli, L.R. and Luo, Z.-X. (2004) *Mammals from the Age of Dinosaurs: Origins, Evolution, and Structure*. Columbia University Press. Available at: https://doi.org/10.7312/kiel11918.

Kielan-Jaworowska, Z. and Hurum, J.H. (1997) 'Djadochtatheria - a new suborder of multituberculate mammals', *Acta Palaeontologica Polonica*, 42(2), pp. 201–242. Available at: https://www.app.pan.pl/archive/published/app42/app42-201.pdf.

Kielan-Jaworowska, Z. and Hurum, J.H. (2001) 'Phylogeny and systematics of multituberculate mammals', *Palaeontology*, 44(3), pp. 389–429. Available at: https://doi.org/10.1111/1475-4983.00185.

King, B. and Beck, R.M.D. (2020) 'Tip dating supports novel resolutions of controversial relationships among early mammals', *Proceedings of the Royal Society B: Biological Sciences*, 287(20200943). Available at: https://doi.org/10.1098/rspb.2020.0943.

Krause, D.W. (1982) 'Jaw movement, dental function, and diet in the Paleocene multituberculate *Ptilodus*', *Paleobiology*, 8(3), pp. 265–281. Available at: https://doi.org/10.1017/S0094837300006989.

Krause, D.W. (1986) 'Competitive exclusion and taxonomic displacement in the fossil record; the case of rodents and multituberculates in North America', *Rocky Mountain Geology*, 24(3), pp. 95–117. Available at: http://dx.doi.org/10.2113/gsrocky.24.special_paper_3.95.

Krause, D.W., Hoffmann, S. and Werning, S. (2017) 'First postcranial remains of Multituberculata (Allotheria, Mammalia) from Gondwana', *Cretaceous Research*, 80, pp. 91–100. Available at: http://dx.doi.org/10.1016/j.cretres.2017.08.009.

Krishtalka, L., Emry, R.J., Storer, J.E. and Sutton, J.F. (1982) 'Oligocene multituberculates (Mammalia: Allotheria): youngest known record', *Journal of Paleontology*, 56(3), pp. 791–794. Available at: https://www.jstor.org/stable/1304407.

Landry, S.O. (1965) 'The status of the theory of the replacement of the Multituberculata by the Rodentia', *Journal of Mammalogy*, 46(2), pp. 280–286. Available at: https://doi.org/10.2307/1377848.

Landry, S.O. (1970) 'The rodentia as omnivores', *The Quarterly Review of Biology*, 45(4), pp. 351–372. Available at: https://doi.org/doi: 10.1086/406647.

Li, Q., Mao, F.-Y. and Wang, Y.-Q. (2018) 'First record of Eocene fossil rodent assemblages from the lower part of the Erden Obo Section, Erlian Basin (Nei Mongol, China) and its biochronological implications', *Palaeobiodiversity and Palaeoenvironments*, 98, pp. 259–276. Available at: https://doi.org/10.1007/s12549-017-0303-2.

Lopatin, A.V. (2020) 'A review of the Mesozoic and Cenozoic mammals of Mongolia', *Paleontological Journal*, 54(7), pp. 779–808. Available at: https://doi.org/10.1134/S0031030120070084.

Lopatin, A.V. and Averianov, A.O. (2004a) 'A new species of Tribosphenomys (Mammalia: Rodentiaformes) from the Paleocene of Mongolia', in S.G. Lucas, K.E. Zeigler, and P.E. Kondrashov (eds) *Paleogene Mammals*. New Mexico Museum of Natural History and Science (Bulletin, 26), pp. 169–175.

Lopatin, A.V. and Averianov, A.O. (2004b) 'The Earliest Rodents of the Genus Tribosphenomys from the Paleocene of Central Asia', *Doklady Biological Sciences*, 397, pp. 336–337. Available at: https://doi.org/10.1023/b:dobs.0000039709.02953.dc.

Mao, F., Wang, Y. and Meng, J.I.N. (2016) 'New specimens of the multituberculate mammal *Sphenopsalis* from China: Implications for phylogeny and biology of taeniolabidoids', *Acta Palaeontologica Polonica*, 61(2), pp. 429–454.

Marandat, B., Adnet, S., Marivaux, L., Martinez, A., Vianey-Liaud, M. and Tabuce, R. (2012) 'A new mammalian fauna from the earliest Eocene (Ilerdian) of the Corbières (Southern France): palaeobiogeographical implications', *Swiss Journal of Geosciences*, 105(3), pp. 417–434. Available at: https://doi.org/10.1007/s00015-012-0113-5.

Matthew, W.D. (1897) 'A revision of the Puerco Fauna', *Bulletin of the American Museum of Natural History*, 9, pp. 259–323.

Matthew, W.D. and Granger, W. (1925) 'Fauna and correlation of the Gashato Formation of Mongolia', *American Museum Novitates*, 189, pp. 1–12.

Matthew, W.D. and Granger, W. (1928) 'Paleocene multituberculates of Mongolia', *American Museum Novitates*, 331.

McKenna, M.C. (1961) 'A note on the origin of rodents', *American Museum Novitates*, 2037, pp. 1–5. Available at: https://core.ac.uk/download/pdf/18225923.pdf.

McKenna, M.C. (1975) 'Toward a phylogenetic classification of the Mammalia', in W.P. Luckett and F.S. Szalay (eds) *Phylogeny of the Primates*. Boston, MA: Springer, pp. 21–46. Available at: https://doi.org/10.1007/978-1-4684-2166-8_2.

Ostrander, G., E. (1984) 'The Early Oligocene (Chadronian) Raben Ranch local fauna, Northwest Nebraska: Multituberculata; with comments on the extinction of the Allotheria', *Transactions of the Nebraska Academy of Sciences and Affiliated Societies*, 239. Available at: https://digitalcommons.unl.edu/tnas/239?utm_source=digitalcommons.unl.edu%2Ftnas%2F239&utm_medium=PDF&utm_campaign=PDFCoverPages.

Parmar, V., Prasad, G.V.R. and Kumar, D. (2013) 'The first multituberculate mammal from India', *Naturwissenschaften*, 100, pp. 515–523. Available at: https://doi.org/10.1007/s00114-013-1047-0.

Pillai, K.C.S. (1955) 'Some new test criteria in Multivariate Analysis', *The Annals of Mathematical Statistics*, 26(1), pp. 117–121. Available at: https://doi.org/10.1214/aoms/1177728599.

Rich, T., Trusler, P., Kool, L., White, M.A., Bevitt, J., Morton, S. and Vickers−Rich, P. (2022) 'Second specimen of *Corriebaatar marywaltersae* from the Lower Cretaceous of Australia confirms its multituberculate affinities', *Acta Palaeontologica Polonica*, 67(1), pp. 115–134. Available at: https://doi.org/10.4202/app.00924.2021.

Rich, T.H., Vickers-Rich, P., Flannery, T.F., Kear, B.P., Cantrill, D.J., Komarower, P., Kool, L., Pickering, D., Trusler, P., Morton, S., Van Klaveren, N. and Fitzgerald, E.M.G. (2009) 'An Australian multituberculate and its palaeobiogeographic implications', *Acta Palaeontologica Polonica*, 54(1), pp. 1–6. Available at: https://doi.org/10.4202/app.2009.0101.

Robinson, J.G. and Redford, K.H. (1986) 'Body size, diet, and population density of neotropical forest mammals', *The American Naturalist*, 128(5), pp. 665–680. Available at: https://www.jstor.org/stable/2461950.

Ross, C.F. and Iriarte-Diaz, J. (2014) 'What does feeding system morphology tell us about feeding?', *Evolutionary Anthropology*, 23(3), pp. 105–120. Available at: https://doi.org/10.1002/evan.21410.

Samuels, J.X. and Hopkins, S.S.B. (2017) 'The impacts of Cenozoic climate and habitat changes on small mammal diversity of North America', *Global and Planetary Change*, 149, pp. 36–52. Available at: http://dx.doi.org/10.1016/j.gloplacha.2016.12.014.

Schumaker, K.K. and Kihm, A.J. (2006) 'Multituberculates from the Medicine Pole Hills local fauna (Chadronian) of Bowman County, North Dakota', *Paludicola*, 6(1), pp. 9–21.

Simpson, G.G. (1926) 'Mesozoic Mammalia, IV; the multituberculates as living animals', *American Journal of Science*, 11, pp. 228–250. Available at: https://doi.org/10.2475/AJS.S5-11.63.228.

Simpson, G.G. (1953) *The Major Features of Evolution*. New York Chichester, West Sussex: Columbia University Press (Columbia Biological Series, 3). Available at: https://doi.org/10.7312/simp93764.

Sloan, R.E. (1979) 'Multituberculata', in R.W. Fairbridge and D. Jablonski (eds) *The Encyclopedia of Paleontology*. Springer Berlin, Heidelberg, pp. 492–498. Available at: https://doi.org/10.1007/3-540-31078-9.

Sloan, R.E. and Van Valen, L. (1965) 'Cretaceous mammals from Montana', *Science*, 148, pp. 220–227. Available at: https://doi.org/10.1126/science.148.3667.220.

Smith, T., Codrea, V.A., Devillet, G. and Solomon, A.A. (2022) 'A new mammal skull from the Late Cretaceous of Romania and phylogenetic affinities of kogaionid multituberculates', *Journal of Mammalian Evolution*, 29, pp. 1–26. Available at: https://doi.org/10.1007/s10914-021-09564-7.

Smith, T. and Smith, R. (2003) 'Terrestrial mammals as biostratigraphic indicators in upper Paleocene-lower Eocene marine deposits of the southern North Sea Basin', in S. L. Wing, P. D. Gingerich, B. Schmitz, and E. Thomas, *Causes and consequences of globally warm climates in the early Paleogene*. Geological Society of America (GSA Special Papers, 369). Available at: https://doi.org/10.1130/0-8137-2369-8.513.

Valen, L.V. and Sloan, R.E. (1966) 'The extinction of the multituberculates', *Systematic Zoology*, 15(4), pp. 261–278.

Wall, C.E. and Krause, D.W. (1992) 'A biomechanical analysis of the masticatory apparatus of *Ptilodus (Multituberculata)*', *Journal of Vertebrate Paleontology*, 12(2), pp. 172–187. Available at: http://www.jstor.org/stable/4523439.

Weaver, L.N., Fulghum, H.Z., Grossnickle, D.M., Brightly, W.H., Kulik, Z.T., Wilson Mantilla, G.P. and Whitney, M.R. (2022) 'Multituberculate Mammals Show Evidence of a Life History Strategy Similar to That of Placentals, Not Marsupials', *The American Naturalist*, 200(3), pp. 383–400. Available at: https://doi.org/10.1086/720410.

Weaver, L.N. and Wilson, G.P. (2021) 'Shape disparity in the blade-like premolars of multituberculate mammals: functional constraints and the evolution of herbivory', *Journal of Mammalogy*. Edited by R. Powell, 102(4), pp. 967–985. Available at: https://doi.org/10.1093/jmammal/gyaa029.

Wilks, S.S. (1932) 'Certain generalizations in the analysis of variance', *Biometrika*, 24(3), pp. 471–494. Available at: https://doi.org/10.2307/2331979.

Williamson, T.E., Brusatte, S.L., Secord, R. and Shelley, S. (2016) 'A new taeniolabidoid multituberculate (Mammalia) from the middle Puercan of the Nacimiento Formation, New Mexico, and a revision of taeniolabidoid systematics and phylogeny: Revision of Taeniolabidoidea', *Zoological Journal of the Linnean Society*, 177, pp. 183–208. Available at: https://doi.org/10.1111/zoj.12336.

Wilson, G.P., Evans, A.R., Corfe, I.J., Smits, P.D., Fortelius, M. and Jernvall, J. (2012) 'Adaptive radiation of multituberculate mammals before the extinction of dinosaurs', *Nature*, 483, pp. 457–460. Available at: https://doi.org/10.1038/nature10880.

Wilson, R.W. (1951) 'Evolution of the Early Tertiary rodents', *Evolution*, 5(3), pp. 207–215. Available at: https://doi.org/10.2307/2405460.

Wood, A.E. (1962) *The early Tertiary rodents of the family Paramyidae*. American Philosophical Society (Transactions of the American Philosophical Society).

Wood, D.J. (2010) *The Extinction of the Multituberculates Outside North America: a Global Approach to Testing the Competition Model*. MSc Thesis. The Ohio State

University. Available at:
http://rave.ohiolink.edu/etdc/view?acc_num=osu1275595604.

Xu, L., Zhang, X., Pu, H., Jia, S., Zhang, J. and Lü, J. (2015) 'Largest known Mesozoic multituberculate from Eurasia and implications for multituberculate evolution and biology', *Scientific Reports* [Preprint], (September). Available at:
https://doi.org/10.1038/srep14950.

Yuan, C.-X., Ji, Q., Meng, Q.-J. and Luo, Z.-X. (2013) 'Earliest evolution of multituberculate mammals revealed by a new Jurassic fossil', *Science*, 341(August), pp. 779–783. Available at: https://doi.org/10.1126/science.1237970.

Chapter 5 – Discussion and conclusions

This project set out to evaluate the variation in masticatory muscles and their efficiency, and compare morphotype groupings within rodents, and then compare these with multituberculates. Together, Chapters 2, 3, and 4 accomplish this.

Several hypotheses were established throughout the project, and all have been either accepted or rejected. Detail was discussed in their corresponding chapters, so only a short summary will be presented here.

In Chapter 2, **H1.1** hypothesised that the morphotype categories would not be distinctly different during a zero-gape incisor bite due to the variation within each category. This hypothesis is supported. **H1.2** hypothesised that there would be no significant phylogenetic signal in zero-gape incisor biting due to the para/polyphyletic nature of morphotype categories. The **T** and **EP** exhibited a significant phylogenetic signal, but no other muscles did.

In Chapter 3, **H2.1** hypothesised that the group means of morphotype categories would be significantly different, and that gape would have an observable correlation with the variation in mechanical advantage. **H2.2** hypothesised that the variance of mechanical advantage in incisor biting would be smaller than in molar biting, due to the established knowledge of rodents as having conservative anatomy adapted for gnawing. Both of these hypotheses are supported. In addition, I anticipated overlap between morphotypes on multiple PCs, also due to homoplasy and convergence, which was observed.

In Chapter 4, **H3.1** hypothesised that multituberculates would possess several muscle attachments homologous to those of rodents, suitable for comparison with the sample established in the preceding chapters. **H3.2** proposed that on the PC plots, multituberculates would be more similar to each other than to rodents, due to their own distinct characteristics (like their offset jaw joint, different skull & mandible shape,

etc). **H3.3** hypothesised that the variation among rodents would be greater than the difference between them an multituberculates, due to the difference in sample sizes and how 2D methods do not account for certain anatomical and mechanical differences between the two groups. **H3.4** hypothesised that gape would affect the variance in mechanical advantage in similar ways to those observed in Chapter 3. All four of these were also, broadly, supported.

There is nuance to be found in the conclusions drawn, however.

The morphotype categories appear to be broad and varied anatomical groupings of a range of nuanced functional approaches, and the anatomy of individual taxa is typically more impactful than the morphotype category itself. Some established interpretations of differences between them are supported, however; for example the **ADM** and **DM** are more significantly different during incisor biting than molar biting, with the **ADM** often behaving similarly to the **IOZM** in the raw data, supporting the idea that the expansion of the in **IOZM** hystricomorphs may fulfil a similar role to the **ADM** in myomorphs and sciuromorphs, as an anterior muscle with high mechanical advantage (Wood, 1965; Druzinsky, 2010). Comparisons in Chapter 3 suggest that the two muscles might be distinct, however, with the morphotypes being identified as significantly different when the **ADM** and **IOZM** are compared against one another; the two muscles are less different than the **ADM** and **DM**. Hystricomorphs group distinctly from sciuromorphs quite often, loosely supporting the existing theory that they are specialised for chewing and gnawing respectively (Becht, 1953; Wood, 1965; Druzinsky, 2010; Cox *et al.*, 2012; Cox, Kirkham and Herrel, 2013; Cox, 2017). Both rodents and multituberculates are more diverse in their mechanical advantage during molar biting, than in incisor biting, likely due to specialisation within their niches despite the homoplasy. Many muscles in multituberculates are homologous to those of rodents, but notably I did not identify a **SM** with a *pars reflexa* as I mapped in all rodents. The multituberculates are established as significantly different to hystricomorphs and myomorphs, but not protrogomorphs and sciuromorphs. All muscles contributed to the variance within Chapters 3 and 4, especially at the low or

high extremes of the studied gape range, but different muscles contributed positively or negatively to the variance on different PCs. Distinct patterns and trends of mechanical advantage against gape occur in different muscles across the data, which could provide an interesting focus for studies of optimum gape in the future. Furthermore, recent papers are calling into question simplified assertions regarding and definitions of morphotypes, a conclusion which aligns with the observed variation within each category in this study; one recent paper applied dissection and comparative anatomy to several taxa in suborder Anomaluramorpha, and concluded that the group's hystricomorphy is distinct from that of Ctenohystrica and Dipodidae (Da Cunha, Fabre and Hautier, 2024). Perhaps due to the sampling in this study, such a distinction is not identified in the phylogenetic signal test in Chapter 2; with further expansion of the sample, this intricacy can be more fully explored.

Some results are of less significance to the focus of this project, but still worth highlighting here. Some differences are proposed between the reconstruction of *N. gobiensis* conducted in this project and the established reconstructions, both regarding skull shape and regarding muscle attachments. In Chapter 2, the origins of the **EP** were suggested to have variation in their position; this may perhaps be associated with variation in the form of the muscle and where it begins its development during the embryonic stage of the organism, or a result of using only muscle mapping on the bones.

Functional comparisons between multituberculates and rodents, or between rodent morphotypes, could be expanded further with additional mechanical and anatomical factors to illuminate the intricacies of the groups. Specific assumptions about an individual taxon within one of the groupings in this study should be made with caution if that taxon has not been studied, due to the observable variance in such a 'conservative' group as rodents. Since this study aims to quantify the variance and compare groupings, it doesn't really compare the *effectiveness* of the groups; as such, I am not making assertions regarding the competitive exclusion hypothesis based on

these results alone. Though the multituberculates do appear to be mechanically distinct, this does not necessarily imply a competitive advantage on the part of one order or the other, especially since these are Cretaceous multituberculates and not those contemporaneous with rodents during the multituberculates' decline and extinction.

Regardless, future studies should ensure they incorporate multiple bite points and gape angles into their analyses, as the introduction of these in Chapter 3 revealed differences between morphotypes that were not observed in Chapter 2.

To further explore the variation within and between morphotypes, rodents, and multituberculate fossils, and explore the possibility of competitive exclusion, several particular subjects need further study in the coming years: dissections and detailed anatomical information on the muscles of extant taxa; incorporation of more complex muscle characteristics such as pennation and force into the analyses; pairing with study of skull and mandible shape to further explore variation in form; studies of dentition and its potential relationships with musculature; detailed dietary analysis, perhaps including identifying the material properties of food objects or doing physical testing of model jaws on plausible food objects; and expanding the digitised fossil sample of both orders.

Bibliography

Becht, G. (1953) 'Comparative biologic-anatomical researches on mastication in some mammals', *Proc. Koninklijke Nederlandse Akademie van Wetenschappen, Ser C*, 56, pp. 508–527.

Cox, P.G. (2017) 'The jaw is a second-class lever in *Pedetes capensis* (Rodentia: Pedetidae)', *PeerJ*, 5:e3741. Available at: https://doi.org/10.7717/peerj.3741.

Cox, P.G., Kirkham, J. and Herrel, A. (2013) 'Masticatory biomechanics of the Laotian rock rat, *Laonastes aenigmamus*, and the function of the zygomaticomandibularis muscle', *PeerJ*, 1:e160. Available at: https://doi.org/10.7717/peerj.160.

Cox, P.G., Rayfield, E.J., Fagan, M.J., Herrel, A., Pataky, T.C. and Jeffery, N. (2012) 'Functional evolution of the feeding system in rodents', *PLOS One*, 7(4). Available at: https://doi.org/10.1371/journal.pone.0036299.

Da Cunha, L., Fabre, P.-H. and Hautier, L. (2024) 'Springhares, flying and flightless scaly-tailed squirrels (Anomaluromorpha, Rodentia) are the squirrely mouse: comparative anatomy of the masticatory musculature and its implications on the evolution of hystricomorphy in rodents', *Journal of Anatomy*, 244(6), pp. 887–1101. Available at: https://doi.org/10.1111/joa.14013.

Druzinsky, R.E. (2010) 'Functional anatomy of incisal biting in *Aplodontia rufa* and sciuromorph rodents – Part 1: Masticatory muscles, skull shape and digging', *Cells Tissues Organs*, 191(6), pp. 510–522. Available at: https://doi.org/10.1159/000284931.

Wood, A.E. (1965) 'Grades and clades among rodents', *Society for the Study of Evolution*, 19(1), pp. 115–130. Available at: https://doi.org/10.2307/2406300.